

# Chapter 4

## Composite Structure Design and Analysis

Zhen Shen, Xianxin Tong, Naibin Yang, Mingjiu Xie,  
Ye Li and Puhui Chen

### 4.1 General

#### 4.1.1 Overview

The term advanced composite materials is given to an innovative range of materials that were developed toward the end of the 1960s. These material systems have since found a wide range of applications and continue to be widely developed. Currently, advanced composites, in particular, polymer matrix composites, are widely used in aerospace structures. Such composites are considered one of the four aerospace structural materials together with Al, Ti, and steel alloys.

Reducing structural weight is particularly important for modern aerospace vehicles. Advanced composite materials offer many advantages, such as high specific strength and specific modulus, tailorable performance, good resistance to fatigue and corrosion, and the potential for integrated processing. These factors may permit weight reductions of up to 25–30%, if composites are used to replace conventional metal structures in aerospace applications. Furthermore, air-elastic properties can be considerably improved, which is difficult or impossible to achieve with the use of other materials. Some advanced composites may facilitate stealth and intelligent flight structures in aerospace applications. Owing to their superior performance, advanced composite materials are also widely applied in infrastructures such as bridges and pipelines, and other vehicles including automobiles and

---

Z. Shen (✉) · X. Tong · M. Xie · Y. Li  
Aircraft Strength Research Institute of China, Xi'an, Shaanxi 710065, China  
e-mail: Shenzhen623@yahoo.com.cn

N. Yang  
Beihang University, Beijing 100191, China

P. Chen  
Nanjing University of Aeronautics and Astronautics, Nanjing, Jiangsu 210016, China

ships. Applications of composite began in aerospace structures. Hence, resources for design and analysis of advanced composite materials have been adopted from aerospace experiences to benefit other transportation industries in both military and commercial sectors.

#### ***4.1.2 Applications of Advanced Composite Materials in Aircraft Structures***

In the USA and Europe, development of advanced composite materials began in the 1960s and was first applied in the early 1970s. Fighter jets in service in the 1980s used advanced composite materials in their wing and tail structures, comprising 20–30% of the total aircraft weight. The wing structures of the stealth B-2 developed in the 1980s was made up of ~60% composite materials.

Applications of advanced composite materials in civil aircraft proceeded more cautiously because of safety and cost considerations. To promote confidence in composite technologies for civil aerospace applications, many programs were implemented in the USA in the 1970s. These include the Aircraft Energy Efficiency (ACEE) and Advanced Composite Technology (ACT) programs, and the Composite Affordability Initiative (CAI). In Europe, the Technology Application to the Near-Term Business Goals and Objectives (TANGO) project was initiated with the aim of producing composite wing and fuselage components at a competitive cost. In the recently launched A380, A350, and Boeing 787, contributions of advanced composite materials to the structural weight were 22, 52, and 50%, respectively.

In helicopters, the use of composites has reached 50–60% of the total structure weight in military helicopters. Advanced composite materials make up 41% of the structural weight of the US RAH-66. The vertical landing and tilt rotor V22 Osprey contains up to 51% composite materials by weight and is considered to be a full-composite vehicle. To date, many small full-composite airplanes have been launched. Among these, the well-known passenger-goods dual-purpose “ship star” has passed the airworthiness certification. The world-famous “voyager” has set the world record for a continuous flight around the world without refueling or landing. These successes are an excellent showcase for the effectiveness of advanced composite materials.

In China, research and development of advanced composite materials and their applications in aircraft structures were initiated in the late 1960s. In the mid-1970s, the first composite structural components were successfully used in the air duct wall of aircraft fighter. In 1985, a jet fighter with a composite vertical tail made its first flight. In 1995, a composite wing with an integrated fuel tank was successfully developed. This advance marked a new milestone in composite material applications in aircraft structures in China. Almost all aircraft currently in service now use composite parts to some extent. In 2000, the commercial airplane-Y7, with a

composite vertical tail, passed the airworthiness certification ushering in a new era of composite material applications in civil aircraft. Many large-scale commercial aircrafts currently being planned will feature large proportions of advanced composite materials. Applications of composite materials in helicopters have also considerably advanced. Imported manufacturing technologies have been replaced by native design approaches to next generation helicopters in China.

### ***4.1.3 Properties of Advanced Composite Materials***

#### **4.1.3.1 Structural Performance**

##### **(1) Specific strength and specific modulus**

Carbon fiber/epoxy resin composites are most often used in aircraft structures. The use of these materials can greatly reduce the structural weight because of their high specific strength ( $\sigma_b/\rho$ ) and specific modulus ( $E/\rho$ ). In Table 4.1, the performance of unidirectional composites and conventional metals is compared. The advanced T800/modified epoxy resin can, respectively, provide specific strength and specific modulus 10 and 4 times as high as that of aluminum alloys [1, 2].

##### **(2) Anisotropy and tailorable performance**

Currently, laminated structures, prepared by unidirectional prepreg laying-up and curing, are the main materials used in aircraft structures. Unidirectional prepreg tapes are strongly orthotropic, i.e., performance in the fiber direction is different to that vertical to fibers. To satisfy the performances requirements in specific directions in a structural plane, it is necessary to place unidirectional tape in different directions at certain ratios. The designed laminates may be either isotropic or anisotropic and may be either symmetrically balanced or asymmetrically balanced. This unique feature offers considerable flexibility to designers. The use of low-density advanced composite materials requires new structural design methods to be applied at an early stage to fully take advantage of the properties of composite materials. Composite forward-swept aircraft wing and the zero thermal expansion coefficient structures are typical applications of laminating anisotropy, which offers tailorable performance. However, anisotropy also presents some challenges for structural design, analysis, and manufacture of composite structures.

Another characteristic of composite laminate anisotropy is that interlaminar performance is typically much lower than that in-plane. There are also large differences in the performance of different constituents, i.e., the mechanical properties of the fiber and matrix. These factors typically contribute to failure mechanisms of laminated composite structures, which are to very different from those of metal structures. Impact damage and delamination are key design considerations.

**Table 4.1** Comparison between composite and metal materials

Materials	T. strength/MPa	T. modulus/GPa	Specific strength/MPa·g <sup>-1</sup> ·cm <sup>3</sup>	Specific modulus/GPa·g <sup>-1</sup> ·cm <sup>3</sup>	Density/g·cm <sup>-3</sup>
Al alloy	420	72.0	151.1	25.9	2.78
Steel (structure)	1200	206.0	152.9	26.3	7.85
Ti alloy	1000	116.7	221.2	25.8	4.52
H.S/C/epoxy	1471	137.3	1014	94.7	1.45
H.M/C/epoxy	1049	235.0	656.0	146.9	1.60
Kevlar/epoxy	1373	78.4	981.0	56.0	1.40

**(3) Damage, fracture, and fatigue behavior**

Features of advanced composite materials often include anisotropy, brittleness, and inhomogeneity. These features, and the inferior interlaminar properties compared with those in-plane, cause the failure mechanisms of laminate composites are very different from those of metals. Their damage, fracture, and fatigue performances are also very different. Although the laying-up and autoclave processing used for composite components is simple, impacts by foreign objects during machining and delivery are more likely to damage or induce defects in composite parts than equivalent metal parts. Table 4.2 summarizes the fatigue and damage tolerance of metal and composite structures.

- ① Main defect/damage types: Cracks are the main damage mode of metal structures. For composite structures, the critical defect/damage modes include interlaminar debonding, delamination, and low-energy (low-speed) impact damage. Impact damage can cause critical damage to composites by significantly decreasing their actual compression load-bearing ability. While no visible damage may be apparent from inspection of the outer surface, impacts may induce cracking of the internal matrix or delamination. Visible checks are only reliable once the compression strength has decreased to 40% of its original value after an impact. Delamination is a unique damage mode of laminated composites. Impacts from tools, and foreign bodies such as runway chippings, hail stones, and birds, together with the local interlaminar stress concentration and over-loading, may all contribute to internal delamination. The occurrence and growth of this type of damage greatly reduce the strength and stiffness of laminate components.

**Table 4.2** Comparison of factors affecting fatigue and damage tolerance

Content		Metal	Composites
Main damage cause		Fatigue, corrosion and stress corrosion	Foreign impact, processing defects
Critical damage		Crack	Impact damage/delamination
Danger loads		Tensile	Compression
Stress-strain behavior		Show yielding	Linear until final failure
Notch sensitivity	Static strength	Insensitive	Very sensitive
	Fatigue	Very sensitive	Insensitive
Damage check before failure		Possible for visible check	Impossible for visible check
Damage growth		Along main crack with regularity	Multi-damage propagation without regularity
Dispersion for static and fatigue strength		Small	Large

- ② Notch sensitivity: Generally, metals possess a yielding stage; however, composites typically show a linear stress–strain curve up until final failure occurs. Hence, composites have much higher static strength notch sensitivity than metals. Conversely, composites show much lower fatigue notch sensitivity than that of metals. The fatigue notch coefficient (i.e., the ratio of the fatigue strength between a non-notched and notched specimen under a certain number of fatigue cycles) is much smaller than the static stress coefficient and close to 1 over the long term.
- ③ Fatigue performance: Metals are often sensitive to fatigue. For notched structures, in particular, the fatigue strength will quickly decrease under a tensile–tensile fatigue load; composites can offer much better fatigue resistance. Fiber-dominated multi-direction laminates can pass  $10^6$  cycles in a tensile–tensile fatigue test under a maximum stress equal to 80% of the ultimate tensile load. Under tensile–compression, or compression–compression fatigue, the fatigue strength decreases slightly; however, after  $10^6$  cycles the fatigue strength remains at approximately 50% of the static strength value. For notched specimens subjected to compression–compression fatigue tests, the fatigue strength corresponding to  $10^6$  cycles will be greater than 60% of the static strength. Although impact damage and delaminated composites do not usually show crack growth under high fatigue loads, such damage may occur at later stages of the component life. It remains challenging to determine the probability of crack propagation in composite materials.
- ④ Stiffness reduction: For metal structures, the stiffness changes caused by fatigue load are usually not accounted for; however, this factor must be considered for composite structures bearing high-cycled fatigue, in particular, helicopter components such as rotor blades.
- ⑤ Dispersion: The dispersions in static strength and fatigue strength for composite materials are more than for metals. So, not only the life dispersion coefficient, but also the load enlarging coefficient should be considered in composite structure fatigue certification.

#### (4) Environmental effects

Besides extreme high temperatures, the effects of hot/wet environments on metals are generally not considered. For composites, the combination of environmental effects must be carefully considered. Composite matrices are made of polymer materials, which can be affected by heat and moisture. The glass transition temperature ( $T_g$ ) of a composite may be decreased on environmental exposure resulting in a considerable decrease in matrix-dominated mechanical properties, such as compression and shear. Although corrosion is a serious problem for metals, composites typically show good corrosion resistance.

## (5) **Electrical Conductivity**

Compared with metals, composites have very low electrical conductivity. Special lightning-proof measures must be considered in composite component design and special attention should be given to the oil tank design and to avoid static electrical shocks to compartments containing electrical instruments and devices.

### **4.1.3.2 Structure Design and Processing**

Metal airplane structures usually consist of parts such as the skin, beams, stringers, rib, and frame. These parts are mechanically assembled with a large quantity of fastening components. Metal parts can be processed by machining, rolling, forging, casting, and welding.

For composites, the material and structure can be manufactured simultaneously. Structural elements can be connected simultaneously with material processing through co-curing, knitting, braiding, and Z-pin technologies. Thus a large and integrated structure can be designed and manufactured in one time. The number of elements and fastening parts as well as the machining and assembling work can be greatly reduced. Hence, the structure weight and production costs can be considerably reduced. Owing to the above features, integration of design and processing is a serious concern for composite structures.

## **4.1.4 Overview of Composite Structure Design and Certification**

### **4.1.4.1 Design Essentials**

According to specifications for composites in military or civil airplanes applications, the design and certification of composite aircraft structures involve the following working phases: structural materials selection, determination of design allowables, structural type selection, quality assurance, and building block approach (BBA) certification. The composite structure design workflow includes the following steps [1, 2].

#### **(1) Material selection**

In addition to a material's fundamental properties, processing ability, and cost, for composite part design, the toughness, i.e., compression strength after impact (CAI), and the maximum service temperature and environmental effects should also be considered.

## (2) **Determination of design allowables**

A typical laminating code and skin thickness are used for testing and determination of the design allowables. Critical issues include the structural properties of laminate specimens with typical stacking, such as compression failure strain, open hole tensile/compression, filled hole compression failure strain, and assembly allowables. Furthermore, the effects of heat and moisture should be included, as well as fatigue properties. Defects are unavoidable in composites, and initial defects (in particular impact damage) can greatly affect the strength of the component. Thus, the effect of initial defects should be considered even if the design allowables only consider the static strength certification.

## (3) **Structure type selection**

On the basis of the structure design requirements and an outline of the external load conditions, proper structure types are selected. If necessary, selection tests should be performed to determine the optimized structure type. For the critical damage tolerance locations, the structures should be designed with the ability to resist impact damage. In the detailed design, special attention should be paid to out-of-plane loads that could be applied to the structures. Care should also be taken for open hole strengthening design. Honeycomb structures and thin skin structures, are susceptible to impact damage and should receive special attention.

## (4) **Certification of typical structures and assemblies with key structural features**

BBA certification tests, from simple to complex in different phases, can verify that a selected structure type can meet the design requirements in key areas. The durability/damage tolerance of the composite components should be verified in this phase particularly for blended metal/composite structures.

## (5) **Full-size part certification**

To verify that a part meets its structural integrity requirements, full-size part static strength verification is typically performed. The durability and damage tolerance of metal structures in blended metal/composite structures are assessed.

### **4.1.4.2 Affordability of Composite Structures in Low-Cost Design and Manufacture**

Although composites can satisfy the high-performance requirements of aircraft structures and effectively reduce the structural weight, processing of this material is expensive. In large-scale aerospace applications, lowering the cost of design and manufacture are key goals of composite research. Currently, areas for cost-saving in composite technologies include lowering the cost of materials and molding. Automatic fiber placement technologies have also been developed, including automated tape-lying (ATL), automated tow placement (ATP), and liquid



composite molding (LCM), such as resin transfer molding (RTM), resin film infusion (RFI), and vacuum assisted RTM (VARTM). More affordable ACM structures have received considerable attention for integrated structure design and manufacture.

## **4.2 Requirements of Structure Design**

### **4.2.1 General Requirements of Structure Design**

The following requirements should be satisfied in composite structure design, in addition to the general requirements for metal structure design.

- ① Co-curing, knitting, or adhering should be used as much as possible to reduce the number of components and eliminate stress concentration sources. Structure integration should be considered as much as possible to take full advantage of composites. For large parts, it is also necessary to consider delivery and repair.
- ② Out-of-plane loading should be avoided as much as possible in composite structures. Special attention should be paid to the out-of-plane load caused by off-axis or structural deformation.
- ③ It is necessary to consider the detectability of damage in manufacture and service. If reliable inspection methods are not available, the potential for large defects or damage should be considered in the design.
- ④ Environmental effects on materials should be considered, including heat, moisture, and the largest potential impact damage that may be encountered in service.
- ⑤ If all the possible failure modes have been considered, buckling or twisting may be allowed in thin laminated composites; however, buckling in thick laminates should be avoided.
- ⑥ Owing to the lower conductivity of composites than that of metals anti-static electrical, lightning proofing, and electromagnetic compatibility design and certification should be performed for certain parts of the airplane to satisfy the safety requirements.
- ⑦ The cost of the design should be considered at all phases of the structure design.

### **4.2.2 Requirements of Military Aircraft Structure Design**

#### **4.2.2.1 Static Strength**

The static strength design requirements of metal structures can also be applied to composite structures. Additional special requirements for composite structures include: the combined effects of operation temperature and moisture absorption to

determine the allowables for the composite structures. The uncertainty coefficient used in this case (the original safety coefficient) will remain as 15. The strength of composite structures is related to the laminating code, geometrical shape, and applied load. Hence, these factors should be also considered in the determination of B-allowables. Large numbers of complex structural tests are used to determine which of the B-allowables of composite structures are not applicable. It is acceptable to use a specimen that can replicate the structure laminating code, geometrical shape, and load to determine the B-allowables.

#### 4.2.2.2 Durability

##### (1) General requirements

The durability design requirements of metal structures can be generally be applied for composite structures. The key consideration for composite durability design is to control the matrix strain level. Unlike metal structures, the fatigue life and corrosion are not major factors to consider in the design of composite structure durability; however, for the impact damage resistance, the following requirements should be satisfied:

- ① The design should allow for checking and repair of damage caused by low-energy impacts such as tool dropping.
- ② Special attention should be paid to the organic polymer matrix composites, taking into account damage induced during services such as low-energy impacts, and the potential for damage during production, delivery, and maintenance. The repair of damage, maintenance, and function of the component should be carefully investigated.
- ③ It should be confirmed that no invisible surface defects exist, which may contribute to performance degradation of a part, requiring repair.
- ④ It should be confirmed that any impact will not result in damage to structures that may become critical over two designed life cycles under typical environmental conditions.

##### (2) Requirements for impact damage resistance

- ① Tool impact: On the basis of the probability of tool impact occurring, composite structures can be divided into two categories. The different structural requirements in durability design of these two structural zones are listed in Table 4.3.
- ② Hail stones and runway chippings: There are two possible impact sources that could bring about serious effects to structures; hail stone impacts during parking time, and stone impacts during aircraft movement on a runway. The selection of hail sizes will depend on the aircraft capacity and should cover a range greater than 90% of possible hail

**Table 4.3** Low-energy impact damage and durability testing requirements (tool impact)

Zone	Damage source	Damage level	Requirement
Zone 1 Easily impacted	Impactor diameter, in 12.7 mm low speed	Impact energy less than 8.1 J, or visible damage (energy not below 5.5 J)	No functional problems, no need for structure repair, and no water leakage over two designed life cycles
	Vertical to surface		No visible damage caused by a single impact of 5.5 J
Zone 2 Not easily impacted	Same as zone 1	Impact energy less than 8.1 J, or visible damage	No functional problem over two designed life cycles, no visible damage, no water leakage after site repair

**Table 4.4** Low-energy impact damage and its durability testing requirement (hail stones and runway chippings)

Zone	Damage source	Damage level	Requirement
All vertical surfaces and upward horizontal surfaces	Hail: Diameter: 20.3 mm Specific weight = 0.9 27.4 m/s Vertical to horizontal surface 45° angle with vertical surface	Uniformly distributed Central distance between impact points 20 mm	No functional problem over two designed life cycles, no need for structure repair No visible damage
Possibly impacted structures	Runway: Diameter: 12.7 mm Specific weight = 3 Equivalent to aircraft speed	None	No functional problem over two designed life cycles, no visible damage, no water leakage after site repair

stone sizes. The majority of stones that will likely be encountered by aircraft moving on a runway will be small and the speed of their impact will depend on the aircraft performance. In Table 4.4 the requirements of durability design for these two impact sources are given.

- ③ Load from operation and stampede: Apart from the impact load, it is necessary to consider the resistance on the operation and pedal loads encountered in manufacturing processes or in a service environment. The requirement on loads should be considered as follows:
  - a. Operation load:
    - Very difficult to reach, i.e., finger touching.
    - Easy to reach from top, i.e., one-hand catching and hanging.
  - b. Pedal load:
    - Very difficult to reach, i.e., difficult to stand on structure with one foot.

Easy to reach from top, i.e., two feet can be placed on the structure.  
Note: It is necessary to define the contact zone, position, and weight related to each of the conditions above.

### (3) Honeycomb sandwich structure control

This type of structure should be used in design elements requiring very light weight, and in parts that can be easily replaced or be accessible for repair. These structures are not permitted for use in environments exposed to water or for parts that require immediate replacement. The impact energy level acceptable for this kind of structure could be appropriately decreased, for example, to the level where no visible damage 2.5 mm in depth or penetration could be produced by an impact of 0.5–0.7 J.

### (4) Damage sensitive zone and details

Special care should be paid to some damage sensitive zones of the airplane, including the lower fuselage and the radome, inside the flap lower surface, and cabin doors. These zones need to be strengthened with thicker structures, possibly using glass-fiber to replace carbon fiber. Furthermore, the potential for a tire burst necessitates special attention to be paid to the damage sensitivity of the tire zone. Similar structures include components near the jet thrust reverser, which are sensitive to damage from ice and debris on the runway.

- ① Minimum-weight structure: Components such as the radome structure may not operate if the weight is designed to be too small. Another example is sandwich structures with low core density. The surface plates should have the minimum required thickness built into the design to prevent water invading the core. Surface coatings should not be considered as the only water resistance measure. Coatings may become corroded or abraded exposing the component to water.
- ② Joints of thin skin honeycomb sandwich structures are easily damaged during assembly and disassembly. Thus, it is necessary to use solid laminated structures in appropriate joining areas.
- ③ The rear edge of control surfaces is very sensitive to damage, the area located 102 mm from the back may be easily damaged by ground impact, loading and unloading impact, or by lightning strikes. These components are difficult to repair because of the need to strengthen the skin and the rear edge. It is acceptable in the design to add a load-bearing element to resist the load ahead of the rear edge. The rear edge itself or its surface should be reinforced with a material that is easily repaired, which will not endanger the functional parts when damaged. Considering the possibility of cracking leading to sealing problems, sealing agents should not be used at the ends of components.
- ④ The edge of laminates should not be directly exposed to an air stream to avoid delamination.

Possible measures include:

- (a) Use of corrosion-resistant edge protection, such as co-cured metal edge element.
- (b) Use of an easily replaced sacrificial material to wrap the edge.
- (c) The pre-cruise edge of wall plates should be placed in a lower position than the after-air edge of adjacent preceding wall plates.

### 4.2.2.3 Damage Tolerance

Damage tolerance design principals of metal structures can generally be adopted for composite aircraft structures. The major source of damage to composite structures is impact damage. The feature of impact damage is that damage may not be visible on the component's surface, but underlying delamination can considerably decrease the compression strength of the component. Composite structures are defined as undetectable structures in design. In this section, some particular requirements of composite structures are outlined [1–3].

#### (1) Assumption of defect dimensions

The damage tolerance of a component containing a defect should be sufficient that the component has enough residual strength over the specified operation period. Here defect refers to both initial and service defects. Defects caused by foreign low-speed impacts can occur at any time during service, including directly after being put into service. It is very difficult to detect such defects visibly over the service time, and thus, this type of defects is defined as an initial defect for the purposes of damage tolerance analysis and certification.

- ① Initial defect size assumption: Initial defects may be divided into three types: impact damage, delamination, and scratches.
  - a. Impact damage: Considering the features of composite impact damage, composite structures are defined as undetectable structures to ensure structure safety. The initial defect size can be determined by the basic concept defined as barely visible identification (BVID). The following standards can be used in general cases:
    - (a) The BVID dent caused by a half-sphere impactor with 25.4-mm diameter (depth less than 2.5 mm).
    - (b) The damage caused by a half-sphere impactor, with 25.4 mm diameter, at the maximum energy possibly encountered in service (typically less than 136 J).

The required energy for a BVID dent is related to the structure thickness. The former of the conditions mentioned above is used for medium thickness structures (less than 6 mm), while the latter is used for thicker structures (greater than 6 mm). For general cases, the smaller value is selected from the above two conditions.

When structures are not exposed to external impact or under threat of damage or the parts can be checked carefully before the structure is closed a lower impact damage requirement can be adopted. To pass certification under such decreased impact energy criterion, the proposed impact energy should be approved by the users; the impact damage, including damage which expanded to critical dimensions over a two-life-cycle spectrum load, can be detected by NDI techniques that have been verified for manufacture acceptance.

b. Delamination and scratches: The initial defect/damage size assumptions can be selected from Table 4.5.

- ② Service damage size assumption: Service damage refers to visibly detectable damage caused by high-energy impacts with foreign objects such as bird impacts or lighting strikes. The size assumption for this kind of damage should be determined and analyzed supported by testing.

## (2) Residual strength requirements

The structural residual strength should meet the following requirements:

- ① Initial defect-contained structures: The requirement for residual strength of composite structures containing initial defects is specified in the section above and is the same as those for metal structures, i.e., the ability to stand a maximum load occurring over 20 life cycles. If the load is smaller than the limit load, the residual strength should meet the requirements of the retaining load. If this load is larger than the limit load, it will not be restricted by 1.2 times the maximum load occurring over the structure life. This requirement is different from that of metal structures.
- ② Service defect-contained structures: The requirements are the same as those of metal structures.

## (3) Damage propagation requirements

Usually, composite structures are considered as slow-growing “crack” structures. No damage propagation models are currently used. In general, the absence of damage propagation should be verified by analysis supported by testing. Fatigue tests of small parts, elements, or substructural components may be used. Cycle numbers of zero damage propagation should consider the dispersion of the composite fatigue data and environmental effects. If structures designed with no consideration of damage propagation show obvious defects or damage at inspection intervals, the component should be re-designed.

**Table 4.5** Initial defect assumption

Defect/damage	Defect/damage dimensions
Scratch	Surface scratch of 100 mm in length, 0.50 mm in depth
Delamination	Delaminated area equal to a circle 50 mm in diameter

### 4.2.3 Requirements for Civil Aircraft Structure Design

The requirements for military aircraft structure design are generally suitable for civil aircraft with the following differences.

#### 4.2.3.1 Advisory Circular AC 20-107A “Composite Structure”

Some items involved in AC 20-107A “Composite Structure” are given below. (The following has been simplified, the reader can refer to the original.)

5.d Impact damage is generally accommodated by limiting the design strain level.

6.g It should be shown that impact damage that can be realistically expected from manufacturing and service (but not more than the established threshold of detectability) for the selected inspection procedure will not reduce the structural strength below ultimate load capability.

7. Verification of structure fatigue/damage tolerance: The evaluation of composite structure should be based on the applicable requirements of FAR 23.571, 23.572, 25.571, 27.571, and 29.571. The following considerations are unique to the use of composite material systems and should be observed for the method of substantiation selected by the applicant. When selecting the damage tolerance or safe life approach, attention should be given to geometry, inspectability, good design practice, and the type of damage/degradation of the structure under consideration.

(1) Damage tolerance (fail-safe) evaluation.

- ① Structural details, elements, and subcomponents of critical structural areas should be tested under repeated loads to define the sensitivity of the structure to damage growth.
- ② The extent of initially detectable damage should be established and be consistent with the inspection techniques employed during manufacture and in service. Flaw/damage growth data should be obtained by repeated load cycling of intrinsic flaws or mechanically introduced damage.
- ③ The extent of damage for residual strength assessments should be established. Residual strength evaluation by component or sub-component testing or by analysis supported by test evidence should be performed considering that damage.
- ④ An inspection program should be developed consisting of frequency, extent, and methods of inspection for inclusion in the maintenance plan.
- ⑤ The structure should be able to withstand static loads (considered as ultimate loads) which are reasonably expected during a completion of the flight on which damage resulting from obvious discrete sources occurs (i.e., uncontained engine failures).

- ⑥ The effects of temperature, humidity, and other environmental factors which may result in material property degradation should be addressed in the damage tolerance evaluation.
- (2) Fatigue (safe-life) evaluation fatigue substantiation should be accomplished by component fatigue tests or by analysis supported by test evidence, accounting for the effects of the appropriate environment. The test articles should be fabricated and assembled in accordance with production specifications and processes so that the test articles are representative of production structure. Sufficient component, subcomponent, element, or coupon tests should be performed to establish the fatigue scatter and the environmental effects.

#### **4.2.3.2 Differences from Military Aircraft Requirement**

##### **(1) Residual strength level**

For civil aircraft structures with defects and damage that have not been detected during manufacture and in service, the structure should be able to withstand the ultimate load in its expected life, without any effects on its operation function. For military aircraft structures, the requirement is lower; the load to be withstood will be the maximum internal element load occurring once in 20 life cycles of undetectable structures [1–5].

##### **(2) Initial defect dimension assumptions**

For military aircraft, the impact damage dimension is clearly specified, either as the maximum impact energy (136 J for thicker panels), or by the defined dent depth detectability (deep dent in 1.5 mm for thin panels). For civil aircraft, there is no such specification, and it is defined only by the impact damage that can be realistically expected from manufacturing and service (but not more than the established threshold of detectability). Although a visual check is not specified for inspection, it is commonly used, and lighting should be considered. Some civil aircraft composite structures (such as the horizontal stabilizer box in the Boeing 7J7) have used the military aircraft initial defect dimension assumption. This is currently based on a statistical analysis, and a smaller initial defect size assumption has been adopted, i.e., 0.3–0.5 mm. A smaller impact energy cutoff value (36 J) has also been certified by the FAA.

##### **(3) Particular conditions for adhesive joint damage tolerance (with reference to military aircraft)**

If currently available manufacture technologies cannot ensure each adhesive joint can meet its designed strength, and NDI cannot detect debonding and weak adhering defects, one or two of the methods described below should be used to



verify the adherence of any joint regarded as a key safety flight element and any joints that have a load-bearing ability not lower than their design limit load:

- ① Use analysis, testing or both to determine the maximum acceptable debonding area of each joint under the load in the most serious case. The detailed design should avoid the possibility of debonding over a greater area.
- ② Proof testing should be performed for each end product, i.e., the largest potential load should be applied to each key adhered joint.

#### 4.2.3.3 AC20-107A Conformity Requirements

##### (1) Static strength [1–6]

- ① The impact damage possibly occurring during manufacture and in service should be considered as inherent damage of the structure to be assessed. It is necessary to consider locations where a tool box or repair tool may drop and impact.
- ② Evaluation of the static strength should include the expected critical failure areas, the corresponding failure mode, and the strain level. If the failure modes under the expected different environmental conditions (such as R.M. Dried and hot/wet) have the same probability of occurring, these two ambient conditions are both needed for verification, or one case should be eliminated from the design, without implementing verification.
- ③ Special attention should be paid to out-of-plane loads caused by design elements such as local thickening, which could induce early damage.

Figure 4.1 shows a flowchart of composite structure static strength verification, in which the items in brackets are cited from AC 29-107A.

##### (2) Damage tolerance

In establishing structure verification plans, the damage tolerance requirements of FAR AC25.471 and Item 7(a) in AC20-107A should be considered. Figure 4.2 is a flowchart for composite aircraft structure damage tolerance evaluation, in which the items in brackets are cited from AC 29-107A.

For example, the following aspects should be verified:

- ① Accidental damage (Failure-Safety) evaluation: Serious accidental damage (Failure-Safety) evaluation should be performed. The primary structural components or part of primary structure components should be cut off to verify that the other structures can withstand design load limits.
- ② Check intervals: By following the intervals defined by 7.a(4) in AC20-107A, the possibility of a missed inspection should be considered in the regular damage inspection.

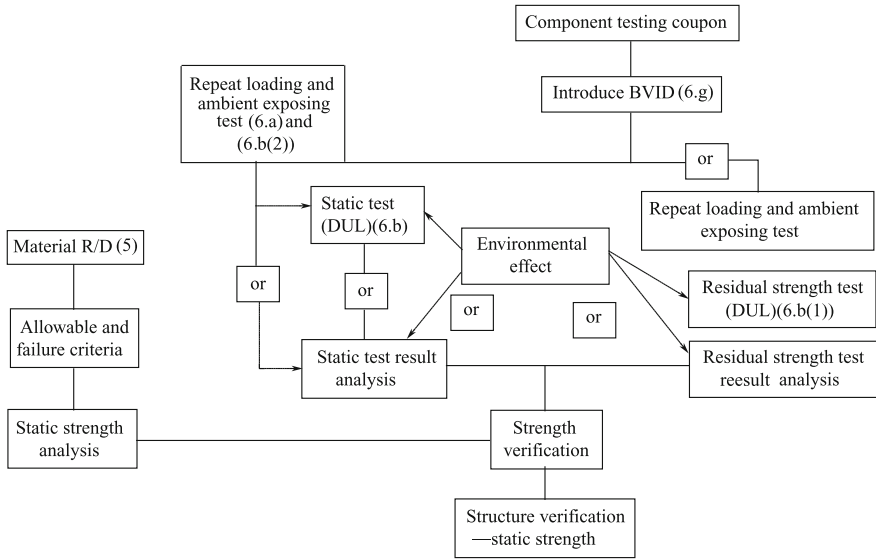


Fig. 4.1 Flowchart of composite structure static strength verification

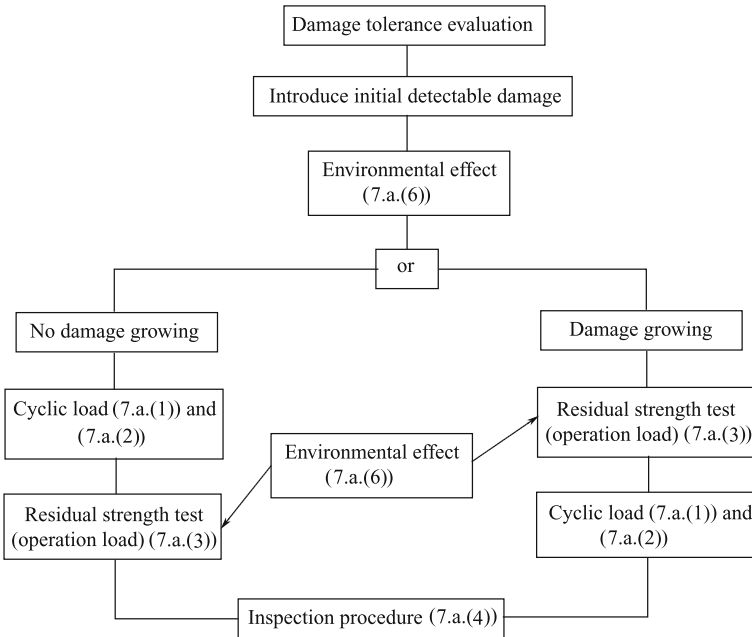


Fig. 4.2 Flowchart of composite structure damage tolerance verification

- ③ The load spectrum and load removal method as well as all other aspects related to damage tolerance evaluation should be written into testing programs, and submitted for FAA certification.
- ④ The B-allowable repeated load verification on flight safety redundant structures as well as the single-load transferring route structures should have Failure-Safety capacity. Here, the Failure-Safety capacity refers to the capacity to withstanding the designed limit load after a major part of a single-load transferring route structure is damaged.
- ⑤ Ice hail impact should be included in damage analysis items.

### **4.3 Material Selection in Structure Design and Structural Processing**

#### ***4.3.1 Principles of Structural Material Selection***

##### **4.3.1.1 General Principles**

- ① We should prefer materials with adequately characterized performance, service experience, and reliable supply sources as much as possible. If a new material that has been used in structures, is selected, it should pass “building block approach” verification including element, typical component, and structural assemble tests, according to the structure production [2].
- ② Similar to metal materials, we should select cheap materials when possible if structural integrity can be satisfied. The cost assessment should cover the following aspects: material cost, processing cost (consider processing feasibility, processing temperature and pressure, as well as the requirement for auxiliary materials) and maintenance costs.
- ③ Materials should have good processing ability. Consider processes such as curing, machining, and repair. Processing and curing performances include: resin viscosity, tack and drape, curing method, temperature and pressure, pressure applying window, shelf life, and flow ability.
- ④ Materials should meet the requirements of the service environment and mechanical properties of structures, including:
  - (a) The service temperature should be higher than the maximum operation temperature of the structure. Under most ambient operation environments (hot/wet), the mechanical performance cannot obviously decrease, and should remain stable in long-term service.
  - (b) Can resist impacts, including impact damage resistance, as well as the residual strength after defect/damage.

- (c) Open-hole tensile and compression strength, and joining bearing strength.
  - (d) Fuel resistance, anti-medium, aging resistance, sand abrasion, and rain corrosion proof.
- ⑤ Materials should meet some special requirement in certain structures.
- (a) Requirements for electromagnetic performances such as electromagnetic shielding, overlap resistance.
  - (b) Requirements as fire retardants, smoke and toxic release behaviors.
  - (c) Good compatibility with related materials.
  - (d) Low input to ensure environment protection.

In general, it is necessary to select resins and fibers of different types and grades to meet the requirements of different applications and structures, even at different locations within the same structure. This allows materials to be utilized to their full potential to reduce costs. Avoid over estimation of the temperature and toughness, which may increase the material and production costs.

#### 4.3.1.2 Property Data Sources

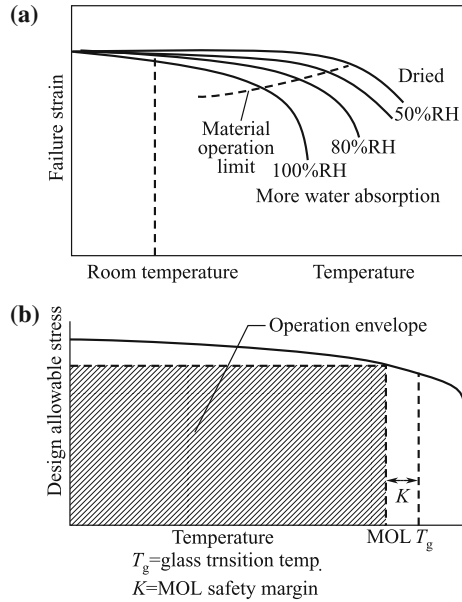
Data sources for mechanical properties of composite materials system and sandwich composite should be authorized and approved for design purposes. The adopted data should meet the following requirements:

- ① Performance characterization based on statistics should be used to establish design data.
- ② All factors affecting the required strength, stiffness, and reliability should be adequately considered in performance characterization, especially the combined action of moisture and high temperature, as well as the effect of defects/damage possibly occurring during manufacture or in service (mainly open hole and low-speed impact).

#### 4.3.1.3 Evaluation of Replacement Materials

- ① Before using replacement materials in production, an evaluation of the equivalence of the replacement and original materials should be performed in accordance with related standards, to ensure no harmful effects on structural performance.
- ② Changes in the original material constituents, material formula, elimination of a processing step, use of alternate processing equipment, or other procedure change should be considered as a major modification, and properties of the new material should be re-evaluated. The necessary evaluation of the effects of changes should be performed in accordance with related standards, to ensure no harmful effects on the structural performance.

**Fig. 4.3** Material selection criterion after considering the effect of hot/wet ambient conditions. **a** Temperature/wetness effect on the matrix-dominated failure; **b** Material selection criterion



### 4.3.2 Environmental Effects of Material Performances

The properties of composite materials are resin matrix-dominated and sensitive to ambient conditions. To reduce environmental problems in a verification program as much as possible, it is necessary to consider environmental effects in the material selection phase of structure design. The materials selection should be performed based on the relationship between the aircraft hot/wet envelope and the material’s maximum operation temperature or material operation limit (MOL). The material’s maximum operation temperature can be defined as shown in Fig. 4.3. The gray area indicates the material operation envelope, in which the aircraft operates.

The envelope helps guide the selection of materials that can be used under typical normal conditions, and environment issues in the verification program to be reduced. The difference  $K$  between the glass transition temperature  $T_g$  under the maximum moisture absorption conditions and MOL is defined as the basis for the determination of the maximum operation temperature. The determination of a  $K$  is related to design considerations. For an epoxy resin matrix, the  $K$  value will be no less than 30 °C.

### 4.3.3 Selection and Use of Matrices and Fibers

Resin matrices have an important influence on mechanical properties of composites. The transverse performance, compression, and shear properties are all resin

**Table 4.6** Comparison of commonly used resin matrices and their performance

Performance	Resin				
	Epoxy	Phenolic	BMI	Polyimide	High performance thermoplastics
Processing ability	Excellent	Good	Good	Bad	Good
Mechanical property	Excellent	Medium	Excellent	Good	Excellent
Heat resistance (°C)	Below 130	Below 177	Below 230	Above 288	Above 120
Toughness	Good	Bad	Good	Bad	Excellent
Dimension stability	Excellent	Excellent	Excellent	Excellent	Excellent
Cost	Low	Low	Medium	High	High

dependent. Toughened resin can improve the damage resistance of a composite, and absorb energy simultaneously.

Composite performances such as heat resistance, aging resistance, fire retardant, hot/wet behavior, anti-corrosion, and electromagnet performance are mainly determined by the resin matrix.

Composite processing abilities such as rheological properties, tack and drape, gel time, prepreg shelf stability, processing temperature, pressure, and time are also directly dominated by the resin matrix. Common requirements of advanced composite resin matrices are: high strength, good toughness, medium-proofing, low processing temperature and pressure, long prepreg shelf life, a wide applied pressure window, low cured shrinkage, low toxicity, and suitability for prepreg solution or melting preparations. The performances of commonly available resin matrices are given in Table 4.6.

Reinforcing fibers offer composites with high strength and moduli and can also greatly increase damage resistance. Fiber selection should be optimized through a combined evaluation of performance and cost. Table 4.7 lists some aspects to consider for fiber selection. Table 4.8 includes data on environmental effects on the materials.

### 4.3.4 Structural Processing Ability

Structural processing ability includes the ability to use cure processing and assembling processing methods. Different processing methods have different requirements and different structural processing capabilities. Critical issues in considering structural processing capability will vary depending on the structure, so it is important to select a proper curing processing method during design. The curing process of a composite structure can be simultaneously completed with the

**Table 4.7** Evaluation of different fibers

Criterion	Powering factor 1–3	Nominated value for different fiber powering		
		Carbon fiber	Kevlar	E-glass-fiber
Tensile strength	3	9	9	9
Compression strength	2	6	0	4
Modulus	3	9	6	3
Long-term performance	3	9	6	3
Fatigue properties	2	6	4	2
Density	2	4	6	2
Alkali proof	2	6	4	0
Price	3	6	6	9
Total		55	41	32

**Table 4.8** Ambient powering factor of materials

Performance	Materials			
	Steel	Kevlar fiber composite	Carbon fiber composite	Glass-fiber composite
Relaxation and creep	3	1	3	2
Wet resistance	2	2	3	1
Alkali proof	3	2	3	1
Thermal stability	2	2	3	1
Salt water resistance	1	2	3	2
Fatigue behavior	1	3	3	2
Total	13	12	18	8

*Note* power factor (3, very good; 2, good; 1, meets requirements; 0, cannot meet requirements)

material processing. Hence, the design of the structure and its processing are linked. Structure design should consider the feasibility of processing methods, particularly for integrated part processing.

**4.3.4.1 Principles of Processing Method Selection**

The feasibility of processing methods should be considered in the structure design phase, to determine the structure processing capability. Principles for processing method selection include the following:

- ① The selected processing method should be able to ensure the structure performance can satisfy design standards and that the fitting accuracy meets the assembly requirements.
- ② Equipment requirements should be satisfied, including currently used and new added equipment. Autoclave size, in particular, should be considered.

- ③ The cost over the lifetime of the component should be considered, including the production continuity, end product rate, and maintenance.
- ④ Processing methods with the greatest level of operation experience should be prioritized.

#### 4.3.4.2 Typical Structure Processing Methods

- ① Autoclave processing is mainly selected for panel structures but liquid resin molding (LCM) processes, such as RTM and RFI, are also widely applied.
- ② Sandwich structures mainly use vacuum bag and pressure bag methods.
- ③ Cylinder structures use filament winding (FW).
- ④ Co-curing, secondary curing or secondary adhering is suitable for integrated part manufacturing.

### 4.4 Structure Design—Determination of Design Allowables

#### 4.4.1 Allowables and Design Allowables

Allowables are mainly used to characterize material performance and are defined as characteristic values of material performance, with a certain confidence and reliability, determined by statistical analysis of coupon testing data under certain loads and environmental conditions. Design allowables are mainly used in structural design. These are defined as the design limits determined on the basis of material allowables and the testing results of typical coupons, elements, and structures. These allowable may be determined for project requirements and structure integrity, and also based on previous design and operation experiences. Designers should follow requirements for structural integrity, such as static strength, stiffness, durability, and damage tolerance to specify design allowables. The design allowables of a composite system are commonly expressed as strain values. The components are subject to the testing verification performed on subcomponents and full-size scale parts, to guarantee that structures designed by following the design allowables can meet these requirements [1, 2].

Material allowables are characteristic mechanical properties of material systems, and mainly used for material selection, acceptance, and equivalence evaluation. These values are usually not directly used in design except for the modulus, which needs detailed analysis of open hole, delamination, and impact damage in analytical models. When performing structural strength verification, design allowables should be used rather than material allowables.



#### 4.4.2 *General Principles for Design Allowables Determination*

To determine design allowables, the following principles should be followed:

- ① The tensile design allowables of skin structures should mainly derive from test results on hole-contained specimens with typical structural laminating code. The compression design allowables of skin structures should mainly derive from the testing results of impact damage containing and filled hole-containing specimens with typical structural laminating code.
- ② For thin skin or surface honeycomb sandwich structures, the determination of design allowables should account for buckling effects. If the design allowables mainly depend on buckling effects, the additional coefficient (less than 1) of impact damage effect should be taken into account.
- ③ The mechanical fastener bearing design allowables should derive from the bearing strength allowables of single pin specimens and should consider the effects of the degree of importance, structural features, load type, durability, and operation environment.
- ④ The design allowables of important joints, and details should derive from test results of corresponding typical structures, or from practically verified past experiences.
- ⑤ Combinations of extreme environmental conditions should be considered for design allowables of composite structures.

#### 4.4.3 *Current Status*

On the basis of documents available from aircraft companies, for current carbon fiber resin matrix composites, the allowable strain values under the designed ultimate loads are as follows:

Compression  $[\varepsilon_c] = 4000 \mu\varepsilon$ ; tensile  $[\varepsilon_t] = 5500 \mu\varepsilon$ ; Shear  $[\gamma] = 7600 \mu\varepsilon$ .

Table 4.9 indicates some design allowables of current aircraft structures for reference.

#### 4.4.4 *Approach to Increasing Design Allowables*

Currently used design allowables have been lowered, to further reduce weight and fully utilize the high specific strength and specific stiffness of composite materials [7].

In aircraft primary structures, it is necessary to increase the structural design allowables, especially the compression design allowables. This approach can be summarized as:

**Table 4.9** Part of design allowables of current aircraft structures

Co.	Structure component	Material	T. design		C. design	
			Uni.	Fabric	Uni.	Fabric
Lockheed	L-1011 vertical stabilizer	T300/5208	4500	3900	4000	4000
Boeing	B727 horizontal stabilizer	T300/5208			4000	
Boeing	B1 horizontal stabilizer	AS/3501			3600	
M.D.	F18A/B wing	AS4/3501-6	4000		4000	
M.D.	AV-8B wing	AS4/3501-6	4000		4000	
BAe	Stabilizer	XAS/914C	4500	3530	3900	2830
MBB	A310 vertical stabilizer	T300/913C	2800		2800	
MBB	A320 vertical stabilizer	T300/913C	3200		3200	
DA	TORNADO main cabin door	T800/5245	5500		4200	

### (1) Increase the damage tolerance of the composite system

The design allowables of composite structures mainly depend on the properties of the composite that can meet requirements for structural damage tolerance. Attention should be paid to the ability of composites to resist impact damage (damage resistance), which is different to the physical damage tolerance of composites. Damage resistance refers to the ability of a component to resist an impact event, while damage tolerance refers to the effect of a certain damage state on the performance of the structure. In the past, the compression strength of standard specimen impacted by 6.7 J/mm (denoted as CAI) was used to evaluate composite damage tolerance. Some studies have shown that this method can give conflicting results. Hence, in recent years, the compression strength after impact by several energy levels is evaluated. Alternatively the compression strength of a standard specimen can be evaluated after impact and induction of a 1-mm dent. The relevant evaluation methods for composite impact resistance can be seen in Sect. 4.9 of this chapter.

### (2) Increase the damage tolerance of the structure through design

This approach includes the application of soften and harden bands, soft skin and stiffened plates with mechanical fasteners.

### (3) Modify the damage tolerance requirements

Currently used damage tolerance requirements have strict specifications for initial defect dimensions, especially for military aircraft structures. If these specifications can be guaranteed, i.e., supported by extensive studies on manufacture and operation in an ambient environment, or by taking effective measures, the specifications can be decreased, and the design allowables can be increased. For civil aircraft, the

design allowables could be increased based on statistical data of processing composite structures and the use of a lower impact energy threshold, such as 35 J.

## **4.5 Building Block Approach for Composite Structure Design Verification**

### ***4.5.1 Introduction and Philosophy***

Owing to the lack of effective analysis and extensive design and use the experience of composite structures the structural integrity needs to be ensured in some way [1–3]. The BBA consists of multiple level testing and certification, at the level of coupons, structural elements, subcomponents, components, and finally a complete full-scale product. This approach is used to solve (and certify) challenging issues such as environmental effects and damage. This approach can also reduce the complexity of full-size tests, qualify the safety of cost reduction measures, and ensure a pass on full-size verification.

For widely used composite/metal structures, the BBA verification approach can also be applied for testing below the substructure component level, and used to complement verification of composite durability and damage tolerance.

For the static strength verification tests of full-size parts, it is difficult to simulate a full range of combined ambient effects, thus the verification may not be fully comprehensive. However, the overall integration can be guaranteed for composite structure static verification, if a BBA verification test program is properly organized.

On the basis of the maturity of materials and design, and the accumulation of experience, the testing content and coupon numbers may be reduced to decrease development costs.

The application of the BBA has not yet been standardized. Relationships between numbers of specimens and material bases values are well defined for specimen tests at the lowest level (see part 15), the numbers of specimens required at higher levels of complexity are somewhat arbitrary and largely based on historical experience, structural criticality, engineering judgment, and economic considerations. Thus, there is currently no standardized methodology for statistically validating each level of the process, although some attempts have been made to develop models that relate specimen quantities to overall reliability.

The sensitivity to out-of-plane loads, failure mode multiplicity, sensitivity to ambient operation conditions, and the absence of mature and reliable analysis for comparing composite and metal structures, motivate the use BBA for structural certification of composite structures [1–3].

The multiplicity of potential failure modes is perhaps the main reason that the BBA is essential for the development of composite structural substantiation. The

many failure modes in composite structures are mainly caused by defects, environmental effects, and out-of-plane sensitivities of the materials.

### 4.5.2 General Procedures for BBA Implementation

Figure 4.4 shows the building block integration. BBA analysis/testing verification is generally divided into five steps described as follows [3]:

- ① Coupon: Small dimension test specimens used for the evaluation of laminar and laminate performances, as well as general structural characteristics. Test specimens including commonly used laminate strips, and adhered or mechanically joined strip joints, may be used to gain material allowables. This approach is also used for evaluation of material notch sensitivity, ambient effects, and specimen failure modes. At this level, the number of specimens is usually large, sometimes on the order of thousands.
- ② Element: Includes elements and typical structures, i.e., typical load-bearing units in complex configuration structures, such as skin,

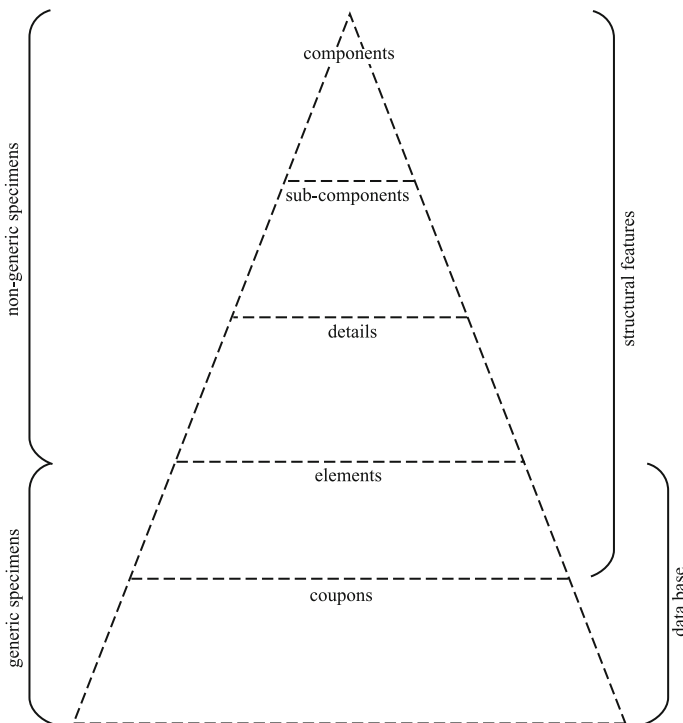


**Fig. 4.4** Pyramid of tests

spars, shear panels, laminate and varied joints. Elements also include weaker components in complex configuration structures such as specially designed complex configuration joints, mechanical fasteners, stranger ends, and large inspection ports. The purpose is to verify the load-bearing ability, failure modes, environmental effects, and analysis methods for a variety of elements. Design allowables will be generated at this testing level on the basis of the material allowables, with a large number of specimens on the order of hundreds.

- ③ Subcomponent: Large 3-dimensional structures that feature all the properties of an integral structure section, such as a box segment, frame segment, wing panel, fuselage panel, wing rib, cabin sector, or frame. These features all represent a typical section of an integral structure and their load-bearing ability, environmental effects, damage tolerance, durability, and analytical methods can be verified. The determination of design allowables is also generated at this testing level. Fewer specimens are used at this level, usually of the order of tens, but occasional hundreds.
- ④ Component: Refers to the main structural section of a wing, fuselage, vertical tail, and horizontal stabilizer, which can be used as an integral aircraft body structure in verification tests. A small number of specimens will be used at this level, usually one or more. Considering current application status, verification of structural integrity can be performed at this level.
- ⑤ Full-size scale: At this level, full-size scale aircraft structures are used for analysis and verification and full-size scale static and fatigue tests should be performed to verify structural integrity and the internal load distribution, deflection, and entire structure failure modes predicted by finite element analysis (FEA). The requirements for full-size tests should be proposed by the customer, verification agency, or by the airworthiness certification body, based on safety and durability requirements. The numbers of specimens at this level is usually one or two. For metal/composite combined structures, the main purpose of verification at this level is to verify the metal structure. Full-size tests can also include testing content at the component level, which may overlap with lower levels.

The BBA has been accepted by all composite designers and manufacturers globally; however, different individuals may use different procedures. On the basis of the different tasks, verification levels, and test items, the numbers of specimens may change. Furthermore, the testing sequence may change or overlap. For example, testing and analysis at the element or subcomponent levels should be performed in advance, to gain knowledge of potential risks as soon as possible. In this sense, the current BBA/verification approaches are not yet fully standardized or documented and certain flexibility is allowed in practical use.

### 4.5.3 Boeing 777 Aircraft Composite Primary Structure Building Block Approach

In Boeing 777, 9.9 t composites have been used to make up 11% of the total structural weight [3]. The horizontal and vertical stabilizers of Boeing 777 are all made of carbon fiber-reinforced composites. The horizontal tail is a main torque box main torque box structure consisting of two spar and multi-rib construction. The BBA for Boeing airplane primary structures (Fig. 4.5) include the following tests.

- (1) Specimens and elements;
- (2) Subcomponents (Table 4.10);
- (3) Components;
- (4) 777 Pre-production horizontal stabilizer test (Table 4.11);
- (5) Stabilizer root attachment test;
- (6) 777 Horizontal stabilizer tests;
- (7) 777 Vertical stabilizer test.

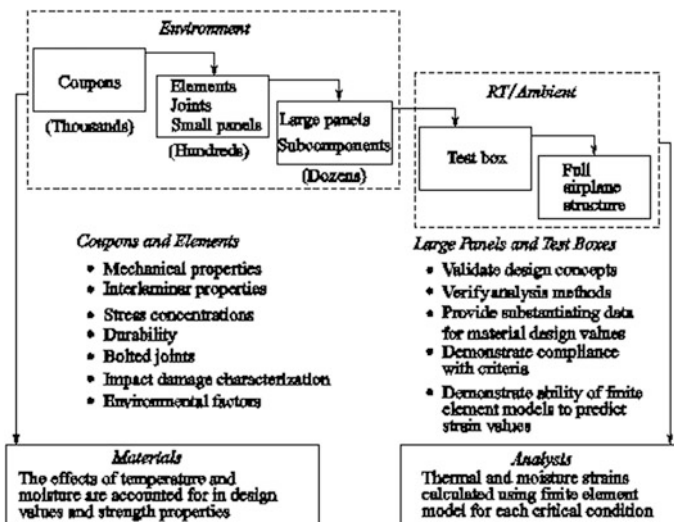


Fig. 4.5 Building block approach for commercial aircraft primary structure

**Table 4.10** Summary of subcomponent tests for 777 empennage

Test type	Number of tests
Bolted joints (major splices)	110
Rib details	90
Spar chord crippling	50
Skin/stringer compression panels	26
Skin/stringer tension panels	4
Skin/stringer shear/compression	6
Skin/stringer repair panels	6
Skin splice panels	2
Stringer runouts	4
Spar shear beams	6
Total	305

**Table 4.11** Pre-production test box load and damage sequence

Test sequence	Damage types and test loadings
1	Perform all small (BVID) damages
2	Design limit load static strain survey
3	One lifetime fatigue spectrum, 50,000 flights, including 1.15 LEF (Load Enhancement Factor)
4	Design limit load static strain survey
5	One lifetime fatigue spectrum, 50,000 flights, including 1.15 LEF
6	Design limit load static strain survey
7	Design ultimate (select cases) load static strain survey
8	Two (C) check fatigue spectrum (8000 flights) with small and visible damages, including 1.15 LEF
9	“Fail-safe” test; 100% design limit load static strain survey with small and visible damage
10	“Continued safe flight $\pm$ loads test”: 70% design limit load static strain survey with small, visible, and element damages
11	Visible and element damages repaired. Design ultimate load static strain survey
12	Destruction test. Strain survey up to destruction

## 4.6 Structural Design and Strength and Stiffness Analysis

### 4.6.1 Composite Structure Design Concepts

To reduce structural weight and to meet load-bearing requirements, most aircraft bodies are designed as a thin-wall construction consisting of several curved planar thin-wall structures. Traditional metal aircraft frames have a thin-wall construction

consisting of a large number of thin-wall components such as skin, beam, stringer, and rib (frame) joined by a large number of mechanical fasteners.

Fiber composites are a kind of artificial structural material. The main advantage of this material is its very high specific strength and stiffness along the fiber direction, which offers great potential for structural weight reduction. Composites also have very different processing techniques from metal materials. Most thin plane structures must withstand in-plane loads, and composites are typically used as laminates or laminated structures in aircraft structures. Laminated composites can offer advantages such as high specific strength and specific stiffness, tailorable properties, and easy processing. On the other hand, composites also have some drawbacks such as low interlaminar strength, stress concentration at open holes, and the occurrence of electrochemical corrosion at composite/aluminum joints. The design concepts used for composite structures are different from those of traditional metal structures. Composite materials are better suited to innovative design concepts.

## 4.6.2 *Laminate Design and Analysis*

### 4.6.2.1 **Ply Design Guidelines**

After the determination of laminate total thickness and its local variation based on the application requirements, ply laminate design should be performed [2, 3, 11, 13]. This step will mainly involve:

- ① Selection of proper ply angles;
- ② Determination of the ply ratio at different angles;
- ③ Provision of proper laminating stacking sequence (LSS).

In addition, ply design also includes local ply alternation, such as the ply design in connecting zones and at the edges of open hole, as well as the ply transitions for sudden changes in the thickness of the structure. It may be said that ply design is one of main factors influencing the characteristics of composite materials. Rational design will directly affect the composite structural strength, stiffness, stability, and other important properties such as delamination, damage, failure, and dimensional stability, as well as processing performance. These factors have direct implications for load-carrying capacity and operation functions. The critical issues of laminate ply design are as follows:

- (1) A LSS is said to be homogeneous if the ply angles are evenly distributed throughout the laminate thickness. Homogeneous LSS is recommended for strength controlled designs.
- (2) A laminate is considered to be symmetric if the plies and property parameters are symmetrical to the mid-plane. A balanced laminate is defined as having equal numbers of  $+\theta$  and  $-\theta$  plies, where  $\theta$  is measured from the primary



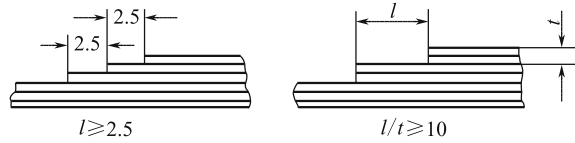
load direction. A laminate having both balanced and symmetrical plies is referred to as balanced and symmetric. If possible, laminates should be balanced and symmetric about the mid-plane to avoid warpage caused by couplings. If this is not possible due to other requirements, locate the asymmetry or imbalance as near to the laminate mid-plane as possible.

- (3) A LSS should have at least four distinct ply angles (e.g.,  $0^\circ$ ,  $90^\circ$ ,  $\pm 45^\circ$ ) with a minimum of 10% of the plies oriented at each angle.
- (4) Minimize groupings of plies with the same orientation. For tape plies, stack no more than four plies of the same orientation together (i.e., limit stacked ply group thicknesses 0.03 in. (0.8 mm). In addition, stacked ply group thicknesses with orientations perpendicular to a free edge should be limited to 0.015 in. (0.38 mm) to avoid delamination, matrix cracking, and shear-out failure in bolted joints.
- (5) The ply orientation should be consistent with the primary load direction. That is,  $0^\circ$  ply should be preferentially used for laminates that are primarily subjected to tensile or compressive loads. For the laminates primarily under shear load, ply with  $\pm 45^\circ$  is preferred. In addition, the plies for primary load transmission should not be placed on outer surfaces.
- (6) For ply design in joint zones, the ratio of the ply in  $\pm 45^\circ$  against the pin load direction should not be less than 40%. The ply ratio in the direction consistent with the pin load should be greater than 25%, to ensure enough shear strength and bearing strength in the joint zone, and reduce stress concentration.
- (7) For the laminates subject to buckling as a critical condition, the outer surface should be a feature  $\pm 45^\circ$  plies. To enhance impact resistance, hybrid composite layers should be used such as aromatic or glass-fiber plies.
- (8) The  $\pm\theta$  plies should be placed as close to each other as possible to reduce bending/twisting coupling and avoid the negative effects on the effective stiffness and stability. However, separation of  $\pm\theta$  plies can offer the benefits in terms of reducing interlaminar stress.
- (9) Attention should be paid to avoid the high interlaminar stress ( $\sigma_z$ ) that may occur at the free edges of laminates. The stacking sequence should be properly selected to reduce the delaminating stress and strain levels at free edges.
- (10) Mismatch of the Poisson's ratio between two laminates co-cured or adhered together should be reduced as much as possible. Otherwise, delamination and/or debonding can easily take place. The following equation is recommended for assessing this risk:

$$|v_{xy}(\text{laminat e 1}) - v_{xy}(\text{laminat e 2})| < 0.1$$

- (11) Usually, ply decreasing is used to realize laminate thickness alternation. The step length of each ply transition zone should not be less than 2.5 mm, or be followed by  $l/t > 10$  to realize a ply decrease, as illustrated in Fig. 4.6. In general, there should be no more than two ply numbers simultaneously decreasing and no ply decreasing is allowed on the width direction of a raised

**Fig. 4.6** Requirements for ply decreases



flange of a beam, frame, or rib of skin. It is specified that certain continuous plies should be used on laminate surfaces to avoid ply tear-off.

Ply splicing is allowed in the direction parallel to the applied load but not permitted in the load vertical direction. The splicing gap should be less than 2 mm, with no overlap. The spliced plies should be separated by four other layers, if less than four layers are applied the intersplicing width should be at least 15 mm, to reduce weak laminating.

The above-mentioned guidelines for ply design cannot always be completely achieved and are sometimes even conflict with the principal needs of satisfying the primary load-bearing and operation functions requirements.

**4.6.2.2 Laminate Stiffness Analysis**

Laminate stiffness is not only dependent on its thickness, but also related to its constituent lamina and their stacking sequence. The stiffness of laminate can be calculated by classical laminate theory [8–10, 12].

**(1) Lamina on-axis and off-axis stiffness**

Lamina on-axis stiffness (also known as on-axis modulus) refers to the lamina stiffness along the fiber direction (1). The matrix for laminar on-axis stress–strain is given as:

$$\begin{Bmatrix} \varepsilon_1 \\ \varepsilon_2 \\ \gamma_{12} \end{Bmatrix} = \begin{bmatrix} \frac{1}{E_1} & -\frac{\nu_2}{E_2} & 0 \\ -\frac{\nu_1}{E_1} & \frac{1}{E_2} & 0 \\ 0 & 0 & \frac{1}{G_{12}} \end{bmatrix} \begin{Bmatrix} \sigma_1 \\ \sigma_2 \\ \tau_{12} \end{Bmatrix} \tag{4.1}$$

where  $\varepsilon_1, \varepsilon_2, \gamma_{12}$  are on-axis strains;  $\sigma_1, \sigma_2, \tau_{12}$  are on-axis stresses;  $E_1, E_2, \nu_1, G_{12}$  are the four independent stiffness coefficients;

$$\frac{\nu_1}{E_1} = \frac{\nu_2}{E_2}$$

From the lamina on-axis stiffness matrix expression, then:

$$\begin{Bmatrix} \sigma_1 \\ \sigma_2 \\ \tau_{12} \end{Bmatrix} = \begin{bmatrix} Q_{11} & Q_{12} & 0 \\ Q_{21} & Q_{22} & 0 \\ 0 & 0 & Q_{66} \end{bmatrix} \begin{Bmatrix} \varepsilon_1 \\ \varepsilon_2 \\ \gamma_{12} \end{Bmatrix} \tag{4.2}$$

where  $Q_{11}$ ,  $Q_{22}$ ,  $Q_{12}$ ,  $Q_{21}$ , and  $Q_{66}$  are the lamina on-axis stiffness coefficients:

$$Q_{11} = mE_1$$

$$Q_{22} = mE_2$$

$$Q_{12} = Q_{21} = mvE_1 = mv_1E_2, v_1/v_2 = E_1/E_2$$

$$M = 1/(1 - v_1v_2)$$

$$Q_{66} = G_{12}$$

$$Q_{16} = Q_{26} = Q_{61} = Q_{62} = 0$$

Lamina off-axis stiffness (also known as the off-axis modulus) refers to the lamina stiffness along the direction forming an angle  $\theta$  with the fiber direction. The off-axis stiffness of a lamina at angle  $\theta$  can be expressed by the matrix:

$$[\bar{Q}] = \begin{bmatrix} \bar{Q}_{11} & \bar{Q}_{12} & \bar{Q}_{16} \\ \bar{Q}_{21} & \bar{Q}_{22} & \bar{Q}_{26} \\ \bar{Q}_{61} & \bar{Q}_{62} & \bar{Q}_{66} \end{bmatrix} \tag{4.3}$$

where  $\bar{Q}_{11}$ ,  $\bar{Q}_{12}$ ,  $\bar{Q}_{22}$ ,  $\bar{Q}_{16}$ ,  $\bar{Q}_{26}$  and  $\bar{Q}_{66}$  are lamina off-axis stiffness coefficients.

$[\bar{Q}]$  is a symmetrical matrix, so that the off-axis stiffness coefficient  $\bar{Q}_{12} = \bar{Q}_{21}$ ;  $\bar{Q}_{16} = \bar{Q}_{61}$ ;  $\bar{Q}_{26} = \bar{Q}_{62}$ .

The conversion between the off-axis stiffness coefficient and the on-axis stiffness coefficient can be expressed by trigonometric functions of the off-axis angle as given in the table:

	$Q_{11}$	$Q_{22}$	$Q_{12}$	$Q_{66}$
$\bar{Q}_{11}$	$m^4$	$n^4$	$2m^2n^2$	$4m^2n^2$
$\bar{Q}_{22}$	$n^4$	$m^4$	$2m^2n^2$	$4m^2n^2$
$\bar{Q}_{12}$	$m^2n^2$	$m^2n^2$	$m^4 + n^4$	$-4m^2n^2$
$\bar{Q}_{66}$	$m^2n^2$	$m^2n^2$	$-2m^2n^2$	$(m^2 - n^2)^2$
$\bar{Q}_{16}$	$m^3n$	$-mn^3$	$mn^3 - m^3n$	$2(mn^3 - m^3n)$
$\bar{Q}_{26}$	$mn^3$	$-m^3n$	$m^3n - mn^3$	$2(m^3n - mn^3)$

where  $m = \cos\theta$ ,  $n = \sin\theta$ .

Note:

- ①  $\bar{Q}_{11}$  and  $\bar{Q}_{22}$  have an intermirror relationship, i.e.,  $\bar{Q}_{11}(\theta + 90^\circ) = \bar{Q}_{22}(\theta)$ .
- $\bar{Q}_{16}$  and  $\bar{Q}_{26}$  have an intermirror relationship, i.e.,  $\bar{Q}_{16}(\theta + 90^\circ) = -\bar{Q}_{26}(\theta)$ .

- ②  $\bar{Q}_{11}, \bar{Q}_{22}, \bar{Q}_{12},$  and  $\bar{Q}_{66}$  are even functions and thus independent of the polarity of the angle  $\theta$ ,  $\bar{Q}_{16}$  and  $\bar{Q}_{26}$  are odd functions, and thus dependent on the polarity of the angle  $\theta$ .
- ③  $\frac{\partial \bar{Q}_{11}}{\partial \theta} = 4\bar{Q}_{16}, \frac{\partial \bar{Q}_{22}}{\partial \theta} = 4\bar{Q}_{26}.$

Hence, only four of the six off-axis stiffness coefficients are independent.

Off-axis stiffness coefficients can also be expressed as a combination of the on-axis stiffness coefficients as listed in the table:

	1	$U_2$	$U_3$
$\bar{Q}_{11}$	$U_1$	$\cos 2\theta$	$\cos 4\theta$
$\bar{Q}_{22}$	$U_1$	$-\cos 2\theta$	$\cos 4\theta$
$\bar{Q}_{12}$	$U_4$		$-\cos 4\theta$
$\bar{Q}_{66}$	$U_5$		$-\cos 4\theta$
$\bar{Q}_{16}$		$\frac{1}{2} \sin 2\theta$	$\sin 4\theta$
$\bar{Q}_{26}$		$\frac{1}{2} \sin 2\theta$	$-\sin 4\theta$

The combination of on-axis stiffness coefficients in the table:

$$U_1 = \frac{1}{8}(3Q_{11} + 3Q_{22} + 2Q_{12} + 4Q_{66})$$

$$U_2 = \frac{1}{2}(Q_{11} - Q_{22})$$

$$U_3 = \frac{1}{8}(Q_{11} + Q_{22} - 2Q_{12} - 4Q_{66})$$

$$U_4 = \frac{1}{8}(Q_{11} + Q_{22} + 6Q_{12} - 4Q_{66})$$

$$U_5 = \frac{1}{8}(Q_{11} + Q_{22} - 2Q_{12} + 4Q_{66}) = \frac{1}{2}(U_1 - U_4)$$

From the lamina stiffness expression, it can be seen that the off-axis stiffness coefficient  $\bar{Q}_{ij}$  is a function of the off-axis angle  $\theta$ . Thus, the off-axis angle  $\theta$  can determine the lamina off-axis stiffness. In general, i.e., when  $\theta \neq 0^\circ$  or  $90^\circ$ , the lamina off-axis coupling stiffness coefficients  $\bar{Q}_{16}$  and  $\bar{Q}_{26}$  will not be zero. This means that tensile–shear coupling or compression–shear coupling will exist, as shown in Fig. 4.7.

The off-axis angle also refers to the ply laminating angle. The design the lamina off-axis stiffness based on the laminating angle is the main approach to tailoring laminate properties.

**Fig. 4.7** Schematic of unidirectional laminate off-axis tensile deformation ( $\bar{Q}_{16} \neq 0$ )

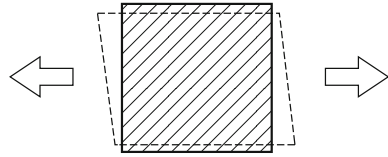


**Fig. 4.8** Laminate stiffness analysis model

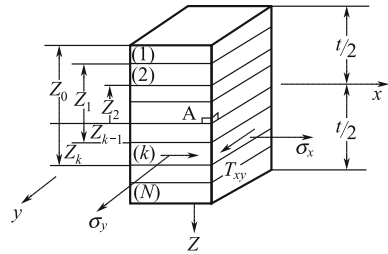


**Fig. 4.9** Resultant force on laminate

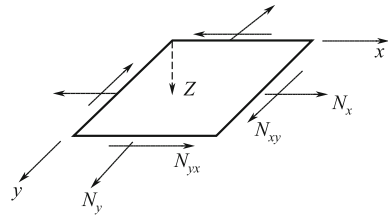
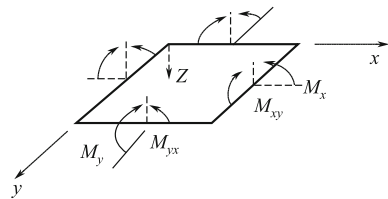


**Fig. 4.10** Resultant moment on laminate



**(2) Laminate stiffness analysis**

In the laminate stiffness analysis model, the mid-plane resultant force  $\{N\}$ , and mid-plane resultant moment  $\{M\}$  scheme are given in Figs. 4.8, 4.9 and 4.10.

In the analysis, the lamina is assumed to be a homogeneous material, and their properties can be determined from unidirectional composite testing.

On the basis of classical laminate theory, the physical equation of laminate can be expressed as:

$$\begin{Bmatrix} N \\ M \end{Bmatrix} = \begin{bmatrix} A & B \\ B & D \end{bmatrix} \begin{Bmatrix} \varepsilon^0 \\ k \end{Bmatrix} \tag{4.4}$$

where

- $\{N\}$  laminate mid-plane resultant force array;
- $\{M\}$  laminate mid-plane resultant moment array;
- $\{\varepsilon^0\}$  laminate mid-plane strain array;
- $\{k\}$  laminate mid-plane curvature array;
- $[A]$  laminate tensile stiffness matrix ( $3 \times 3$  matrix), where each tensile stiffness coefficient can be calculated from the equation:

$$A_{ij} = \sum_1^N (\bar{Q}_{ij})_k (Z_k - Z_{k-1}) = \sum_1^N (\bar{Q}_{ij})_k h_k l \quad (4.5)$$

where  $(\bar{Q}_{ij})_k$  is the off-axis stiffness coefficient of layer  $k$  and  $h_k l$  is the area of layer  $k$ .

$[B]$ —laminated coupling stiffness matrix ( $3 \times 3$  matrix), wherein each coupling stiffness coefficient can be calculated by the equation:

$$B_{ij} = \frac{1}{2} \sum_1^N (\bar{Q}_{ij})_k (Z_k^2 - Z_{k-1}^2) = \sum_1^N (\bar{Q}_{ij})_k \bar{Z}_k h_k l \quad (4.6)$$

where  $\bar{Z}_k h_k l$  is the static moment from layer  $k$  to the mid-plane.

$[D]$ —laminated bending stiffness matrix ( $3 \times 3$  matrix), wherein each bending stiffness coefficient can be calculated by the equation:

$$D_{ij} = \frac{1}{2} \sum_1^N (\bar{Q}_{ij})_k (Z_k^3 - Z_{k-1}^3) = \sum_1^N (\bar{Q}_{ij})_k \left( \frac{h_k^3}{12} + \bar{Z}_k h_k l \right) \quad (4.7)$$

where  $\left( \frac{h_k^3}{12} + \bar{Z}_k h_k l \right)$  is the inertia moment from the layer  $k$  to mid-plane.

The strain on laminate cross section  $\{\varepsilon\}_Z$  is expressed as:

$$\{\varepsilon\}_Z = \{\varepsilon^0\} + Z\{k\} \quad \left( -\frac{t}{2} \leq Z \leq \frac{t}{2} \right) \quad (4.8)$$

Clearly, the strain on cross section changes continuously and linearly.

The strain on layer  $k$  is:

$$\{\varepsilon\}_k = \{\varepsilon^0\} + Z\{k\} \quad (Z_{k-1} \leq Z \leq Z_k) \quad (4.9)$$

The stress of each lamina depends on the lamina strain and stiffness. The stress in layer  $k$   $\{\sigma\}_k$  can be expressed as:

$$\{\sigma\}_k = [\bar{Q}]_k \{\varepsilon\}_k = [\bar{Q}]_k \{\varepsilon^0\} + [\bar{Q}]_k Z \{k\} \quad (Z_{k-1} \leq Z \leq Z_k) \quad (4.10)$$

It can be seen that the stress in cross section is not constant and may be summarized based on the analysis of stiffness matrices  $[A]$ ,  $[B]$ , and  $[D]$ :

- ① The expected laminate stiffness and strength can be derived from the proper selection of each lamina laying-up angles, ply percentages and stacking sequences, similar to cloth tailoring, and so-called tailoring design.
- ② Coupling is a unique feature possessed by laminates, and it is the basis of aeroelastic tailoring design of aircraft wing surfaces.

Laminate stiffness design analysis generally begins from the matrix  $[A]$  and goes through parameter adjustment (ply sequence, laying-up angle and axis moving) to generate matrices  $[D]$  and  $[B]$ .

With the use of symmetrical laminating sequences, where each lamina is of the same material and has the same thickness, then  $[B] = 0$ ; however, in-plane tensile–shear coupling ( $A_{16} \neq 0$ ,  $A_{26} \neq 0$ ) and bending–twisting coupling ( $D_{16} \neq 0$ ,  $D_{26} \neq 0$ ) will exist.

If an asymmetrical laminating sequence is used, when each lamina has the same material and thickness, then  $[B] \neq 0$ . Thus, in-plane tensile–shear and out-of-plane bending–twisting coupling will take place in the laminates.

If a symmetrical and balanced stacking sequence is used, such as  $[\pm\alpha/-\alpha]$ , or  $[\pm\alpha]_{ns}$ ,  $[0/90/\pm\alpha]_s$ , where each lamina is composed of the same material and has the same thickness, symmetrical laminating will make  $[B] = 0$ . Simultaneously, balanced laminating will make  $A_{16} = A_{26} = 0$ . The values of  $D_{16}$  and  $D_{26}$  will depend on the number of plies (i.e., the more the plies, the smaller the coupling effect). When the ply number is equal to or greater than 12,  $D_{16}$  and  $D_{26} \approx 0$ . In this type of laminate, there will be no in-plane tensile–shear coupling, and no out-of-plane bending–twisting coupling. It is also possible to obtain larger in-plane shear stiffness and out-of-plane twisting stiffness. Hence in structural design, symmetrical and balanced laminating is usually preferred.

Symmetrical laminating or symmetrical unbalanced laminating may be used to give unique composite coupling deformation features, and gives great freedom to composite structural designs, for example, to meet the aerodynamic tailoring requirements.

### (3) Typical laminate stiffness

Typical laminate stiffness is an example of how to describe the designed ability of laminate stiffness. Common laminates are listed below to illustrate the concept of laminate stiffness.

- ① Stiffness of quasi-isotropic laminates: For example, laminates with a ply sequence of  $[0/\pm 45/90]$ ,  $[0/\pm 60]$  are quasi-isotropic laminates. The stiffness coefficients  $A_{11}$ ,  $A_{22}$ ,  $A_{12}$ , and  $A_{66}$  in the in-plane stiffness matrix will correlate as:

$$A_{11} = A_{22} = U_1t; A_{12} = U_4t$$

$$A_{66} = U_5t = \frac{1}{2}(U_1 - U_2)t = \frac{1}{2}(A_{11} - A_{12})$$

where,  $U_1, U_2, U_4,$  and  $U_5$ —material on-axis stiffness coefficient combination,

$t$ —laminate thickness.

This equation indicates that only two of the four stiffness coefficients  $A_{11}, A_{22}, A_{12}, A_{66}$  are independent. This is similar to the case of isotropic materials, where only two of four properties  $E, G, \nu,$  and  $G = \frac{E}{2(1+\nu)}$  are independent. Thus laminates  $[0/\pm 45/90], [0/\pm 60]$  are referred to as quasi-isotropic laminates.

The stiffness coefficients in the matrix  $[A]$  are independent of the laminating sequence when it is symmetric and balanced; however, in matrix  $[B]$  and  $[D]$ , the stiffness coefficients are dependent on the laminating sequences. Quasi-isotropic laminating has the stiffness matrix:

$$\begin{bmatrix} A_{11} & A_{12} & 0 & & & \\ A_{12} & A_{11} & 0 & & & \\ 0 & 0 & \frac{1}{2}(A_{11} - A_{12}) & & & \\ & [B] & & & & \\ & & & & & [D] \end{bmatrix}$$

- ② Stiffness of symmetrical orthotropic laminates: Symmetrical laminates consisting of  $0^\circ$  and  $90^\circ$  plies are referred to as symmetrical orthotropic laminates, for example  $[0/90]_s, [0_2/90]_s$ .

In this type of laminates, each lamina (in  $0^\circ$  or  $90^\circ$ ) will not have tensile–shear coupling in their off-axis stiffness, namely  $(\bar{Q}_{16})_k = (\bar{Q}_{26})_k = 0$ . Accordingly, the in-plane stiffness cross term  $A_{16} = A_{26} = 0$  and bending–twisting stiffness cross term  $D_{16} = D_{26} = 0$  can be derived. Again, for symmetrical laminated plies,  $[B] = 0$ .

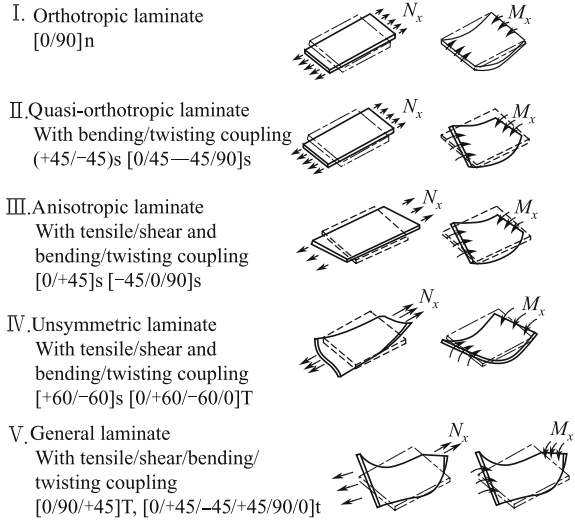
The deformation of symmetrical orthotropic laminates is shown as in Fig. 4.11(I). Because of the absence of cross-ply, symmetrical orthotropic laminates have very small in-plane shear stiffness and out-of-plane twisting stiffness. These systems are only suitable for withstanding in-plane biaxial loads.

The stiffness matrix of symmetrical orthotropic laminates is given as:

$$\begin{bmatrix} A_{11} & A_{12} & 0 & & & & \\ A_{12} & A_{22} & 0 & & & & \\ 0 & 0 & A_{66} & & & & \\ & & & D_{11} & D_{12} & 0 & \\ & & & D_{12} & D_{22} & 0 & \\ & & & 0 & 0 & D_{66} & \end{bmatrix}$$



**Fig. 4.11** Schematic illustration of typical laminate deformations



③ Stiffness of symmetrical and balance laminates: Laminates consisting of  $[\pm\alpha]_s$  ply combinations are referred to as symmetrical and balanced laminates.

For lamina with  $+\alpha$  and lamina with  $-\alpha$ ,  $\bar{Q}_{16}(\alpha) = -\bar{Q}_{16}(-\alpha)$ ,  $\bar{Q}_{26}(\alpha) = -\bar{Q}_{26}(-\alpha)$ . If the number of lamina with  $+\alpha$  is equal to that with  $-\alpha$ , then  $A_{16} = A_{26} = 0$ , laminates will show in-plane orthotropic behaviors.

For symmetrical laminating, then  $[B] = 0$  and each stiffness coefficient  $D_{ij}$  is independent of the stacking sequence. Generally,  $D_{16} \neq 0$ ,  $D_{26} \neq 0$ . Only in laminates with a sufficient number of plies (12 or more plies), can  $D_{16}$  and  $D_{26}$  be reduced and ignored.

The deformation of symmetrical and balanced laminates is shown as in Fig. 4.11(II). Balanced laminates with  $[\pm\alpha]_s$  are referred to as cross-ply laminates, with large in-plane shear stiffness and out-of-plane twisting stiffness. If  $0^\circ$  and  $90^\circ$  plies are arranged, laminates will be enhanced with improved positive stress bearing ability. This arrangement can be used to meet the design requirements of complex load-bearing conditions. The difference between symmetrical and balanced laminates and quasi-isotropic laminates is that the former is not limited by  $A_{11} = A_{12}$  and  $A_{66} = (A_{11} - A_{12})/2$ , which allows greater design freedom. However, owing to their low degree of processing deformation and the ease of quality control, symmetrical and balance laminates are most commonly used in composite structures.



$$\begin{bmatrix} A_{11} & A_{12} & 0 & 0 & 0 & B_{16} \\ A_{12} & A_{22} & 0 & 0 & 0 & B_{26} \\ 0 & 0 & A_{66} & B_{16} & B_{26} & 0 \\ 0 & 0 & B_{16} & D_{11} & D_{12} & 0 \\ 0 & 0 & B_{26} & D_{12} & D_{22} & 0 \\ B_{16} & B_{26} & 0 & 0 & 0 & D_{66} \end{bmatrix}$$

- ⑥ Stiffness of unsymmetrical orthotropic laminates: Laminates containing alternative arrangement of  $0^\circ$  and  $90^\circ$  plies, and with an even total ply number, such as  $[0/90/0/90]$ , are referred to as unsymmetrical orthotropic laminates.

The analysis of matrix  $[A]$  and  $[D]$  is the same as that used for symmetrical orthotropic laminates. It can be proven that  $B_{11} = -B_{22}$ ,  $B_{12} = B_{66} = B_{16} = B_{26} = 0$  in matrix  $[B]$ . As ply number increases, the coupling stiffness coefficient  $B_{11} = -B_{22}$  tends to zero when the ply number is less than eight such that  $B_{11} = -B_{22} = 0$ . Unsymmetrical orthotropic laminates have a stiffness matrix given by:

$$\begin{bmatrix} A_{11} & A_{12} & 0 & B_{11} & 0 & 0 \\ A_{12} & A_{22} & 0 & 0 & -B_{11} & 0 \\ 0 & 0 & A_{66} & 0 & 0 & 0 \\ B_{11} & 0 & 0 & D_{11} & D_{12} & 0 \\ 0 & -B_{11} & 0 & D_{12} & D_{22} & 0 \\ 0 & 0 & 0 & 0 & 0 & D_{66} \end{bmatrix}$$

- ⑦ Stiffness of general laminates: General laminates, referred to as asymmetrical and unbalance laminates, feature a stiffness matrix containing all the coupling terms. The deformation of these laminates is illustrated in Fig. 4.11(V), and the stiffness matrix is given by:

$$\begin{bmatrix} A_{11} & A_{12} & A_{16} & B_{11} & B_{12} & B_{16} \\ A_{12} & A_{22} & A_{26} & B_{12} & B_{22} & B_{26} \\ A_{16} & A_{26} & A_{66} & B_{16} & B_{26} & B_{66} \\ B_{11} & B_{12} & B_{16} & D_{11} & D_{12} & D_{16} \\ B_{12} & B_{22} & B_{26} & D_{12} & D_{22} & D_{26} \\ B_{16} & B_{26} & B_{66} & D_{16} & D_{26} & D_{66} \end{bmatrix}$$

### 4.6.2.3 Laminate Strength and Failure Analysis

#### (1) Ply strength criterion

The strength criterion provides an analytical relationship (mathematical model) of the strength under a combination of stresses. The aim of establishing strength criterion (failure criterion) is to create a material failure envelope under combined stresses based on a simple load-bearing strength index [8–10, 12, 13].

(1) Maximum (on-axis) stress criterion and maximum (on-axis) strain criterion

- ① Maximum (on-axis) stress criterion: All on-axis stresses in a ply should be low, or equal to zero. The corresponding material strength and failure are determined by the ply. Expressions of maximum stress criterion are given by:

$$\begin{aligned} \sigma_1 &\leq X_t & |\sigma_1| &\leq X_c \\ \sigma_2 &\leq Y_t & |\sigma_2| &\leq Y_c \\ & & |\tau_{12}| &\leq S \end{aligned} \quad (4.11)$$

If one of these inequalities cannot be satisfied, a corresponding failure will occur in the ply.

- ② Maximum (on-axis) stress criterion: All the on-axis strain in a ply should be less than the correspond material ultimate strain, otherwise failure will take place in the ply. The expression for maximum strain criterion is given by:

$$\begin{aligned} \varepsilon_1 &\leq X_{te} = X_t/E_1 & |\varepsilon_1| &\leq X_{ce} = X_c/E_1 \\ \varepsilon_2 &\leq Y_{te} = Y_t/E_2 & |\varepsilon_2| &\leq Y_{ce} = Y_c/E_2 \\ & & |\gamma_{12}| &\leq S_e = S/G \end{aligned} \quad (4.12)$$

If one of the inequalities cannot be satisfied, then corresponding failure will occur in the ply.

- ③ Discussion: Each component with maximum (on-axis) stress criterion and maximum (on-axis) strain criterion should have independent criterion. Each criterion has five subcriteria, such that the failure envelope described by the criterion shows a tipping point. The difference between these criteria is that Poisson's effect is involved in the strain criterion.

(2) Tsai–Hill criterion: The Tsai–Hill criterion follows the expression:

$$\left(\frac{\sigma_1}{X}\right)^2 + \left(\frac{\sigma_2}{Y}\right)^2 - \frac{\sigma_1\sigma_2}{X^2} + \left(\frac{\tau_{12}}{S}\right)^2 = 1 \quad (4.13)$$

The Tsai–Hill criterion can give a smooth and continuous failure envelope, with small differences between the theoretical values and testing results. The main problem is that the interaction terms  $\sigma_1$  and  $\sigma_2$  are only related to

$X$  and have no first power terms (without considering  $X \neq X'$ ,  $Y \neq Y'$ ). Under the reduced conditions,  $Y = Z$  and  $S_{12} = S_{13} = S$  are used in derivation, such that this expression cannot be used for biaxial woven reinforcement. More details are given in Tsai's published work.

- (3) Tsai–Wu criterion: In stress space, unidirectional composite failure can be expressed by the quadratic tensor of the failure envelope:

$$F_{ij}\sigma_i\sigma_j + F_i\sigma_i = 1, \quad (4.14)$$

referred to as the quadratic interaction criterion.

For plane stress conditions, the expression can be simplified as:

$$F_{11}\sigma_1^2 + 2F_{12}\sigma_1\sigma_2 + F_{22}\sigma_2^2 + F_{66}\sigma_6^2 + F_1\sigma_1 + F_2\sigma_2 = 1 \quad (4.15)$$

In the equation, there are four quadratic strength parameters and two linear strength parameters. Of these six material strength parameters, five can be determined by simple tensile, compression, and shear tests.

$$F_{11} = \frac{1}{XX'} \quad F_1 = \frac{1}{X} - \frac{1}{X'}$$

$$F_{22} = \frac{1}{YY'} \quad F_2 = \frac{1}{Y} - \frac{1}{Y'}$$

$$F_{66} = \frac{1}{S^2}$$

It is more complex to determine  $F_{12}$ , because of the interaction of  $\sigma_1$  and  $\sigma_2$  is involved. Tsai recommended the use of:

$$F_{12} = -\frac{\sqrt{F_{11}F_{22}}}{2}$$

Compared with the Tsai–Hill criterion, the Tsai–Wu criterion can give more information about strength standards, such as the inequality between tensile and compression strength and how the interaction terms  $\sigma_1$  and  $\sigma_2$  depend on  $X$ ,  $X'$ ,  $Y$ , and  $Y'$  values.

Tsai–Wu criterion can also be expressed in terms of strain parameters (refer to Tsai's publication for details).

- (4) Strength ratio: Strength criterion gives the material failure criterion under operation stress. To describe the safety margin of materials under proportional loading conditions, the concept of the strength ratio is introduced. The strength ratio is defined as the ratio between allowable and operation stress:

$$R = \frac{\sigma_i(\alpha)}{\sigma_i}$$

When the strength ratio is used to describe the safety margin under proportional loads, it is assumed that the deformation of a composite is linear until its final failure.

If  $R = 1$ ,  $\sigma_i = \sigma_i(\alpha)$ , failure occurs.

When  $R > 1$ ,  $\sigma_i < \sigma_i(\alpha)$ ,  $R$  denotes an operation stress  $\sigma_i$  smaller than the allowable stress  $\sigma_i(\alpha)$ . Hence the factor of proportional load increases, within the safety margin. When  $R = 2$ , the operation stress doubles and failure occurs. Hence, if a load is proportionally applied and doubled material failure will occur.

When  $R < 1$ ,  $\sigma_i > \sigma_i(\alpha)$  material failure occurs, or the situation is not physically possible.

The strength ratio can be also used in strain space. The Tsai–Wu criterion in strain space can be expressed as:

$$G_{11}\varepsilon_1^2 + 2G_{12}\varepsilon_1\varepsilon_2 + G_{22}\varepsilon_2^2 + G_{66}\varepsilon_6^2 + G_1\varepsilon_1 + G_2\varepsilon_2 = 1 \quad (4.16)$$

where

$$\begin{aligned} G_{11} &= F_{11}Q_{11}^2 + 2F_{12}Q_{11}Q_{12} + F_{22}Q_{12}^2G_{22} \\ &= F_{11}Q_{11}^2 + 2F_{12}Q_{12}Q_{22} + F_{22}Q_{12}^2 \end{aligned}$$

$$G_{12} = F_{11}Q_{11}Q_{12} + F_{12}(Q_{11}Q_{12} + Q_{12}^2) + F_{22}Q_{12}G_{22}$$

$$G_{66} = F_{66}Q_{66}^2$$

$$G_1 = F_1Q_{11} + F_2Q_{12}$$

$$G_2 = F_1Q_{12} + F_2Q_{22}$$

When using the strength ratio, then

$$\begin{aligned} (G_{11}\varepsilon_1^2 + 2G_{12}\varepsilon_1\varepsilon_2 + G_{22}\varepsilon_2^2 + G_{66}\varepsilon_6^2)R^2 \\ + (G_1\varepsilon_1 + G_2\varepsilon_2)R = 1 \end{aligned} \quad (4.17)$$

This expression can also be used to obtain  $R$ , to determine if failure occurs in a ply.

## (2) Strength estimation of laminates

- (1) Strength failure features of laminates: Laminate strength is based on that of individual ply. Under loading, laminate failure will begin first at a single ply, and will then take place at other ply successively, until total failure occurs, as shown in Fig. 4.12. The failure process proceeds from single ply

failure to total failure. In estimating the laminate strength, it is necessary to determine the first ply failure (FPF) load and the final failure ultimate load. The estimation of laminate strength involves the following aspects:

- ① Select the ply failure criterion,
  - ② Determine the FPF load,
  - ③ Laminate stiffness modification,
  - ④ Calculate ultimate load.
- (2) Determination of FPF load: When a laminate is under loading (including additional temperature loading), the load causing a FPF ( $R = 1$ ) is defined as the FPF load.
- (3) Modification of laminate stiffness: After FPF, the following models can be used for laminate stiffness modification:
- ① Ply-deeply model: Set the stiffness of failure ply ( $R = 1$ ) in the laminate to zero, i.e.,  $[\bar{Q}]_{k(R=1)} = 0$ .
  - ② Fiber successive load-bearing model: Longitudinal cracks usually occur during failure ply ( $R = 1$ ). The ply will separate into fiber bundles, which can only withstand loads in the fiber axial direction, as shown in Fig. 4.13. Hence the stiffness matrix becomes  $\bar{Q}_{11} \neq 0$  and all other terms zero:

$$[\bar{Q}]_{k(R=1)} = \begin{bmatrix} \bar{Q}_{11} & 0 & 0 \\ 0 & 0 & 0 \\ 0 & 0 & 0 \end{bmatrix}$$

- ③ Shear failure model: When shear failure occurs in a ply of laminate ( $R = 1$ ), let the shear stiffness  $Q_{66}$  and the tensile–shear coupling stiffness  $Q_{16}$  and  $Q_{26}$  be zero, such that:

$$[\bar{Q}]_{k(R=1)} = \begin{bmatrix} \bar{Q}_{11} & \bar{Q}_{12} & 0 \\ \bar{Q}_{12} & \bar{Q}_{22} & 0 \\ 0 & 0 & 0 \end{bmatrix}$$

**Fig. 4.12** Load versus displacement curve of laminate

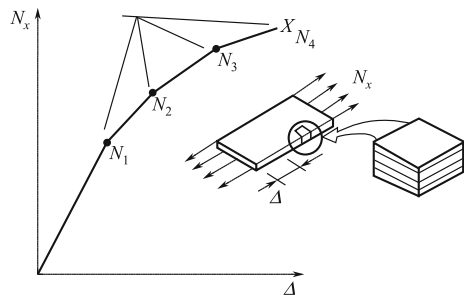
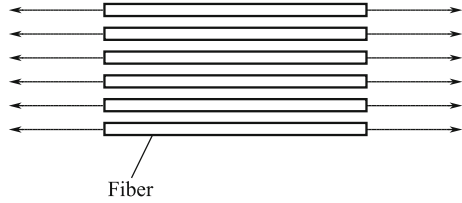


**Fig. 4.13** Fiber successive load-bearing model

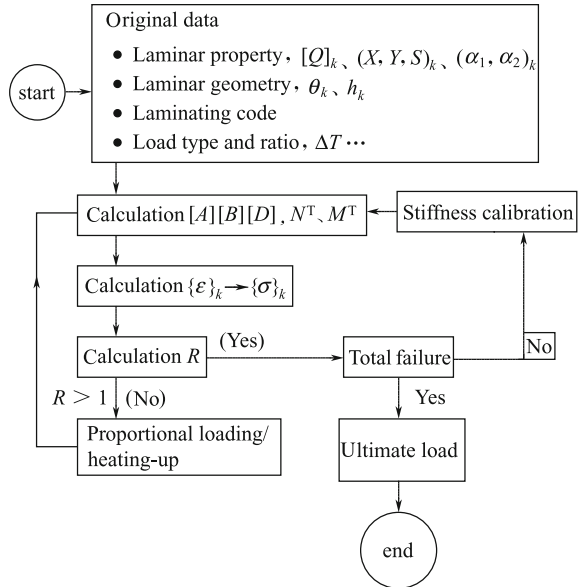


(4) Determination of laminate ultimate load: Fig. 4.14 shows a frame chart of the process from ply successive failure to total damage. This is an iterative calculation process.

Note:

- ① Ply failure criterion is considered suitable for other laminate plies.
- ② Assume that Kirchhoff hypothesis can be always applicable in laminate successive ply failure.
- ③ Decide and select stiffness modification models based on the ply failure modes.

**Fig. 4.14** Analytical chart of laminate ultimate load





### 4.6.2.4 Examples of Laminate Structure Design

#### (1) Symmetrical and unbalance composite skin design

Figure 4.15 shows the canard wing of a jet plane. Symmetrical and unbalanced skin is used in the composite to achieve bending–twisting effects, which allow the canard wing to meet many requirements in terms of strength, stiffness, aerodynamics, and weight reduction [2].

The design steps of symmetrical and unbalanced skin are as follows:

- ① On the basis of static strength requirements, determine the coordinate system (in the  $0^\circ$  ply direction) and perform preliminary ply design. The  $0^\circ$  ply direction in a symmetric and balanced skin is usually consistent with the structural primary load direction, as shown if Fig. 4.16a.

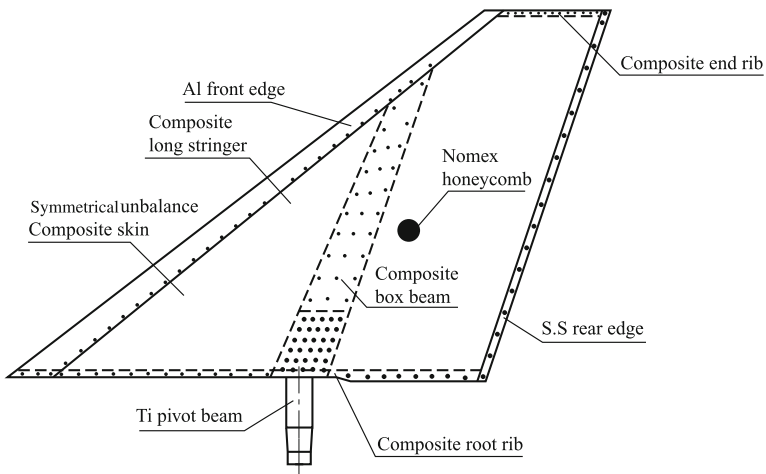


**Fig. 4.15** Schematic of rudder canard wing with symmetrical and unbalanced full-height honeycomb

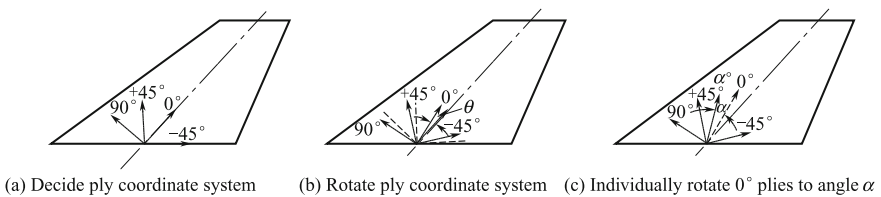


**Fig. 4.16** Conversion of coordinate system during symmetrical and balance skin design

- ② Rotate the symmetrical and balance coordinate system to an angle  $\theta$ , as shown in Fig. 4.16b, and adjust the ply numbers to fully meet the requirements of strength, stiffness, and aerodynamics. The obtained skin laminating is still symmetric and balanced.
- ③ Individually rotate  $0^\circ$  plies to angle  $\alpha$ , as shown in Fig. 4.16c (or  $\pm 45^\circ$  plies), and optimized the design to minimize the weight. The obtained skin laminating will be symmetrical and balanced.

## (2) Aeroelastic tailoring design of a composite forward-swept wing [13]

Because isotropic metal materials encounter insurmountable forces in forward-swept wing designs caused by twisting divergence, great attention should be given to aluminum forward-swept wings in terms of structural weight (Fig. 4.17).

Controlling forward-swept wing wash-in, and changing it into wash-out is the fundamental approach to increasing divergence speed. Wing surface cross-coupling stiffness and the coupling stiffness between bending curvature and twisting curvature play a key role in the control of wing wash-in and wash-out.

When the bending–twisting coupling stiffness coefficients  $D_{16}$  and  $D_{26}$  in the composite laminated wing skin bending–twisting stiffness matrix have different values, different bending–twisting coupling deformations will take place. These effects can produce wash-in or wash-out effects, as shown in Fig. 4.18.

When  $D_{16} = D_{26} = 0$ , there will be no bending–twisting coupling in wing skin laminates (Fig. 4.18a).

When  $D_{16}$  and  $D_{26}$  take negative values, and up-forward bending occurs in the wing skin, twisting will cause the front edge to deform down and forward such that a wash-out effect will take place (Fig. 4.18b).

When  $D_{16}$  and  $D_{26}$  take positive values, and up and forward bending occurs in the wing skin. Twisting will cause the front edge to deform in this manner giving rise to wash-in effects (Fig. 4.18c).

The basis of forward-swept wing aerodynamic tailoring design is to engineer bending–twisting coupling stiffness coefficients  $D_{16}$  and  $D_{26}$  with negative values.

Symmetrical and unbalanced ply design can be used to make  $D_{16}$  and  $D_{26}$  with a negative value. This is the main approach in composite forward-swept wing aerodynamic design. Symmetrical plies can make  $[B] = 0$ , in which no deformation exists coupling between the in-plane and out-of-plane loads. This is useful for cure

**Fig. 4.17** Correlation between wing weight and sweep angle

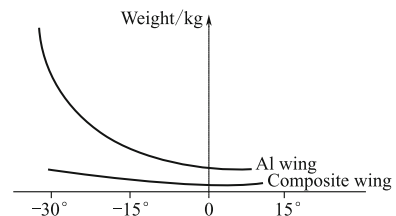
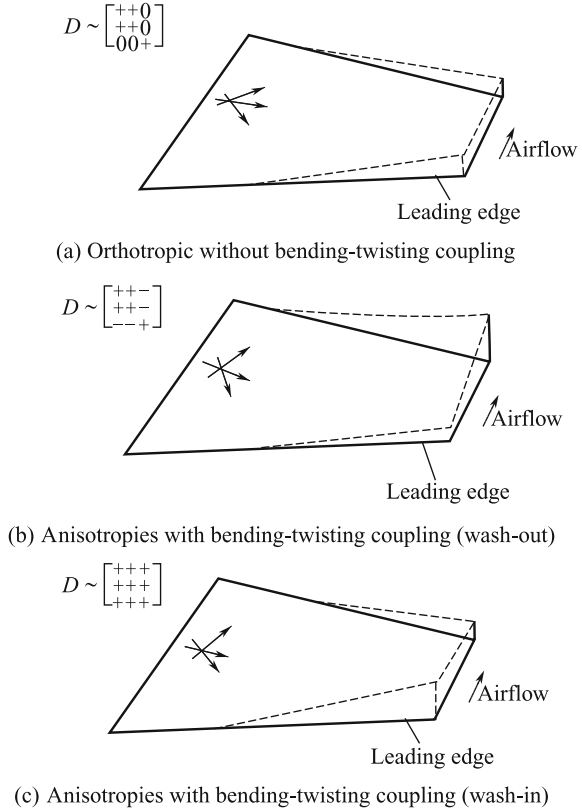


**Fig. 4.18** Correlation between positive/negative values of bending–twisting coupling stiffness and wing skin wash-in/wash-out



deformation control. Unbalanced ply design can be realized with unequal numbers of plies with ply angles  $+\theta$  and  $-\theta$ , or by changing the ply angle in balanced laminates. These choices will depend on the requirements of the design program.

In the above discussion on forward-swept wing design, the focus is on a technical approach to increase the divergence speed. In fact, aeroelastic tailoring is the height of a combined design approach, giving many benefits in aeroelastic performances, besides increasing divergence speed. For forward-swept wings, this approach can also increase buffet speed, improve operational safety, reduce motor load, and improve the lift-to-drag ratio in aerodynamic quality curves. These performances are closely related to aeroelastic deformation control, reflecting wash-in, washout, and chord wise deflection, simultaneously. There is often conflict between these technical approaches, for example, the contradiction between divergence and buffet speed. In general, wing washout is useful for divergence prevention, while wash-in is useful to increase buffet speed. Hence aero elastic tailoring should try to reach a combined optimized design.

(3) **Hollow step grid structure** [15]

This design includes skin and hollow step grids. Grids are mounted on a skin as shown in Fig. 4.19. The grid width and thickness can be changed based on the application requirements. It can be manufactured as an integrated component without additional fasteners, and weight reduction can be realized, with guaranteed strength and stiffness. In Fig. 4.20, the design concept of a cabin door design is shown.

**4.6.3 Sandwich Structure Design and Analysis**

**4.6.3.1 Basic Design Concept of Sandwich Structure**

(1) **Load-bearing and failure modes of sandwich structures**

Owing to their light weight and high bending stiffness, sandwich structures are widely used in aircraft structures, as shown in Fig. 4.21. Sandwich structures consist of a pair of thin surface panels and a honeycomb core. Core materials

**Fig. 4.19** Step grid design concept

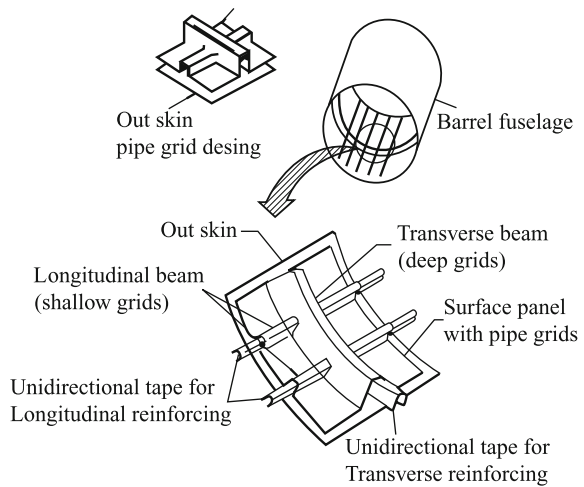


**Fig. 4.20** Hollow step grid cabin door design

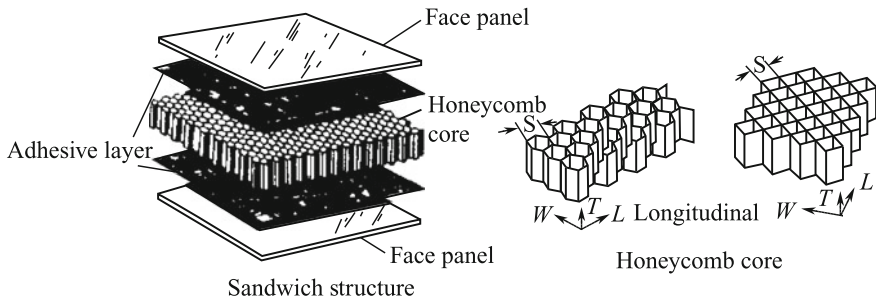
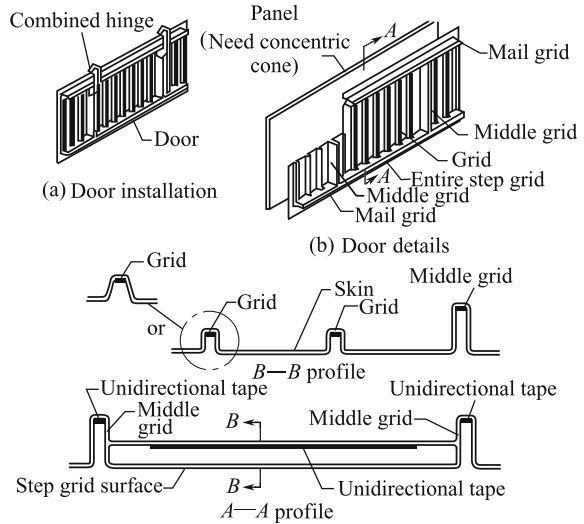
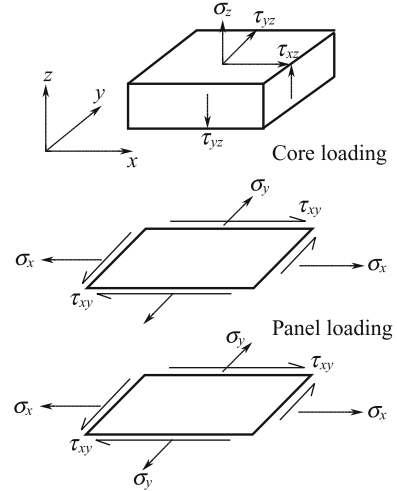


**Fig. 4.21** Honeycomb sandwich construction

may be classed as longitudinal (L) and transverse (W), and have very low stiffness in the LW plane, i.e.,  $G_{LW}, E_L, E_W = 0$ , and give a definite value to  $E_T$  and  $G_{LT}$  and  $G_{WT}$ . The load-bearing conditions are shown in Fig. 4.22, surface panels will withstand tensile, compression, and shear loads in the  $xy$  plane, where the  $xy$  axes are in the same plane as LW. Core materials provide support to the surface panels and can only withstand transverse shear load and loads vertical to the  $xy$  plane [2].

The failure modes of sandwich structures include: total buckling, surface panel wrinkling and buckling, surface bending failure, transverse shear failure, local crash, and impact damage failure. Several failures can occur at the same time during practical applications, and hence strength corrections should be performed for several failure modes.

**Fig. 4.22** Load-bearing of sandwich structure component



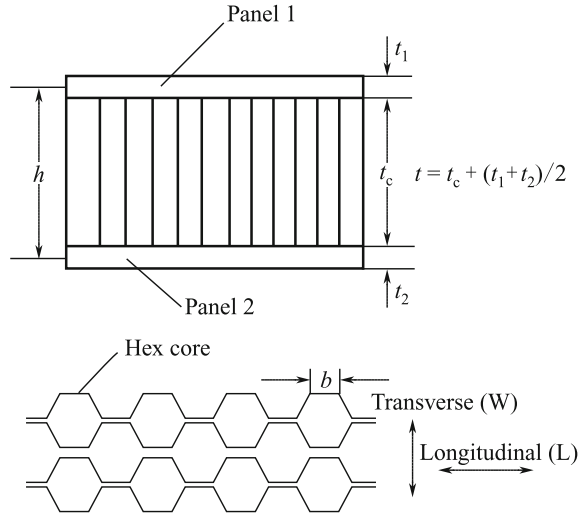
(2) **Sandwich structure preliminary design—engineering beam approach**

Sandwich structures have similar load-bearing features to I-cross-section beams. Thus, in preliminary design, the simple engineering beam approach can be used to determine the preliminary dimensions of sandwich structures. The dimensional definition of sandwich structures is shown as in Fig. 4.23.

- ① Mechanical properties of sandwich panels: First use laminate theory to determine the mechanical properties of the surface panels:  $E_x$ ,  $E_y$  and  $\nu_{xy}$ ,  $\nu_{yx}$ . The mechanical properties of the core materials include: longitudinal shear modulus  $G_{TL}$ , transverse shear modulus  $G_{TW}$ , longitudinal shear strength  $[\tau_{TL}]$ , transverse shear strength  $[\tau_{TW}]$ , compression modulus  $E_c$ , tensile modulus  $E_T$  (usually replaced by  $E_c$ ), compression strength  $[\sigma_c]$ , tensile strength  $[\sigma_c^t]$  (usually replaced by  $[\sigma_c]$ ), and normal tensile modulus. Subscripts L, W, and T represent the longitudinal, transverse, and normal directions, as shown in Fig. 4.23.

In some references, several equations are provided for the calculating the mechanical properties of sandwich structures, but in engineering, test results should be used in the structure design.

**Fig. 4.23** Dimensional definition of sandwich structures



The followings should be taken into account in the application of the above properties:

- (a)  $[\tau_{TL}]$  and  $[\tau_{TW}]$  are related to core thickness and highly reliable test results should be used, or, thickness modification should be engineered in. A value of 0.7 is recommended as a conservative correction factor.
- (b) The normal tensile modulus is usually replaced by the compression modulus.
- (c) The property data of core materials should be based on material specifications.

② Sandwich panel stiffness

- (a) The bending stiffness of sandwich panels: The bending stiffness per unit width of a panel in the  $i$  direction ( $i = x, y$ ) (units N-mm) can be calculated by:

$$D_i = \frac{E_{i1}t_1E_{i2}t_2h^2}{(E_{i1}t_1 + E_{i2}t_2)\lambda} + \frac{1}{12\lambda}(E_{i1}t_1^3 + E_{i2}t_2^3) \quad (4.18)$$

where  $\lambda = (1 - \nu_{xy}\nu_{yx})$ ,

$\nu_{xy}, \nu_{yx}$  are the panel Poisson's ratio, and subscripts 1 and 2 denote the top and bottom surface panels. When the panel is very thin, the second term in the equation can be ignored.

- (b) The shear stiffness of sandwich panels: The transverse shear stiffness of a unit width of panel (N/mm) can be calculated by the following equation:

$$U = h^2 G_c / t_c \quad (4.19)$$

where  $G_c$  is the core shear modulus. In some special cases ( $G_c = G_{TL}$  or  $G_{TW}$ )

$$U = h^2 G_{TL} / t_c \quad (4.20)$$

$$U = h^2 G_{TW} / t_c$$

- ③ Core material density: Core density is an important index reflecting the core mechanical properties and weight. Core density is the same concept as volumetric weight, a dimensional unit. A regular hexagon honeycomb cell has a core density ( $\text{kg/m}^3$ ) given by:

$$\rho = \frac{8}{3\sqrt{3}} \rho_m (t_m / b) \quad (4.21a)$$

A square honeycomb cell has a core density given by:

$$\rho_c = \frac{2t_m}{b} \rho_m \quad (4.21b)$$

where

- $\rho_m$  —core cell wall material density,  $\text{kg/m}^3$ ;  
 $t_m$  —core cell wall material thickness, mm;  
 $b$  —cell side length, mm.

In general, the above equations underestimate the actual core density.

- ④ Sandwich beam design and analysis: When sandwich panels have an aspect ratio (length versus width) greater than or equal to 3:1, the system can be simplified as a sandwich beam for design purposes. The shorter side can be considered to be the beam width. Following the external load, material selection and preliminary design can be performed to determine the sandwich beam dimensions. Following the local pressure (or absorbing force), core density can be determined from the following equation:

$$[\sigma_c] / \sigma_c = 3$$

Preliminary design of sandwich beams can be performed by following the engineering beam equations:



(a) Bending stress on a surface panel given by:

$$\sigma_{\bar{n}} = M / (t_{\bar{n}}hb) \quad (4.22)$$

(b) Shear stress on core cell is given by:

$$\tau_c = V / (hb) \quad (4.23)$$

(c) Deflection is given by:

$$\Delta = \frac{2k_b PL^3 \lambda}{E_f t_f h^2 b} + \frac{k_b PL}{h G_c b} \quad (4.24a)$$

or

$$\Delta = \frac{k_b PL^3}{D} + \frac{k_b PL}{h G_c b} \quad (4.24b)$$

(d) The wrinkle stress on a surface panel is given by:

$$\sigma_{cr} = \frac{2E_f}{S} \left( \frac{t_f}{S} \right)^2 \quad (4.25)$$

(e) The buckling stress on a surface panel is given by:

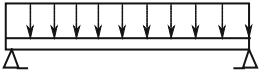
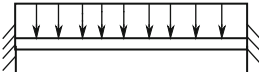
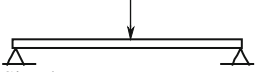
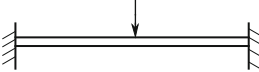
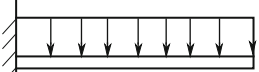
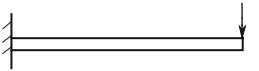
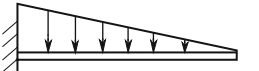
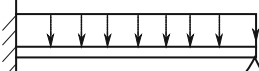
$$\sigma_{cr} = 0.82E_f \left( \frac{E_c \cdot t_f}{E_f \cdot t_c} \right)^{\frac{1}{2}} \quad (4.26)$$

where  $M$ ,  $V$ ,  $K_b$ , and  $K_s$  are given in Table 4.12.

- $M$  maximum bending moment;
- $V$  maximum shear force;
- $k_b$  bending deflection constant;
- $D$  bending stiffness;
- $P$  total load;
- $\sigma_{\bar{n}}$  surface panel stress;
- $t_f$  surface panel thickness;
- $\tau_c$  core shear stress;
- $\Delta$  deflection;
- $E_f$  surface panel modulus, taking the values in beam axial direction;
- $\sigma_{cr}$  surface critical stress;
- $\lambda$   $1 - \nu_{xy}\nu_{yx}$ ;
- $S$  core cell dimensions (core cell inscribed circle diameter);
- $E_c$  core compression modulus;
- $t_c$  core thickness.

Others variables are shown in Fig. 4.23.

**Table 4.12** Calculation of  $V$ ,  $M$ ,  $K_b$ , and  $K_s$  of beams

Beam type	Max. shear force $V$	Max. bending moment $M$	Bending deflection constant $K_b$	Shear deflection constant $K_s$
 Simple support Uniform force	$0.5P$ ( $P = qL$ )	$0.125PL$	0.01302	0.125
 Two-point Fixed-support Uniform force	$5P$ ( $P = qL$ )	$0.08333PL$	0.002604	0.125
 Simple support Concentrated force	$0.5P$	$0.25PL$	0.02083	0.25
 Two-point Fixed-support Concentrated force	$0.5P$	$0.125PL$	0.00521	0.25
 Suspend beam Uniform force	$P$ ( $P = qL$ )	$0.5PL$	0.125	0.5
 Suspend beam Concentrated force	$P$	$PL$	0.3333	1
 Suspend beam Triangle distribution	$P$ ( $P = 0.5qL$ )	$0.3333PL$	0.06666	0.3333
 One end fixed, one end uniform force	$0.625P$ ( $P = qL$ )	$0.125PL$	0.005403	0.07042

**4.6.3.2 Sandwich Stress Analysis and Strength Correction**

Composite panels and honeycomb cores feature anisotropic properties, complex structure configurations, and a wide range of changing parameters. Hence, simplified engineering beam design approaches cannot meet the requirements for sandwich structure design and analysis. Currently, the finite element method (FEM) is used for stress and stability analysis in structural design. An example is the MSC/NASTRAN program analysis.

(1) **FEM for sandwich structures**

In applications of FEM to sandwich structures, the membrane stress unit is used for the surface modeling, and a special volume unit is used to simulate the honeycomb core.

- ① Special volume unit: Taking the axis L, W, and T of the core material as the coordinate system, the unit stress–strain relationship can be given as:

$$\begin{Bmatrix} \sigma_L \\ \sigma_W \\ \sigma_T \\ \tau_{LW} \\ \tau_{WT} \\ \tau_{TL} \end{Bmatrix} = \begin{bmatrix} G_{11} & & & & & & \\ G_{21} & G_{22} & & & & & \\ G_{31} & G_{32} & G_{33} & & & & \\ G_{41} & G_{42} & G_{43} & G_{44} & & & \\ G_{51} & G_{52} & G_{53} & G_{54} & G_{55} & & \\ G_{61} & G_{62} & G_{63} & G_{64} & G_{65} & G_{66} & \end{bmatrix} \begin{Bmatrix} \varepsilon_L \\ \varepsilon_W \\ \varepsilon_T \\ \gamma_{LW} \\ \gamma_{WT} \\ \gamma_{TL} \end{Bmatrix} - \begin{Bmatrix} A_1 \\ A_2 \\ A_3 \\ A_4 \\ A_5 \\ A_6 \end{Bmatrix} \Delta T \quad (4.27)$$

where

{ $A_i$ } is the thermal expansion coefficient,  
 $\Delta T$  is the temperature difference.

The subscripts 1–6 of the stiffness coefficient  $G_{ij}$  are used for the axes L, W, T, LW, WT, and TL of the core material, respectively. In the case of a core special body unit, then:  $G_{33} = E_c$ ,  $G_{55} = G_{WT}$ ,  $G_{66} = G_{TL}$ ,  $E_c$  is the compression modulus,  $G_{WT}$  and  $G_{TL}$  are the

shear modulus in two directions, and  $G_{ij}$  is zero. To avoid value overflow in the calculation,  $G_{11}$ ,  $G_{22}$ ,  $G_{44}$  use 1% of the minimum values of  $G_{33}$ ,  $G_{55}$ , and  $G_{66}$ .

$$G_{11} = G_{22} = G_{44} = \min(G_{33}, G_{55}, G_{66}) \times 0.001$$

For the coordinate system in arbitrary  $X$ ,  $Y$ ,  $Z$  axes the stiffness coefficients in the stress–strain relationship should be calculated by tensor algorithms, which are automatically processed by FEM programs.

② Use of MSC/NASTRAN program

- (a) Separation between a panel and core. The panel uses plate elements; the core uses a special body unit.
- (b) The core special body unit can be divided into hexahedron (CHEXH), pentahedral (CPENTA) or tetrahedron (CTETRA) units. For a sandwich panel with a rectangular projection, either QUAD4 or HEXA units can be used, based on the sandwich structure construction.
- (c) Use the MAT9 card to denote the core modulus  $G_i$  in the coordinate system  $L$ ,  $W$ ,  $T_j$ .
- (d) Define the material coordinate system.

When the volume unit orientation is in an arbitrary coordinate system, the correlation between MAT9 and the arbitrary orientation should be established through a CORDM domain in the PSOLID card. In such a case, the output special body unit stress components will be the components in the defined coordinate axes in CORDM domain.

③ Finite element mesh partition concept

- (a) For full-height sandwich structures, external loads will be mainly distributed asymmetrically. If the core material strength is critical, the core special body unit should be analyzed as a multiple-layer partition from top to bottom. If the core material strength is not critical, a single-layer partition can be used.
- (b) For in-plane load sandwich structures, the core can be analyzed as a single-layer partition for total buckling analysis.
- (c) In buckling analysis, the mesh partition should be of an appropriate size to properly reflect the buckling behavior. Attention should be paid to the rational modeling of boundary conditions.

(2) **Sandwich strength corrections**

A design load is used for stress analysis, and the results can be used for strength correction and structural design modifications.

① In-plane strength correction

- (a) Operation strain  $\leq$  allowable strain.
  - (b) Modification of operation stress under design load should be performed with the modifying factor is  $f_m$ .  
Operation stress  $\times f_m \leq$  panel allowable strength.  
For composite panels,  $f_m = 1.06\text{--}1.15$ .
- ② Core material strength correction: The FEM results  $\sigma_z$  (stress at cell center) should be modified by the factor  $f_c$ .

$$\sigma_z \times f_c \leq [\sigma_c]$$

where

$[\sigma_c]$ —core material allowable compression strength,  
 $f_c$ —modification factor, depending on the core partition layer number as well as loading conditions usually  $f_c = 1.0\text{--}2.0$ ,

In the case of a core “single-layer” partition and a normally distributed load applied to a sandwich panel, then  $f_c \approx 2.0$ .

Core shear strength can be corrected by the following equation:

$$\begin{aligned}\tau_{LT} &\leq [\tau_{LT}] \times 0.7 \\ \tau_{WT} &\leq [\tau_{WT}] \times 0.7\end{aligned}$$

where  $[\tau_{LT}]$   $[\tau_{WT}]$ —core allowable shear strength.

## 4.6.4 Composite Structure Anti-crash and Energy Absorption Design

### 4.6.4.1 Aircraft Body Structure Crash Resistant Design Features

When an aircraft crashes, the body structure is subjected to a large instantaneous deformation to absorb the impact energy. Theoretical analysis of large structural impact deformation involves multiple complex fields of study, such as collision mechanics and material high strain rate and impact damage mechanics. Hence, body structure anti-crash and energy absorbing design should be performed by combining digital stimulation analysis and testing verification. Testing plays a particularly important role. The design should be started from the crash/absorption of structural components [3].

The measures taken for structural crash absorption will increase structural weight. This increase is considered to be a fixed additional weight, so low mass composites with high energy absorption are important for structural crash/absorption design. Many studies have indicated that energy absorption components, such as agamid/epoxy composite sine-wave beams, offer better energy

absorption capacities than that of aluminum alloy components. Use of composite components may also reduce the weight requirements of crash absorption designs.

#### 4.6.4.2 Composite Crash Absorption Component Design

Composite body structures should be able to provide at least the same level of crash safety as metal structures. The design of energy absorption components provides a basis for materials selection and selection of configuration parameters in crash absorption structure designs. Thus, composite crash/absorption component design is an important part of the design process. Anti-crash and energy absorption components can be classified as follows:

##### (1) Metal crash absorption components

Structural metal materials such as Al alloy are the tough materials, which can produce large deformations to absorb crash impact energies. The toughness of metals can be used to design crash/absorption body structures.

##### (2) Composite crash/absorption components

Fiber-reinforced composites show linear elastic behaviors at  $0^\circ$  tensile and compression loads with a small failure strain. However, nonlinear  $\pm 45^\circ$  off-axis tensile and compression loads have a large failure strain and show tough material behavior. Thus, in composite crash/absorption component design, a design scheme with tube and wave beams with  $\pm 45^\circ$  plies as the base, and  $0^\circ$  plies as supplements are preferred, as shown in Fig. 4.24. Tube components may be easily manufactured at low cost, and the test result analysis is straightforward.

Composite sine-wave web beams are a high stiffness and stability structural component with both load-bearing and energy absorption abilities. The shapes of sine waves and ply stacking can be designed to give good processing ability. An energy absorption component made of a sandwiched web beam with a ladder core is shown in Fig. 4.25. This structure is used in the helicopter NH90. Its absorbing ability is equivalent to that of a sine-wave web beam, but it can be processed more easily.

**Fig. 4.24** Composite crash/absorption components

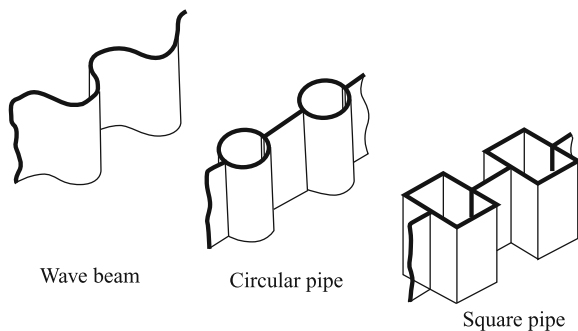
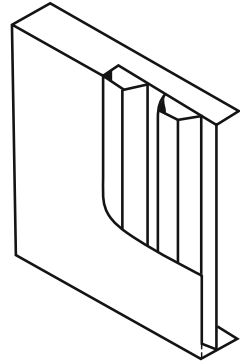


**Fig. 4.25** Energy absorption component made of sandwich web beam with ladder cores



Material selection for crash absorption components and common structural components requires materials with high toughness and energy absorption capacity, which also have good mechanical properties and processing ability. Currently, Kevlar/carbon hybrids or woven Kevlar are selected as reinforcing materials and an epoxy or thermoplastic (such as PEEK) resin matrix is selected with high toughness. For RTM processing, a special resin matrix is required. Test-based verification is needed for all selected composite systems.

#### 4.6.4.3 Structural Design of Composite Crash/Absorption Floor

Crash/absorption floor structures are an important part of aircraft crash resistance design. In designing these structures, the first consideration is energy absorption and the second is their load-bearing ability. With a selection of a proper structural configuration, parameters, and materials a balance between the load-bearing and crash absorption requirements can be realized.

##### (1) Structural design principle of crash/absorption composite floor

Crash/absorption composite floor structures consist of a fuselage structural floor and energy absorbing structure as shown in Fig. 4.26. In an airplane crash, the impact energy to the aircraft body will be mainly absorbed by an energy absorption structure. The floor deformation will absorb part of the residual energy. The energy absorption ability of the energy absorption structure is controlled through its structural design.

##### (2) Structural design of sine-wave beam crash/absorption floor

As an energy absorbing component, sine-wave beams are commonly used in crash/absorption floor design. The sine-wave beam crash/absorption floor construction used in the front body of a “Tiger” helicopter is shown in Fig. 4.27. Crash

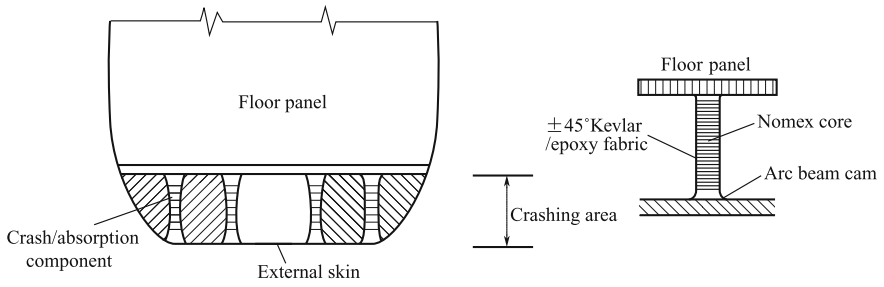


Fig. 4.26 Structural design principle of crash/absorption floor

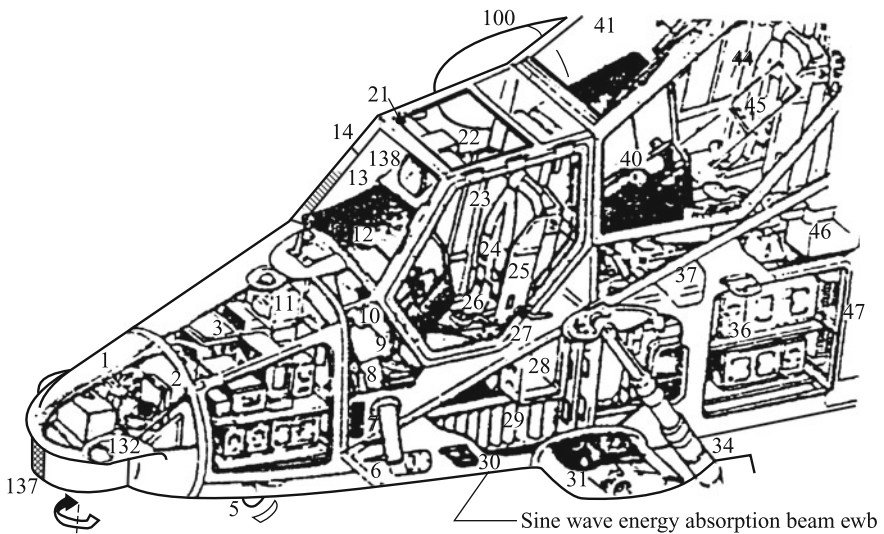
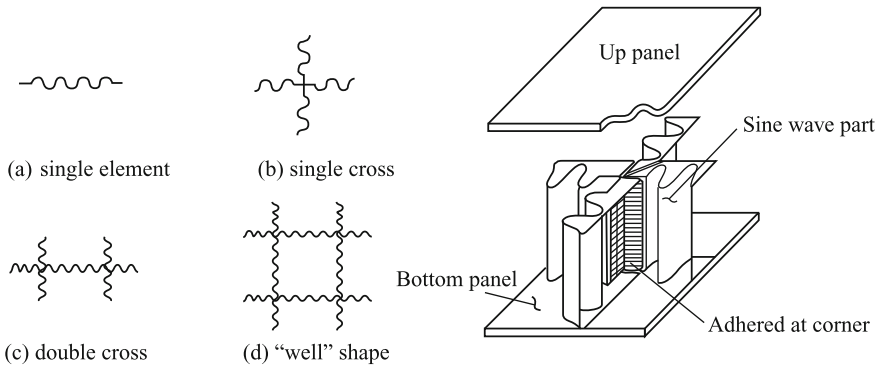


Fig. 4.27 Crash/absorption floor in "Tiger" front helicopter body

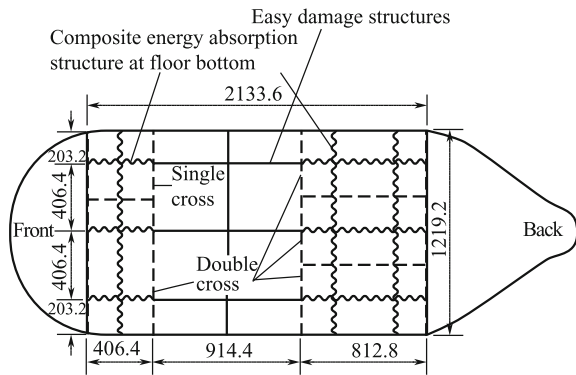
absorption structures feature a longitudinal/transverse cross-beam construction, which can be a single component in a single cross, double cross, or well-shape configuration, as shown in Fig. 4.28. A recommended configuration is shown in Fig. 4.29.





**Fig. 4.28** Basic pattern of a sine-wave web assembly

**Fig. 4.29** Recommended optimized energy absorption construction configuration



### 4.6.5 Analysis of Thick Cross-sectional Composite (Thick Laminate)

Thick cross-section composites refer to thick laminates containing a large number of plies.

Currently, thin composite laminates are most often used in aerospace engineering. However, thick composite laminates are becoming more common. For example, the panel thickness in the wing root of a large commercial airplane is 30–45 mm.

In an A380, some panels of the central wing critical joints have thicknesses up to 160 mm and the number of plies is of the order of hundreds or thousands.

Compared with thin laminates, thick laminates can offer higher impact and damage resistances. Their damage tolerance is a less serious concern and thick laminates can also provide improved thermal resistance and hot/wet properties, and

operation performances. However, in terms of processing and property testing, the analysis and design of thick laminates require special care to be taken.

#### 4.6.5.1 Features of Thick Cross-section Composites

Owing to the dimensional increase in the thickness direction, the stress component in this direction cannot be ignored. Hence, 3D stress analysis should be performed on thick laminates. Even under a single in-plane load, thick laminates will also show a 3D stress distribution. Any stress components reaching a critical state can result in thick laminate failure. Therefore, the above-mentioned thin laminate 2D stress analysis and the corresponding failure criteria are not appropriate for thick laminates.

In addition, the 3D effects in thick laminate composite are more significant than those in uniform isotropic materials. The strength along the thickness direction is very low, and has a high sensitivity to matrix cracking and delamination. Thus, it is necessary to perform 3D stress analysis to establish the failure criterion for thick laminates. The failure modes governed by the fiber, matrix, and interface should all be considered.

Many new problems will be encountered in thick composite processing, such as decreasing residual stress, reducing void content, and ensuring full curing. To minimize these effects, it is necessary to use special resin matrices, processing techniques, modes, and curing conditions. Special attention should be given to two main issues in thick composite processing: A low-level residual stress should be achieved; the production efficiency should be high, i.e., the time required for full curing should be as short as possible. Rapid heating and cooling can reduce the curing time, but can also induce higher residual stress. Slow curing cycles will result in a low production rate and high cost; however, a fully cured part can be expected. Cure modeling is very important for thick composite manufacture and can provide a good understanding of the cure kinetics and instant cure degree in the cure cycle. This knowledge is useful for predicting the processing stress and is an important approach to guaranteeing processing quality.

In thick composite laminate analysis and design, it is necessary to understand the multi-axial strength and stiffness to fully take advantage of thick composites. Currently, there is a lack of studies on thick composite design, analysis, and materials testing.

In Fig. 4.30, a flowchart of thick composite analysis is given.

#### 4.6.5.2 3D Stress Analysis of Thick Composites

As mentioned above, 3D stress analysis should be performed for thick composites. The effects of interlaminar tensile stress and shear stress should be considered when thick laminate is under out-plane loading conditions. Furthermore, 3D stress

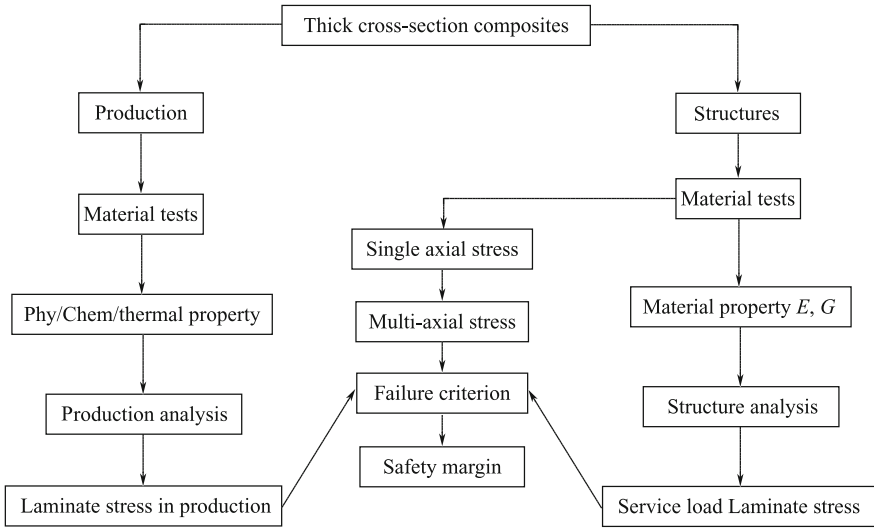


Fig. 4.30 Flow chart of thick composite analysis

analysis is needed in unidirectional isotropic laminates. The stress–strain expression is given as:

$$\begin{Bmatrix} \varepsilon_1 \\ \varepsilon_2 \\ \varepsilon_3 \\ \gamma_{23} \\ \gamma_{31} \\ \gamma_{12} \end{Bmatrix} = \begin{bmatrix} S_{11} & S_{12} & S_{13} & 0 & 0 & 0 \\ S_{12} & S_{22} & S_{23} & 0 & 0 & 0 \\ S_{13} & S_{23} & S_{33} & 0 & 0 & 0 \\ 0 & 0 & 0 & S_{44} & 0 & 0 \\ 0 & 0 & 0 & 0 & S_{55} & 0 \\ 0 & 0 & 0 & 0 & 0 & S_{66} \end{bmatrix} \begin{Bmatrix} \sigma_1 \\ \sigma_2 \\ \sigma_3 \\ \tau_{23} \\ \tau_{31} \\ \tau_{12} \end{Bmatrix} \quad (4.28)$$

If engineering constants are used, then:

$$\begin{Bmatrix} \varepsilon_1 \\ \varepsilon_2 \\ \varepsilon_3 \\ \gamma_{23} \\ \gamma_{31} \\ \gamma_{12} \end{Bmatrix} = \begin{bmatrix} \frac{1}{E_1} & -\frac{\nu_{21}}{E_2} & -\frac{\nu_{31}}{E_3} & 0 & 0 & 0 \\ -\frac{\nu_{12}}{E_1} & \frac{1}{E_2} & -\frac{\nu_{32}}{E_3} & 0 & 0 & 0 \\ -\frac{\nu_{13}}{E_1} & -\frac{\nu_{23}}{E_2} & \frac{1}{E_3} & 0 & 0 & 0 \\ 0 & 0 & 0 & \frac{1}{G_{23}} & 0 & 0 \\ 0 & 0 & 0 & 0 & \frac{1}{G_{13}} & 0 \\ 0 & 0 & 0 & 0 & 0 & \frac{1}{G_{12}} \end{bmatrix} \begin{Bmatrix} \sigma_1 \\ \sigma_2 \\ \sigma_3 \\ \tau_{23} \\ \tau_{31} \\ \tau_{12} \end{Bmatrix} \quad (4.29)$$

where

$$\frac{\nu_{12}}{E_1} = \frac{\nu_{21}}{E_2}, \frac{\nu_{13}}{E_1} = \frac{\nu_{31}}{E_3}, \frac{\nu_{23}}{E_2} = \frac{\nu_{32}}{E_3} \quad (4.30)$$

Nine independent elastic parameters are involved:  $E_1, E_2, E_3, G_{12}, G_{13}, G_{23}, \nu_{12}, \nu_{13},$  and  $\nu_{23}$ .

If a difference exists between the tensile modulus and compression modulus, the mean value of the two should be used for small differences; for large differences, the applied external load should be used for the tensile and compression moduli.

Symmetrical and balanced laminates can be treated as orthotropic laminates, by changing the subscripts 1, 2, 3 in the above equation to  $x, y, z$  coordinate axes to derive the laminate stress–strain relationship. Hence, the laminate takes the nine independent elastic parameters:  $E_x, E_y, E_z, G_{xy}, G_{xz}, G_{yz}, \nu_{xy}, \nu_{xz}, \nu_{yz}$ .

#### 4.6.5.3 Determination of the Properties of Thick Composites

For design and establishing failure criterion of thick composites, it is necessary to determine their properties and behavior. Determination of the 3D properties of thick composites is more complex than that of thin 2D laminates. The use of testing supported by theoretical calculations is the main approach to analyzing these structures:

##### (1) Testing Methods

Problems may arise with the testing methods, specimens, equipment, and fixtures used for thick composite testing. In general, the following aspects should be considered:

- Fixtures and clamping
- Specimen design and optimization
- Computer control interface
- Proper control of displacement in the central zone of the specimen
- The internal stress state of thick composites
- Multi-axial extensometers and other measuring devices
- Environmental considerations
- Data collection and processing
- Multi-axial yielding and failure criterion
- Dimensional effects and magnifications
- Static and dynamic testing, including fatigue and impact
- Sensitivity of stress concentration
- NDT evaluation

- ① Single-axis testing: Conventional 2D single-axis testing of unidirectional laminates includes measurements of in-plane tensile moduli ( $E_{1t}, E_{2t}$ ), compression moduli ( $E_{1c}, E_{2c}$ ), shear modulus ( $G_{12}$ ), and tensile–compression strengths ( $T_X, X_{-C}, \bar{Y}_t, \bar{Y}_c$ ) and tensile–compression failure strains ( $\varepsilon_{1t}, \varepsilon_{1c}, \varepsilon_{2t}, \varepsilon_{2c}$ ). In 3D single-axis testing, new characteristics for testing, include: the tensile modulus in the thickness direction ( $E_{3t}$ ); compression modulus ( $E_{3c}$ ) and shear

moduli ( $G_{13}, G_{23}$ ) related to thickness; and the tensile–compression strengths ( $T_{zu}, Z_c$ ) and tensile–compression failure strain ( $\epsilon_{3t}, \epsilon_{3c}$ ).

In compression testing of thick composites, special attention should be paid to the design and bonding of the specimen end tabs as well as the end supports. Any impact, end cracking or improper fixturing, may negatively affect the material’s properties and give inconclusive data. Tables 4.13 and 4.14 present typical room-temperature testing data from medium modulus C-fiber/epoxy unidirectional laminates and multi-directional laminates.

- ② Multi-axis testing: Multi-axis testing is needed to evaluate the behavior of thick laminates under 3D loading conditions. Two- or three-axis testing machines are needed. The load can be applied along two intervertical or three intervertical axes. Figures 4.31 and 4.32 show two-axis and three-axis tensile–compression testing systems, respectively.

Specimens for multi-axis testing should be specially designed, having a 3D construction, as shown in Fig. 4.33.

(2) **Calculation Methods**

When theoretical methods are used to calculate composite mechanical properties, the constituent mechanical properties and micromechanics should be considered.

**Table 4.13** Typical 3D test data of medium modulus C-fiber/epoxy unidirectional laminates

Item	$x_t$	$E_{1t}$	$\epsilon_{1t}$	$x_c$	$E_{1c}$	$\epsilon_{1c}$	$\bar{Y}_t$	$E_{2t}$	$\epsilon_{2t}$
Property	1720	114	15,200	1170	114	10,300	55.2	9.65	5700
Item	$\bar{Y}_c$	$E_{2c}$	$\epsilon_{2c}$	$S$	$G_{12}$	$r_{12}$	$Z_t$	$E_{3t}$	$\epsilon_{3t}$
Property	207	9.65	21,500	103	6.0	17,000	55.2	9.65	5700
Item	$z_c$	$E_{3c}$	$\epsilon_{3c}$	$S_{13}$	$G_{13}$	$r_{13}$	$S_{23}$	$G_{23}$	$\gamma_{23}$
Property	207	9.65	21,500	82.7	6.0	4000	82.7	3.8	22,000

Note 1. Units: Strength in MPa, modulus in GPa, strain in  $\mu\epsilon$ ; 2. Laminate thickness: >6.35 mm; 3. Assume transverse isotropy in 2–3 plane

**Table 4.14** Typical 3D test data of medium modulus C-fiber/epoxy cross-ply laminates  $[0_3/90]_n$

Item	$\sigma_{xt}$	$E_{xt}$	$\epsilon_{xt}$	$\sigma_{xc}$	$E_{xc}$	$\epsilon_{xc}$	$\sigma_{yt}$	$E_{yt}$	$\epsilon_{yt}$
Property	965	103	9330	765	88.9	8600	241	39.0	12,900
Item	$\sigma_{yc}$	$E_{yc}$	$\epsilon_{yc}$	$S_{xy}$	$G_{xy}$	$\gamma_{xy}$	$\sigma_{zt}$	$E_{zt}$	$\epsilon_{zx}$
Property	503	39.0	12,900	105	4.8	22,000	23.4	7.72	3040
Item	$\sigma_{zc}$	$E_{zc}$	$\epsilon_{zc}$	$S_{xz}$	$G_{xz}$	$\gamma_{xz}$	$S_{yz}$	$G_{yz}$	$\gamma_{yz}$
Property	414	11.3	3600	28.0	3.7	7700	42.4	4.6	9300

Note 1. Units: same as above; 2. Laminate thickness: 15 mm; 3.  $V_f = 61.4\%$ , void content 0.04%

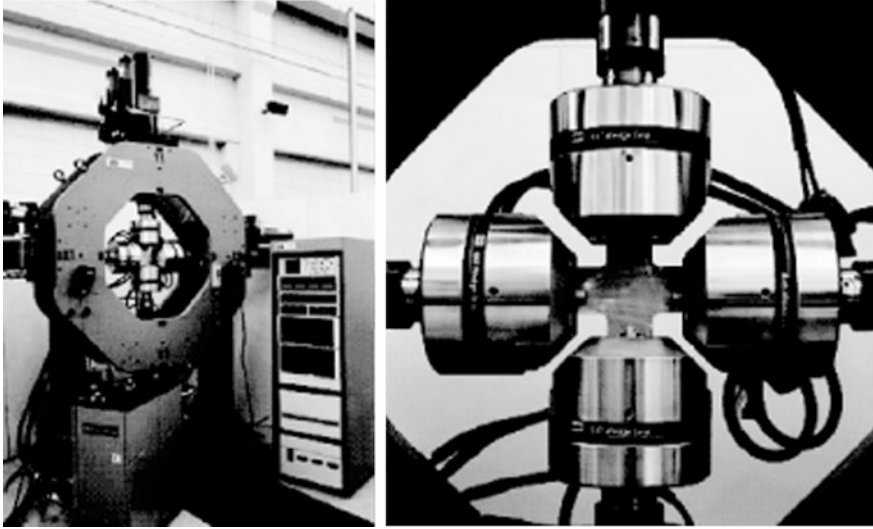


Fig. 4.31 Two-axis tensile-compression testing (I)

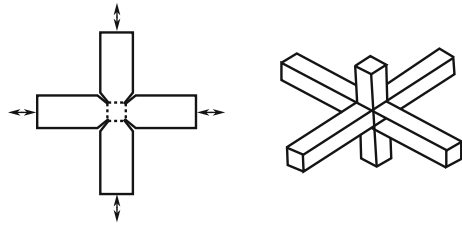


Fig. 4.32 Three-axis tensile-compression testing (II)

A data processing method is introduced below.

- ① 3D properties of unidirectional laminates: As mentioned above, unidirectional laminates have nine material properties, i.e.,  $E_1$ ,  $E_2$ ,  $E_3$ ,  $G_{12}$ ,  $G_{13}$ ,  $G_{23}$ ,  $\nu_{12}$ ,  $\nu_{13}$ ,  $\nu_{23}$ . The values of  $E_1$ ,  $E_2$ ,  $G_{12}$  and  $\nu_{12}$  are

**Fig. 4.33** Two-axis testing specimen



**Table 4.15** 3D elastic constants of composite materials

Material	Performance								
	$E_1/$ GPa	$E_2/$ GPa	$E_3/$ GPa	$G_{12}/$ GPa	$G_{13}/$ GPa	$G_{23}/$ GPa	$\nu_{12}$	$\nu_{13}$	$\nu_{23}$
AS4/3501-6	113.6	9.65	9.65	6.0	6.0	3.1	0.334	0.328	0.540
S2/3501-6	49.3	4.7	4.7	6.8	6.8	4.9	0.296	0.306	0.499

easily derived from conventional testing. For a calculation, assuming that the 2–3 plane is transverse isotropic, then:

$$E_3 = E_2, G_{13} = G_{12}, \nu_{13} = \nu_{12}, G_{23} = \frac{E_2}{2(1 + \nu_{23})}.$$

In this way, only the term  $\nu_{23}$  needs to be experimentally determined. The test values of  $\nu_{23}$  can be found in some sources. Table 4.15 presents the 3D elastic constants of CF and GF S2 reinforced epoxy composites. The values of  $E_1, E_2, \nu_{12}, \nu_{13},$  and  $\nu_{23}$  are derived from thick composite compression testing.

② 3D properties of multi-directional laminates (thick laminates):

As mentioned above, multi-directional laminates have nine material properties. The values of  $E_x, E_y, G_{xy}, \nu_{xy}$  can be easily derived from conventional testing or calculated by classical laminate theory; however, determining the out-of-plane properties is complex by both testing and theoretical approaches. Hence, there are fewer test data available for multi-directional laminates. Several theoretical methods are available; however, these approaches are based on unidirectional in-plane properties. Owing to the lack of available 3D testing data, it is difficult to verify theoretical calculations.

## 4.7 Analysis of Structural Stability

### 4.7.1 Stability Analysis of Laminates

The failure mode of thin panel structures of composite materials under compressive or shear loads is an instability known as buckling. Therefore, stability analysis is required to design these structures [2, 14].

For analysis the structure may be simplified as three components: ① rectangle laminates; ② stiffened stringers; ③ stiffened laminates.

Rectangular flat plates are widely used in numerous aerospace structures in the form of unstiffened panels and panels between the stiffened stringer of a stiffened panel, elements of a stiffened stringer and the skin of the air foil. The bending of the air foil skin is usually ignored in the analysis. The results of simulations with this assumption are relatively safe, but not conservative. The bending of fuselage skin cannot be ignored; however, in this section, only the air foil structure is discussed.

The stiffened stringer is an important component for enforcing the stability of the air foil skin. Commonly used section configurations include angle-, T-, Z-, I-, channel-, and hat-shaped stiffened stringers. It can be assumed that there is no shear load on the stiffened stringer; hence, only the compressive stability needs to be considered.

The skins of airfoils and the empennage are usually made of stiffened laminates. Hence these are the most widely studied components in stability analysis. Although global analysis is highly complex, programs based on the FEM are frequently used for calculations performed by computer. The performance of a preliminary design can be estimated by considering the rectangular plate and stiffened stringer separately.

Next, the stability analysis of three typical components/elements will be introduced.

#### 4.7.1.1 Buckling Analysis of Rectangular Flat Plates

Stability analysis of rectangle plates, also known as buckling analysis, is mainly concerned with the initial buckling load (or simply the buckling load).

Buckling load is related to the stiffness of the laminate, its dimensions (i.e., thickness, length, and width), and peripheral supporting conditions. Compared with isotropic metal plates, the stiffness of anisotropic laminates made from composite materials is complex. Stiffness not only depends on the thickness of laminates but also on the stacking sequence. In the case of symmetrical and balanced laminated plates, if  $\pm\theta$  cross-layers are stacked adjacently there are many layers with rigidity coefficients  $B_{ij} = 0$ ,  $D_{16} \approx 0$ , and  $D_{26} \approx 0$ . Commonly used laminated plates are orthotropic and can be simply considered under ideal boundary conditions (i.e., simply supported, fixed, and free) and under an evenly distributed load for axial pressure, and shear and transverse compression. With these assumptions, the



buckling load has a closed analytical solution. Therefore, the four edges of orthotropic laminated plate in supported conditions can be properly simplified: The ideal conditions are simply supported, fixed supported, and free boundary conditions. Engineers can apply existing closed formulae to calculate the buckling loads.

The calculation of buckling load in unbalanced and asymmetrical laminates is difficult. Calculations based on numerical methods are commonly used.

The next eight sections introduce calculations used to determine the buckling load of orthogonal anisotropic laminates under different loads and boundary conditions.

**(1) Uniaxial load, rectangular flat plate with all sides simply supported**

In the case of a rectangular flat plate with all sides simply supported and a compressive pressure applied equally to the two edges of a rectangular flat plate (Fig. 4.34), the formula of the buckling load is:

$$N_{xcr} = \frac{\pi^2}{b^2} \left[ D_{11} \left( \frac{b}{a} \right)^2 m^2 + 2(D_{12} + 2D_{66}) + \left( \frac{a}{b} \right)^2 \frac{D_{22}}{m^2} \right] \quad (4.31)$$

In this formula:

- $N_{xcr}$  —axial compressive buckling load per unit length;
- $m$  —buckling half-wave number along the  $x$ -axis of plate;
- $a, b$  —length and width of the plate;
- $D_{ij}$  ( $i, j = 1, 2, 6$ ) —bending stiffness factor of plate.

The parameter  $m$  can take the values 1, 2, 3, ... in the calculation, to determine a corresponding set. The minimum value of the set is the buckling load of the laminate,  $N_{xcr}$ .

**(2) Uniaxial load, laminates with loaded edges simply supported and unloaded edges fixed**

The case of a uniaxially loaded plate with the loaded sides simply supported and unloaded sides fixed is considered in Fig. 4.35. In this case, the calculation formula of the buckling load is:

**Fig. 4.34** Uniaxial load, rectangular flat plate with all sides simply supported

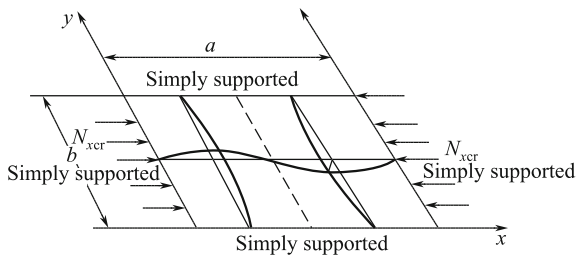


**Fig. 4.35** Uniaxial load, rectangular flat plate with loaded edges simply supported and unloaded edges fixed

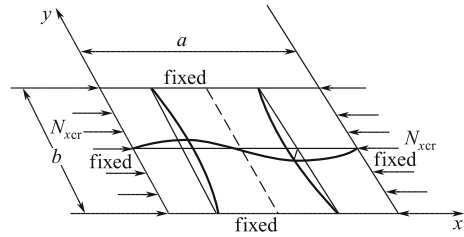
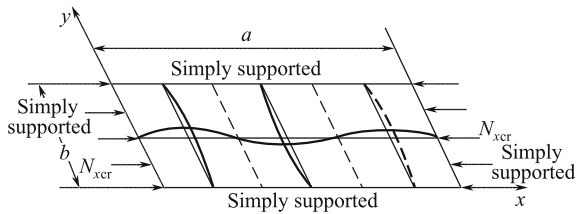


**Fig. 4.36** Uniaxial load, long plate with all sides simply supported



$$N_{xcr} = \frac{\pi^2}{b^2} \left\{ \begin{array}{l} D_{11} \left(\frac{b}{a}\right)^2 m^2 + 2.67D_{12} + \\ 5.33 \left[ D_{22} \left(\frac{a}{b}\right)^2 + D_{66} \frac{1}{m^2} \right] \end{array} \right\} \quad (4.32)$$

The parameter  $m$  can be 1, 2, 3, ... in the calculation to determine a corresponding set. The minimum value of the set is the buckling load of the laminate,  $N_{xcr}$ .

**(3) Uniaxial load of a long plate with all sides simply supported**

To calculate the buckling load of a long plate with a length-to-width ratio of  $a/b > 4$  and all sides simply supported under a compressive pressure applied equally to two edges (Fig. 4.36), the following formula is used:

$$N_{xcr} = \frac{2\pi^2}{b^2} \left[ \sqrt{D_{11}D_{22}} + D_{12} + 2D_{66} \right] \quad (4.33)$$

This formula can also be applied under the conditions when the two compressed edges are fixed.

Supporting experiments have demonstrated that the error of this calculation is within 10% for a long plate with a width-to-thickness ratio of  $b/t > 35$ ; however, in the case of a narrow plate with  $b/t < 35$ , the transverse shear effect must be considered and the calculation results should be revised.

**(4) Uniaxial load, long plate with all sides fixed**

In the case of a long plate with a length-to-width ratio  $a/b > 4$  and all edges fixed, when an even compressive pressure is applied to two edges (Fig. 4.37), the buckling load can be calculated from the formula:

**Fig. 4.37** Uniaxial load, long plate with all sides fixed

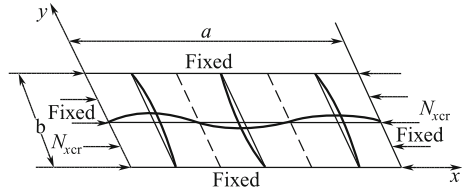
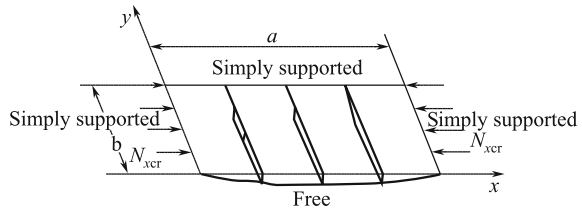


**Fig. 4.38** Uniaxial load, rectangular plate with three edges simply supported and one unloaded edge free



$$N_{xcr} = \frac{\pi^2}{b^2} (4.6\sqrt{D_{11}D_{22}} + 2.67D_{12} + 5.33D_{66}) \tag{4.34}$$

This formula can also be applied in the situation of two simply supported loading edges.

In the case of a narrow flat plate with a width-to-thickness ratio of  $b/t < 35$ , it is also necessary to consider the transverse shear effect and correct the calculation result.

**(5) Uniaxial load, long plate with three edges simply supported and one unloaded edge free**

When an equal compressive pressure is applied to two edges of a long plate with a length-to-width ratio of  $a/b > 4$  having three edges simply supported and one free unloaded edge (Fig. 4.38), the calculation to determine the buckling load is:

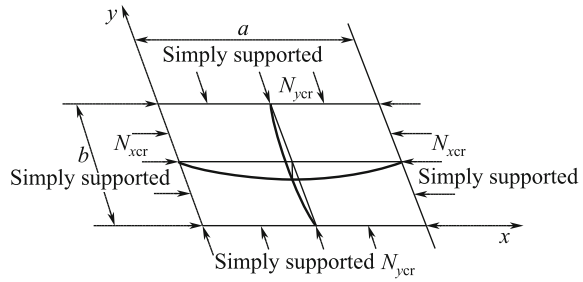
$$N_{xcr} = \frac{12D_{66}}{b^2} + \frac{\pi^2D_{11}}{a^2} \tag{4.35}$$

For a narrow flat plate, with a width-to-thickness ratio  $b/t < 20$ , it is also necessary to correct the calculation for the transverse shear effect.

**(6) Biaxial load, rectangular flat plate with all edges simply supported**

In the case of a rectangular flat plate with all edges simply supported and the short edges under an equal longitudinal compressive pressure  $N_x$  and the long edges under an equal transverse compressive pressure  $N_y$  (Fig. 4.39), the buckling load can be calculated from the formula:

**Fig. 4.39** Biaxial load, rectangular flat plate with all edges simply supported



$$N_{xcr} = \frac{\pi^2}{b^2} \left[ \frac{D_{11} \left(\frac{b}{a}\right)^4 m^4 + 2(D_{12} + 2D_{66}) \left(\frac{b}{a}\right)^4 m^2 n^2 + D_{22} n^4}{\left(\frac{b}{a}\right)^2 m^2 + \phi n^2} \right] \tag{4.36}$$

$$N_{ycr} = \phi N_{xcr}$$

In this formula:  $\phi$ —ratio of loading, i.e., the ratio of applied transverse to longitudinal loading;

$$\phi = N_y / N_x$$

$m$ —longitudinal buckling half-wave number;  
 $n$ —transverse buckling half-wave number.

For calculations, with  $m = 1, 2, 3, \dots$  and  $n = 1, 2, 3, \dots$ , then a corresponding set of  $N_x$  can be determined and the minimum value of  $N_x$  is  $N_{xcr}$ . The calculation gives good results with the use of  $n = 1$  and  $m = 1$ .

**(7) Shear load, flat laminate with all edges simply supported or fixed**

In the case of all four edges of rectangular flat laminate under an equal shear pressure (Fig. 4.40), the buckling load values of the four edges, in simply supported or fixed cases, can be calculated from the following formula:

$$N_{xycr} = K_s \frac{\pi^2 \sqrt{4D_{11}D_{22}^3}}{b^2} \tag{4.37}$$

where  $K_s$ —shear buckling load factor.

The  $K_s$  values of the four edges simply supported or fixed are different, and can be determined from the nine variables as the dimensionless parameters  $\alpha$  and  $\beta$  as illustrated in Figs. 4.41 and 4.42.

**Fig. 4.40** Shear load, rectangular flat plate with all edges simply supported or fixed

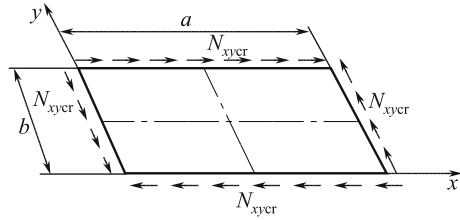


**Fig. 4.41** Shear buckling coefficient of rectangular flat plate with all edges simply supported

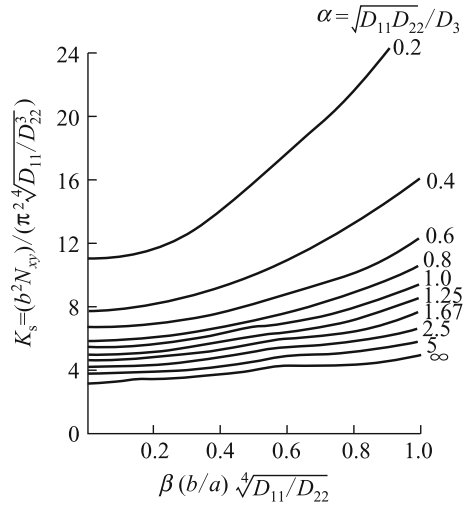


**Fig. 4.42** Shear buckling coefficient of rectangular flat plate with all edges fixed

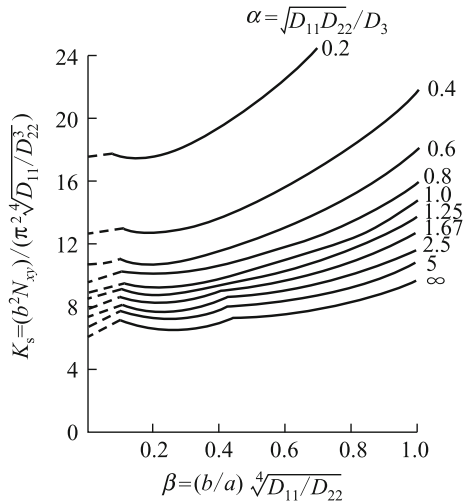
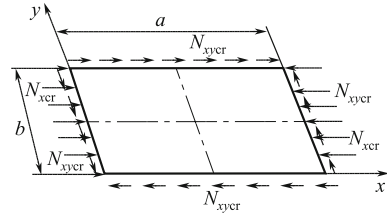


**Fig. 4.43** Rectangular flat plate with shear and compressive complex load



$$\alpha = \sqrt{D_{11}D_{22}/D_3}, \beta = \left(\frac{b}{a}\right) \sqrt{4D_{11}/D_{22}}, D_3 = D_{12} + 2D_{66}.$$

**(8) Flat laminate with complex shear and compression load**

In the case of a load on an orthogonal anisotropic rectangular flat plate, where two edges are under equal stress from complex shearing and compression  $N_x + N_y$  and an equal shear loading  $N_{xy}$  is applied to the side edge (Fig. 4.43), the buckling load value can be estimated from:

$$R_x + R_{xy}^2 = 1 \tag{4.38}$$

In this formula:  $R_x, R_{xy}$ —ratio of loading;

$$R_x = N_x/N_{xcr}^0, R_{xy} = N_{xy}/N_{xycr}^0$$

$N_{xcr}^0, N_{xycr}^0$ —buckling load of a laminate with uniaxial and pure shearing buckling load, respectively.

The safety margin of shearing and compression of laminates  $MS$  can be calculated from the method illustrated in Fig. 4.44.

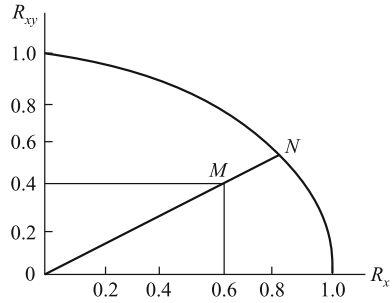
$$MS = \frac{\overline{ON}}{\overline{OM}} - 1$$

A flat laminate with all edges supported, which has already undergone buckling may still have some load-bearing ability, which is known as post-buckling strength. This parameter must be considered for supporting components/elements, and more details on post-buckling strength will be discussed in Sects. 4.7.1.2 and 4.7.2.3 of this chapter.

**4.7.1.2 Analysis of Buckling and Crippling of Stiffened Stringer**

Stiffened stringers used in construction are commonly composed of thin panel components made of laminated laths. In the analysis of the design of this

**Fig. 4.44** Diagram used to identify buckling safety margin of a rectangular flat plate with shear and compressive complex load



component, stiffened stringers can be decomposed or simplified into two kinds of laths: first, one long lath with one edge free, i.e., one unloaded edge simply supported, while another unloaded edge (or flange) is free; second, a long lath with no free edges, i.e., a web plate with two unloaded edges simply supported, as shown in Fig. 4.45. Analysis of stiffened stringer buckling and crippling should integrate estimated characteristics for all the constituent laths.

**(1) Buckling analysis of stiffened stringer components**

The buckling load values of two laths can be calculated with the formula presented in Sect. 4.1.1 of this chapter.

The buckling load of a web plate of a long lath with no free edge is given by:

$$N_{xcr} = \frac{2\pi^2}{b^2} [\sqrt{D_{11}D_{12}} + D_{12} + 2D_{66}] \tag{4.39}$$

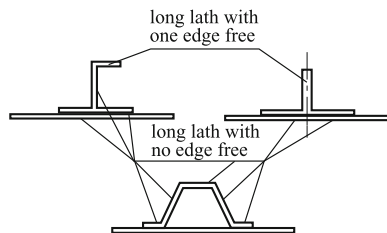
The buckling load of the flange of long lath with one free edge is given by:

$$N_{xcr} = \frac{12D_{66}}{b^2} + \frac{\pi^2 D_{11}}{L^2} \tag{4.40}$$

In these formula, the length of the stiffened stringer L is used instead of the length of the lath a, which appeared in the initial formula.

Equations (4.39) and (4.40) are only suitably for use with orthogonal anisotropic laminates and do not consider the effects of bending and torsion rigidity of laminates, i.e.,  $D_{16}$  and  $D_{26}$ . However, these two formulae are correct for most

**Fig. 4.45** Separation of stiffened stringer into long lath with one free edge and long lath with no free edges



symmetrical and balanced laminated plates. If the layering of laminates is slightly asymmetrical, the following equation can be applied for asymmetrical laminates to give results equivalent to those for orthogonal anisotropic laminates. Use the equivalent bending rigidity  $\bar{D}_{ij}$  in place of  $D_{ij}$  in previous formula, calculated as:

$$[\bar{D}] = [D] - [B][A]^{-1}[B] \tag{4.41}$$

In this formula:  $[A]$ ,  $[B]$ ,  $[D]$ —(tension) stiffness matrix, coupling stiffness matrix, bending stiffness matrix of in-plane laminate, respectively;

$[\bar{D}]$ —equivalent bending stiffness matrix of an equivalent orthotropic plate.

The partial buckling load of a stiffened stringer corresponds to the minimum buckling value of the constitute laths and can be determined by the following method:

It is assumed that the initial buckling stress  $\sigma_{cri}$  of the  $n$ th component of a stiffened stringer, where  $k$ -plate buckling stress  $\sigma_{crk}$  is minimum, is given by  $\sigma_{cri} = N_{xcri}/t_i$ ,  $\sigma_{crk} = N_{xcrk}/t_k$ .

The partial buckling stress of a stiffened stringer  $\sigma_{cr}^{st}$  is:

$$\sigma_{cr}^{st} = E_{xc}^{st} \left( \frac{N_{xcrk}}{t_k E_{xc}k} \right) \tag{4.42}$$

where:

- $N_{xcri}$  buckling load of  $i$ th plate element;
- $N_{xcrk}$  buckling load of  $k$ th plate element;
- $\sigma_{cri}$  buckling stress of  $i$ th plate element;
- $\sigma_{crk}$  buckling stress of  $k$ th plate element;
- $E_{xc}k$  equivalent compressive modulus along  $x$ -axial of  $k$ th plate element.

$$E_{xc}k = \frac{1}{t_k} \left( A_{11k} - \frac{A_{12k}^2}{A_{22k}} \right)$$

$E_{xc}^{st}$ —equivalent compressive modulus along  $x$ -axial of stiffened stringer;

$$E_{xc}^{st} = \frac{\sum_{i=1}^n \left( A_{11i} - \frac{A_{12i}^2}{A_{22i}} \right) b_i}{\sum_{i=1}^n b_i t_i}$$

- $t_k$  thickness of  $k$ th plate element;
- $t_i$  thickness of  $i$ th plate element;
- $b_i$  width of  $i$ th plate element;
- $A_{11k}, A_{12k}, A_{22k}$  in-plane stiffness coefficient of  $k$ th plate element;
- $A_{11i}, A_{12i}, A_{22i}$  in-plane stiffness coefficient of  $i$ th plate element.



## (2) Crippling of stiffened stringer

After one layer of a stiffened stringer undergoes initial buckling, i.e., an externally applied load reaches the partial buckling load, the stiffened stringer may continue to bear some load. For a stiffened stringer in this post-buckling phase, further increases in the externally applied load, i.e., the axial compressive load, may induce two modes of deterioration. One mode is an overall buckling instability for long stiffened stringers; another is deterioration through partial crippling for a short stiffened stringer, also known as crippling.

Post-buckling analyses of the two kinds of laminated plates that are used in stiffened stringers involve geometric nonlinearities. Furthermore, the stress–strain curve of a laminate with a higher percentage of  $\pm 45^\circ$  layers shows considerable nonlinear behavior before initial buckling. Thus, specific programs based on nonlinear buckling theory are required to analyze the intensity of crippling.

At the beginning of the design, designers are reluctant to or unwilling to analyze the complicated nonlinear characteristics of a large number of preselected laminates, including the layering characteristics and width-to-thickness ratio of  $b/t$ . Thus, to estimate the intensity of crippling, a better solution is to apply the results of experiments and semiempirical relationships.

Here we introduce experiments used to determine the crippling intensity of a stiffened stringer, and calculation methods used to estimate the crippling intensity of a long stiffened stringer.

- (1) Crippling intensity experiments of a stiffened stringer: Fig. 4.46 shows the shape deformation of angle- and channel-shaped stiffened stringers undergoing crippling. The in-plane cross section of a stiffened stringer becomes distorted because part of the plate elements is buckled. However, the whole stiffened stringer is not deflected and cross lines (i.e., crest lines) of all the plate elements remain straight.

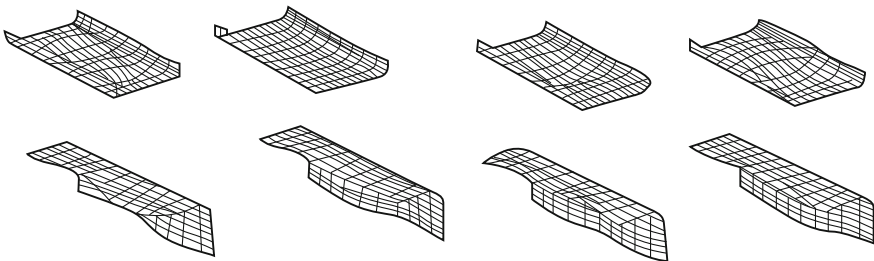


**Fig. 4.46** Crippling deformation of angle- and channel-shaped stiffened stringers

**Fig. 4.47** Loading–displacement diagram of a plate element with no free edge

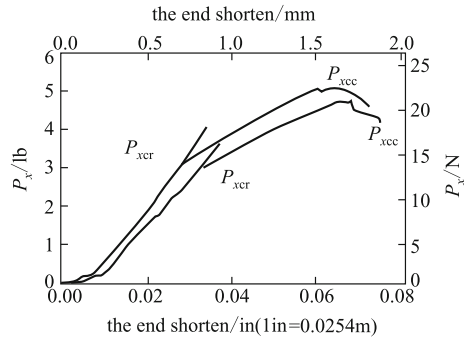
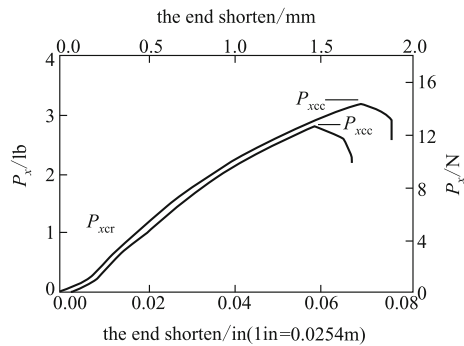


**Fig. 4.48** Loading–displacement diagram of a plate element with one free edge



An experiment, which is specific to two typical plate elements of the stiffened stringers, may be performed. Figures 4.47 and 4.48 show loading displacement diagrams for no free edge and one free edge test specimens, respectively, under axial compression. After the phase of initial buckling ( $P_{xcr}$ ), the rigidity of the plate considerably decreased in the post-buckling phase. When the pressure reached  $P_{xcc}$ , the test specimens were destroyed.

Figures 4.49 and 4.50 show experimental dimensionless crippling curves,  $\sigma_{cc}/\sigma_{cu} \sim b/t$ , of laminates with no free edge and one free edge, respectively. In these dimensionless curves the  $y$ -coordinate is the ratio of the crippling stress to the compressive strength limit of the materials comprising the laminate. The  $x$ -coordinate is the width-to-thickness ratio  $b/t$  of the laminate. However, in these crippling curves, the compressive ability of the laminate is dimensionless and the effects of bending rigidity of the laminates are not considered. Although the compressive ability of materials may be similar, the buckling and crippling may be different owing to different layering order, which gives different bending rigidity.

For this reason, the curves in Figs. 4.49 and 4.50 have little practical value, and further work is necessary to determine the effect of the layering order of laminates on bending rigidity.

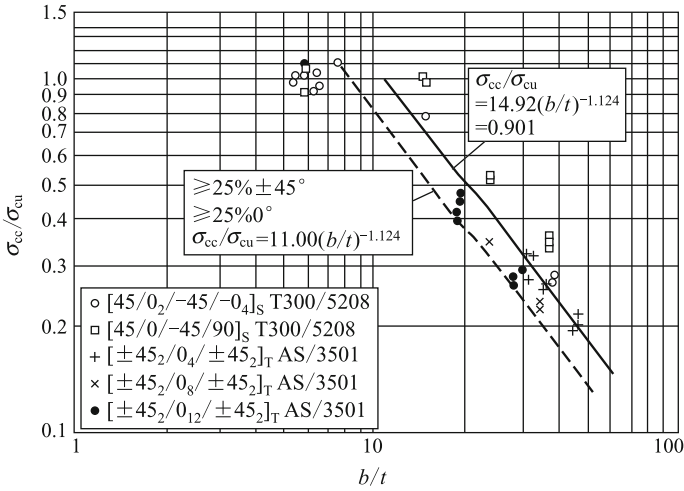


Fig. 4.49 Crippling curve of plate element with no free edge

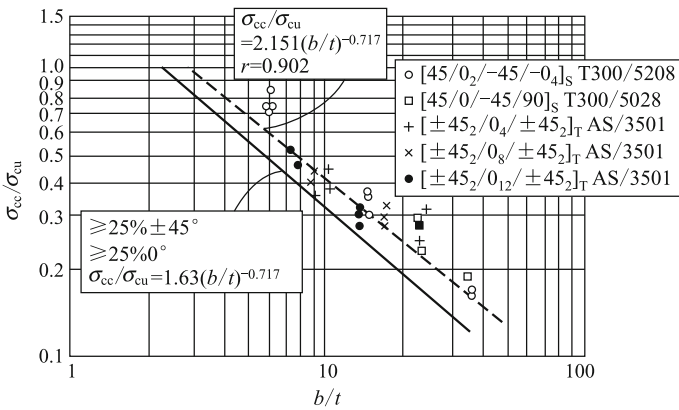


Fig. 4.50 Crippling curve of plate element with one free edge

The crippling curves in Figs. 4.51 and 4.52 are corrected crippling curves of two kinds of laminates with one free edge and no free edge, respectively.

The y-coordinate is the dimensionless crippling stress  $\frac{\sigma_{cc}}{\sigma_{cu}} \left( \frac{E_{xc}}{E} \right)$ ; the x-coordinate is the dimensionless ratio of width to thickness  $\frac{b}{t} \left( \frac{\bar{E}}{E_{xc}} \sqrt{\frac{\sigma_{cu}}{E_{xc} E_{yc}}} \right)$ , and

$$\bar{E} = \frac{12D_{11}}{t^3} (1 - \nu_{xy}\nu_{yx}) \tag{4.43}$$

**Fig. 4.51** Corrected crippling curve of laminated plate element with one free edge

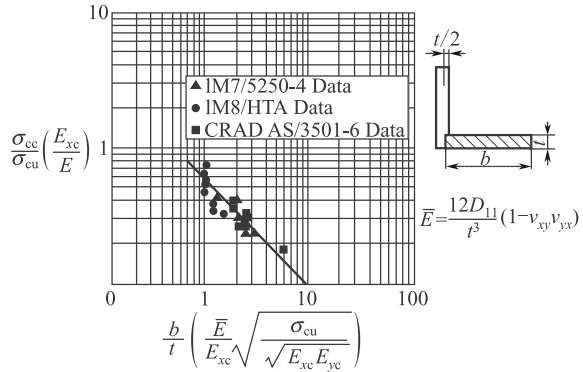
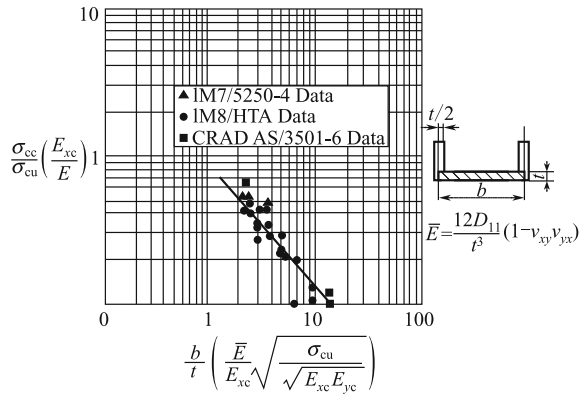


**Fig. 4.52** Corrected crippling curve of laminated plate element with no free edge



where

- $D_{11}$  —bending stiffness coefficient of laminate;
- $\nu_{xy}, \nu_{yx}$  —Poisson’s ratio of the laminate;
- $E_{xc}, E_{yc}$  —equivalent longitudinal and transverse compressive moduli of laminate;
- $b$  —laminated width;
- $t$  —laminated thickness;
- $\sigma_{cu}$  —compressive strength (ultimate);
- $\sigma_{cc}$  —crippling strength (stress).

The values of  $E_x$  ( $E_{xc}$ ),  $E_y$  ( $E_{yc}$ ),  $\nu_{xy}$  and  $\nu_{yx}$  of a symmetric laminated plate can be calculated from the following formulae.

$$E_x = \frac{1}{t} \left( A_{11} - \frac{A_{12}^2}{A_{22}} \right)$$

$$E_y = \frac{1}{t} \left( A_{22} - \frac{A_{12}^2}{A_{11}} \right) \quad (4.44)$$

$$\nu_{xy} = \frac{A_{12}}{A_{22}}$$

$$\nu_{yx} = \frac{A_{12}}{A_{11}}$$

(2) Identification of crippling rigidity of a stiffened stringer: According to curves from previous experiments, the crippling rigidity of a stiffened stringer can be identified by the following procedures:

- ① Break down the stiffened stringers into two plate element groups, i.e., one-free-edge and no-free-edge groups.
- ② Certify the crippling stress of every plate element according to Figs. 4.51 and 4.52; when applying the width-to-thickness ratio determine  $\sigma_{cc}$  for every plate element, the values of  $E_x$ ,  $E_y$ ,  $\nu_{xy}$ ,  $\nu_{yx}$ , and  $\bar{E}$  should be calculated from Eqs. 4.44 and 4.45 to determine the value of  $\sigma_{cu}$ .
- ③ The limiting value of the crippling stress of a laminated plate  $\sigma_{cu}$  can be determined experimentally or estimated from the following formula:

$$\sigma_{cu} = E_{xc} \varepsilon_c$$

where

$E_{xc}$  —equivalent longitudinal modulus of elasticity of laminate;

$\varepsilon_c$  —compressive strain design allowable value of composite laminate.

- ④ Apply the following formula to determine the weighted contribution of crippling stress of each plate element of the composite laminated plate. The crippling stress of a stiffened stringer can be determined from:

$$\sigma_{cc}^{st} = \frac{\sum_{i=1}^N \sigma_{cci} b_i t_i}{\sum_{i=1}^N b_i t_i} \quad (4.45)$$

where

$\sigma_{cci}$  —crippling stress of  $i$ th stringer;

$b_i$  —width of  $i$ th stringer;

$t_i$  —thickness of  $i$ th stringer;

$N$  —number of stringer.

Note: if the value  $\sigma_{cc}$  of one plate element is higher than its  $\sigma_{cu}$ , the whole calculation should use  $\sigma_{cu}$  instead.

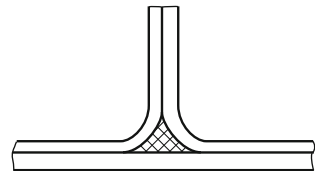
- (3) Some issues should be considered when calculating the crippling stress of a stiffened stringer.
- ① The data in Figs. 4.51 and 4.52 are taken from experiments based on a stiffened stringer with uniform thickness. If the thickness of a single plate element in the stiffened stringer differs greatly, the thicker plate elements will give greater resistance than the thinner plate elements and enhance the buckling and crippling stress of the thinner plate elements. However, the buckling and crippling stress of the thicker plate elements will also be reduced. Therefore, the crippling stress of the affected plate element should be modified. The crippling stress of a stiffened stringer depends on the plate elements that will undergo buckling or crippling first.
  - ② Consideration of fillets: As shown in Fig. 4.53, a 0°-material is used to fill the corners of stiffened stringers, and these materials can boost the crippling rigidity of the stiffened stringer. The area of the fillets under pressure is directly proportional to the square of the corner radius. Thus, the larger the corner radius, the greater the enhancement on the crippling rigidity. The following formula can be used to estimate the enhanced crippling stress:

$$\bar{\sigma}_{cc}^{st} = \left( \frac{1 + \frac{E_f A_f}{\sum E_i b_i t_i}}{1 + \frac{A_f}{\sum b_i t_i}} \right) \sigma_{cc}^{st} \quad (4.46)$$

where

- $\sigma_{cc}^{st}$  crippling stress of stiffeners (without fillets);
- $\bar{\sigma}_{cc}^{st}$  crippling stress of stiffeners (with fillets);
- $A_f$  cross-sectional area of fillets;
- $E_f$  equivalent longitudinal modulus of elasticity of fillets.

**Fig. 4.53** Sketch of corner stuffing in a stiffened stringer



- ③ Modification of the slenderness ratio: A stiffened stringer may become unstable as its length is increased, but it will not undergo partial crippling. A modification engineering method is introduced to adjust the crippling stress by considering the slenderness ratio. The slenderness ratio  $L'/\rho$  of a stiffened stringer can be considered as a pressured column, where  $L' = L/\sqrt{C}$  is a valid length of a stiffened stringer, and  $C$  is the supporting coefficient of the end of the stiffened stringer. The value of  $C$  can be in the range 1–4, but it is generally assumed that  $C$  is 2.0.  $\rho$  is the gyration radius of the cross section of the stiffened stringer. With the use of the formula:

$$\rho = \sqrt{\frac{(EI)_{st}}{(EA)_{st}}} \tag{4.47}$$

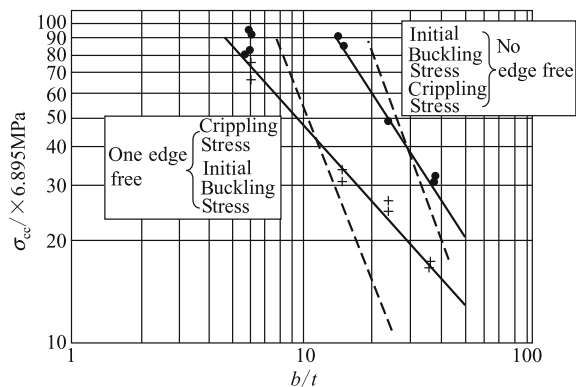
where  $(EA)_{st}$  and  $(EI)_{st}$  are the tensile or compression rigidity and the bending rigidity, respectively. These two values may be calculated from Eqs. (4.53) and (4.54), given in Sect. 4.7.2.3 of this chapter. The critical stress of a stiffened stringer is:

$$\sigma_{cr} = \sigma_{cc} \left[ 1 - \frac{\sigma_{cc}}{4\pi^2 E_{xc}} \left( \frac{L'}{\rho} \right)^2 \right] \tag{4.48}$$

If the value of  $L'/\rho$  is greater than 12, this formula may require some modifications.

- ④ In Fig. 4.54, the broken line represents the calculated initial buckling stress compared with experimental results from plate elements with one free edge and with no free edges. The solid lines show crippling stress data from corresponding experiments. The calculated initial buckling stress is smaller than the experimental values when  $b/t$  is great, i.e., in the case of a thin plate. The value of the calculated initial buckling stress is larger than the experimental value when  $b/t$

**Fig. 4.54** Comparison of calculated initial buckling and crippling stresses with experiment results for plate elements with one free edge and no free edge



$t$  is small, i.e., in the case of a thick plate. Thin plates undergo buckling at a lower stress; however, thin plates can undergo greater loading in the post-buckling phase. Therefore, the estimate of the loading of a thin plate from its initial buckling stress is conservative. For the thick plate, the loading will recede because of the crosswise shear effect and these calculations do not give reliable results.

In summary, it is necessary to consider partial buckling and crippling intensity together when analyzing the stability of a stiffened stringer. If the laminated plate elements are thin, the lower initial partial buckling stress is a conservative estimate of the loading of a plate element. If the laminated plate elements are thick, applying the initial partial buckling stress without consideration of the crosswise shear effect will overestimate the loading of the stiffened stringer.

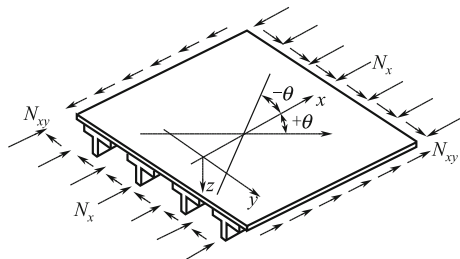
#### 4.7.1.3 Stability Analysis of Stiffened Stringer

Stiffened stringers are a typical component used in airfoil structures. The stability of a stringer is enhanced when it is reinforced with a cover. Part of the stiffened stringer between two wing ribs and two wing spars should be analyzed to consider the stability of the whole design. For convenience, the structure can be simplified as a set of parallel stringers and the dimensions and materials (i.e., layering) of a section plane of the stringers are same, with equal spacing. The slight lateral curvature of a stiffened stringer may be ignored, as shown in Fig. 4.55. This approach is widely accepted by engineers.

The loading situations of stiffened stringers can be divided into three categories: axial compression loading (along the length direction of the stiffened stringer), shear loading, and combinations of shear and compression loadings.

Failure modes of instability can be divided into four categories: ① covers between stringers or parts of the stringers buckling; ② general instabilities of the stiffened stringer. A long stiffened stringer can be considered as a wide column with the use of Euler instability under axial compression; ③ crippling damage that may occur in a short stiffened stringer under axial pressure; ④ a combination of the previously mentioned Modes ① and ②.

**Fig. 4.55** Diagram of laminated reinforced stringer





Medium long stiffened stringers, widely used in airfoils, typically undergo failure through Mode ④. The covers between stringers become partially buckled and enter into the post-buckling phase. Under greater loading, the partial flexural wave of the cover gradually expands and passes through the stiffened stringers. These stringers are subjected to strong bending and torsion, leading to instability. Sometimes, the load on damaged stiffened stringers may be reduced by damage to the cover or stringer before general instability occurs.

The stability analysis of stiffened stringers is complex and requires special programs based on FEMs, including: MSC/NASTRAN, BAFLCP, CPANDA, and COMPOSS. These programs have different merits and scopes of application. Most of these programs are based on linear buckling theory and thus can only be applied to calculate the partial buckling load of covers or stringers and the general buckling load of a stiffened stringer. Only the COMPOSS program can be used to analyze the loading of a stiffened stringer in the post-buckling phase and give the limiting loading of a reinforced stringer.

In the initial design phase, the following simplified methods are used to estimate the stability of a stiffened stringer:

- (1) A dense stiffened stringer, which has a compact arrangement of stringers, can be considered to be a smooth plate for estimates of its general buckling load. The method for calculating the equivalent rigidity of a stiffened stringer is given in Appendix A: Directory of structural stability analysis of composited materials.
- (2) In the case of widely spaced stiffened stringers, the partial initial buckling load and crippling intensity of the covers between the stringers and that of the reinforcing stringer can be estimated separately. The partial initial buckling load of covers between stringers can be calculated from the formula given in Sect. 4.7.1.1 of this chapter. Initially, the supporting conditions of all sides of the covers should be regarded as ideal boundary (supporting) conditions. The ideal boundary of a reinforced stringer or wing rib is the supported boundary condition. The reinforced stringer or wing rib can be regarded as a fixed supported boundary condition. The subjacent end of a reinforced stringer connected with the cover can be regarded as a no free edge plate element, with two edges simply supported, when calculating the initial buckling load and crippling intensity of a stiffened stringer.
- (3) Some specific programs can be applied to the simplify the methods for estimating the general stability of a whole stiffened stringer.
- (4) Continuous loading analysis of covers or parts of reinforced stringers in the post-buckling phase can only be estimated for the limiting loading of a reinforced stringer at a certain axial pressures. This topic will be introduced in Sect. 4.7.2.3.

### 4.7.1.4 Influence of Layering Order on Stability

Structural stability depends on the rigidity of the structure and the rigidity of the support conditions (i.e., the boundary supporting conditions). The structural stability of laminated plate is closely related to the layering order. Hence, it is necessary to consider the influence of layering order on stability in the design phase.

#### (1) Influence of layering order on buckling of laminated plate

The buckling load of laminated plate is related to layering order, loading environment, geometric dimensions, and boundary supporting conditions. Thus, there are no general rules for setting the best layering order of a laminated plate. Specific analyses are needed for specific loading situations, geometric dimensions, and boundary conditions.

To enhance the buckling load of a laminated plate, the following observations may help guide layering design:

- (1) Symmetrical and balanced laminated layering are adopted in most cases, except for situations with special requirements, such as requirements for aeroelastic tailoring. To avoid plate deflection caused by coupling of flexural tension and bending, let  $B_{ij} = 0$ ,  $D_{16} \approx 0$  and  $D_{26} \approx 0$ . This deflection is equal to the amount of initial deflection of a laminated plate and it will decrease the buckling load.
- (2) For a rectangular laminated plate that is under pressure along its length, a higher buckling load may be achieved when  $\pm 45^\circ$  plies are layered on the surface of the laminated plate.
- (3) For a rectangular laminated plate that is under pressure along its width, a higher buckling load may be achieved when  $0^\circ$  plies are layered on the surface of the laminated plate.
- (4) The maximum buckling load of a laminated plate under a given shear stress is achieved when  $\pm 45^\circ$  plies are layered on the surface of the laminated plate. The buckling load value of a plate under positive shear stress is lower, than that of a plate under negative shear stress, as shown in Fig. 4.56. This effect is attributed to the  $D_{16}$  and  $D_{26}$  values of the plate. The buckling loads of an orthotropic plate are the same no matter if the plate is under positive or negative shear stress.

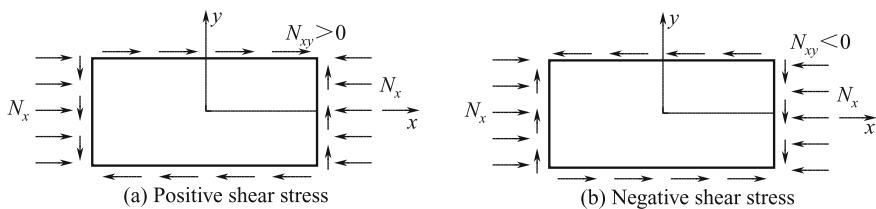
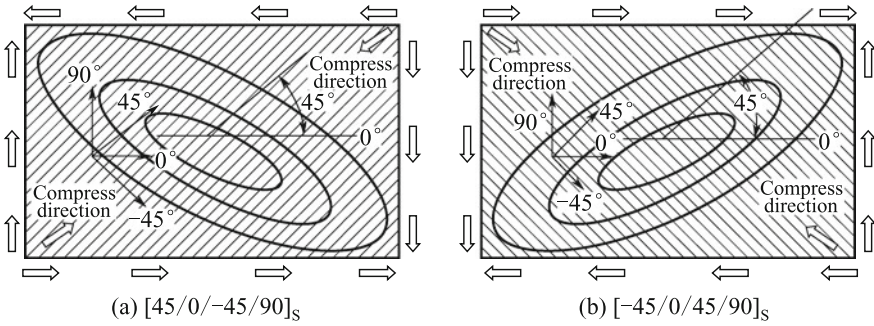


Fig. 4.56 Rules for shear plates under positive and negative shear stress



**Fig. 4.57** Illustration of the 45°-surface fibers along the compression direction under combined shear stress

For symmetrical laminated plates, where  $D_{16} \neq 0$  and  $D_{26} \neq 0$ , the fibers on the outer surfaces may allow for a higher buckling load when the plate is under a combination of shear stress in the pressure direction, as illustrated in Fig. 4.57.

- (5) The behavior of a laminated plate under combined stress from pressure and shear loading is an unusual situation because of the effects of  $D_{16}$  and  $D_{26}$ . In Sect. 4.1.1 of this chapter, a pressure and shear stress formula is presented for orthotropic laminated plates ( $D_{16} = 0, D_{26} = 0$ ):

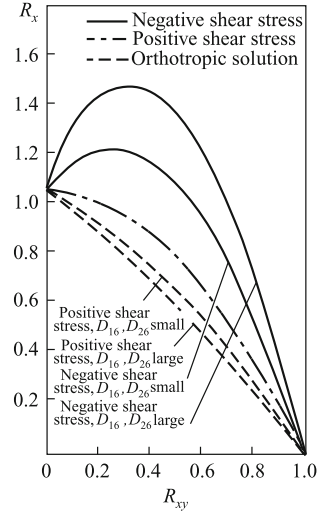
$$R_x + R_{xy}^2 = 1$$

Thus, a parabola may be defined in this the coordinate plane, to describe the pressure load-to-shear load ratio with  $R_x$  and  $R_{xy}$  as coordinates.

A related parabola for shear buckling of a symmetrical laminated plate under pressure and shear stress loading can also be defined. When  $D_{16} \neq 0$  and  $D_{26} \neq 0$ , the parabola may be distorted becoming more prominent or concave according to the different direction of the shear stress (i.e., positive or negative shear stress). Figure 4.58 shows buckling curves of a symmetrical laminated plate, with  $D_{16} > 0$  and  $D_{26} > 0$ , undergoing combined pressure and shear stress loading in the positive and negative directions. As shown in the figure:

- ① In the case of  $D_{16} > 0$  and  $D_{26} > 0$ , a negative shear stress makes the parabola more prominent, indicating an enhancement of the buckling load under axial pressure. A positive shear stress makes the parabola concave and reduces the buckling load under axial pressure. Furthermore, higher values of  $D_{16}$  and  $D_{26}$  have a more prominent effect on the concaving of the parabola.
- ② In the case of  $D_{16} < 0$  and  $D_{26} < 0$ , the influences of negative or positive shear stress on the buckling curves have the opposite effect. Thus, negative shear stress makes the parabola concave and decreases the buckling load under axial pressure; however, a

**Fig. 4.58** Curves of pressure and shear stress buckling of symmetric laminated plate under negative/positive shear stress, with  $D_{16} > 0$  and  $D_{26} > 0$



positive shear stress makes the parabola more prominent and increases the buckling load under axial pressure.

According to results from experiments, the influence of this effect is related to the length-to-thickness ratio, boundary conditions, and the ratio of the lateral elasticity modulus to the transverse elasticity modulus ( $E_x/E_y$ ). In the case of a laminated plate with four fixed supported edges, the effects of the shear stress direction (positive or negative) are stronger than the case of a laminated plate with four edges simply supported. A higher value of  $E_x/E_y$  indicates a stronger influence of the shear stress direction.

To increase the buckling load, the outer plies should have a fiber direction  $45^\circ$  to the compressive direction of the combined shear forces.

**(2) Effects of layering order on partial buckling and crippling of stiffened stringer**

Experimental data indicate that a  $0^\circ$  ply layer near the surface layer of a laminated plate element in a stiffened stringer will induce minimum values of partial buckling and crippling load of the reinforced stringer.

However, in terms of bending rigidity, the influence of the dimensions of the stiffened stringer is stronger than the influence of the layering order. For example, the Euler buckling load of an I-shaped reinforced stringer section depends on the cross-sectional dimensions of its flange and web plate. The influence of layering order is considerably reduced as the height of a middle I-shaped web plate is increased. Hence, the Euler buckling load has no relationship with layering order.

**(3) The influence of layering order on stability of a stiffened stringer**

The influence of layering order on the stability of a stiffened stringer is complicated and related to the instability failure modes of the reinforced stringer as well as the support conditions of the reinforced stringer with a cover.

- (1) Partial buckling or crippling of a stiffened stringer are unrelated to the layering order. However, the buckling load of a covered composite stiffened stringer, as well as post-buckling of the cover are affected by the layering order of the cover.
- (2) For the case of a stiffened panel with stronger stiffeners under an axial pressure, the buckling load of the axial pressure will decrease because the transverse distortion of the cover is restricted. Namely, the transverse distortion of the cover (free expansion) is restricted by the stiffened panel and additional transverse pressure is introduced because of the Poisson effect. Thus, the cover is under a two-way compression such that its buckling load in the axial pressure direction decreases. The level of this decrease is directly proportional to the Poisson ratio of the cover ( $\nu_{yx}$ ). The value of  $\nu_{yx}$  can be calculated from the following formula:

$$\nu_{yx} = A_{12}/A_{11}$$

where  $A_{11}$ ,  $A_{12}$ —in-plane stiffness coefficients of the skin.

In this situation, the design should aim to reduce the  $\nu_{yx}$  value of the layering.

### ***4.7.2 Overview of Post-buckling and Post-buckling Strength Analysis***

The classic theory of linear buckling has been used to analyze the stability of structures in engineering. According to this theory, when a structure has achieved the critical state of initial buckling, its normal deformation (deflection) suddenly increases arbitrarily. This means that the structure loses its load-bearing capacity. In practice, when the skin of a thin-walled stiffened structure of a plane features local buckling, the structure generally maintains the ability to bear load, which is known as post-buckling strength. For structures designed according to their initial local buckling stress as the limiting allowable stress, the post-buckling strength of the structure is not used. Thus, the potential load-bearing capability of a structure is not fully accounted for [3, 16].

To explain the differences between the practical stabilities of structures and the stability calculated based on the theory of linear buckling, nonlinear large deflection buckling theory has been proposed. This theory is based on in-depth theoretical and experimental studies of post-buckling behavior of structures.

The structural stability analysis involves complicated elastic–plastic and mathematical theory. Analysis of a simple rectangular symmetric laminated panel by linear buckling theory requires the solution of high-order partial differential equations. However, nonlinear large deflection buckling theory requires even more complex calculations. Thus, although the foundations of this theory were laid in at the beginning of the twentieth century, it has not been widely applied in practice. In the 1960s, the emergence and rapid development of the FEM and advances in computing power provided the necessary tools to resolve the issues of a nonlinear field and enable practical application of the theory. Over the past three decades, post-buckling strength issues of structures have aroused considerable interest in the engineering sector.

The development and application of advanced composite materials has to on some extent depend on the discovery and use of this capability to determine the load a material can withstand beyond its initial buckling.

The analysis and solution of the large deflection theory of nonlinear buckling are complex and burdensome. The following sections introduce the basic concepts of nonlinear large deflection buckling theory and present a few examples of its application to analyzing post-buckling structural characteristics. The use of this theory in projects is also discussed.

#### **4.7.2.1 Characteristics of Post-buckling Analysis**

In this section, nonlinear large deflection buckling theory and linear buckling theory are compared in terms of analysis, processing, and the solutions derived. The basic concepts and features of post-buckling issues are introduced.

- (1) The post-buckling problem involves analysis of a structure from initial buckling to damage and failure.

Linear buckling theory analysis indicates that when a structure has achieved the critical state of initial buckling, its deformation (deflection) increases arbitrarily, and the load-bearing capacity is suddenly lost. It necessary to determine the load and buckling mode of the initial buckling of a structure.

Nonlinear post-buckling theory can be used to solve the deformation and forces acting on a structure from the initial buckling to damage to the failure. This approach involves both stability analysis and requires judgement of the failure related to the intensity of the damage. Thus, analysis of post-buckling unifies the analysis of the stability and the issue of strength. In the analysis, many factors that affect the stability and strength of the structure should be considered, including: the impact of damage, initial defects, temperature and humidity, and guidelines of material damage.

- (2) In the analysis of post-buckling of a structure, the impact of a large deformation needs to be considered to accurately describe the state and strength characteristics.

Linear buckling theory analysis establishes the equilibrium equations for the initial position and shape of the structure and, therefore, does not reflect the impact of structural deformation on the equilibrium state.

In practice, a structure under a load undergoes some deformation. After the initial post-buckling deformation, the structure will enter a buckled state. Analysis by theory of nonlinear buckling considers the structure and processes that might change the position and shape of the structure from their equilibrium values. This analysis allows for a more accurate description of the structure and the forces acting on it and can more truly reflect the characteristics of the system.

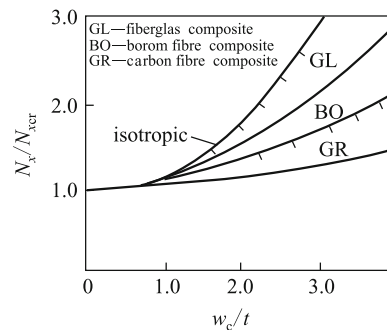
- (3) Post-buckling analysis of a structure is calculated from progressive data sets in the moment after a load is applied to the structure. The structure's stiffness after deformation as well as changes in its position and shape are recalculated in iterations. This analysis can determine whether a process will undermine the strength of a structure but requires an understanding of the structure and the acting forces.
- (4) The use of FEMs for linear buckling analysis of a structure can be reduced to solving a set of linear algebraic equations equal to zero for the determinant of a coefficient matrix of the eigenvalue problem.

The FEM and nonlinear buckling analysis require the solution of the nonlinear algebraic equations in repeated iterations. Accurate calculations and convergence are not always achieved. Thus, nonlinear analysis calculations are a specialized research field.

#### 4.7.2.2 Reinforced Laminates and Post-buckling Laminate Properties

Recently, some practical post-buckling analysis procedures based on nonlinear buckling theory of structures have been introduced. These include ABAQUS, ADINA, ANSYS, ASKA, and MARC. For analysis of the buckling of composite structures and destruction post-buckling, a dedicated software, COMPOSS, has been developed in China.

**Fig. 4.59** Axial load–deflection curves for laminated square plate simply supported on four sides by metal square plates



The following procedures may be followed for calculations of laminate composite materials, reinforced laminates with COMPOSS based on post-buckling analysis of a phase curve (path), to reveal the characteristics of subsequent buckling.

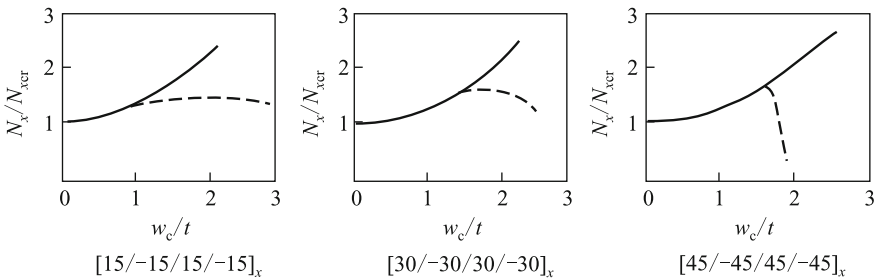
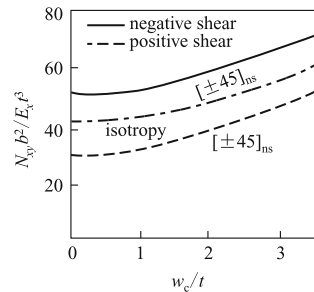
Figure 4.59 shows the axial load–deflection curve ( $N_x/N_{xcr}-t$ ) for an isotropic laminated composite simply supported on four sides with metal side plates.  $N_x$  is the initial buckling load,  $w_c$  is the normal displacement of center point (deflection), and  $t$  is the thickness. For initial post-buckling as the deflection increased, the plates continued to show considerable load-bearing capacity.

Figure 4.60 shows the  $N_{xy}$ -deflection curve ( $N_{xy}b^2/E_x t^3 - w_c/t$ ) of a laminated composite square plate simply supported on four sides with metal side panels, under a pure shear load.

With  $b$  as the width and  $t$  as the thickness, along the  $x$  direction for the plate, having a Young’s modulus  $w_c$ . The positive and negative shear loads of the laminates show different post-buckling performance.

Figure 4.61 shows axial damage path diagrams ( $N_x/N_{xcr} - w_c/t$ ) of clamped laminated composite square plates in a post-buckling state. The solid lines in the figure represent a calculation, which does not consider an internal damage path,

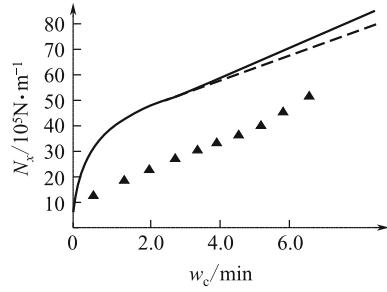
**Fig. 4.60** Shear load–deflection curves of, laminated square plate simply supported on four sides by metal side panels



**Fig. 4.61** Damage path in clamped laminated square plates composed of three layers with axis 15°, 45°, 30°



**Fig. 4.62** Axial load–deflection curves of longitudinally reinforced laminates



while the dashed line shows a calculation considering the path of an internal damage. The laminate may undergo gradual failure indicated by the dashed line showing a gradual downward trend or a more sudden failure indicated by a sharp downward trend. Analysis of the former case suggests that failure occurred owing to tension caused by destruction of fibers. The latter case reflects tension (pressure) caused by the destruction of the matrix.

Figure 4.62 shows the load–deflection curve ( $N_x$ – $w_c$ ) of a vertical reinforced composite laminate material and skin layer, clamped at both ends under axial compression with two simply supported edges (taken from a NASA report). The focal points for deflection of the skin map, respectively, are given for a thin mesh (solid line), a dense grid (dashed lines), and theoretical calculations and experimental measurement points (triangles).

There is clearly a large difference between the theoretical values and the test results. In the theoretical analysis and experimental measurements of the reinforced laminates, the presence of geometric defects and internal damage, or improper handling of boundary conditions will cause errors in the results of theoretical calculations and experimental measurements.

### 4.7.2.3 Post-buckling Strength in a Project

Wing structures based on laminate composite materials and reinforced laminates have been the focus of most post-buckling analysis. It is desirable to evaluate the buckling load-bearing capacity to further reduce weight and increase efficiency.

FEMs are useful analytical procedures, but other factors that can affect the results must also be considered, such as initial flaws in the geometry and materials. Factors such as internal damage and the degree of damage require further evaluation by the user. Minimizing the number of iterations necessary for convergence of an analysis also requires the user to have sufficient professional knowledge and problem-solving experience. Furthermore, finite element analysis features a number

of common problems, including element selection, model simplification, mesh generation, and boundary condition treatment. These features bring considerable difficulties when used in engineering. Thus, it is necessary to adopt a consistent approach to experimental studies and projects as a whole.

Here, the subjects of axial compression of laminates and stiffened panel structures are discussed in terms of developing practical approaches to a project:

- (1) For the skin, the post-buckling laminate load-bearing capacity can be estimated by the effective width method;
- (2) For reinforcement of the post-buckling load-bearing capacity, tests can be used based on pressure loss curve estimates;
- (3) For a stiffened plate, the post-buckling load-bearing capacity can be estimated with the use of subtreatment and effective width methods.

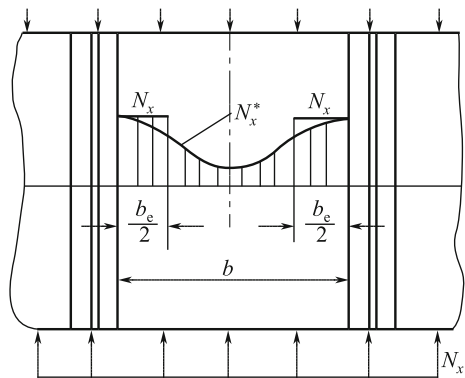
Test data are lacking for complex shear and pressure loading behavior. Therefore, the following considers a limited number of topics, including: axial load on laminated boards, reinforced laminates, and post-buckling load-bearing capacity.

- (1) Estimation of post-buckling laminate load-bearing capacity:

In the case of a reinforced laminate (skin) under uniform pressure at both ends and with both edges supported, the initial post-buckling and the distribution of compressive stress gradually become uneven. Before buckling occurs, as the pressure increases the middle part of the plate will feature alleviated stress. Test results show that the lateral distribution of stress takes the form shown in Fig. 4.63. With reference to treatments of metal plates, an effective width, or reduced width may be introduced. The width of the pressure effect may be reduced by multiplication by  $N_x$  to estimate the change in stress distribution over the board and the post-buckling load-bearing capacity. The effective width can be expressed as:

$$b_e = \varphi b \tag{4.49}$$

**Fig. 4.63** Reinforced skin between the local buckling stress distribution



where  $b_e$  is the width and  $\varphi$  is the effective width coefficient, determined from experimental data.

A relationship for estimating the post-buckling load-bearing capacity of a stiffened plate of a given width is presented in subsection (3).

(2) Estimation of reinforced post-buckling load-bearing capacity:

A reinforced  $B_e$  in the buckling and pressure loss analysis may be divided into two types of stiffened plates. FEMs and experimental studies of the two types of plate elements have been used to study the buckling pressure loss after destruction in pressure loss curves. The  $B_e$  of components in a reinforced plate element under pressure loss can be considered to be a stress-weighted sum of estimates of the post-buckling load-bearing capacity.

(3) Estimation of stiffened panel post-buckling load-bearing capacity:

Here, two pilot projects based on this estimation method are introduced.

- ① The subsection approach used for metal plates can be applied to composites subject to axial compression. A long board is divided into shorter board panels based on the slenderness ratio ( $L'/\rho$ ). Figure 4.64 illustrates three regimes for division of boards.

In a stiffened panel  $L' = L/\sqrt{C}$  for an effective column length  $C$ , where the end of the stiffened plate support profile or  $\rho$  factor can take  $C = 1-4$ , although it is generally assumed that  $C = 2.0$ . The value of  $\rho$  for a stiffened plate radius of gyration can be determined by the following equation:

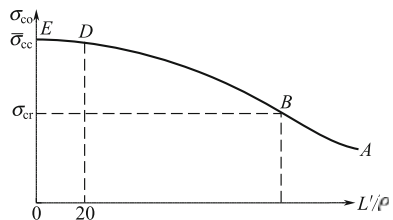
$$\rho = \sqrt{\frac{(EI)}{(EA)}}$$

where  $(EA)$  and  $(EI)$  are the stiffened plate tensile (compression) stiffness and bending stiffness, respectively, according to Eqs. 4.53 and 4.54.

In the pilot study and mechanical analysis:

- (a) In the  $D-E$  section the short-board features pressure damage, where  $0 < L'/\rho \leq 20$ .
- (b) In the  $B-A$  section a long board features damage leading to overall instability.

**Fig. 4.64** Subprocessing curves of axial load-bearing capacity of longitudinally reinforced laminates



(c) In the *D-B* section of medium and long boards, before damage to the reinforcement between the skins local buckling occurs first. Thus, it is necessary to account for the post-buckling load-bearing capacity.

The *D-E* between each section, where  $L/\rho = 20$ , can be defined separately for the *D-B* sections and the *B-A* cutoff points between sections. For *B* the skin between the reinforced parts determines the initial buckling stress.

The actual structures of a stiffened panel include medium and long boards and stiffened plates. Thus, these are the focus of post-buckling load-bearing capacity analysis. Test results show that in the *D-B* section of a stiffened plate, the post-buckling load-bearing capacity and average failure stress can be fitted by a parabola. The vertex of the parabola is *D*, the other point is *B*. This allows estimation of the post-buckling load-bearing capacity of reinforced pressed plates from the equation:

$$\bar{\sigma}_{co} = \left[ 1 - \left( 1 - \frac{\sigma_{cr}}{\bar{\sigma}_{cc}} \right) \frac{\sigma_{cr}}{\sigma_r} \right] \bar{\sigma}_{cc} \tag{4.50}$$

where

- $\bar{\sigma}_{co}$  stiffened panel average failure stress;
- $\bar{\sigma}_{cc}$  Type of short stiffened plate ( $0 < L/\rho \leq 20$ ) average pressure loss of the failure stress;
- $\sigma_{cr}$  reinforcement between the skin of the initial local buckling stress;
- $\sigma_r$  A factor to discount the skin or  $b_e$  reinforcement after the effects of local buckling decreases the stiffness. In the calculation of the overall instability of stiffened plate stress, for  $b_e$  reinforcement of more than 4, the system can be considered a side support with the width determined by the Euler column formula.

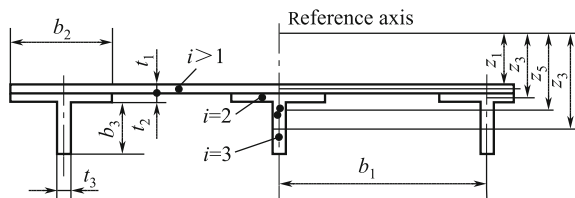
In preliminary design, the following simplified formula are used for preliminary estimates

$$\bar{\sigma}_{co} = \bar{\sigma}_{cc} - (\bar{\sigma}_{cc})^2 (L'/\rho)^2 / (4\pi^2 \bar{E}_x) \tag{4.51}$$

where

- $\bar{E}_x$  stiffened plate *x* direction equivalent elastic modulus;
- $\rho$  stiffened plate section radius of gyration;

**Fig. 4.65** Schematic diagram of laminate reinforced vertical plate element



$L'$  stiffened panel effective column length.

A stiffened plate can generally be divided into sections by symmetric laminates  $m$  yen (also known as a skin plate element. A calculation model (Fig. 4.65) can used based on the following equation A,  $(EA)$  and  $(EI)$ .

$$A = \sum_{i=1}^m b_i t_i \quad (4.52)$$

$$(EA) = \sum_{i=1}^m \left( A_{11i} - \frac{A_{12i}^2}{A_{22i}} \right) b_i \quad (4.53)$$

$$(EI) = \sum_{i=1}^m \left[ \left( A_{11i} - \frac{A_{12i}^2}{A_{22i}} \right) b_i (z_i - z_c)^2 + \left( D_{11i} - \frac{D_{12i}^2}{D_{22i}} \right) b_i \right] \quad (4.54)$$

where

$b_i$  first plate element of width  $i$ ;  
 $t_i$  thickness of the  $i$ th plate element;  
 $A_{11i}, A_{12i}, A_{22i}$  first plate element of the  $i$ th plane stiffness coefficient;  
 $D_{11i}, D_{12i}, D_{22i}$  first plate element  $i$  of the bending stiffness coefficient;  
 $(z_i - z_c)$  first section  $i$  of a plate element on the neutral axis from the center;  
 $Z_c$  stiffened plate section on the neutral axis position (from calculation of the distance between the reference axis).

$$z_c = \frac{\sum_{i=1}^m E_{xi} b_i t_i z_i}{\sum_{i=1}^m E_{xi} b_i t_i}$$

where

$E_{xi}$  first plate element  $i$  in  $x$  direction of the equivalent modulus of elasticity;  
 $z_i$  part  $i$  of a plate element calculation of the reference section of the center distance from the axis;

In general, Eq. (4.54) is used, when the second part is negligible compared with the first; see “Stability Analysis of Composite Structures Guide” in Appendix A.

- ② The effective width method for skin damage occurring prior to local buckling of a stiffened panel, can be used to estimate the post-buckling load-bearing capacity of the skin. For  $b_e$  reinforcement, the buckling

pressure loss or damage can be used to estimate the damage of the stiffened plate load.

The stiffened panel features skin  $n_1, n_2$  arranged in a geometric space, such that the size and material properties of all reinforced features are the same for each article. The buckling load-bearing capacity can be calculated as:

$$P = (n_1 b_e t E_x^s + n_2 F E_x^{st}) \varepsilon_b \quad (4.55)$$

where

- $P$  stiffened plate load damage;  
 $E_x^s$  direction of the skin equivalent elastic modulus;  
 $E_x^{st}$  reinforced  $b_e$  equivalent  $x$  direction modulus of elasticity,  
 $E_x^s = \frac{1}{t} \left( A_{11} - \frac{A_{12}^2}{A_{22}} \right)$ ;  
 $t$  thickness of skin;  
 $F$  reinforced area profiles;  
 $\varepsilon_b$  reinforcement of the buckling pressure loss or strain;  
 $b_e$  effective width of skin.  
 $A_{11}, A_{12}, A_{22}$  skin stiffness coefficient of the plane.

When the computation can be divided into  $m$  articles reinforcing a symmetric laminated plate element, the following equations may be used:

$$E_x^{st} = \frac{1}{F} \sum_{i=1}^m \left( A_{11i} - \frac{A_{12i}^2}{A_{22i}} \right) b_i$$

$$F = \sum_{i=1}^m b_i t_i$$

where

- $b_i$  reinforcement  $b_e$  of the first plate element of width  $i$ ;  
 $t_i$  reinforcement  $b_e$  of the first  $i$  of the thickness of a plate element;  
 $A_{11i}, A_{12i}, A_{22i}$  reinforced articles in the first  $i$ -plane of the plate element stiffness coefficient.

The  $b_e$  reinforcement between the skin of the effective width can be determined by the following equations:

$$b_e = \varphi b$$

$$\varphi = \zeta + (1 - \zeta) \varepsilon_{cr}^s / \varepsilon_b$$

$$\xi = 1 - 2 / \left[ 3 + \eta \left( \frac{a}{b} \right)^4 \right] \quad (4.56)$$

where

- $a, b$   $b_e$  reinforcement between the length and width of skin;  
 $\varphi$   $b_e$  reinforcement of a skin with the effective width coefficient;  
 $\varepsilon_{cr}^s$  local buckling of the strain skin;  
 $\varepsilon_b$  reinforcement of the buckling strain;  
 $\eta$  anisotropy degree of the skin,  $\eta = A_{22}/A_{11}$ .

In addition, the articles reinforcing the effective width between the skin can also be determined from the following equation:

$$b_e = \frac{b}{2} \left( 1 + \frac{\sigma_{cr}^s}{\sigma_{cc}^f} \right) \quad (4.57)$$

where

- $b_e$  reinforcement between the effective width of the skin;  
 $b$  reinforcement between the width of the skin;  
 $\sigma_{cr}^s$  local buckling stress of the skin;  
 $\sigma_{cc}^f$  pressure loss stress of skin attached to the end of the reinforced section.

If Eq. (4.57) is used, to estimate the damage to a stiffened plate,  $b_e$  can be determined from  $\varepsilon_b$  of the load  $P$ , with Eq. (4.55) where the response of the pressure loss is given by:

$$\sigma_b = \varepsilon_{cc}^{st} = \sigma_{cc}^{st} / E_x \quad (4.58)$$

where  $\sigma_{cc}^{st}$  is described in Sect. 4.7.1.2 of the method [Eq. (4.45)].

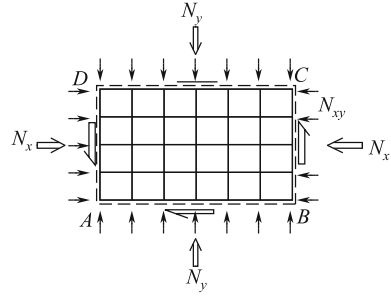
### 4.7.3 Buckling Analysis of Sandwich Structures

#### (1) Overall buckling analysis of sandwich structure

A large number of calculated and experimental results show that the FEM for overall buckling analysis of sandwich structures is well suited to their complexities. In buckling finite element analysis, note the following issues [2, 14]:

- ① Model grid segmentation: Grid partitions should maintain the principle of the instability mode, and the core thickness direction should be selected as a monolayer element. The rest of the other analysis is same as that for stress analysis;

**Fig. 4.66** Finite element analysis grid



② For simulation of the supported edges, refer to Fig. 4.66.

In the case of all sides simply supported, the points of all sides  $AB, BC, CD, DA$   $w_i = 0$ .

Corner points  $u_A = v_A = 0, v_B = 0$  (or  $u_A = v_A = 0, u_D = 0$ ).

All sides fixed: the points of all sides  $AB, BC, CD, DA, w_i = 0, \theta_{xi} = \theta_{yi} = 0$

$$u_A = v_A = 0, v_B = 0 \text{ (or } u_D = 0).$$

Other supported boundary conditions can be used with this method. In the case of a support for an elastic boundary, the corresponding  $w$  and  $\theta_{xi}, \theta_{yi}$  values are given by the stiffness of the elastic support. For the sides of a fixed supported plate,  $\theta_{xi}$  or  $\theta_{yi}$  is 0; for the sides of simply supported plate  $w_i = 0$  or replaced by the stiffness of the elastic support.

- ③ Loading, as shown in Fig. 4.66. Put in-plane load  $N_x, N_y, N_{xy}$  to the nodes of each side, with upper and lower points corresponding to the same node. If the load changes along the edge, the load of each node can be not same.

- ④ Critical buckling load:  $N_{icr} = \lambda_{\min} N_i$

where  $\lambda_{\min}$ —minimum eigenvalue;

$N_i$ —stress of analysis with design load.

**(2) Local buckling analysis of laminate**

In the local buckling analysis of laminates, the panel can be considered to be a beam support for the core, or flexibility base. The flexibility base has the bending stiffness and shear stiffness of the core.

Local buckling failure modes of laminates can be divided into three types: damage to laminated panels, damage to the core, and damage to the interface.

Failure modes of laminated panels include: single-layer instability, folding of the intergrid, laminated panel buckling.

Failure modes of the core: sandwich core crush, shear failure of sandwich core; interface damage of the sandwich core and panel debonding from the core.

The calculation methods of various failure modes are introduced as follows:



## ① Single-layer instability

$$\frac{\sigma_{jcr}}{G_z} = \begin{cases} \xi_j(2 - \xi_j) & \xi_j < 1 \\ 1 & \xi_j > 1 \end{cases} \quad j = x, y, xy \quad (4.59)$$

where

$\sigma_{jcr}$  buckling stress of single-layer,  $j = x, y, xy$ , compressive buckling stress and shear buckling stress along the x- and y-axis. respectively;

$G_z$  interlaminar shear modulus;

$\xi_j$  stiffness parameter,  $\xi_j = \frac{\sqrt{DB_j}}{S_j}$ ,  $j = x, y, xy$ ;

$B_j$  base stiffness,  $B_j = \frac{LbE_z}{r}$ ,  $j = x, y, xy$ ;

$D$  bending stiffness,  $D = \frac{\pi d_f^3 E_f b}{64W_f}$ ;

$S_j$  shear stiffness,  $S_j = \frac{bt'G_z}{L_j}$ ,  $j = x, y, xy$ .

Carbon fiber material:

$d_f$  fiber diameter, recommended value is 0.007 mm;

$W_f$  fiber spacing, recommended value is 0.005842 mm;

$E_f$  fiber modulus, recommended value is 255,162 MPa;

$E_z$  normal tensile modulus of composite panel, recommended value is  $E_z = 0.5 \times (E_{22T} + E_{22C})$ ;

$L_j$  effective layup percent along loading direction  $j = x, y, xy$ , calculation formula is:

$$L_x = SPL0 + SPL9 \times \frac{E_{22C}}{E_{11C}} + 0.5 \times SPL45 \\ \times \left( 1 + 2.5 \times \frac{E_{22C}}{E_{11C}} \right)$$

$$L_y = SPL9 + SPL0 \times \frac{E_{22C}}{E_{11C}} + 0.5 \times SPL45 \\ \times \left( 1 + 2.5 \times \frac{E_{22C}}{E_{11C}} \right)$$

$$L_{xy} = SPL45 \times \left( 1 + \frac{E_{22C}}{E_{11C}} \right) + 0.25 \\ \times (SPL0 + SPL9) \times \left( 1 + 2.5 \times \frac{E_{22C}}{E_{11C}} \right)$$

where

*SPL0* percent of fiber in  $0^\circ$  direction;  
*SPL9* percent of fiber in  $90^\circ$  direction;  
*SPL45* percent of fiber in  $45^\circ$  direction:

$$SPL45 = 0.5 \times (1 - SPL0 - SPL9)$$

- ② Panel buckling: Panel instability refers to local panel buckling when a surface is under a compressive or shear load. The following formula applies to local buckling analysis of the compressive surface of an anti-symmetric sandwich structure (for example, a full-size wing).

The panel instability can be calculated by Eq. (4.59), the calculation of parameters  $D$ ,  $S$ , and  $B$  require the following changes:

Base stiffness  $B$

$$B = \frac{2E_c}{t_c} \quad (4.60)$$

Bending stiffness of panel  $D_j$ ,  $j = x, y, xy$

$$D_{ij} = \int_{-0.5t_f}^{0.5t_f} Q_{ij}^{(K)} z^2 dz \quad i, j = 1, 2, 6 \quad (4.61)$$

$$D_x = D_{11}$$

$$D_y = D_{22}$$

$$D_{xy} = 0.25 \times (D_{11} + D_{22}) + 0.5 \times (D_{12} + 2D_{66})$$

Shear stiffness  $S_j$ ,  $j = x, y, xy$

$$S_x = \frac{D_{11}^2}{DEN1}$$

$$S_y = \frac{D_{22}^2}{DEN2} \quad (4.62)$$

$$S_{xy} = \frac{D_{xy}^2}{\sqrt{DEN1 \times DEN2}}$$

where

$$DEN1 = \sum_1^N CA(i) \times t(i)/G_{13}$$

$$DEN2 = \sum_1^N CB(i) \times t(i)/G_{13}$$

$$CA(i) = \sum_1^i Q_{11}(k) \times AB2(k) \times t(k)$$

$$i_{\max} = N; k = 1, 2, \dots, i$$

$$CB(i) = \sum_1^i Q_{22}(k) \times AB2(k) \times t(k)$$

$$i_{\max} = N; k = 1, 2, \dots, i$$

$$AB2(k) = 0.5 \times h + (t_f - \sum_1^{k-1} t(i) - 0.5 \times t(k))$$

$$k = 1, 2, \dots, N$$

$$Q_{11}(k) = m(k) \times E_L(k)$$

$$Q_{22}(k) = m(k) \times E_T(k)$$

$$m(k) = (1 - \nu_{LT}(k) \times \nu_{TL}(k))^{-1}$$

② Folding of intergrid can be calculated as follows:

$$\sigma_{cr} = 2 \frac{E'_f}{\lambda} \left( \frac{t_f}{S_c} \right)^2 \quad (4.63)$$

where  $E'_f = \sqrt{E_{1f} E_{2f}}$

$$\lambda = 1 - \nu_{12} \nu_{21}$$

$E_{1f}, E_{2f}$  moduli of orthogonal axis of panel;

$t_f$  thickness of panel;

$S_c$  dimensions of a core-wise sandwich structure (diameter of inscribed circle for core-wise structure).

③ Shear failure of sandwich core

$$\sigma_{xcr} = \frac{V_x}{1 + \frac{\delta_0 \times B_7 \times \sqrt{4B/D_{11}}}{h \times \tau_{13b}}} \tag{4.64}$$

$$\sigma_{ycr} = \frac{V_y}{1 + \frac{\delta_0 \times B_8 \times \sqrt{4B/D_{22}}}{h \times \tau_{23b}}} \tag{4.65}$$

$$\sigma_{xycr} = \frac{V_{xy}}{1 + \frac{\delta_0 \times \sqrt{B_7 \times B_8} \times \sqrt{4B/D_{xy}}}{h \times \sqrt{\tau_{13b} \times \tau_{23b}}}} \tag{4.66}$$

$$B_7 = DD_{11}^2 / DDEN1$$

$$B_8 = DD_{22}^2 / DDEN2$$

where  $DD_{11}$  and  $DD_{22}$  are equivalent conversion bending stiffness of the composite panel, the equivalent conversion formula is:

$$[DD] = [D] - [B][A]^{-1}[B]$$

$$B_{ij} = \int_{-0.5t_f}^{0.5t_f} Q_{ij}^{(K)} z dz \quad i, j = 1, 2, 6$$

$$A_{ij} = \int_{-0.5t_f}^{0.5t_f} Q_{ij}^{(K)} dz \quad i, j = 1, 2, 6$$

where

$$DDEN1 = 2 \times DEN1 + CA(N)^2 \times \frac{h}{G_{C13}}$$

$$DDEN2 = 2 \times DEN2 + CB(N)^2 \times \frac{h}{G_{C23}}$$

- $\delta_0$  initial wave range of panel;
- $\tau_{13b}$  normal shear strength of sandwich core;
- $\tau_{23b}$  normal shear strength of sandwich core;
- $V_x, V_y$  compression along  $x$ - and  $y$ -axis; (i.e., the lowest value of the following: overall critical buckling stress of panel, critical buckling stress of layer, critical core-wise buckling stress of panel);

$V_{xy}$  — shear; (i.e., the lowest value of the following: overall critical buckling stress of panel, critical buckling stress of layer, critical core-wise buckling stress of panel);

④ Sandwich core crush

$$\sigma_{jcr} = \frac{V_j}{1 + B \frac{\delta_0}{\sigma_{cc}}}, \quad j = x, y, xy \quad (4.67)$$

where

$\sigma_{cc}$  compressive strength of sandwich core;  
 $\delta_0, B, V_j, j = x, y, xy$  see definition above.

⑤ Interface failure of sandwich core and panel

$$\sigma_{jcr} = \frac{V_j}{1 + B \frac{\delta_0}{\sigma_{bt}}}, \quad j = x, y, xy \quad (4.68)$$

where

$\sigma_{bt}$  bonding strength of sandwich structure panel;  
 $\delta_0, B, V_j, j = x, y, xy$  definition see above.

The local buckling analysis described above is compiled in the calculation software BUCKLSCP.

## 4.8 Joint Design and Analysis

Advanced composites have an important advantage over metals in terms of structural integrity. However, technological limitations and the need for maintenance require some separate components to be connected. Proper analytical techniques are necessary to solve the problem of load transmission at joints. Thus, joint design is an important aspect of composite structure design.

Joints represent one of the greatest challenges in the design of structures in general, particularly for anisotropic composite structures. Joints represent potential weak points in a structure; thus, the design of the overall structure tends to follow from, and be limited by, the features of joints in the structure. Failure of the entire structure often originates at the joints. The reason for this is that joints involve interruptions of the geometry of the structure and discontinuities in materials, which

almost always produce local highly stressed areas. Stress concentration in composites is not only more severe but also more complex than that in metals. Stress concentration in metals depends only on geometry; however, composites are affected by the layering pattern as well as geometric parameters. Well-established joining technologies for metallic structures are not directly applicable to composites.

Stress concentration in mechanically fastened joints is particularly severe because the load transfer between the elements of the joint has to take place over a fraction of the available area.

Composite joint strength is closely related to the layering pattern, load direction, and environment. There are more failure modes of composite joints, and moreover, strength prediction is more difficult. These complicating factors require careful consideration.

This section deals with the joining of advanced fiber composites, mainly focusing on mechanically fastened and adhesively bonded joints.

### ***4.8.1 Characteristics of Composite Joints***

There are two methods of advanced composite joining: adhesive bonded and mechanical fastening [2, 13, 17, 18].

#### **4.8.1.1 Characteristics of Adhesively Bonded Joints**

Adhesively bonded joints have the following advantages:

- (1) No stress concentration caused by drilled holes and strength of basic laminate does not decrease;
- (2) Lower number of parts, lightweight structure, and high joint efficiency;
- (3) Anti-fatigue, sealing, shock absorption, and good insulation performance;
- (4) Good damage tolerance and fail-safe performance;
- (5) Smooth surface contours;
- (6) No fretting problems created by dissimilar materials;
- (7) Non-corrosive, i.e., no galvanic atmosphere created by the presence of dissimilar materials.

Adhesive bonded joints have the following disadvantages:

- (1) Difficultly of inspection of bond quality, poor reliability;
- (2) Large dispersibility, low peel strength, difficultly of transferring large loads;
- (3) Sensitive to hygrothermal and corrosive environments, aging problems;
- (4) Requirements for high-quality surface preparation and strict processing, which can result in residual stress;
- (5) Strict fitting tolerance between adherends and difficultly of repair;

- (6) Permanent joint formed which cannot be disassembled.

#### **4.8.1.2 Characteristics of Mechanically Fastened Joints**

Mechanically fastened joints have the following positive attributes:

- (1) Ease of quality inspection, good reliability;
- (2) Ease of disassembly and reassembly in manufacture, replacement, and maintenance;
- (3) No special surface preparation requirements;
- (4) Residual stresses are generally not a problem;
- (5) Environmentally insensitive;

Mechanically fastened joints have the following drawbacks:

- (1) Require machining of holes in the members, thereby weakening the members;
- (2) Require local reinforcement, resulting in increased weight and considerable stress concentration;
- (3) Cost can increase because of increased manufacture capacity;
- (4) Galvanic corrosion may occur when metallic fasteners are in direct contact with composite materials, thus fasteners should be composed of a material that has a small potential difference with the composite.

#### **4.8.1.3 Characteristics of Combined Bonded-and-Bolted (or Riveted) Joints**

Bonded-riveted (bolted) combined joints are used based on considerations of fail-safety and the need for additional assurance of joint safety and integrity over a bonded or bolted joint design alone.

Basic principles for use of combined bonded-and-bolted (or riveted) joints are as follows:

- 1. Select a ductile adhesive;
- 2. Improve the fit precision of the pin in the hole.

The following points should be noted for use of combined joints:

- (1) The use of fastener strengthening in a bonded structure is a complex question. On the one hand, the addition of fasteners may arrest and relax damage progression and improve anti-impact, anti-fatigue, and anti-creep performances. On the other hand, the fasteners may have an adverse effect on stress concentration and should be carefully considered in different situations;
- (2) Deformation of mechanically fastened joints is generally greater than that of adhesively bonded joints. Deformation behavior of combined bonds shows more similarities to the deformation of mechanically fastened joints;

- (3) The precision of the fastener fit with the hole is important. A poor fit will increase the shear deformation of the joint, resulting in shear failure of the bond-line, and induce shear failure of the fasteners and bearing failure of holes. Hence, there may be no net benefit to the use of fasteners and bonding.

#### **4.8.1.4 Principles for Selecting Composite Joint Methods**

The selection of the joining methods should seek to take advantage of the respective features of joint types. In general, some basic principles should be followed:

- (1) Bonded joints are generally suitable for thin structures with low running loads (load per unit width, i.e., stress  $\times$  element thickness) or structures carrying shear load. The main advantages of bonded joints are their lightweight nature and high joint efficiency. Thus, bonded construction tends to be more prevalent in small light aircraft and secondary aircraft structures. Well-designed, bonded joints can also transmit large loads;
- (2) Mechanically fastened joints are mainly used in structures where concentrated loads occur or an emphasis on high reliability is required. Bolted joints can transfer greater loads than riveted joints. Thus, bolted joints are mainly used in primary aircraft structural components. The main disadvantage of mechanically fastened joints is the decrease in the strength of the basic laminate owing to the fastener holes;
- (3) Combined joints are generally suitable for jointing places requiring greater margins and for medium thickness laminates.

#### **4.8.2 Adhesively Bonded Joints**

Bonded joints have advantages in terms of their lightweight and high joint efficiency; thus, their use in aircraft structural components has grown. For example, the spar of the B-737 horizontal stabilizers; the root-stepped joints of the F-14 all-movable horizontal stabilizers; the joints of wing panel-to-root rib of the F-15 aircraft; Joints of fuselage panels to frame and joints of skin-to-skin for the Lear Fan 2100 all composite plane; joints of the skin of the pelvic fin of the clapboard for the Y7-200B; the skin-stringer joint of the Y7-FC vertical stabilizer; joints of the  $\pi$ -stringer to panels, and the  $\pi$ -stringer to web for the DC-10 vertical stabilizer wall. Bonded step lap joints are used in the attachments for the F-14 and F-15 horizontal stabilizers as well as the F-18 wing root fitting, and the majority of the airframe components in the Lear Fan and the Beech Starship [2, 17–24].



### 4.8.2.1 Characteristics of Bonded Joint Design

The following points should be noted for bonded joint design:

- (1) The difference in the thermal expansion coefficient of carbon fiber composites and metals is relatively large. Elevated temperature bonding of composites to metallic components will generate considerable internal stress and deformation. Therefore, whenever possible, structural adhesive bonding of composites to metallic components in design, particularly aluminum, should be avoided. If necessary, titanium components with lower thermal expansion coefficients can be used.
- (2) Adhesive joints work best in shear and are poor in peel. Thus, the adhesive layer should carry the load in the maximum strength direction. Whenever possible, normal and peeling forces should be avoided. The interlaminar tension strength of carbon fiber-reinforced polymers is very low, and composites are prone to interlaminar tension failure, whereas metals tend to show peeling failure at bond-lines. Therefore, thick adherends are suitable for stepped and tapered joints.

It is vital to avoid letting the adhesive layer be the weak link in the joint; this means that, whenever possible, the joint should be designed to ensure that the adherends fail before the bond layer.

### 4.8.2.2 Main Factors Affecting Adhesive Joints Strength

The main factors affecting adhesive joints strength include: material of the adherends, stiffness ratio and thermal expansion coefficients of the adherends, joint configuration and geometry, fiber orientation of the bond-line, temperature and moisture, adhesive, and manufacturing procedure.

- (1) Effects of unbalanced adherend stiffness: All types of joint geometry are adversely affected by unequal adherend stiffness, where the stiffness is defined as the axial or in-plane shear modulus multiplied by the adherend thickness. As an example, for single-lap joints, if the stiffness of the adherends is balanced, the bending moments at two ends of the joint will be the same and the deformation of the adherends will be equal. If the stiffness of the adherends is unequal, the bending moment at two ends of the joint will be different and a higher deformation will generally occur at the loaded end of the more flexible adherend.

Where possible, the stiffness of adherends should be kept approximately equal. For example, for step lap and scarf joints between quasi-isotropic carbon/epoxy and titanium (Young's moduli: 55 and 110 GPa, respectively) ideally, the ratio of the maximum thickness (the thickness just beyond the end of the joint) of the composite adherend to that of the titanium should be  $110/55 = 2.0$ .

- (2) Thermal mismatch of adherends: Adherent thermal mismatch relates to dissimilar thermal expansion coefficients, which can induce initial curvatures in single-lap joints. These curvatures may influence the already eccentric load path and thereby change the bending moments at the ends of the joint. This effect can in turn change the adhesive shear and peel stress distribution. In general, the joint load capacity is usually decreased because one end of the joint is more critical than other.
- (3) Effects of ductile adhesive response: Adhesive ductility is an important factor in minimizing the adverse effects of shear and peel stress peaks in the bond layer. Ductility has a pronounced influence on the mechanical response of bonded joints. The elastic response may prevent applications in situations where a considerable amount of additional structural capability is required.
- (4) Temperature and humidity: Temperature and humidity have a pronounced influence on the performance of composite components and these environment variables must be considered. When a composite with a polymeric matrix is placed in a wet environment, the matrix will absorb moisture, which may cause material swelling. Particularly at higher temperatures, the material may soften and weaken the matrix and matrix/fiber interface. Absorbed moisture lowers the glass transition temperature and maximum operating temperature of the material. If the adhesive can be used over a range of operating temperatures, the influence of temperature is not important. However, combinations of temperature and humidity conditions should be considered. At high temperatures, the ability of moisture to absorb and diffuse in the material may increase, which could severely degrade the strength of the material.

Long-term environmental effects will obviously decrease bonded joint strength. In engineering design and analysis, these situations should be fully considered. To avoid any adverse effects from temperature and humidity, consider the following points:

- ① Bond-lines are sealed with an adhesive, which is effective against moisture;
  - ② The most severe potential environmental conditions should be precisely determined;
  - ③ The temperature and humidity range of the bonded joint should be precisely defined;
  - ④ The most effective adhesive should be selected considering the aforementioned points;
- (5) Effects of bond defects: Defects in adhesive joints, which are of concern include: debonding, flaws, cracking, cure imperfections, surface preparation deficiencies, voids and porosity, and thickness variations in the bond layer. Of the various defects that are of interest, debonding, cracking, and surface preparation deficiencies are likely of the greatest concern.

Any bond defects will result in load redistribution along the entire bond-line and stress from discontinuity of the bond-line will increase. When the defect size of debonding and cracks is small compared with the length of the bond-line, any increase in stress will not be obvious. The stress will increase markedly as the defect size increases. Thus, it is necessary to establish standards for bond quality.

#### 4.8.2.3 Adhesives

##### (1) General requirements of adhesives

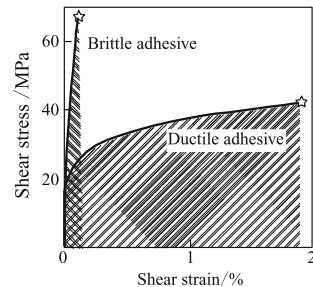
Adhesives should have the following features:

- (1) Compatibility with the adherends and high bonded strength, such that bond-interface failures will not occur;
- (2) The curing temperature should be as low as possible;
- (3) The thermal expansion coefficient of the adhesive should be nearly identical to that of the adherends;
- (4) Temperature effects should be minimal;
- (5) Good mechanical properties;
- (6) Simple processing;
- (7) The durability of the bond should be greater than the anticipated life of the structure.

##### (2) Types of adhesive and their selection

Adhesives can be broadly classified into two major groups on the basis of their stress–strain curve, i.e., ductile and brittle adhesives (Fig. 4.67). The limit of shear strain of a ductile adhesive is greater than 0.05, whereas that of brittle adhesive is typically far less than 0.05.

**Fig. 4.67** Ductile and brittle adhesives



As shown in Fig. 4.67, the shear strength of a brittle adhesive is higher than that of a ductile adhesive. However, peel stresses can be eliminated from consideration by approaches such as adherend tapering. The static shear strength of the bonded joint does not depend only on a single parameter and is determined by the strain energy to failure of the adhesive under a shear load (i.e., the area under the curve). Therefore, joints based on ductile adhesives have greater strength. From the viewpoint of fatigue performance, a brittle adhesive will rupture near the inflexion and its fatigue life is lower. The ultimate strain of a ductile adhesive is also greater. Ductility in aerospace adhesives is beneficial in reducing stress peaks in the adhesive, i.e., lowering the stress concentration. If higher fatigue stresses can be withstood, the fatigue life will be longer. When the environment temperature does not exceed 70 °C, ductile adhesives should be used as far as possible.

Near the engine or in ultrasonic airplanes, high operating temperatures necessitate that the brittle adhesives are used despite the loss of strength.

It is necessary to consider the effects of temperature. If the temperature remains below the glass transition temperature of the adhesive, the bond strength will not be sensitive to temperature effects. However, the strength will be reduced at low temperature.

Materials commonly used in structural adhesive bonding of composite structures are thermosetting resins, which can be subdivided into four basic chemical classes: epoxy, polyimide, phenolic, and silicone.

- (1) Epoxy: The advantages of epoxy resins include its high strength and modulus, low levels of volatiles, excellent adhesion, low shrinkage, low moisture absorption, good adhesion, good chemical resistance, and ease of processing. Therefore, epoxy resins are the most widely used structural adhesives. Forms are packed with resin and curing agents, which are mixed and cured with heat. The major disadvantages of epoxy resins include brittleness, generic hardness, low thermal strength, and poor wear characteristics. The curing is usually accomplished by the application of heat under pressure. For example, a cure will typically be performed at 145 °C and 0.7 MPa and be complete within 20 min. Some cures will also be completed at room temperature.
- (2) Epoxy–Phenolic: This class of adhesives are a modified epoxy, which can be completed within 60 min at 250–350 °C. Its advantages include high strength and good performance at low temperatures; its major disadvantages are the need to heat during curing, porosity of the bond, and poor electrical performance.
- (3) Polyimides: This class of adhesives requires high temperature curing, usually between 250–400 °C. A post-cure is also required to attain maximum strength. The highest operating temperatures of these adhesives are in the range of 250–400 °C. Advantages of this class of adhesives include their resistance to temperature, moisture, fire, and corrosion as well as their low coefficient of thermal expansion. Disadvantages of polyimides include their high cost, porosity, and corrosiveness.

- (4) Phenolic: Mixed resin adhesives are usually composed of a phenolic resin mixed with another resin. The advantages of such mixtures include high thermal strength, acid resistance, low cost, and good electric performance. Their major disadvantages are the need for high curing temperatures, high shrinkage, and corrosiveness. Common used resins include:
- ① Phenolic polyamide: Shear strength can be as high as 36 MPa and maintains excellent strength at high temperature.
  - ② Phenolic ethylene: Shear strength can be as high as 30 MPa and can operate at very low temperatures. Performance is rapidly degraded above 100 °C.
- (5) Silicone has good resistance to heat, cold, radiation, and good isolation; however, its strength is low. Therefore, joints requiring high stability and the high mechanical strength may be achieved with the use of this resin in combination with others. Epoxy–silicone can be used continuously at temperatures as high as 340 °C and discontinuously at temperatures up to 510 °C.

**(3) Adhesives suitable for bonding different materials**

Adhesives for bonding different materials may be selected as outlined in Table 4.16. Blank entries for material/adhesive combinations in the tables indicate that it may be difficult to achieve bonding.

Adhesives suitable for aeronautic structures are listed in Table 4.17.

**(4) Measurements of the mechanical properties of the bond-line**

Stress–strain characterization of adhesive films and their mechanical performances form the basis of static strength design for adhesive bonded joints. Because the bond-line is very thin, the interface will have some influence and the specimens used for testing must have the same configuration as that of the actual part.

Measurement results show that the actual stress–strain curve (Fig. 4.68) is complicated and may be difficult to apply directly for joint analysis. Equivalent elastic–plastic and bilinear stress–strain curves are commonly used simplified models. The elastic–plastic curve is particularly useful and the simplification allows closed form analytical solutions to be obtained. The principles of this simplification are that any adhesive is defined by two straight lines having the same strain energy and failure stress and strain. The peak allowable shear stress should be multiplied by a factor of 0.8 to account for both bonding defects and the differences between laboratory and production fabrication. The peel strength and other data needed for design can be measured from related test standards.

**Table 4.16** Adhesives suitable for the bonding different materials

	Metal	Polyamide	Silicone	Ceramics and glass	Polyflon	Polyurethane	Phenolic	Epoxy
Metal	E/T	E	S					
Polyamide	E	P	-	-				
Silicone	S	-	S	-	-			
Ceramics and glass	E	-	-	-	-	-		
Polyflon	E/T	-	-	-	E/T	-	-	
Polyurethane	E	-	S	-	-	E	-	-
Phenolic	E	-	-	E	-	-	E	-
Epoxy	E	-	-	-	E/T	-	E/T	E/T

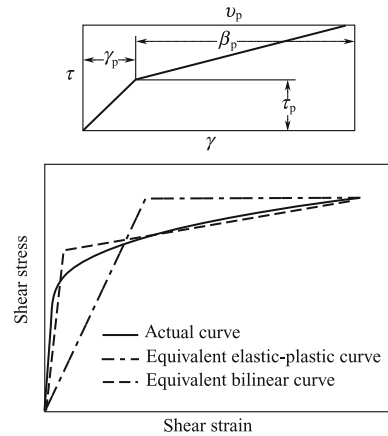
*Note* E epoxy; P polyamides; S silicone; T polysulfide rubber

**Table 4.17** Properties of commonly used adhesives in aeronautical structures

Item	Trademarks of the adhesives							
	SY-24C (primer SY-D9)	SY-18 (primer SY-18)	J-47A (primer J-47B)	J-95 (primer J-96)	SY-14A (primer SY-D8)	J-99 (primer J-100)	J-116B <sup>ⓐ</sup> (primer J-117)	
Test standard	Q/6S928-93 Q/6S927-93	Q/6S348-83 (film) Q/6S347-83 (flour)	CB-SH-0037 -85	Q/HSY022-92 Q/HSY023-92	Q/6S104-88 Q/6S1234-95	Q/HSY039-92 Q/HSY026-92	Q/HSY043-93	
Basic components	Epoxy, dicyandiamide	Epoxy, nitrile rubber, curing agent, accelerator	Epoxy, nitrile rubber, amine, curing agent	Epoxy, nitrile rubber, epoxy amine	Epoxy, polysulfone, curing agent	Epoxy, polysulfone, curing agent	Epoxy, elastomeric, curing agent nylon carrier	
Shear strength MPa	55 °C	≥ 33		≥ 33	≥ 28	≥ 28	24.5	
	25 °C	≥ 33	≥ 30	≥ 33	≥ 30	≥ 28	24.5	
	80 °C	≥ 21(70 °C)		≥ 21 (70 °C)				
	100 °C		≥ 18	≥ 15				
	150 °C		≥ 10 (130 °C)		≥ 20	≥ 15	13.3	
175 °C					≥ 18			
90° peel strength/(kN/m)	≤ 55 °C	≥ 4.5 <sup>ⓐ</sup>		≥ 4.5 <sup>ⓐ</sup>			7.5	
	25 °C	≥ 6.0 <sup>ⓐ</sup>		≥ 6.0 <sup>ⓐ</sup>	≥ 5.9	≥ 7.0	4.0	
	150 °C				≥ 3.9		HIP	
Manufacturers	BIAM	BIAM	HIP	HIP	BIAM	HIP	HIP	
Overseas similar trademarks	Metland 1113.06 Metlbond 6726			Metland 1113.06 Metlbond 6726		Redux 319A Redux 119		
	DHS172-292 DHS186-211			DHS172-292 DHS186-211		DHS174-292 DHS186-231		

Note <sup>ⓐ</sup>. All data of J-116B adhesives are B-basis; <sup>ⓑ</sup>. Bell peel strength

**Fig. 4.68** Shear stress–strain curves of adhesive layer



#### 4.8.2.4 General Design Requirements for Adhesive Bonded Joints

##### (1) General principles for adhesive bonded joints

Effective bonded joints should be designed to ensure that the bonded strength is not less than that of the adherends. Otherwise, the adhesives will become weak links, resulting in the premature failure of the bonded structure.

From the standpoint of increasing strength and reducing costs, the basic principles for bonded joint design are as follows:

- (1) A rational joint configuration should be selected to ensure that the shear loads are carried by the bond-line in the maximum strength direction. Whenever possible, normal stress, cleavage, and peel forces should be avoided to prevent peeling failure;
- (2) Minimize joint eccentricities and stress concentration. Reduce peel stress. Interlaminar peel failure of end laminates should be avoided;
- (3) Balanced adherend stiffness is required to reduce peel stress;
- (4) Use adherends with similar coefficients of thermal expansion. The coefficient of thermal expansion of the adhesives should be close to that of the adherends to reduce residual stress;
- (5) Ductile adhesives are preferred over brittle ones;
- (6) Film adhesives are preferred over paste adhesives for large area bonds;
- (7) Ensure the bonded joint configuration can be visually inspected to improve reliability and confidence. It is important to emphasize the process control;
- (8) It should be recognized that slow cyclic loading is a major factor affecting the durability of adhesive joints. Avoid the worst effects of this type of loading by providing sufficient overlap to ensure that some of the adhesive is lightly loaded. Ensure that creep cannot occur at that position under the most severe potential humidity and temperature, to which the component will be exposed.



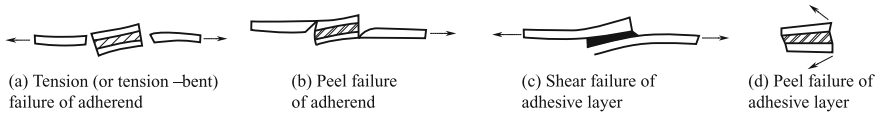
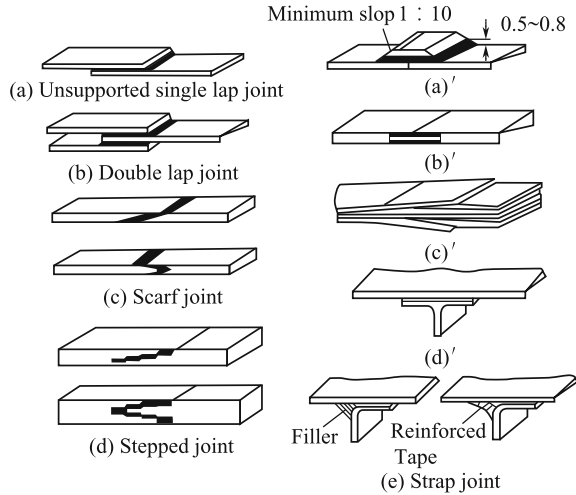


**Fig. 4.69** Basic failure modes for bonded joints

**Fig. 4.70** Basic configurations of bonded joints



The overall purpose of these principles is to ensure that the strength of the bonded layer is higher than or close to that of the adherends. Therefore, it is necessary to adopt measures to ensure that the configuration and geometric parameter satisfy these requirements.

**(2) Failure modes of bonded joints**

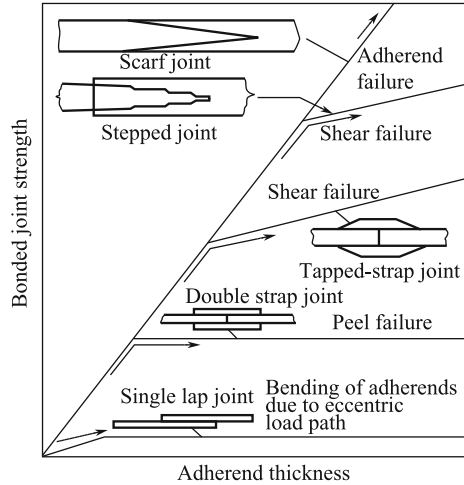
Basic failure modes for adhesively bonded composite joints are as follows (shown in Fig. 4.69):

- (1) Tension (or tension-bending) failure of adherend;
- (2) Shear failure of glue-line;
- (3) Peel failure of bond-line and adherends.

Alongside these three basic failure modes, combined modes may also occur. The failure modes of bonded joints will depend on the joint configuration, geometric parameters, fiber direction near the glue-line, and loading properties. The adherend thickness is the most important geometric parameter, as outlined for the following cases:

- (1) Tension (or tension-bending) failure of adherend will occur when adherends are very thin, and joint strength is sufficient;

**Fig. 4.71** Influence of adherend thickness on selection of joint configuration



- (2) Shear failure of the glue-line will occur when the adherends are thick and the eccentric moment is small;
- (3) Peel failure will occur under eccentric moments when the adherend thickness reaches a certain value and the bond length is not long. The interlaminar tension strength of CFRP is very low; thus, composites are prone to interlaminar tension failure. Peel failure will reduce the load capability greatly and should be avoided.

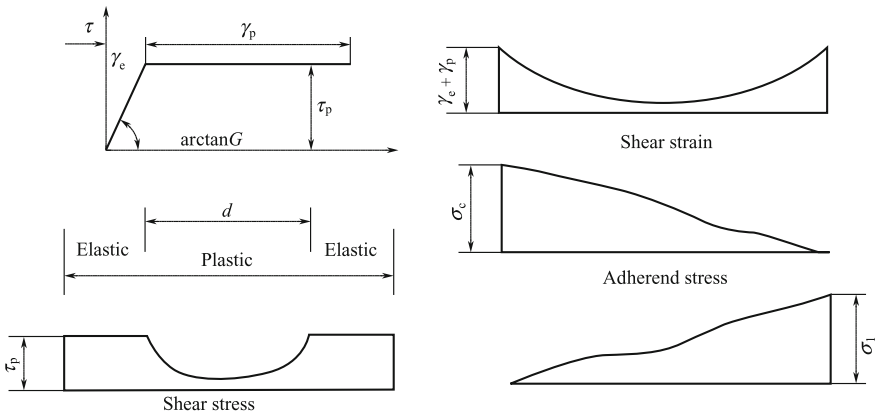
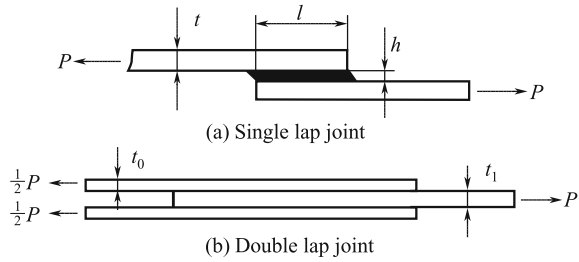
### (3) Selection of basic joint configuration for bonded joints

Figure 4.70 shows some basic joint configurations for panel components of aircraft.

The selection of a joint configuration is key for bonded joint design. Joints must be designed to transfer their maximum load in the shear direction with smaller loads in other directions. This will avoid the occurrence of large peel stress. Figure 4.71 illustrates the strengths of basic joint classifications as a function of the adherend thickness. Each curve shown represents the best strength that can possibly be obtained for each joint type.

- (1) Single-lap joints may be used when adherends are thin ( $\leq 1.8$  mm). Note that additional bending moments, caused by eccentricity of the load path, will result in very high peel stress at both ends of the bonded joint, which will reduce the joint strength. Therefore, it is necessary to increase the overlap-to-thickness ratio. Bending moments may be alleviated through the use of a high ratio  $L/t = 50\text{--}100$ . When adherends feature an imbalance of stiffness, eccentricity effects will be greater. The use of single-lap joints should be avoided. However, in a single-lap joint supported against bending, eccentricity effects may be alleviated and deformations restricted. Such joints

**Fig. 4.72** Geometric parameters of bonded joints



**Fig. 4.73** Stress and strain distribution of balanced stiffness double-lap joint

may be treated as double-lap joints in analysis, by considering the single-lap joint as half of a double-lap joint. Secondary adhesive bonding is used extensively for thin, lightly loaded composite structures, to reduce the need for mechanical fastening.

- (2) Adherends of moderate thickness ( $L/t \approx 30$ ) are suitable for double-lap joints.
- (3) Thick adherends are suitable for stepped and tapered joints, where stepped joints are most commonly used. Stepped-lap joints share some characteristics of both scarf and uniform lap joints. The pure shear state for every step can be closely attained and as the number of steps is increased a higher joint efficiency will result. As a rule, scarf joints are only used for repairs of thin structures.

**(4) Selection of geometric parameters for bonded joints**

As an example, the geometric parameters of single-lap joints under a tension load are: adherend thickness  $t$ , bond layer thickness  $h$ , and overlap length  $L$  (Fig. 4.72).

The adherend thickness is determined by the required transfer load  $P$ .

The thickness of an adhesive layer has an effect on joint strength. For most practical joints, adhesive layer thickness is maintained in the range 0.10–0.25 mm. Stress concentration can be reduced and joint strength can be improved by increasing the thickness of adhesive layer. However, thicker layers tend to have a high void content, and strength will be reduced. Furthermore, high-precision fitting

between adherends is required for thin adhesive layers such that a very thin glue-line may not be possible.

The design of simple, bonded splices of uniform thickness for near quasi-isotropic carbon/epoxy is simple. Use a  $30t$ -overlap for double shear,  $80t$ -overlap for single-lap joints, and a 1-in-50 slope for scarf joints. Overlapping ends should taper to 0.51 mm with a slope of 1/10.

Analysis and test results indicate that the shear stress distribution is not uniform throughout the bonded area under an applied load. Most of the load is transferred through two end zones which form a low stress elastic trough (Fig. 4.73).

Because of the presence of these elastic troughs, the load carrying capacity of the bonded joint increases gradually in the beginning. However, the width and depth of the elastic trough only increases continuously when the length of the overlap attains a certain value. Increases in overlap length above this value do not add to the joint's load carrying capacity. From the viewpoint of static strength, there is no need to increase the overlap length; however, service life and durability should also be considered and longer overlaps are often used. For very short overlap and transfer of large loads, the minimum shear stress and strain in the middle of the overlap area are nearly equal to that at both ends. Thus, the entire bond is in a plastic state. When the load is removed, the adhesive in the middle cannot recover, and the joint will fail soon. Analysis results demonstrate that at a minimum stress equal to 10% of the maximum stress the glue-line can recover its original state. For double-lap joints, an elastic trough width of  $6/\lambda$  is sufficient to ensure a minimum adhesive shear stress distribution, which is no greater than 10% of the maximum stress.

#### (5) **Fiber orientation of the bond surface**

The surface fiber direction of the laminate should be in the primary load direction or  $45^\circ$  to the load direction, but not perpendicular to the load direction, to prevent adherend premature interlaminar tension (peel) failure.

#### (6) **Surface preparation of adherends**

The bonding of adhesive is a complicated activation process between the adherends and adhesives. It is important to prepare a quality adherend surface for good quality bonds in terms of static strength and durability. The bond should meet prescriptive technical specifications. Strict quality control and inspection should be performed in the bond processing. Nondestructive inspection should be performed for all important parts. Surface preparation deficiencies are particularly troublesome because there are currently no nondestructive evaluation techniques for detecting low interfacial strength between the bond and adherends.

For bonds between carbon-epoxy composites, solvents may be used to clean the surface together with mechanical abrasion of the surface. For bonds between composites and metal, in addition to the surface preparation the metal will require a surface treatment. Corrosion barriers (such as fiberglass and sealants) are placed at the interfaces between the composites and aluminum or steel to prevent galvanic corrosion.

Globally, surface treatment processes for metals include: stainless steel, no-treatment; titanium, phosphoric acid anodization or no-treatment; aluminum, chromic acid anodization.

Phosphoric acid anodization is a common surface treatment for aluminum in China. To prevent galvanic corrosion, a fiberglass or Kevlar insulated layer should be placed between the aluminum and composite.

#### 4.8.2.5 Design of Thick Section Joints

Thin section joints can only transfer small loads; however, it is possible to transfer larger loads through thick section joints. Failure will occur preferentially in the adhesive for thick adherends in a simple joint configuration. Thick adherends cannot perform effectively and joint efficiency will be low. To ensure the glue-line is not a weak link in the joint and to make full use of the load-bearing capacity of the adherends and avoid premature failure, the bond surfaces should be increased and peel stress reduced. Complex stepped and tapped joints are typically used.

- (1) Selection of stepped and scarf joints: Thick adherends under a large load are suitable for stepped or tapped joints. The use of stepped or scarf joints is effective for reducing peel stress. The advantages of stepped joints over scarf joints are their ease of fit and high strength achievable by adjusting structural parameters. Therefore, higher joint efficiency may be attained. Composite-to-titanium stepped joints are used extensively throughout the aerospace industry for high load transfer.

Stepped and scarf joints are appropriate for highly loaded thick plate bonded joints. The use of scarf and stepped joints is effective for reducing peel stress. Unlike scarf lap joints, stepped joints have simple processing and can achieve high strength by adjusting structural parameters. Stepped-lap joints are commonly used for joining cover panels and titanium structures, see Fig. 4.74.

- (2) Strain-level requirements: In the design of strain levels for thick adherend structures, values should be properly lowered considering the need for future repair. It is impractical to repair thick structures by bonding because of the taper ratio requirement, i.e., 1:50. When there is no need for repairs such as one-shot

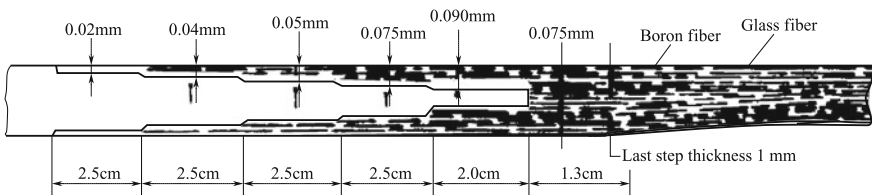


Fig. 4.74 Root-stepped joints of F-14 all-movable horizontal stabilizers

and throwaway structures, in missiles and unmanned aircraft, bonding permits extremely high structural efficiencies to be obtained, even on thick structures.

- (3) Geometric requirements of stepped-lap joints: Complex stepped joints are required to obtain sufficient joint efficiency in thick structures. Many steps are required to transfer load, and to ensure that the glue-line provides adherend strength. The thickness at the end step should be a minimum of 0.76 mm and the step length no longer than 9.5 mm, to prevent failure of the end step. Tapered ends of bonded overlaps should taper to a thickness of 0.51 mm with a 1-in-10 slope. This minimizes the induced peel stress that cause premature failure.
- (4) Layering requirements of stepped-lap joints: If possible,  $\pm 45^\circ$  plies should be used on the first and last step of bonded step joints to reduce the peak inter-laminar shear stress at end steps.  
If possible, do not end with more than two  $0^\circ$  plies, which have a thickness less than 0.36 mm, on any step surface. For  $0^\circ$  plies ending on the last step (longest  $0^\circ$  ply), serrated edges have been shown to reduce the stress concentration and reduced stress concentration at the end of the joint.  $90^\circ$  plies should butt up against the first step of a step joint.
- (5) The differences in thermal expansion coefficient between the adherends need to be minimized to reduce thermal stress for composite-to-metal joints. Bonding composites to titanium is preferred; steel is acceptable; aluminum is not recommended.
- (6) Technological considerations. Co-cured joints are preferred over pro-cured joints if there are fit-up problems. For pre-cured parts, machined scarfs are preferred over layered scarfs for improving the fit.

#### 4.8.2.6 Detailed Design of Composite Bonded Structure

Detail design of composite bonded structures should not only consider the static strength of the bonded structure but also the durability, bonding technology, and cost of the bonded structure. In addition to the aforementioned basic principles, the following issues should be noted for detailed design of composite bonded structures.

- (1) Selection of bonded joint configuration: The configuration of a bonded joint is a critical design aspect. The load-bearing capabilities of bonded joints work best in the shear direction and have poor resistance to peeling. The maximum load should be transferred in the shear direction and minimum loading should be induced in other directions. The use of stepped-lap or scarf-lap joints is effective for reducing peel stress and ensuring the joint strength is not lower than that beyond the joint.

- (2) Procedures for reducing stress concentration and peel stress for adhesive joints: Whenever possible, the peel stress in the structure should be reduced by induction of eccentricities in the load path and asymmetry. For example, the use of a symmetric double-lap joint increases the bending stiffness of the outer adherend, and tapering of the edges of the overlap in single joints. Three procedures for decreasing stress concentration are illustrated in Fig. 4.75.

**Fig. 4.75** Procedures for decreasing stress concentration

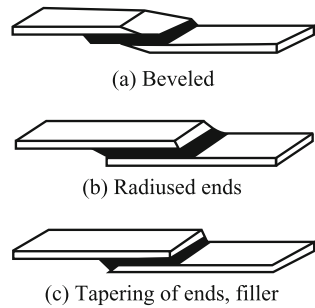


**Fig. 4.76** Single-lap joint with transverse support

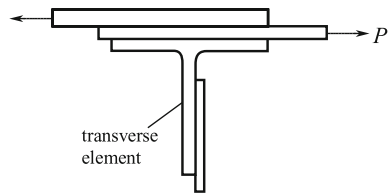


**Fig. 4.77** Joint of corner reinforcement to skin

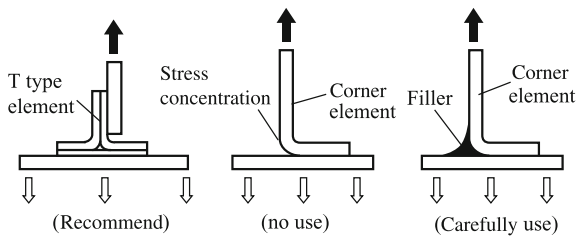
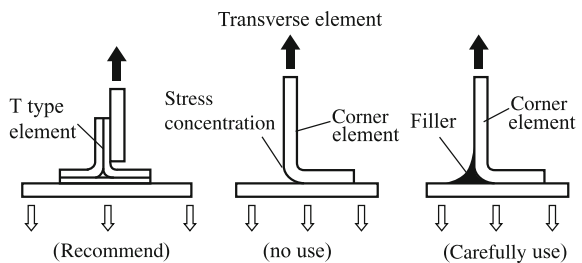


**Fig. 4.78** Stress distribution of T-type reinforcement



A high stress concentration at both ends of the joint occurs owing to eccentricity in the load path for single joints. Thus, the peel stress can result in the premature failure of the adherends. The load-bearing capacity will be improved by supporting a joint with a transverse fully stiffened restraint (Fig. 4.76).

- (3) Skin (web) strengthening procedure: The use of T-type components rather than angled components is recommended. Peeling at the corner of the angle reinforcement can occur easily if there is a tension force. Premature peeling may be prevented with the use of filler at the corner (Fig. 4.77). When a T-type element is used, peeling can be prevented if there are tension forces. Peeling will be improved by edge tapering of the profile element and balancing the stiffness between the profile element and web. The stress distribution of T strengthened elements is shown in Fig. 4.78.
- (4) Thermal stress of bonded structures: In the bonding of carbon/epoxy, boron/epoxy composites to metals, such as titanium and steel, Thermal residual stress arises due to differences in thermal expansion coefficient of the materials. In particular, the thermal stress is proportional to the difference between the operating and cured temperature. Thermal stress can be reduced through the use of laminate layering design.
- (5) Avoidance of galvanic corrosion: In the bonding of composites to metal, galvanic corrosion may occur owing to differences between the electrode potentials of materials. Surface treatment of metal elements should be performed. Whenever possible, direct bonding of carbon composites to aluminum should be avoided and an isolating layer should be placed between the materials.  
Carbon fibers must be isolated from aluminum or steel through the use of an adhesive layer and/or a thin glass-fiber ply at such interfaces. The galvanic interaction between carbon and aluminum or steel will cause corrosion of the metal.
- (6) Prevention of moisture entering adhesive layer: Unlike metal adherends, composite adherends are subject to the effects of moisture diffusion. As a result, moisture is more likely to affect the whole component rather than be confined near the exposed edges of the joint in the case of metal adherends. The response of adhesives to moisture is an important issue for composite joints.
- (7) Tooling design and manufacture: The quality of bonded joints is influenced greatly by tooling. Therefore, careful attention is required for the design and processing of bonded joints to minimize thermal deformation and residual stress. Tools should be applied under uniform pressure to the adherends.
- (8) Quality control: Adhesive quality should be controlled based on allowable values for defects prescribed for different positions.



### 4.8.2.7 Durability Design of Bonded Structures

Durability of composites relates to their fatigue performance under cyclic loading and different environmental conditions. Like metals, it is difficult to reliably estimate the life of composite structures. Durability of composite structures is mostly assured by performing constant or variable amplitude cyclic loading tests.

Durability of bonded structures is based on adhesive performance, surface preparation, loading and environmental conditions, structural characteristics, and the detailed design.

The design of adhesive joints should be focused on joint durability rather than static strength and should meet certain conditions. Three major considerations for bonded joint durability, based on the design philosophy of Hart–Smith, are as follows:

① Either the adherent thickness should be limited, or more sophisticated joint configurations, such as scarf and step lap joints, should be used to ensure that adherend failure takes precedence over bond failure; ② The design should minimize peel stress, either by keeping the adherends sufficiently thin or by tapering the adherends for intermediate adherend thicknesses (see discussion of effects of adherend tapering); ③ It is essential that good surface treatment practices are maintained to ensure that the bond between the adhesive and adherends does not fail. When these conditions are met, reliable joint performance can be expected for the most part, except in environmental extremes (hot–wet conditions). The Hart–Smith approach focuses primarily on creep failure associated with slow cyclic loading (i.e., one cycle over several minutes to an hour) under hot–wet conditions.

In fact, the distribution of shear stresses of bonded joints is non-uniform. The maximum stress occurs at both ends of bonded joints and stress in the middle area is basically zero. The Hart–Smith criterion for avoidance of creep failure is that the minimum shear stress along the bond length should be no greater than one tenth the yield stress of the adhesive.

In addition to creep failures under hot–wet conditions, the joint may fail due to cracking in the bonding layer.

### 4.8.2.8 Summary of Bonded Joint Analysis

Stress analyses of adhesive joints range from very simplistic ‘P over A’ formulations in which only the average shear stress in the bond layer are considered, to extremely elegant elasticity approaches that consider fine details—for example, calculation of stress singularities by applications of fracture mechanics concepts. A compromise between these two extremes is desirable, because the adequacy of structural joints does not usually depend on knowledge of their details at the micromechanics level, but rather at the scale of the bond thickness. Practical considerations require bonded joints to incorporate adherends, which are thin relative to their dimensions in the load direction; hence, the stress variation through the thickness of the adherend and the adhesive layer tend to be moderate. Such variations do tend to have a great effect on polymer matrix composite adherends because of their relative softness with respect to transverse shear and thickness

normal stresses. However, design procedures have been developed by neglecting the thickness-wise adherend stress variation. Such approaches involve the use of 1D models in which only variations in the axial direction are accounted for.

FEMs are often used for investigating various features of bonded joint behavior. However, there are serious pitfalls, which the analyst must be aware of to avoid problems in such analyses. There is a tendency for the bond layer thickness to unbalance the finite element model. To achieve adequate accuracy, it is especially important to provide a high degree of mesh refinement around the ends of the overlap and the mesh should transition to a coarser representation away from the ends of the overlap to avoid unneeded computational costs. Without such approaches, the aspect ratios of elements may be limited and will force either a crude representation of the bond layer or an excessively over-refined mesh for the adherends.

Currently, the most useful analytic method is based on the simplified one-dimensional approaches characterized in the work of Hart–Smith. This method emphasizes principles, which have been determined from practical experiences in joint design, and has been successfully applied to aircraft components. Before analyses, a stress–strain diagram of the glue-line and other characteristic parameters, similar to those shown in Fig. 4.68, needs to be measured for the adherends and adhesives. The analytic methods for single-lap, double-lap, stepped, and scarf joints are presented in references [4–7]. It should be noted that design parameters based on these methods consider only static strength. Other factors should be considered separately—specifically, the influence of long-term loading in particular environments. The ultimate design parameters should be determined by the necessary tests.

### **4.8.3 Mechanically Fastened Joints**

#### **4.8.3.1 Design of Mechanically Fastened Joints**

##### Characteristics of Mechanical Joint Design

The following points should be noted for mechanical joints [2, 13, 17]:

- (1) Owing to the brittle nature of composite materials, multiple fastener joint load distributions are non-uniform. The stress and strain of basic laminates will be lower when joints fail;
- (2) The bolted joint strength of laminates with a certain content of  $0^\circ$ -plies is less than the unnotched laminate strength;
- (3) The load-carrying capability of joints does not show a directly proportional increase with the end distance;
- (4) Bolted joints should be designed to carry a load such that the bolt is under a shear force rather than tension. Bolt bending in composites is more common than that in metals.

## Main Factors Affecting Mechanical Joint Strength

There are many more factors that affect the mechanical joint strength of composites than those affecting metals. It is important to understand and consider all factors in design.

These factors can be classified into the following five types:

- (1) Material type and form: unidirectional tape or woven fabric fibers, resin type, fiber orientation of, fiber volume fraction, and laminate pattern;
- (2) Processing methods: prepreg, RFI, RTM, curing, and consolidation processes (vacuum bag molding and oven and autoclave curing);
- (3) Configuration: joint types (single or double lap), geometry (pitch, space, edge distance, side-end distance, thickness, hole diameter and tolerance, hole patterns, and washer size);
- (4) Fastener types (hexagonal head bolt, big foot bolt, blind fastener, protruding and countersunk head fastener), clamp-up force;
- (5) Load: static, dynamic, fatigue load, load direction, loading rate;
- (6) Environment: temperature and humidity.

### (1) Laminate pattern

Laminates used in aerospace structures are generally composed of layers in the  $0^\circ$ ,  $\pm 45^\circ$  and  $90^\circ$  directions with respect to the axes of the laminate. The percentage of  $\pm 45^\circ$  plies has an important effect on laminate bearing strength. Shear-out or cleavage failure can occur more readily when the  $\pm 45^\circ$ -ply content is less than that of the  $0^\circ$  plies. Unlike metals, shear-out failure can only be prevented by increasing the end distance of holes. It is more important that a proper percentage of  $\pm 45^\circ$  plies is maintained. Bearing strength increases with the percentage of  $\pm 45^\circ$  plies. The recommended layering ranges to achieve maximum strength in joint areas are  $\pm 45^\circ$  plies  $\geq 40\%$ ,  $0^\circ$  plies  $\geq 30\%$ ,  $90^\circ$  plies in the range 10–25%, with variations of 5% allowed. Bearing strength will decrease as the percentage of the  $\pm 45^\circ$  layers is increased further.

Characteristics of  $\pm 45^\circ$  layer content  $\geq 50\%$  are as follows:

- (1) Joint strength is less sensitive to load direction;
- (2) Initial failure strength may occur earlier;
- (3) Shear load-bearing ability is stronger and tension load-bearing ability is lower.

Particular care should be given to the tension in multi-row fastener joint design.

### (2) Ply stacking sequence

The stacking sequence is a special parameter effecting the mechanical nature of composites. Laminates of the same ply numbers and proportions can have various stacking sequences, which can change interlaminar stresses, and the mechanical natures of laminates may be affected. Whenever possible, maintain a well-dispersed stacking sequence and avoid grouping similar plies.

### (3) Fastener torque

Bearing strength is sensitive to clamping forces, namely the force in the through-thickness direction caused by tightening the bolt. Bolt clamp-up improves the strength of composite joints. Test results have demonstrated that bearing strength increases with torque moment until a certain value, after which the bearing strength will not increase. Excessive bolt tightening could damage the laminate.

### (4) Joint configuration

Joint configuration is one of the important factors affecting mechanical fastening strength. In comparison with double shear lap joints, lap joint strength decreases because of eccentricity in the load path. The magnitude of the single shear effect depends on plate thickness and has little effect on thin laminates; however, it has a clear effect on the initial bearing failure strength. Single shear effects will increase gradually with plate thickness.

### (5) Width-to-diameter ratio

The width-to-diameter ratio mainly effects the net-tension failure strength of mechanical joints. Failure modes of joints will transform from tension to bearing with increasing plate width, when the end edge distance is sufficient. Because bearing failure is a local phenomenon, further increases in  $W/D$  do not affect the joint strength. However, joint efficiency can be reduced. The  $W/D$  ratios of failure mode transitions from net-tension to bearing are different for various laminates. It is recommended that laminate patterns in joint areas should have a minimum bearing failure of  $W/D = 5$ . For orthotropic ( $0^\circ = 50\%$ ,  $90^\circ = 50\%$ ) and  $100\% \pm 45^\circ$  layers laminates, larger  $W/D$  values are needed for bearing failure to occur.

### (6) End edge distance-to-diameter ratio

The end edge distance-to-diameter ratio mainly affects the shear-out failure strength. Failure modes of joints will change from shear to bearing with increasing  $e/D$  when the plate width is sufficient. It is recommended that patterns in the joint areas should have a minimum  $e/D$  not less than three. For laminates including a lower proportion of  $\pm 45^\circ$  layers, a larger  $e/D$  value is needed. The transition ratios of  $e/D$  will differ among various laminates.

### (7) Hole diameter-to-thickness ratio

When  $W/D$ ,  $e/D$ , and  $D/t$  are constant, failure loads of mechanical joints will increase with hole diameter, but bearing strength will decrease. The joint strength will attain a maximum at approximately  $D/t = 1.0$ . The joint strength will decrease as  $D/t$  is increased further. The bearing strength will decrease about 13% when  $D/t = 3$ .

It should be noted that fastener failure will generally occur if the fastener diameter is smaller than the plate thickness. When the laminate capacity is calculated, the effective thickness  $t_e = d$  should be used:

$$t_e = t \text{ for } t \leq d;$$
$$t_e = d \text{ for } t > d.$$

### (8) Load direction

The angle between the fastener load and 0°-ply direction can affect joint strength owing to the anisotropic nature of the strength and stiffness of composite materials. Test results have indicated that the bearing strength decreases as the angle between the fastener load and 0°-ply direction increases. The more isotropic the layering, the less sensitive the laminate will be to load direction.

### (9) Countersink holes

Countersinks will clearly decrease laminate bearing strength. This effect will decrease gradually with increasing plate thickness.

### (10) Hygrothermal environment

Environmental conditions such as temperature, moisture, and corrosion have a significant effect on laminate bearing strength. The extent of these effects is outlined in Sect. 4.8.3.4 of this chapter.

## Design Basic of Mechanical Joints

### (1) General requirements of mechanical joints

The following basic principles should generally be followed in the design of mechanical joints:

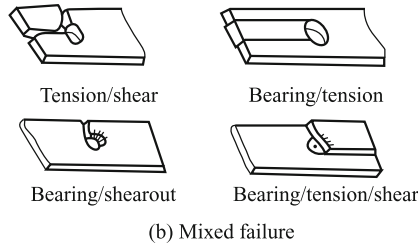
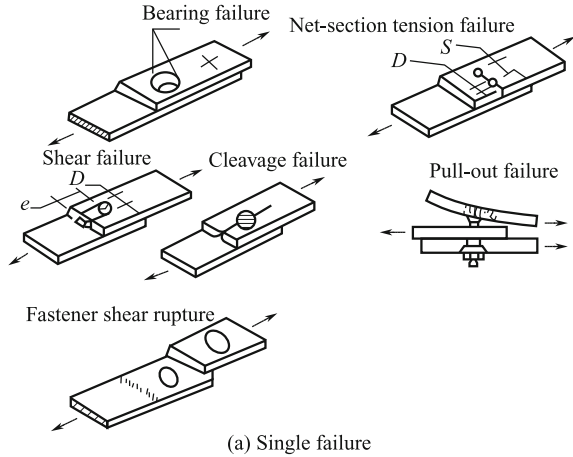
- (1) Strength requirement should be satisfied in terms of the design of joint geometry and laminates. Allowable bearing stress cannot be exceeded in design loads;
- (2) Future repair activities should be considered such that joints can accommodate the next largest fastener size;
- (3) Use double shear joint configurations;
- (4) Fasteners should bear load in shear direction and avoid tension and bending;
- (5) Requirements of galvanic corrosion resistance should be satisfied;
- (6) Consider the environmental effects of operating conditions and special requirements.

### (2) Failure modes of mechanical joints

Composite mechanical joints mainly have the following failure modes:

Single failure modes: Bearing, tension, shear-out, and cleavage failure of laminates (Fig. 4.79a).

**Fig. 4.79** Single and combined failure modes of mechanical joints



Mixed failure modes: bearing-tension, bearing-shear-out, tension-shear-out, bearing-tension-shear-out failure of laminates (Fig. 4.79b); Pull-through, fastener shear rupture, tension and bending failure of fastener modes.

Mechanical joint failure modes mainly depended on the joint geometry and the fiber pattern. Tension and shear-out failures occur when  $W/d$  and  $e/d$  are respectively too small. Note that increasing the end distance will have no benefit if shear and cleavage failure occur because the  $0^\circ$ -ply content is likely too high. Cleavage and shear failures are two kinds of low strength failure modes, which should be prevented. Bearing failures occur when both  $W/d$  and  $e/d$  are too large. Bearing damage is localized and is usually not associated with catastrophic failure of a composite structure. Fastener shear and bending failure may occur when the ratio of plate thickness to the fastener diameter is large. For single-row fastener joints, from the perspective of joint safety and efficiency, whenever possible, mixed modes associated with bearing failure should be designed. Tension failure generally occurs for multirow joints, because this failure mode is governed by bearing-bypass load interactions. Special care should be taken in the design of these joints.

### (3) Configuration and selection of mechanical joints

Composite fastening joints can be classified as single and double shear lap joints. Each joint type has uniform and varying thickness conditions (Fig. 4.80).

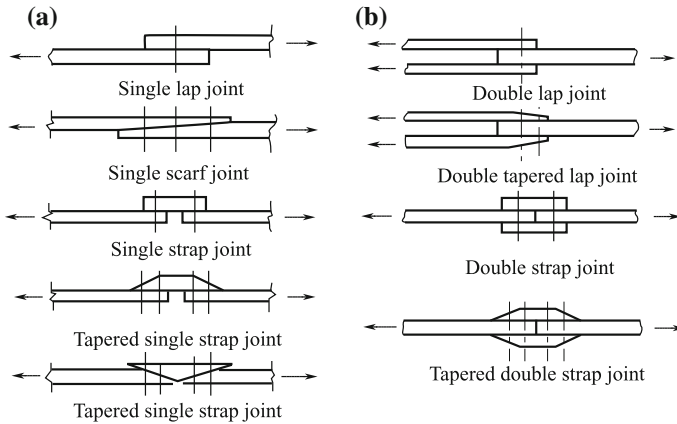


**Fig. 4.80** Basic types of mechanical joints

The following principles are recommended for selection of composite fastening joints:

- (1) Joint design should be suitable for use in double shear lap joints. Whenever possible, unsymmetrical single shear lap joints with low efficiency should be avoided;
- (2) Multiple rows are recommended for unsymmetrical joints such as single shear lap joints. The back pitch should be as high as possible, to minimize bending induced by eccentric loading. Local reinforcement of unsymmetrical joints by arbitrarily increasing the laminate thickness should generally be avoided because the increased resulting eccentricity might increase bending stress. This effect will counteract or negate the increase in the material area;
- (3) Carbon fiber/resin matrix composites do not generally feature plastic deformation. This may result in a severe non-uniform load distribution in multirow fastener joints. Therefore, joints with more than two rows of fasteners should not be used, and hole patterns with parallel-row joints should be used whenever possible;
- (4) Tapered joints can improve the non-uniformity of load distribution in multirow fastener joints and increase the load-bearing capacity of joints. It is important to select tapered splice plate thickness and fastener diameters in the design.

#### (4) Ply-layering requirements in joint areas

To improve the strength and flexibility of mechanical joints, the following principles should be considered in addition to general ply-layering requirements:

- (1) The percentage of  $\pm 45^\circ$ ,  $0^\circ$ , and  $90^\circ$  plies should not be less than 40%, 30%, and 10%, respectively. This is particularly important for mechanical joint design;
- (2) Extremely thin laminates should be reinforced locally at the attachment area to provide greater thickness. This reinforcement will avoid the reduced bearing allowables that result from a  $D/t$  ratio greater than four. The general rules  $D/t \geq 1$  should be followed to avoid failure of the fastener;
- (3) In areas of load induction there should be equal numbers of  $+45^\circ$  and  $-45^\circ$  plies on each side of the mid-plane;
- (4) Butt-splined fibers should be avoided in join areas.

**(5) Geometry requirements**

To prevent low strength failure and ensure high strength of mechanical joints, geometric parameters of jointed plates should be selected according to Table 4.18. Definitions of the geometric parameters are shown in Fig. 4.81.

In addition, the geometric size of joints should consider future repair demands. The next largest size fastener should be useable after the repair.

**(6) Fastener requirements**

To prevent galvanic corrosion, fasteners made from titanium, titanium alloy, stainless steel, and Monel should be used because the electrode potentials of these alloys are close to those of the composites.

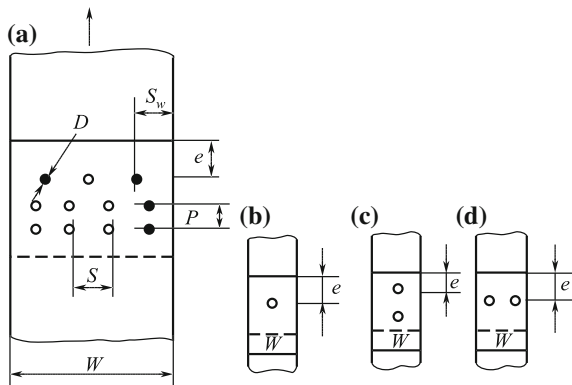
- (1) Principles for selecting fastener diameter: General guidance for selecting fastener diameters are as follows:

- ① Sufficient bearing strength of jointed component should be ensured.

**Table 4.18** Select of geometric parameters of mechanical joints

$S/D$	$p/D$	$S_w/D$	$e/D$	$D/t$	$H/\text{mm}$
$\geq 5$	$\geq 4$	$\geq 2.5$	$\geq 3$	$1 \leq D/t \leq 2$	$H \leq 0.7t$

**Fig. 4.81** Definition of geometric parameters of mechanical joints





The fastener diameter-to-thickness ratio should be properly considered to guarantee sufficient fastener strength. The rated shear strength of fasteners does not usually control the joint design. Bolt diameter is usually governed by the need to avoid exceeding the allowable bearing stress of the laminate.

- ② Fasteners should have sufficient stiffness to prevent any reduction of the laminate allowable bearing stress, owing to severe bending of the fastener.

Primary determination of fastener diameter is based on the occurrence of fastener shear failure and laminate bearing failure at same time, that is,

$$D/t = 4[\sigma_{br}]/\pi[\tau_b] \quad (4.69)$$

where

- $D$  —fastener diameter, mm;
- $t$  —laminate thickness, mm;
- $\sigma_{br}$  —allowable laminate bearing strength, MPa;
- $[\tau_b]$  —allowable fastener shear strength, MPa.

## (2) Selection principles for fastener type

- ① Bolts are used for structural joints transferring high load, which may require reassembly. Rivets are used for structures that are not intended to be disassembled. The laminate thickness range suitable for rivets is generally 1–3 mm;
- ② Carbon fiber laminates in direct contact with aluminum (without a coating), steel components with aluminum- or cadmium-plating should be avoided to prevent galvanic corrosion. If it is necessary to use such parts, insulating layers should be added. Measures to prevent galvanic corrosion may be adopted for carbon fiber laminates in contact with stainless steel. Titanium alloy and stainless steel fasteners are often installed wet with sealant;
- ③ Tension head fasteners are preferred for most applications. Shear head fasteners can lead to local hole bearing damage because of the size of their smaller heads, which can roll. Shear head fasteners may be used in special applications only where stress considerations allow;
- ④ In generic joints, it is recommend that the precision of the fastener-to-hole size is not lower than H9/h9. Precise ream holes are used for important joints. Interference fits should not currently be used because interference fit assembly technology has not yet been fully mastered.

## (3) Requirements of bolt torque

**Table 4.19** Bolt tightening torque /N·m

Screw diameter	Nut type		
	Thick type	Thin type	All types
	Countersunk head tension Hexagonal head	All types	Countersunk head share
M5	3–5	2.3–3.2	2.3–2.9
M6	5–8	2.9–4.9	3.1–3.9
M8	10–15	6.4– 10.8	10.2–11.3
M10	18–25	12.3–19.1	10.8–11.9
M12	25–30		

Proper tightening torque can increase bolt-joint strength. The torque moment should be selected based on the relational standard for various material, diameter, and the bolt type. If there are no special requirements, the tightened torque may be selected according to Table 4.19.

#### (7) Requirements of galvanic corrosion resistance for mechanical joints

The three conditions which lead to galvanic corrosion should be excluded in the design: potential differences between materials, presence of an electrolyte, and the electric connections. The following measures of corrosion prevention should be used:

- ① Material matching can prevent galvanic corrosion. Metals that have electrode potentials that match those of carbon/epoxy composites include: titanium alloy and stainless steel.
- ② Prevention of electrolyte accumulation should be considered in the design; sealing of joints should be performed to prevent infiltration of electrolyte and avoiding corrosion battery formation.
- ③ For materials unsuitable for direct contact, an insulating layer of glass/epoxy or aramid/epoxy should be used. At important joint sites which may be predisposed to corrosion, full sealing of the joints should be used to prevent corrosion.
- ④ Joints can be installed wet with sealant, in addition to insulation. In riveted joints, it is important to wet set with sealant, to prevent galvanic corrosion but also compensate for any manufacturing damage.
- ⑤ Fiber laminates in direct contact with aluminum and aluminum and cadmium plated steel components should be avoided to prevent galvanic corrosion. Otherwise, an insulating layer should be added. Carbon fiber

in direct contact with stainless steel should adopt some measures to prevent corrosion. Titanium may be used directly without any protection.

#### (8) **Gap filling requirements**

The gap between attached parts should not exceed 0.8 mm for non-structural shim. Large gaps cause excessive bolt bending, non-uniform load-bearing stress, and an eccentric load path. Any gap in excess of 0.13 mm should be shimmed to minimize interlaminar stress due to clamp-up.

### Design of Riveted Joints

#### (1) **Design requirements for riveted joints**

Selection of geometric parameters of riveted joints should follow the parameters given in Table 4.18. Laminate design should follow the principle described in section “4.Design Basic of Mechanical Joints”.

#### (2) **Selection principles of rivets**

Principles for selecting rivets are as follows:

- (1) In addition to galvanic corrosion prevention and high strength, rivet materials should have good plasticity to satisfy the requirements of riveting assembly technologies. Titanium alloy, pure titanium and titanium–niobium alloy rivets are preferred to avoid galvanic corrosion. Aluminum and low-alloy-steel rivets are not suitable owing to the large difference between their electrode potential and that of the composites. A286 and Monel are less applicable because of their lower specific strength. Stainless steel fasteners in contact with carbon should be permanent and wet set with sealant.
- (2) Bimetallic and blind rivets should be preferred to avoid damage to the laminate.
- (3) The rivet diameter should generally not exceed 4 mm, to allow for easy formation and avoid damage to the laminates. Flush fastener and round head rivets should be used whenever possible where the structure requirements are satisfied.
- (4) To allow for disassembly and for non-stressed or secondary stressed inner components, a low number of aluminum rivets may be used from the view

point of reducing weight and cost. However, these must be wet set and strict measures taken to prevent galvanic corrosion prevention.

- (5) Avoid buck rivets in composite structures. Squeeze rivets can be used if washer is installed on the tail side.

**(3) Measures to improve pull-out strength**

For outer surface of structures, such as the rudder, a hole cap and countersink can be used to strengthen the structure with titanium alloy or stainless steel to improve the pull-out strength.

**(4) Reliable measures for galvanic corrosion prevention**

**(5) Riveting processing requirements**

- (1) Riveting should follow technology specifications. Strict quality control and inspection should be conducted during hole drilling, countersinking, and riveting. Nondestructive evaluation should be conducted for important parts;
- (2) Damage to the exit site of the drill should be prevented by coating the composite with a layer of film adhesive, glass-cloth, or a pad plate;
- (3) When composites come into direct contact with metallic components, under structure permissive conditions, snap the head of the rivet at the metallic surface whenever possible. If the snapped head of the rivet is on a composite surface, a pure titanium, titanium alloy, or stainless steel washers must be placed on the snap head;
- (4) Whenever possible, squeeze rivets should be used for parts requiring common solid rivets. Bull rivets may be considered where squeeze riveting cannot be conducted. Strong power rivets should be avoided.

## Fatigue of Mechanical Joints

Mechanically fastened joints are the main joint type used in primary composite structures. To meet structural integrality requirements, in addition to meeting strength and stiffness requirements, fatigue, damage tolerance, and functional requirements must also be satisfied. Stress concentration in mechanical joints can create fatigue weak points in the primary composite structure. Fatigue strength is determined mainly by testing now, because methods for pre-estimating the life time of composite joints are not mature, and are complicated by environmental conditions.

Three fatigue failure criteria should be considered in the rational design of mechanical joints under wet-heat conditions and different load spectrums.

Tension, shear-out, and bearing failure of fasteners loaded hole; permanent elongation deformation of fastener holes exceeding allowables; residual strength of joints is lower than the design requirements. The joint life will fail when any one of aforementioned items occurs. Generally, permanent elongate deformation of loading holes is the first limiting value.

Limiting values of permanent elongation of fastener holes depend on the subsequent damage to structure integrity. Control of the deformation value is based on the critical degree of deformation of the specific joint structure. Permanent deformation of a loading hole should not exceed 5% of the hole diameter.

Experimental investigations have shown that symmetric mechanical joints are insensitive to tension–tension and compression–compression fatigue if  $K < 0.67$  in both flight and gust spectrum action. In high-speed aircraft, the hygrothermal conditions spectrum, tension–compression fatigue with high  $K$  values, and unsymmetrical joint design should be considered in fatigue problems. Residual strength should not be lower than the inherent static strength. Fatigue is insensitive to processing defects, delamination, and damage growth resistance. For matrix-dominated laminates in a high loading cycle range and fiber-dominated laminates, signs of macrodamage are not obvious before rapid failure; thus, it is difficult to inspect damage in advance and prevent failure.

#### 4.8.3.2 Design of Main Load Carrying Joints

##### Characteristics of Multirow Fastener Joint Design

One major difference in the mechanical behavior of composite materials and metals is that composites are brittle and anisotropic; while metals are plastic. Metal has the capability to redistribute load, thus allowing each of the fastener holes of a multirow joint to uniformly carry the load distribution. However, for brittle composite materials this is not the case [26–31].

Composite (fiber-dominated) laminates generally show linear behavior up until failure. The material will not yield locally and redistribute stress. Effective joint design should adopt measures to reduce the bolt bearing stress in the most critically loaded locations. Even if at ultimate load non-uniformity of the fastener load distribution shows little improvement in comparison with the initial load for steel or titanium fasteners. Effective joint design requires that the greatest load-bearing fastener row should be reduced.

The strength of multirow bolted joints in composite structures is governed by associated bearing–bypass load interactions under tensile or compressive loads. The key to obtaining high operating strain in bolted joints in fibrous composite laminates is to restrict the bolt bearing stress in the most critically loaded locations. By tailoring the joint geometry, a bolt load distribution can be generated which maintains low bearing high bypass conditions in the first or outermost row of fasteners. With efficient joint design, cross-section strain in basic skin laminates can reach 0.005 in room-temperature tests.

The laminate fiber pattern is a design variable and optimizing the joint for maximum strain does not guarantee the highest strength or the most weight-efficient design. The principle design parameter governing the design of composite joints is the amount of load that must be transferred rather than the operating strain level of the adjacent structure.

## General Principles of Joint Area Design

Design principles for multirow fastener joints include:

- (1) The joint area should be designed first and the basic structure filled later. Optimization of the laminate fiber pattern should be performed considering the amount of load that must be transferred rather than the operating strain level of adjacent structures.
- (2) The load distribution of multirow joints mainly depends on the relative stiffness of jointed members. To obtain even load sharing, joined components need to have similar stiffness. Fastener stiffness also has a slight effect.
- (3) The geometry of joints should be optimized to improve the load-bearing capacity of multirow joints. The bearing stress of load holes can be reduced through the use of variable fastener diameters and thickness. Skins of uniform thickness in combination with tapered splice plates should be used for joints. The use of tapered splice plates can optimize fastener load distribution and reduce the bearing of the most severely affected fastener row. Both analysis and test results have shown these joint geometries are more efficient than other joint geometries. Notably composite tapered splice plates that have tapered washers should be used on spot faces milled at locations that may not be able to accommodate fasteners and nuts, because machining may induce small cracks on the surface.
- (4) Total thickness of the top and bottom splice should be slightly greater than that of the center cover even for the same material and fiber pattern. The reason for this requirement is that stress in the splice plate should be lower than that in the skin to prevent splice delamination. Otherwise, failure will occur at the splice plates. This is because, regardless of whether the applied loads are tensile or compressive, there is also a strong influence from the presence or absence of the through-thickness clamp-up. External splice plates have a relatively small amount of clamp-up provided by fastener bolts and nuts compared with the clamp-up of the center plate sandwiched between two splice members. Therefore, the bearing strength of the center cover is larger than that of the external splice plates.
- (5) Avoid skin reinforcement: As a basic philosophy, skin reinforcements should be avoided wherever possible from the perspective of both cost and basic skin reparability. A skin pad-up is a bolted splice area where the joint operates to its maximum efficiency implying that repairs to bolted joints or bolted repairs will occur in other regions. The pad-up cannot restore the ultimate strength of structure. Thus, pad-ups are allowed if warranted by other design considerations, but the joint itself must not be loaded to the point that the surrounding maximum load on the structure would be unreparable.
- (6) Joint strength is sensitive to the joint geometry as well as the type of fiber and resin used. However, joint strength is insensitive to minor changes in the

fiber pattern for optimal layer compositions. For carbon–epoxy laminates, the optimum  $w/d$  is likely to be in the range 4–5 for multirow joints.

- (7) Adequate consideration of the bolt diameter-to-laminate thickness ratio (or more appropriately, bolt bending stiffness-to-laminate thickness ratio) is warranted in joint design to assure that fasteners are the weak link. Fastener bending elastic deformation may decrease the clamp force and allowable bearing stress and should thus be avoided. Therefore, selection of fastener sizes should not be based only on the rated shear strength of the fasteners but should also consider the fastener stiffness.
- (8) Interference fit systems with a sleeve of fasteners having the same outer diameter as the sleeve, generally do not feature increased strength (strength may actually decrease slightly). This is because any potential benefits are negated by recurrent bolt bending failures.
- (9) Materials should be selected to take advantage of their strengths while avoiding their weakness. Metals should be used in parts for which composite materials are unsuitable.

Metal materials are selected for splice plate members for several reasons.

If protruding head fasteners are used in the subcomponent tension joints of tapered composite splice plates, tapered members require either spot-facing of the splice plate surface or the use of tapered washers under the fastener heads and nuts. These features may cause premature failure owing to the high peel stress and interlaminar forces. The use of tapered washers also increases the cost and complexity of the assembly procedure. Thus, metallic splice plates with spot-facing on tapered surfaces are used to accommodate the fastener seating. The use of metallic splice plates is the simplest and most cost-effective way of avoiding these potential failure modes.

Composite materials are not well-suited to applications where high out of plane forces are present. The T-splice members are likely to encounter such forces, and the magnitude of the forces is very difficult to predict analytically or measure experimentally. The fabrication of the corner fittings based on composite materials would be impractical for similar reasons and cost-prohibitive compared with the use of aluminum parts.

The splice plates may be slightly heavier, owing to the use of metals; however, any small extra weight in the splices (or fasteners) is compensated by maximizing the efficiency of the large heavy skins. For a large airplane, the weight of the splicing elements as a percentage of the total wing weight is small, and splice efficiencies should be evaluated solely on the basis of the minimum splice and fastener weight.

- (10) Joint strength is typically greater under compression than under tension loading. An example of the application of these principles is presented in Fig. 4.82. An optimum splice structure is represented, including a cover of uniform thickness, tapered splice plates and varying diameter fasteners. The bolt diameter of the inner most row near the cover butt is largest,  $S/D = 3$ . There are no bypass loads on the skin. The combination of maximum bearing

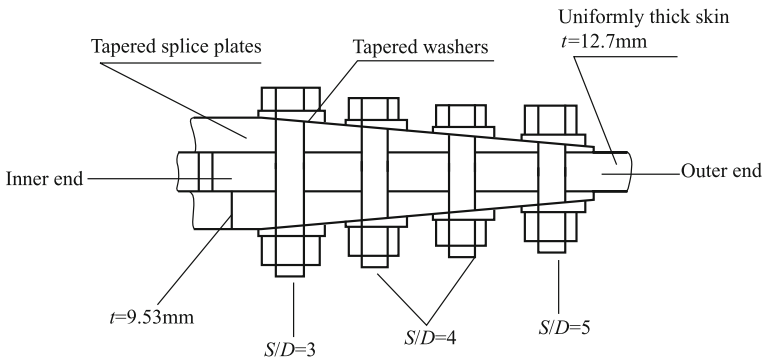


**Fig. 4.82** Optimum proportions for multirow bolted composite joints

and bypass loads act on the splice plate of the innermost skin such that the splice plate thickness must be properly increased. Research results indicated that the optimum splice plate thickness is 1.5 times the basic plate thickness. In the example, the basic plate thickness is 12.7 mm, and the total plate thickness of the taped splice is 19.1 mm, including the thickness of both the top and down taped splice (9.5 mm each). The diameter of the middle two row bolts has an intermediate  $S/D$  value of 4. The diameter of the outermost row of bolts is smallest with  $S/D = 5$ . A low thickness of the splice plate outer end may result in shear failure of laminates under a large load, which should be avoided.

#### 4.8.3.3 Static Analysis of Mechanical Joints

Static analyses of mechanical joints generally include the following three aspects [2, 17, 25–31]:

- (1) Exterior forces acting on the mechanical joint are determined from overall structural analysis of the whole joint.
- (2) These forces are then used to determine individual fastener loads and bypass forces acting at each fastener hole of the joint.
- (3) Joint strength can be assessed by applying two methods: one is the semiempirical failure envelope method; another is to use material failure criteria and characteristic curves.



## Finite Element Analysis of Fastener Load Distribution in Mechanical Joints

Methods of determining the fastener load distribution of mechanical joints can be separated into three classes: classical stiffness methods, elastic mechanics, and FEMs. This section considers the application of FEMs, which also have broader applicability to analysis of other components. FEMs are suitable for both regular multi-row fastener arrangements and complex shaped joints. More information on the other two methods can be found in Ref. [1].

There are two major differences that should be considered when dealing with composite materials: First, composite laminate stiffness is dependent on the direction of the applied force; second, most composite materials tend to exhibit nearly linear stress–strain behavior up until failure and have little load redistribution capability.

The MSC/NASTRAN program has become widely applied in aeronautic design. Therefore, we introduce issues affecting calculations of fastener load sharing with MSC/NASTRAN.

### (1) Element modes

One important point to consider for solving fastener load distribution is that fasteners are regarded as fastener elements. Two end points of the fastener elements are placed at finite element net nodes of the joining members.

- (1) Fastener modes: Fasteners can be modeled with shear fastener type elements (CELAS2 spring element) and beam elements (BAR element). However, beam elements are used more frequently because bending effects can be considered. Beam elements are suitable for both single and double shear joints, but spring elements are only suitable for double shear joints.
- (2) Joined plate modes: Joined plates are modeled with QUAD4 elements, which have membrane and bending type elements. Bending plate elements are used generally when the fasteners are modeled with beam elements. The use of bending plate elements has no meaning if the fasteners are modeled as spring elements. For commonly used geometric sizes of multi-fastener joints, it is suggested that the node numbers placed along the plate width are no less than five, and those placed between fasteners are no less than one.

### (2) Fastener flexibility

The distribution of internal loads within a complex redundant mechanical joint depends upon the plate members and the fasteners connecting them. Each fastener's contribution to joint flexibility is dependent upon fastener stiffness, joint member stiffness, and load eccentricity.

- (1) Linear analysis: In normal practice, the fastener load/deflection behavior is assumed to be linear throughout the loading range. Friction and clearance between the fastener and hole effects are usually ignored. For preliminary

design purposes, the following relation of bolt flexibility can be used, which is simple and satisfies engineering precision requirements.

$$\alpha = L/K_s = L/A_s G \tag{4.70}$$

where

- $K_s$  —shear stiffness of the fastener;
- $A_s$  —shear area of the fastener;
- $G$  —shear modulus of the fastener;
- $L$  —effective length of the fastener.

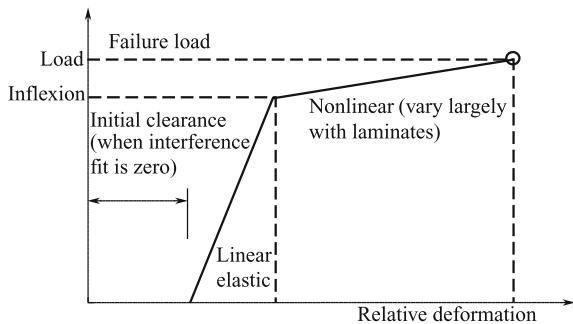
For single shear, the effective length  $l$  can be assumed to be one-fourth the combined thicknesses of the attached sheets. The effective length in double shear can be approximated as half the single shear value. Equation 4.8.2 is used for fasteners where only shear is accounted for; fastener bending and rigid body rotation (in a single-lap joint) are not considered. The fastener load distribution derived from these relations will be slight conservative.

- (2) Nonlinear analysis: Load-deflection ( $P-\delta$ ) curves from single fastener joint tests can be modeled as bilinear curves, as shown in Fig. 4.83. The nonlinear strength analysis should permit some bolts to fail while the structure should still be able to carry loads. Nonlinear analysis can provide more exact load-sharing analysis and ultimate strength predictions.

### Detailed Stress Analysis Methods

Stress analysis methods of single fastener joints are described in detail in Ref. [1].

**Fig. 4.83** Bilinear load-deflection ( $P-\delta$ ) curves



After the load distribution is determined (i.e., the bearing and bypass loads of fastener holes) analytical methods for single fastener joints can be used to calculate the detailed stress and strain near the fastener hole. Finally, joint strength and failure modes can be assessed by applying material failure criteria or characteristic curves.

Theoretical analytical methods of single fastener joints mainly depend on analytical and FEMs. In finite element analysis a fine mesh must be used in regions of high stress gradients, such as around the cutouts and at ply and stiffener drop-offs. Joint analysis should include the effects of shimming to the limits permitted by drawings. The effects of shimming may reduce joint strength. The effects of permissible manufacturing parameters should be considered, for example, hole perpendicularity ( $\pm 10^\circ$ ), shimming, and loose holes.

### Semiempirical Methods

Analyses of mechanical joints in composite structures typically follow the procedures: First, load-sharing analysis is performed; second, detailed analyses are conducted for individual severely loaded holes to determine the stress distribution; finally, failure hypothesis and material failure criteria are used to assess whether a joint will fail or not.

The disadvantages of detailed analysis include the requirements of manpower and material resources and the use of failure criteria. Currently, no single material failure criteria are uniformly endorsed, and moreover, some failure criteria have an empirical nature. Generally, analysis of fastener load distribution is more exact and errors of estimates of the strength derive mainly from the failure criteria. A failure envelope is used by the test judge to determine whether failure will occur, and complicated detailed analysis and disputed failure criteria may be avoided.

Having determined the bearing and bypass load of individual fastener holes by finite element or other methods, joint strengths are pre-estimated by empirical methods. Thus, a failure envelope is determined from test specimens and used to judge the likelihood of joint failure.

#### (1) Tensile load conditions

Under the combined action of bearing and bypass loads, assume that the joint tensile failure will occur when Eq. (4.71) is satisfied:

$$K_{bc}\sigma_{br} + K_{tc}\sigma_{net} = \sigma_b, \quad (4.71)$$

where

- $\sigma_b$  —unnotched laminate tensile strength;
- $\sigma_{br}$  —loaded hole bearing stress;
- $\sigma_{net}$  —laminate net-tension stress caused by bypass loads;
- $K_{bc}$  —composite bearing stress concentration factor, with respect to bearing stress;

$K_{tc}$  —composite stress concentration factor, with respect to net-section tension stress;

$$K_{tc} = 1 + C(K_{te} - 1) \tag{4.72}$$

$$K_{te} = 2 + (1 - D/W)^3 \tag{4.73}$$

$$K_{bc} = \left\{ 1 + C \left[ 1 + (W/D - 1) - 1.5 \times \frac{W/D - 1}{W/D + 1} \times \theta \right] \right\} / (W/D - 1) \tag{4.74}$$

$K_{te}$  —elastic isotropic stress concentration factor, with respect to net-section tension stress;

$W$  —width;

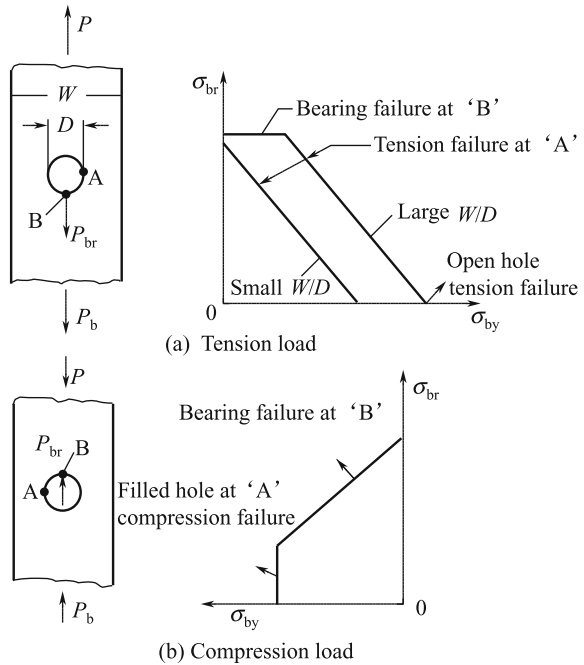
$D$  —hole diameter;

$\theta$  —may be considered as 1.0;

$C$  —stress concentration correlation coefficient, as seen in Fig. 4.85.

The left side of Eq. (4.71) can be regarded as the sum of contributions from the combination of bearing and bypass loads to tensile stress. Failure will occur when it exceeds the laminate tensile strength.

Fig. 4.84 Failure envelope



Otherwise, joint-bearing failure will occur when the bearing stress achieves the bearing strength:

$$\sigma_{br} = \sigma_{bru} \tag{4.75}$$

where  $\sigma_{bru}$ —is bearing strength.

A typical failure envelope is shown in Fig. 4.84a. The inclined line AB represents the tensile failure satisfying Eq. (4.71). The flat line BC represents the bearing failure satisfying Eq. (4.75).

**(2) Compressive load conditions**

Under the combined action of bearing and bypass loads, assume that the joint-bearing failure will occurred when Eq. (4.76) is satisfied:

$$\sigma_{br} + \sigma_{net} = \sigma_{bru} \tag{4.76}$$

Compressive failure will occur when Eq. (4.77) is satisfied:

$$K_{tc}\sigma_{net} = \sigma_c, \tag{4.77}$$

where  $\sigma_c$ —unnotched laminate compressive strength.

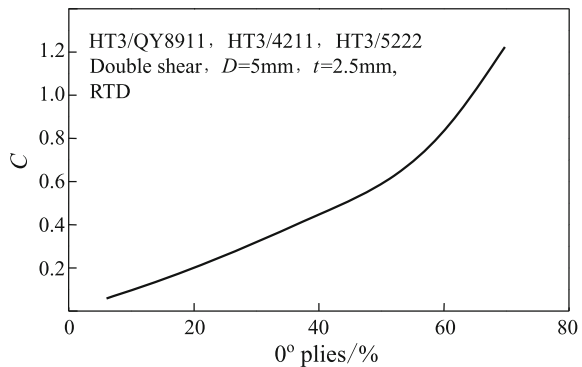
In the absence of a filled hole  $K_{tc}$  value, the mean open hole  $K_{tc}$  value of 1 can be used.

This failure envelope is shown in Fig. 4.84b, where the inclined line represents the bearing failure satisfying Eq. (4.76). The vertical line represents compressive failure satisfying Eq. (4.77).

**(3) Stress concentration correlation coefficient C**

The stress concentration correlation coefficient considers the effects of anisotropy, non-homogeneity, nonlinearity, and damage to the composite material. Test results of composite specimens are used to measure C.

**Fig. 4.85** C curves as a function of ply proportions



The stress concentration correlation coefficient  $C$  is key to applying empirical methods. Because stress concentration factors of open holes and loaded holes for isotropic materials are known. If the  $C$  value is determined, stress concentration factors for composites can be determined by linear relations. Thus, joint strengths can be simply estimated.

Figure 4.85 shows  $C$  curves as a function of ply proportions. The curves are based on test results of HT3/QY8911, HT3/5222, and HT3/4211.

In general,  $C$  takes values between 0 and 1.0. If the proportion of  $0^\circ$ -plies of laminate is too high and that of  $\pm 45^\circ$ -plies is too low,  $C$  may be greater than 1, and loses its meaning as a stress concentration correlation coefficient. Nevertheless, the same, single fastener joint strength can be pre-estimated from the  $C$  value.

In the absence of test data, within the recommended range of layering conditions in joint areas,  $C$  may be considered to be:

$$C = (\%0^\circ \text{ plies})/100$$

#### (4) Failure envelopes

Failure envelopes provide failure criteria for multirow joint analysis. The failure envelope is the foundation for estimating joint strength by empirical approaches. Failure envelopes can be determined for single fastener and unloaded hole specimens by the following methods:

- (1) The bypass stress point at the abscissa can be determined from the tensile and compressive strength of unloaded hole (fill-hole) specimens.
- (2) The cutoff can be determined from the bearing strength of a wide plate ( $W/D = 6-8$ ).
- (3) The inclined line represents the tensile failure, which may be determined from the stress concentration correlation coefficient  $C$  and joint geometry.

#### 4.8.3.4 Checking Mechanical Joint Strength

##### Allowable Bearing Stress of Full Carbon Fiber Composites

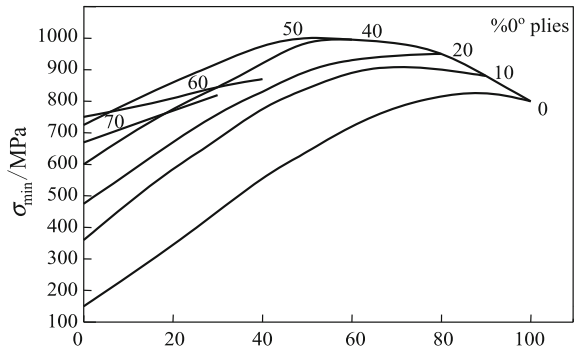
The information presented here is not only applicable to single fastener joints, but also useful for determination of multirow joint strength. All joint strength data are developed from tensile test results, and the results will be conservative for use in compression loads [2, 17].

- (1) **Allowable bearing stress**

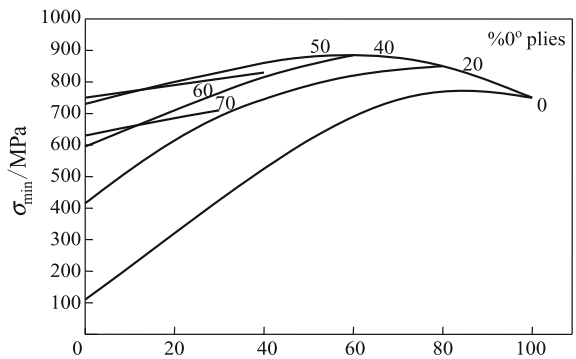
To ensure structure integrity the loading should generally not be greater than the initial bearing failure stress. Therefore, selection of an allowable bearing stress strongly depends on the failure criteria. The initial bearing stress is very different to the definition of failure. Failure criteria can be classified in different ways: One approach is to base failure on stress, which guarantees that structures have sufficient strength; another is based on deflection of the loaded hole, which guarantees that structure have sufficient stiffness. One frequently used approach is based on the degree of hole deformation. However, the failure deflection limits of loaded holes selected by various countries and departments are very different, ranging from 0.5 to 6%.

The following are recommended criteria for determining the initial bearing failure stress of a loaded hole: the lowest value between the first slope inflexion point and bearing deformation of 4% in the load deformation curve. Experience indicates that the minimum initial bearing failure stress can be considered to be half of the ultimate bearing strength  $\sigma_{bru}$ .

**Fig. 4.86** Bearing strengths of three composite systems



(a) HT3/QY8911 and HT3/5222  $\% \pm 45^\circ$  plies



(b) HT3/4211  $\% \pm 45^\circ$  plies

The ratio of the initial bearing failure stress to the ultimate bearing strength depends on the material system and laminate pattern. Generally, the ratio decreases as the proportion of  $\pm 45^\circ$  plies is increased. For laminate frequently used in joint areas, the ratio is in the range 0.55–0.66. Selection of allowable bearing stress should also consider joint importance, structural characteristics, load type, durability and service life and environmental effects.

Allowable bearing stress can be determined from the following:

$$[\sigma_{br}] = C_w C_e C_p C_d C_s C_{en} K \sigma_{bru} \quad (4.78)$$

where

- $C_w$  correlation factor for width;
- $C_e$  correlation factor for end distance;
- $C_p$  correlation factor for load direction;
- $C_d$  correlation factor for hole diameter;
- $C_s$  correlation factor for single shear;
- $C_{en}$  correlation factor for environment;
- $K$  factor considering initial failure, durability, aging, and technological quality. The value of  $K$  is typically in the range 0.50–0.66;
- $\sigma_{bru}$  bearing strength, MPa.

The bearing strengths of several composite laminates are illustrated in Fig. 4.86. Various correlation factors are shown in Fig. 4.86 for  $W/D \geq 6$ ,  $e/D \geq 4$ ,  $D/t = 1.0\text{--}2.0$ ,  $D = 5$  mm, double shear, torque 4 N·m, at room temperature, in dry conditions.

For laminates typically used in joint areas (i.e.,  $0^\circ$ -plies = 25–50%,  $\pm 45^\circ$ -plies  $\geq 40\%$ ,  $90^\circ$ -plies = 10–25%), the allowable bearing stress for HT3/QY891 and HT3/4211 can be taken as 600 and 500 MPa, respectively.

Hence, the formula (4.78) is a concise, convenience, and effective model. The effects of many parameters have been considered in various correlation factors, and therefore, numerous procedures can be avoided. Traditionally, both the bearing strength and tension strength as well as shear strength would require checking. This method has been successfully used in joint design for many aircraft structures.

## (2) Bearing strength

To fully develop the bearing capability, joint geometry selection requires that bearing failure or combined failure modes depending on bearing failure are considered. Full load-bearing failure strengths are the foundation of joint design. Failure modes are dependent not only on geometric parameters but also the fiber pattern. Full bearing failures typically occur when  $W/D = 6$  and  $e/D = 4$  in the laminate pattern range of joint areas. The bearing strengths given in this paragraph are equal to the ultimate load divided by the bearing area  $Dt$ .



The bearing strengths of laminates of HT3/QY8911 and HT3/5222 composites are shown in Fig. 4.86a. The laminate bearing strengths of HT3/4211 composite are given in Fig. 4.86b. The test parameters are as follows: double shear, hole diameter 5 mm,  $W/D \geq 6$ ,  $e/D \geq 4$ ,  $D/t = 2$ , load direction was consistent with the  $0^\circ$  fiber orientation. The fixture was made of steel with a stiffness approximately 8 times as high as that of the specimen. Loading bolts were made of 30CrMnSiA steel. The fit precision of the bolt in the hole was H8/h8, and the bolt tightened torque was 4 N·m. The interior and exterior diameters of the washers were 5.5 and 10 mm, respectively. The environmental conditions were room temperature and a dry atmosphere.

The double shear method is a basic procedure and preferable to single shear joint tests. For double shear joints, the test specimen size is smaller and test fixture is simpler. These features not only can save costs and time, but also give a smaller data dispersion. Moreover, actual aircraft single shear joints with supported structures differ considerably from tests of single shear joints. Therefore, test results of single shear joints may be considered conservative.

### (3) Correlation factors of bearing strength

When the actual applied parameters are different from those in Fig. 4.86, it is necessary to correct the bearing strength in Fig. 4.86. The bearing strength correlation factors are mainly based on HT3/QY8911, HT3/5222, and HT3/4211 laminate test results. Laminate codes names used in this paragraph are described in Table 4.20.

- (1) Width correlation factors  $C_w$ : The width correlation factors  $C_w$  are shown in Fig. 4.87a for several representative laminates.
- (2) Edge distance correlation factor  $C_e$  is shown in Fig. 4.87b for several representative laminates.
- (3) Load orientation correlation factors  $C_p$  are shown in Fig. 4.87c. Generally, the more  $0^\circ$  plies, the greater the load orientation effect, i.e., more  $\pm 45^\circ$ -plies will give a smaller load orientation effect.
- (4) The hole diameter correlation factor  $C_d$ : When geometric sizes ( $W/D$ ,  $e/D$ , and  $D/t$ ) of mechanical joints are all the same, a larger hole diameter will lower strength. Hole diameter correlation factors  $C_d$  are shown in Fig. 4.87d.
- (5) Single shear correlation factor  $C_s$ : The single shear correlation factor  $C_s$  is given in Fig. 4.87e. Note that for single shear joints in actual aircraft

**Table 4.20** Laminate codes

Laminate codes	Percentage ( $0^\circ/\pm 45^\circ/90^\circ$ )	Stacking sequence
2	70/20/10	[45/0/0/-45/0/0/0/90/0/0] <sub>S</sub>
4	50/40/10	[45/0/-45/0/90/0/45/0/-45/0] <sub>S</sub>
6	30/60/10	[45/0/-45/0/45/90/-45/0/45/-45] <sub>S</sub>
8	0/100/0	[ $\pm 45$ ] <sub>SS</sub>
9	50/0/50	[0/90] <sub>SS</sub>
10	25/50/25	[45/0/-45/90] <sub>2S</sub>

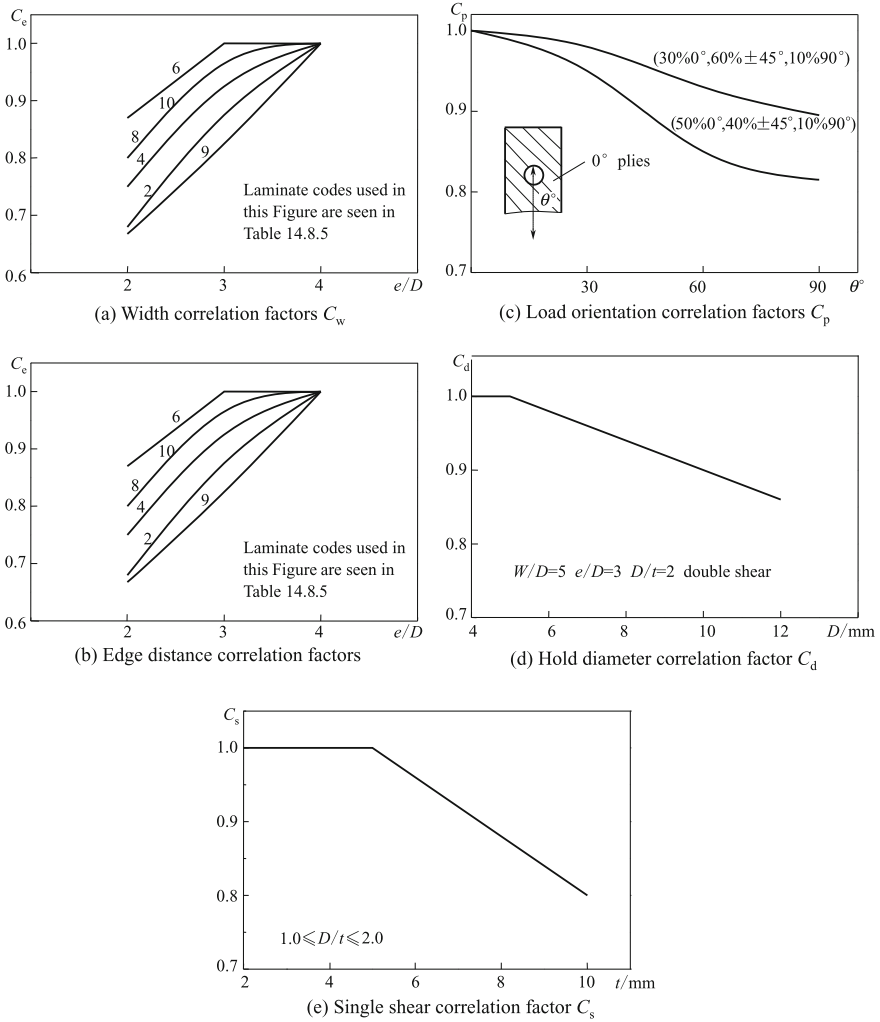


Fig. 4.87 Correlation factors of bearing strength

Table 4.21 Environmental correlation factor  $C_{en}$

Materials	Environmental condition	$C_{en}$	Materials	Environmental condition	$C_{en}$
T300/QY8911	100° moisture content 1%	0.75	T300/4211	82° moisture content 1%	0.83
	130° moisture content 1%	0.67		100° moisture content 1%	0.75

structures, owing to support by surrounding components, practical bending effects will far less than those in test cases. Consequently,  $C_s$  is used to reflect an actual aircraft structure.

- (6) Environmental correlation factor  $C_{en}$ : Environment has strong effects on bearing strength of laminates. In the laminate pattern range recommended for joint areas, the environmental correlation factors  $C_{en}$  of T300/QY8911 and T300/4211 laminates are given in Table 4.21.

**Strength Checking of Single Fastener Joints**

- (1) Strength checking of joined plates: Bearing strength checking is performed as follows:

$$\sigma_{br} = P_{br}/Dt_e \leq [\sigma_{br}] \tag{4.79}$$

where

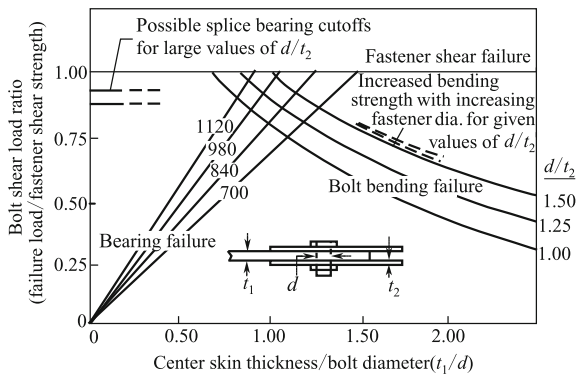
- $P_{br}$  —fastener load, N;
- $D$  —hole diameter, mm;
- $t_e$  —plate effective thickness, defined as:  
 $t_e = t$ , when  $t \leq D$ ,  
 $t_e = D$ , when  $t > D$ ;
- $[\sigma_{br}]$  —allowable bearing value, MPa.

Note that tension and shear strength will be satisfied automatically without checking because the effects of width and edge distance have been considered in the allowable bearing strength value.

- (2) Checking of fastener strength: The shear strengths of single fastener joints can be checked as follows:

$$\tau = 4P_{br}/Dt_e \leq [\tau] \tag{4.80}$$

**Fig. 4.88** Approximate single-row allowables



where  $[\tau]$ —allowable shear strength of fastener.

- (3) Bolt bending failure curves: Design guidelines for the selection of fastener were sizes traditionally based on the fastener shear strength and limitations of the allowable  $d/t$  ratio. However, such a broad criterion can sometimes be either unconservative or overly conservative, depending on the relative dimensions of the members to be joined or the splicing material through which the load is transferred. The chart shown in Fig. 4.88 was developed to provide a more comprehensive method for selecting fastener sizes, with consideration given to the bearing strengths of the materials to be joined, the fastener shear strength, and the potential for bolt bending failures. The bolt bending failure curves were derived from limited test results and assume that the bending failure is a function of the  $d/t$  ratio for both the skin and splice members.

Figure 4.88 was developed for double shear and is nondimensionalized, except for the center skin bearing stress allowables, which are plotted in units of ksi. The chart shows that when the value of  $d/t_2$  ( $t_2$  is the thickness of one splice plate) is low, and the value of  $d/t_1$  (for the central skin) is about 1.0, the bearing stress allowables of composite joints reach maximum. The bending failure curves show that at low  $d/t$  ratios for both the skin and splice plates, bending failure can occur at low percentages of the joint member bearing strength and fastener shear strength. As the  $d/t_2$  ratio increases, the propensity for bolt bending failure decreases owing to the lower eccentricity, and fastener shear strength becomes the limiting factor. Eventually, as the  $d/t_2$  ratio becomes large, the splice plate bearing strength approaches the strength cutoff, as indicated by the dashed lines in the upper left of Fig. 4.88. It should be noted that the bolt bending curves on this chart are approximate, and will likely require modification as more test data are obtained. All potential failure modes can be included on this chart except for net-section failure, which must be calculated separately.

### Strength Checking of Multirow Fastener Joints

#### (1) Tensile load

- (1) Bearing strength checking: With knowledge of fastener loads, bearing strength checking is the same as that of single fastener joints according to formula (4.78). For joints of uniform plate thickness and equal fastener diameter, only the fastener holes of maximum load-carrying capability need to be checked.

- (2) Tensile strength checking: For strength checking, the tensile loading of a multirow joint,  $\sigma_b$ , of the right side of Eq. (4.71) can be replaced by the allowable tension stress of the laminate, i.e.,

$$K_{bc}\sigma_{br} + K_{tc}\sigma_{net} = [\sigma] \quad (4.81)$$

where

- $[\sigma]$  —allowable tension stress of laminate, MPa,  $[\sigma] = E_{xt}[\varepsilon]$ ;  
 $E_{xt}$  —longitudinal tensile elasticity modulus of laminate, MPa;  
 $[\varepsilon]$  —allowable tensile strain of laminate.

Design allowable strains can be classified on A-basis and B-basis. The use of either basis depends on the structure design criteria of the practical engineering project. Generally, for components without a structure test or single path transfer component, A-basis is used; B-basis is used for multi-path transfer or fail-safe components. For carbon fiber resin matrices composites, allowable tension strains are  $[\varepsilon_A] = 0.0082$  for A-basis and  $[\varepsilon_B] = 0.0090$  for B-basis. Shear failure will not occur within the ply range recommend for joint areas when the pitch is not less than 4D and the edge distance is not less than 3D.

(2) **Compressive load**

For strength checking of multirow joints under a compressive load,  $\sigma_{bru}$  on the right side of Eq. (4.71) may be replaced by the allowable bearing stress of the laminate,  $[\sigma_{br}]$ , i.e.,

$$\sigma_{br} + \sigma_{net} = [\sigma_{br}] \quad (4.82)$$

## 4.9 Damage Tolerance and Durability

### 4.9.1 Overview

#### 4.9.1.1 General Concepts

Inspection plans should be combined with knowledge of damage threats, including damage growth rates and residual strength. This concept is referred to as damage tolerance. Specifically, damage tolerance is the ability of a structure to sustain design loads in the presence of damage caused by fatigue, corrosion, environmental effects, accidental events, and other sources until such damage is detected, through inspections or malfunctions, and then repaired. Thus, safety is the primary goal of damage tolerance.

Durability considerations are typically combined with damage tolerance to meet economic and functionality objectives. Specifically, durability is the ability of a structural application to retain adequate strength and stiffness to resist fatigue cracking, corrosion, thermal deterioration, peeling, delamination, wear-off, and external impact damage over the designed operation life time. Structures should have a certain durability under expected loads and environmental conditions to avoid high costs caused by frequent maintenance, repair, and replacement of parts over the designed operation life time. Thus, economics is the primary motivating factor for durability.

#### **4.9.1.2 Composite Damage Tolerance and Durability**

All structural applications should be designed to be damage tolerant and durable. In the use of composite materials, typical design objectives involve meeting or exceeding the design service and reliability objectives for the same structure made of other materials. Generally, the good fatigue and corrosion resistance of composites can help to achieve these objectives. However, the unique characteristics of composite materials also present some challenges for developing safe and durable structures.

The new problems of composites relate to their impact resistance, and residual load-bearing ability after an external impact and before damage is inspected. Damage resistance has become an important topic in composite research in recent years. Although composites offer excellent anti-fatigue and corrosion resistance, they are very sensitive to impact. In particular, thin skin structures or thin skin surface panel sandwich structures are susceptible to small external impacts encountered in manufacture or operation, which can necessitate considerable maintenance and repair. Studies on damage resistance of composites typically focus on two aspects: characterization of the impact resistance of composite systems, and the durability design requirements of composite structures. The feature of composite damage tolerance is that barely visible impact damage (BVID) can decrease compression strength by up to 40%, and the regular inspection and maintenance of composite structures cannot use special NDT equipment. Only visible inspection of dent depth is specified as standard in design. Similarly, studies on composite damage tolerance involve two aspects: characterization of damage resistance of the

composite system and the damage tolerance design requirements of composite structures. The damage resistance and damage tolerance design requirements of composite structures are discussed in Sect. 4.9.2.

The optimum balance of damage resistance and damage tolerance for specific composite applications involves a number of technical and economic issues early in the design process. Damage resistance often competes with damage tolerance during the design process, both at the material and structural level. In addition, materials and fabrication costs, as well as operational costs associated with inspection, repair, and structural weight, are strongly influenced by the selected material and structural configuration. For example, toughened resin material systems typically show improved damage resistance compared with untoughened systems, which results in reduced maintenance costs associated with damage from low-severity impact events. However, these cost savings compete with the higher material costs per unit weight of the toughened systems. In addition, these materials can also result in lower tensile capabilities of the structures with large damage or notches, which might require the additional material to satisfy structural capability requirements at the limiting load. This extra material and increased weight will result in higher material and fuel costs, respectively.

### ***4.9.2 Evaluation of the Effects of Defects/Damage on Strength***

Damage can be divided into two types according to its source: manufacturing defects, which cover structural abnormalities caused by production, and operational damage, which covers structural abnormalities caused in service [1, 2].

#### **4.9.2.1 Manufacturing Defects**

Manufacturing defects can usually be divided into two categories: First, lamination and part curing processes may create defects such as voids, delamination, debonding, inclusions, resin-rich or resin-poor areas, improperly cured resin, deviation of fiber orientation (fiber bending), layering sequence errors, and gaps between fibers. Second, defects may be produced in machining, packing and delivery such as scratches, abrasion, improper hole drilling, and torque and impact damage.

#### **4.9.2.2 Operational Damage**

Operational damage mainly concerns impact damage occurring in service. Impacts can be classified by the type of external impact energies. The impact caused by

external bodies such as bullets, non-inclusive engine fragments and bird-strikes are classed as high-energy impacts. These events are also known as high-speed impacts and can produce penetrating damage with a certain amount of delamination. Lightning can also break through the structure of the skin and produce deep delamination and burning. This type of damage is visibly inspectable and can be detected, allowing the part to be replaced or repaired. During production and maintenance, low-energy impacts include events such as: tool dropping; impact with maintenance facilities such as forklifts, trucks, and work platforms; damage by personnel standing on structures; impacts caused by stones, screws, and tire fragments during taking off or landing; impact of hail stones.

In fact, impact damage modes depend not only on external impact energy, but also the laminate thickness. For thin skins or thin surface panels, impact damage mainly results in fiber fracture, or penetration, resulting in decreased compressive and shear strength. Furthermore, after such damage water may diffuse into the sandwich core and causing durability issues. For medium thickness laminated structures (less than 6 mm), impact damage may not be visible from the surface. However, damage may be induced inside the laminate in the form of delamination or matrix cracking. Such damage will greatly reduce the compression strength of the component and presents damage tolerance safety issues.

#### **4.9.2.3 Evaluation on the Effects of Defects/Damage on Strength**

Great attention has been paid to the effects of defects/damage on the strength of composites. Since their initial use in aircraft primary structures in the 1970s, many tests and investigations have been performed on the effects of damage on composites. On the basis of test data derived from various composite material systems (mainly carbon/epoxy, and carbon/BMI systems), and studies on the effects of defects/damages on the static strength and fatigue strength of specimens under different ambient conditions (room temperature/dry, hot/wet, cold/dry), the effects of defects/damage on composite strength have been established as follows:

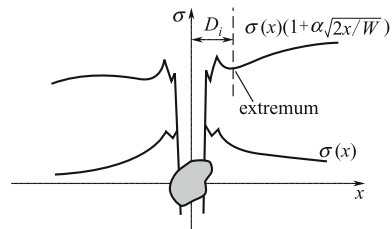
- (1) Tensile loading: Many dangerous defects, such as cuts and slots, are inspectable to some extent. The residual strength of laminates containing cuts will mainly depend on the width, and is basically independent of the cut shape. Test results for an open hole (typically 6.35 mm in diameter) can be used to consider the strength reduction associated with an edge cut of similar size, when the structure design allowable values are to be determined.
- (2) Compression loading



**Table 4.22** Notch sensitivity and applicable failure criterion

Laminate type	Load type	Defect type	Notch sensitivity	Applicable failure criterion	
0° unidirectional	Tensile	Penetration	No	Net cross-section failure criterion	
[±45]nS	Tensile	Penetration	No	Net cross-section failure criterion	
Multi-directional laminates	Tensile	Penetration	Yes	DI criterion, FD criterion, AS criterion, PS criterion	
		Compression	Penetration	Yes	FD criterion
			Delamination		DI criterion
		Impact damage		DI criterion, FD criterion	

*Note* The failure criterion under compression load can only suit the case of no buckling before failure

**Fig. 4.89** DI criterion schematics

- ① Compared with many defects caused in production and operation (including delamination up to 50 mm in diameter, hole making defects, scratches, and void content up to 2%), the low-speed impact damage caused by an impactor 12.7–25.4 mm in diameter will induce more critical damage.
- ② Compression strength reduction caused by filled and load-free hole 6.35 mm in diameter can be used to as a model for the effects of all other defects including: delamination up 38.1 mm in diameter, hole making defects, scratches, and void content up to 2%.
- ③ BVID of the front surface may cause a static compression strength reduction up to 60%.
- ④ The compression fatigue  $S-N$  curve is quite flat and smooth, and the conditional fatigue ultimate strength (the fatigue strength corresponding to  $10^6$  testing cycles) will be 60% of the static residual strength of a specimen containing a defect of the same size. The fatigue threshold value may be higher when structures are load bearing in aircraft with a random fatigue load spectrum.
- ⑤ No clear regularity of damage growth can be found in specimens with impact damage under fatigue loading conditions.

### 4.9.3 Analysis of Durability and Damage Tolerance

#### 4.9.3.1 Analytical Methods Applied to Damage Tolerance

(1) **Notch sensitivity and applicable failure criterion**

The different ply stacking of laminates will result in different notch sensitivities as well as different failure criteria. In Table 4.22, the notch sensitivities of different laminates and their applicable failure criteria are listed. In addition, failure criterion is also related to failure modes, and the criteria listed in the table are applicable for laminates with fiber-dominated failure modes [1, 2, 32–37].

(2) **Introduction to applicable failure criterion**

(1) Damage influence (DI) criterion can be expressed as: the point where weighted normal stress at a characteristic point near the notch (damage) reaches laminate failure strength, at which point the damaged laminate will fail (see Fig. 4.89). The expression for DI is given as:

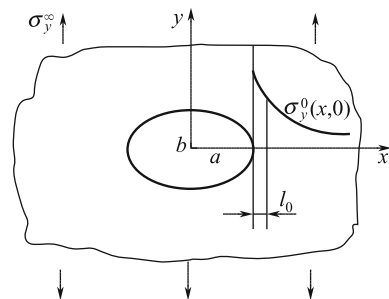
$$\sigma_y(x, 0)(1 + \alpha\sqrt{2x/W}) \Big|_{x=D_i=\sigma_b} \tag{4.83}$$

where  $D_i$  is equal to the  $x$  value,

$$\frac{d}{dx} \left( \sigma_y(x, 0) \left( 1 + \alpha\sqrt{2x/W} \right) \right) = 0 \tag{4.84}$$

Where

**Fig. 4.90** Stress distribution of 0° plies near the notch of laminate with a hole



- $\sigma_b$  — laminate damage-free strength;
- $\sigma_y(x, 0)$  — normal stress distribution near damage;
- $W$  — specimen width;
- $\alpha$  — constant related to the damage types (hole, crack, delamination, impact damage), loading condition and performance. For open hole tensile loading:

$$\alpha = \left| \frac{A_{11} + A_{12}}{2A_{22}(1 + (K_T^\infty - 3)^2)} - \nu \right| + K_T^\infty \left( \sqrt{\left(\frac{2R}{W}\right)^3} - \left(\frac{2R}{W}\right)^2 \right) \quad (4.85)$$

where

- $A_{ij}$  — laminate in-plane stiffness coefficient;
- $\nu$  — laminate Poisson’s ratio;
- $K_T^\infty$  — laminate hole edge stress concentration coefficient.

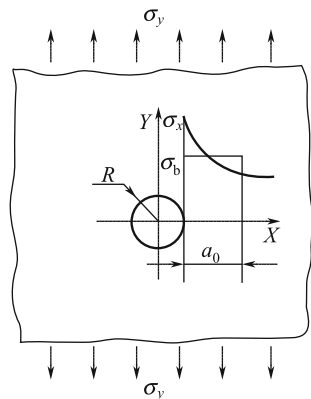
- (2) Failure criterion for fiber breakage in damage zone can be expressed as: the point when average normal stress of  $0^\circ$  plies within the characteristic distance  $l_0$  near the notch (or damage) reach the ultimate strength of a unidirectional laminate (see Fig. 4.90). At this point, the damaged laminate will behave according to the expression:

$$\frac{1}{l_0} \int_a^{a+l_0} \sigma_y^0(x, 0) dx = X_t \quad (4.86)$$

where

- $\sigma_y^0(x, 0)$  —the normal stress distribution of  $0^\circ$  plies on the notch cross section without considering damage zone influence;

**Fig. 4.91** Average stress criterion



- $l_0$  —material system constants independent of ply orientation and notch shape and dimensions;
- $a$  —half the length of a notch in the  $x$ -axis direction;
- $X_t$  —longitudinal tensile or compression strength of unidirectional laminates.

(3) Average stress criterion (AS) and point stress criterion (PS)

- ① Average stress criterion: This criterion considers the average stress within a characteristic distance  $a_0$  from the hole edge, which achieves the ultimate strength of a notch-free laminate. Failure will occur in laminates as shown in Fig. 4.91, according to:

$$\frac{1}{a_0} \int_R^{R+a_0} \sigma_y(x, 0) dx = \sigma_b \tag{4.87}$$

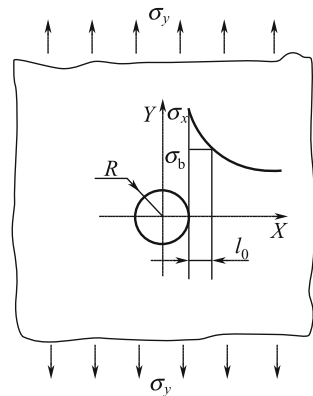
where

- $\sigma_y(x, 0)$  —stress distribution in  $Y$  direction of the minimum cross section with a hole;
- $R$  —hole radius, and half length of the central crack;
- $a_0$  —characteristic length determined by testing.

For orthotropic infinite laminates with a tensile hole, the hole edge stress distribution is substituted into the average stress criterion Eq. (4.87), and the equation for residual stress calculation can be derived as:

$$\sigma_c^\infty = \frac{2\sigma_b(1 - \xi_2)}{2 - \xi_2^2 - \xi_2^4 + (K_T^\infty - 3)(\xi_2^6 - \xi_2^8)}, \tag{4.88}$$

**Fig. 4.92** Point stress criterion



where  $\xi_2 = \frac{R}{R+a_0}$ .

- ② Point stress criterion (PS): This criterion assumes that failure of the laminate will occur if the stress  $\sigma_y$  at a point  $d_0$ , a characteristic distance, reaches the ultimate strength  $\sigma_b$  of a notch-free laminate (Fig. 4.92), that is:

$$\sigma_y(x, 0)|_{R+d_0} = \sigma_b \quad (4.89)$$

For an orthotropic infinite laminate with tensile holes, the hole edge stress distribution is substituted into the point stress criterion expression (4.89), and an equation for residual stress calculation can be derived as:

$$\sigma_c^\infty = \frac{2\sigma_b}{2 + \xi_4^2 + 3\xi_4^4 - (K_T^\infty - 3)(5\xi_4^6 - 7\xi_4^8)} \quad (4.90)$$

where  $\xi_4 = \frac{R}{R+d_0}$ .

- ③ Characteristic length  $a_0$  and  $d_0$ : The characteristic length  $a_0$  and  $d_0$  in average stress criterion and point stress criterion are determined by testing. A number of specimens with different hole sizes and crack lengths are used for tensile failure testing to obtain a set of residual strength data  $(\sigma_c^\infty)_T$ . These data are substituted into the residual calculations by Eqs. (4.88) and (4.90) based on the average stress criterion and point stress criterion. The finite width correction and notch-free specimen tensile strength  $\sigma_0$ , and a set of  $a_0$  and  $d_0$  values corresponding to hole diameter, and crack length can be derived. Their average values will be the characteristic lengths  $a_0$  and  $d_0$ .
- ④ Finite width correction: The above-mentioned open hole laminate or cracked laminate residual strength  $\sigma_c^\infty$  is the stress of a laminate with an infinite width. Thus, corrections should be performed for finite width laminates. Let  $\sigma_c$  be the residual strength of a finite width laminate, such that:

$$\sigma_c^\infty = \eta\sigma_c \quad (4.91)$$

where  $\eta$  is the correction coefficient for a finite width laminate, when the ratio between the defect width and laminate width is equal to or less than 1/3 (laminate width is  $W$ ). For a laminate with a central hole radius  $R$ :

$$\eta_1 = \frac{2 + (1 - 2R/W)^3}{3(1 - 2R/W)} \quad (4.92)$$

For laminates with an ellipse hole (long axis is  $2a$ , short axis is  $2b$ ):

$$\eta_2 = \frac{\lambda^2}{(1 - \lambda)^2} + \frac{1 - 2\lambda}{(1 - \lambda)^2} \sqrt{1 + (\lambda^2 - 1) \left(\frac{2a}{W} M\right)^2} - \frac{\lambda^2}{1 - \lambda} \left(\frac{2a}{W} M\right)^2 \left[1 + (\lambda^2 - 1) \left(\frac{2a}{W} M\right)^2\right]^{-1/2} \quad (4.93)$$

where

$$M^2 = \left( \sqrt{1 - 8 \left[ \frac{3(1 - 2a/w)}{2 + (1 - 2a/w)^3} - 1 \right]} - 1 \right) / 2(2a/w)^2, \lambda = \frac{b}{a}.$$

For laminates with a central crack length  $2a$ :

$$\eta_3 = \sqrt{(W/\pi a) \tan(\pi a/W)} \quad (4.94)$$

### (3) Estimation of residual strength of laminate with penetrating defect

- (1) Tensile loading: The above-mentioned four failure criteria can be used to perform residual strength estimation. The defect shape has no effect and can be simplified as a hole with a diameter equal to the defect width. Because no tests are needed for determination of material constants, DI criterion will become the first selected method.
- (2) Compression loading: Fiber breakage damage failure criterion (FD) can be used for the estimation, as given in Eq. (4.86), where  $X_t$  in the equation is changed into a unidirectional laminate compression strength  $X_c$ , and the characteristic length  $l_0$  should use the value given in the compression load case.

### (4) Estimation of residual compression strength of laminate with impact damage

The estimation of residual compression strength of laminates with impact damage consists of two parts, namely the estimation of impact damage and the estimation of the residual compression strength of the laminate with impact damage.

- (1) Estimation of impact damage: To analyze the residual characteristics of composite laminates after impact, it is necessary to know characteristics of

the impact damage, such as shape, size, and distribution along the thickness. This information can be derived from testing and inspection (such as nondestructive CT-scans and X-ray methods), or from quantitative analytical estimations. The analytical estimation of composite laminate impact damage includes two parts: a) analysis of the impact transient response of laminates, b) the use of appropriate failure criteria to calculate the impact zone, which will be mainly discussed in this section.

Impact damage of composite laminates includes matrix cracking, fiber rupture, and delamination. In the following section, methods for calculating impact damage size will be discussed based on delamination failure criterion, which can be used in composite structural design.

- ① Delamination failure criterion: In terms of bending strain energy density delamination failure criterion, If impact delamination of composite laminates is dominated by matrix strength and interlaminar strength, initial delamination can be derived from the criterion:

$$R = (y_S/Y_S^*)^2 + (y_M/Y_M^*)^2 \geq 1 \quad (4.95)$$

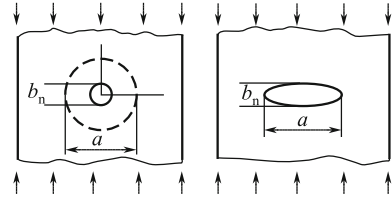
where  $Y_S^* = (9/50)(S_i^2/E_f)$  is the average transverse shear strain energy density, while  $S_i$  is interlaminar shear strength,  $E_f$  is the corresponding bending modulus,  $Y_M^* = (1/2)(S_y^2/E_y)$  is the strain energy density reflecting matrix failure, while  $S_y$  is the tensile strength or compression strength vertical to fiber direction (depending on stress conditions),  $E_y$  is the tensile modulus or compression modulus vertical to fiber direction;  $y_S = (1/2)\tau_{xz}\gamma_{xz,\max}$ , while  $\tau_{xz}$  is interlaminar shear stress,  $\gamma_{xz,\max}$  is the maximum shear strain;  $y_M = (1/2)\sigma_y\varepsilon_y f$ , while  $\sigma_y$ ,  $\varepsilon_y$  are the stress and strain vertical to fiber direction, respectively. Here,  $f$  is an empirical coefficient reflecting stiffness inconsistencies as well as the thickness difference between two adjacent plies, and has the following form:

$$f = (t^L/t^U) / \left[ 1 + \left( \frac{Q_{11}^L - Q_{11}^U}{Q_{11}^L - Q_{22}^U} \right) \right] \quad (4.96)$$

where superscripts L and U indicate the lower and upper plies, respectively. This means that the stiffness should be converted according to the following lower ply fiber direction.

- ② Shear strain energy density delamination failure criterion: This is a new delamination failure criterion from consideration of the effects of transverse strength on delamination failure based on the bending strain energy density delamination failure criterion:

**Fig. 4.93** Analytical model of impact damage



$$e_D = f_1 \left( \frac{\sigma_2^L}{Y^L} \right)^2 + f_2 \left( \frac{\tau_{23}^U}{S_{23}^U} \right)^2 + f_3 \left( \frac{\tau_{31}^L}{S_i} \right)^2 \geq 1 \quad (4.97)$$

where  $f_1$  is the influence coefficient reflecting the stiffness inconsistency between two adjacent plies:

$$f_1 = \left( \frac{t^L}{t^U} \right) \left( \frac{Q_{11}^L - Q_{11}^{nU}}{Q_{11}^L - Q_{22}^U} \right) \quad (4.98)$$

where  $t^L, t^U$  are the upper and lower ply group thickness, respectively.  $Q_{11}^L$  is the stiffness coefficient along fiber direction of lower ply,  $Q_{22}^U$  is the stiffness coefficient vertical to fiber direction of the upper ply,  $Q_{11}^{nU}$  is the off-axis stiffness coefficient of the top ply along the lower ply fiber direction.

$$f_2 = \frac{1}{2} \left( 1 + \frac{G_{23}^U}{G_{23}^L} \cos^2(\Delta\theta) + \frac{G_{23}^U}{G_{31}^L} \sin^2(\Delta\theta) \right) \quad (4.99)$$

$$f_3 = \frac{15}{16} \left( 1 + \frac{G_{31}^U}{G_{31}^L} \cos^2(\Delta\theta) + \frac{G_{31}^U}{G_{23}^L} \sin^2(\Delta\theta) \right) \quad (4.100)$$

This model not only allows determination of bending strain energy density delamination failure criterion, but also reflects the characteristics of impact delamination along the thickness direction.

(2) Estimation of residual strength: In this section, two methods for estimating residual strength of laminates containing impact damages will be discussed.

① Estimations based on the FD criterion have the main steps given below (as shown in Fig. 4.93):

- (a) Testing, determination, or estimation of impact damage;
- (b) Simplify impact damage as an ellipse with its long axis equal to the projected width of delamination, the projected delamination can be determined by NDT or calculated by the following the procedures mentioned above. The short axis is equal to the width of a surface dent that can be measured directly, or is assumed to be 0.3 on the long axis;



**Fig. 4.94** Cross section of damaged zone

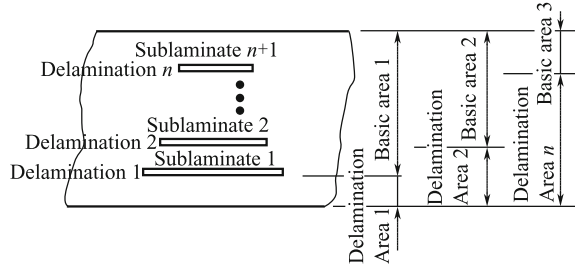
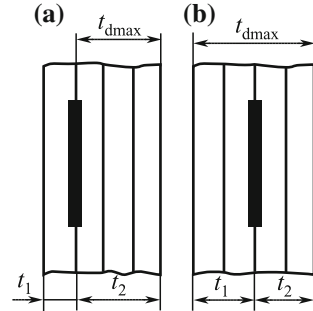


**Fig. 4.95** Calculation method of  $t_{dmax}$



- (c) A complex stress functional method or FEM is used to calculate the normal stress distribution of  $0^\circ$ -plies near the elliptic notch;
  - (d) FD criterion are used [as given in Eq. (4.88)] and the characteristic length  $l_0$  determined by open-hole laminate compression tests.
- ② Estimation based on DI criterion: Estimating methods based on DI criterion can be used to calculate residual compression strength after impact, the main steps are:
- (a) Determine the impact damage conditions (such as delamination, matrix crack, and fiber rupture) by the above-mentioned methods, or by NDT inspection. Store the damage information as a data damage structure (DDS).
  - (b) Assume that the impact causes delamination in the sublaminate with a certain thickness, and perform multi-sublaminate buckling analysis.
  - (c) Use the analytical results to calculate the stiffness reduction of delaminated zone. If fiber rupture or matrix cracks are included in DDS, it is necessary to perform stiffness degradation for the corresponding damaged units, letting the damaged zone be a softened ply. The delamination and delamination zone are defined as represented in Fig. 4.94.

- (d) Use FEM to calculate the stress distribution of the laminate with a softened ply;
- (e) Use DI failure criterion [Eq. (4.82)] to estimate the compression strength. The damage effect distance  $D_i$  is defined in Fig. 4.88. For an impact damaged laminate,  $\alpha$  is the influence factor involving the delamination distribution along the laminate thickness direction, and defined as:

$$\alpha = \left( 2 \left( 1 - \frac{t_{d\max}}{h} \right) \right)^{\left( 1 - \frac{t_{d\max}}{h} \right)} \quad (4.101)$$

where  $t_{d\max}$  is the total thickness of plies (ply group) in a continuous arrangement with the same stiffness degradation coefficients (as shown in Fig. 4.95), and  $h$  is laminate thickness.

**(5) Estimation of residual strength of laminate containing delamination**

The calculation steps are the same as mentioned in the above section on estimations based on DI criterion.

**(6) Estimation of stiffened laminates containing defects/damage**

- (1) Estimation of stiffened laminate with impact damage: As for the estimation of impact damage of laminates, to analyze the residual strength of a stiffened laminate after impact, characteristics of the impact damage shape, size and distribution along the thickness should be derived from NDT inspection or analytical estimations.
- (2) Estimation of stiffened laminates containing damage: The analysis may be divided into two cases: the estimation of residual strength of stiffened laminate containing penetrating defects (hole or cracks) under a tensile load; and the estimation of the residual strength of stiffened laminates containing holes or impact damage under a compression load. In this calculation software, a force calculation of the crack tip stress strength factor, similar to that of a stiffened metal plate, is used, and the stress distribution in the area adjacent to the notch (including crack and ellipse hole) of an anisotropic stiffened laminate can be determined. In this case, both the simplification of the impact damage as an ellipse hole and the DI failure criterion are used simultaneously.

### 4.9.3.2 Analysis of Durability

Composite laminated structures can offer excellent fatigue performance. For common fiber-dominated multi-direction laminates (including specimens with holes), the tensile-tensile fatigue life is  $10^6$  cycles under a maximum stress equal to 80% of the ultimate tensile strength. In the case of tensile-compression fatigue, the fatigue strength will be slightly

lower, with the fatigue strength equal to 50% of the corresponding static strength after  $10^6$  cycles. In particular, for specimens with impact damage, the fatigue strength will not be lower than 60% of the corresponding static strength after  $10^6$  cycles. In thermoplastic composites, values may reach up to 65% under the same conditions. Currently used allowables in composite structure design mainly depend on damage tolerance allowables. Under such strain levels, composite structures can have infinite service life, which is so-called static cover fatigue. Special attention should be paid to adhesive structures because fatigue failure may occur if the design is performed incorrectly. Currently, fatigue failure is not a critical problem in design; however, no mature analytical methods for durability are currently available.

#### **4.9.4 Measures to Improve Durability and Damage Tolerance**

##### **(1) Softened-zone design**

With softened-zone design, the damage tolerance of structures can be effectively improved while maintaining low weight and costs. This is a potentially effective design approach, which has a wide range of applications [1, 2]:

- (1) Tension panels: In this design method, high failure strain fibers (such as a glass-fiber) or prepreg tape (such as  $\pm 45^\circ$  with a high failure strain and low modulus) are spread at intervals in a high modulus fiber that bears main structural load. These constituents can inhibit damage growth and improve damage tolerance. This design method may become an important approach for damage growth inhibition. For example, a number of strips can be selected in the panel and constructed into a glass/carbon fiber hybrid softened zone, arranged at intervals in a high modulus panel parallel to the load direction. This design can inhibit damage growth and direct damage growth along the softened-zone edge, so that the residual tensile strength will be increased. This design approach can be used for the design of carbon/epoxy composite wing skin and fuselage integral stiffened or sandwich panels.
- (2) Mechanical joint zone: Mechanical joining is suitable for high and complex load-bearing situations, and has become a commonly used composite structure joining method. Holes can cause more serious problems in composites than in metals, and will influence the joint strength. In a softened design, low modulus ply or prepreg tape is placed in the mechanical joining zone to improve the connection strength.

##### **(2) Soft skin design approach**

The basic concept in soft skin design is to place ply groups with different ply angles into skin or stiffener to enhance the structural damage tolerance and the allowable strain in the damage tolerance design. The so-called soft skin is a designed low stiffness wing skin with a low thickness. Soft skin mainly uses

low modulus  $\pm 45^\circ$  plies (at a percentage of 70–80%), and contains a certain amount of glass-fibers in some local zones, which can bear shear load and the internal pressure of an oil tank for example. Laminates with a small ratio of  $0^\circ$ ,  $90^\circ$  plies, such as a (10/80/10) ply ratio, can also be used to ensure local strength and structural stability. Stiffeners mainly use  $0^\circ$  plies that are orientated along the wing span direction and can be used to withstand tensile and compression loading in wing panels. The skin and stiffeners are mechanically joined or co-cured to form the wing panel. In some design programs (such as for body panels), a certain proportion of  $0^\circ$  plies are embedded into the soft skin at certain intervals as additional reinforcing elements (crack-blocking zones). This approach is mainly used in shear-bearing transportation aircraft wings.

(3) **Film enclosure**

A layer of adhesive film may be introduced in between laminate plies to increase the interlaminar damage resistance or to reduce the interlaminar stress concentration for easily impacted structures. Epoxy films (such as FM series films) or thermoplastic films (such as HXT series films and PEEK film) can be inserted between the carbon fiber plies to increase damage resistance. A new generation of interlaminar enclosed films can be made by spraying toughened particles on prepreg tapes, which can largely increase the interlaminar toughness and compression strength after impact without increasing the thickness between plies.

(4) **3D reinforcing (Z-axis reinforcing)**

3D reinforcing is mainly used to inhibit the delamination growth caused by impacts and to increase the composite structural damage tolerance. Approaches include reinforcement braiding in the thickness direction (such as 3D braiding and Z-axis knitting performed in combined RFI and RTM processing), as well as fasteners and Z-axial pin joining. Among these methods, dry/knitting and 3D braiding/RTM show great potential for applications in improving damage tolerance.

Z-pin joining is another mechanical joint for Z-axial reinforcement, other than the use of metal fasteners. A foam preform (made of FM) containing small strong carbon/epoxy pins is placed on a laminate structure. These preforms will be pressed into laminates during hot pressing. This approach can be used for reinforcement, locally or over the entire component. This approach can also be used to replace metal fasteners used to fix frame construction. Test results indicate that it may be possible to reduce delamination size and increase damage tolerance with this method.

(5) **Other approaches for durability/damage tolerance improvement**

Three approaches can be used for durability/damage tolerance improvements: use of special designs methods to inhibit damage growth and increase residual strength. On the basis of the analysis of failure mechanisms of laminated structures containing damage (including impact damage), the composite performances can be improved to increase their damage tolerance. Namely, the residual strength can be improved when laminates contain damage of the same

size. On the basis of statistical analysis of external impact energies, and improved production and maintenance conditions (increased supportability), the current damage tolerance requirements may be revised. The initial defect sizes are changed from the current BVID to the external impact energy probability distribution at different locations.

(6) **Special issues**

- (1) Owing to the variety of damage patterns with different formation and expansion mechanisms, proper design approaches should be used for different damage types, such that damage tolerance can be effectively improved.
- (2) In this section, improvements of impact damage tolerance are discussed. Attention should be paid to other possible damages caused under different loading conditions, for example, holes or other penetrating damage may cause potential dangers under tensile or tensile–shear loads. To improve the structural efficiency and design strain level, special design approaches should be used based on the different load conditions and the potential damage modes.
- (3) In practice, no single approach can be used to improve composite structural damage tolerance. Good results can be achieved only through consideration and use of a combination of design concepts.
- (4) It should be noted that damage tolerance is critical, for example, if damage tolerance contributes only a small part to the whole structure (20% for example), the weight may be increased by approximately 4% by increasing the thickness to reduce the strain level. However, the design approaches used for improving damage tolerance can be costly. In practice, a combination of considerations should be taken, including structural strength, stiffness durability, damage tolerance, weight and cost, so that the structure is optimized in terms of cost effectiveness, while balanced performance is achieved.

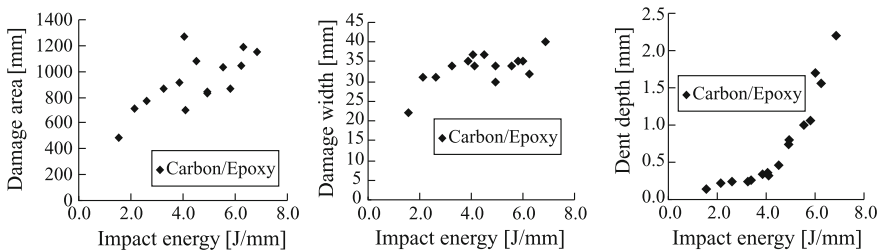


**Fig. 4.96** Typical relationship of damage size and impact energies

### 4.9.5 Characterization of Composite Damage Resistance and Damage Tolerance

#### 4.9.5.1 Review

In fact, the most effective approach to increase composite structure damage tolerance and damage resistance is to develop new material systems with high damage tolerance and high damage resistance. The traditional method to evaluate the composite damage tolerance is use of compression strength after impact (CAI) as detained in NASA RP1142 and SACMA SRM 2R-94; in the recent studies, it has been indicated that CAI obtained in such approaches can only evaluate damage

**Fig. 4.97** Typical relationship of compressive failure strain and damage size

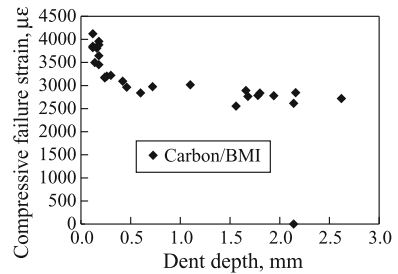


**Fig. 4.98** Typical knee point phenomenon for damage tolerance and damage resistance properties of composite systems

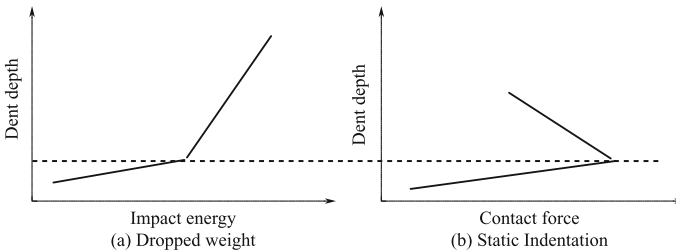
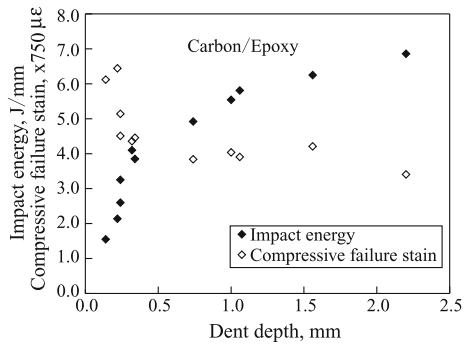
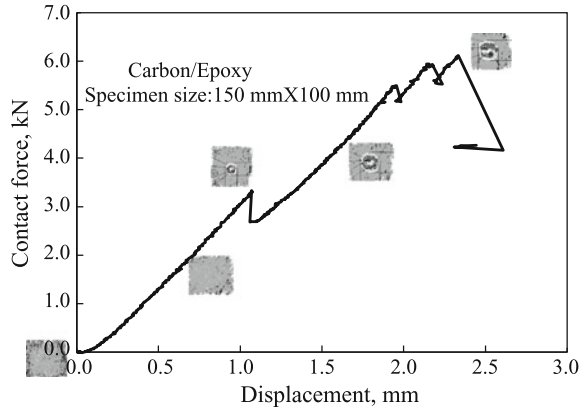


**Fig. 4.99** Comparison of damage resistance behavior obtained by two methods

**Fig. 4.100** Typical contact–displacement curve of composite laminates and corresponding internal damage state



resistance, rather than damage tolerance, which needs a proper evaluation approach [38–45].

In ASTM D 3878–07 Standard Terminology for Composite Materials, definitions on damage resistance and damage tolerance are given, and their differences are also discussed.

#### 4.9.5.2 Complete Description of Damage Resistance, Tolerance and Knee Point

As discussed above, a main parameter describing composite damage resistance is the damage size, which is a function of the impact event. Other parameters describing composite damage tolerance, including the compression load-bearing capacity, are a function of damage size. Usually, impact energy is used as a parameter to describe an impact event. As shown in Fig. 4.96, testing data have indicated that, among the commonly used damage size parameters (such as damage area, damage width and surface dent depth), surface dent depth measured immediately after impact shows a good linear relationship with the impact energy. This measurable is also consistent with the damage parameters required in aircraft structural design. Compression load-bearing capacity is usually expressed by compressive strength or compression failure strain. A comprehensive description of composite damage resistance and tolerance is illustrated in Figs. 4.96 and 4.97. Testing data have indicated that there will be a visible knee point for composite damage resistance and damage tolerance, occurring at the same damage size for a dent depth of approximately 0.5 mm, as shown in Fig. 4.98. It has been verified by theory and experiments, that quasi-static indentation forces can be used to replace hammer dropping to induce damage. The same conclusion is derived as shown in Fig. 4.99. In some studies, supersonic C-scans have been used to study damage propagation with increasing indentation force under quasi-static pressing conditions. The change of damage size was the same as that found for impact energy, as shown in Fig. 4.100. From these studies, we may conclude that when the

indentation force reaches a lower threshold (corresponding to a certain impact energy), apparent delamination occurs inside the specimen, while no dent can be found on the surface. As the indentation force increases (also corresponding to an increase of impact energy), the degree of inner delamination increases gradually as the surface dent depth increases to a depth not larger than 0.3 mm. When the indentation force reaches the ultimate value it drops down quickly and the dent depth will rapidly increase. This is analogous to the impact energy reaching a threshold, such that the dent depth increases markedly, as shown in Figs. 4.99 and 4.100, where the dent depth will not exceed 0.5 mm. Further increases of indentation force or impact energy will not increase the internal damage size further although the dent depth will increase continuously.

In some studies, the two methods described above have been used to induce damage in specimens; damaged specimens from before and after the knee point were soaked with gold chloride ether solution, and ply peeling of the internal damage states was observed. These results have indicated that impact damage prior to the knee point involves matrix cracking and internal delamination. After the knee point, fiber breakage can be found on the front surface of the specimen. Thus, the knee point marks the onset of fiber breakage at the impact point on the front surface. Knee point phenomenon indicates a sudden change of impact (or contact force) resistance in composite laminates. Before the knee point, the impact resistance of a composite derives from both resin and fibers. Damage is induced to the matrix in the form of cracking and delamination; however, the ply, as the basic unit of a composite and, particularly, plies on the surface (including their matrix and inter-laminar structure) are undamaged before the knee point. After that the knee point fiber breakages occur, and damage becomes visible on the surface plies. This indicates that the laminates cannot provide further impact resistance. The damage growth will cause fiber ruptures from the front and back surfaces extending to the center, and internal delamination will also increase. Internal delamination is the main factor contributing to the reduction of the composite laminate compression strength, and the size of delamination will not change greatly after the knee point. Thus, the compression strength will remain unchanged.

For composite laminates, a knee point on the impact energy versus dent depth curve will also be a knee point on the impact energy (dent depth) versus compression failure strength (strain) curve. The former relates to the damage resistance characteristics of a composite laminate, while the latter relates to the damage tolerance characteristics of the laminate. The former denotes a sudden change of damage resistance in composite laminates after an impact event. Before such an event, external impacts are resisted by the combination of matrix and fibers. Damage is caused mainly in the form of internal delamination and small matrix cracking. The same increase in impact energy can result in a small increase in the dent depth, while a larger increase in the damage area and damage width can be expected with good regularity. The presence of a knee point indicates fiber breakage on the surface, and further increases in impact energy will not produce greater delamination beyond that which exists in the damage width. Instead, further increases in the impact energy will produce more fiber breakages from the surface to the inside. Thus, increasing impact energy will increase the dent depth, and



have a smaller effect on the damage area and damage width. The residual compression strength is directly related to the damage width (damage area); thus, a knee point on the impact energy (dent depth) versus compression failure strength (strain) curve will result. Before the knee point, the compression failure strength (strain) will rapidly decrease as the impact energy (dent depth) increases. After the knee point, the compression failure strength (strain) will not change any further or only show a small change.

On the basis of the physical consequences of a knee point, typical values taken from areas adjacent to the knee point can be used to characterize the damage resistance and damage tolerance of composite laminates.

### 4.9.5.3 Characterization of Composite Damage Tolerance and Damage Resistance

It is recommended that the following physical parameters are used to characterize the damage resistance and damage tolerance of composite systems.

- For quasi-isotropic laminates, the maximum indentation force  $F_{max}$  on the indentation force versus displacement curve obtained by static indentation testing can be used to characterize the damage resistance of a composite system.

**Fig. 4.101** Comparison of damage tolerance behavior for two composites with different CAI

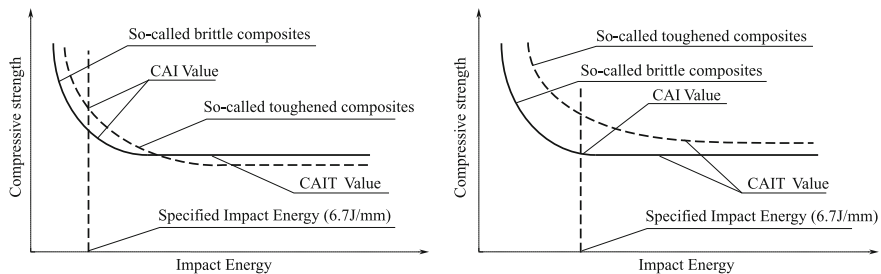
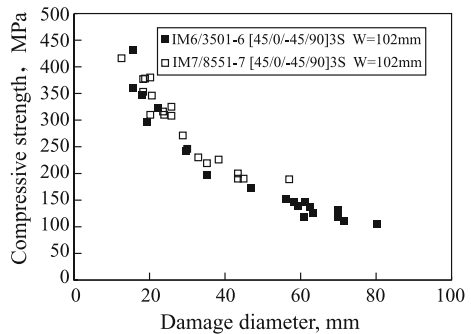


**Fig. 4.102** Comparison of CAI and CAIT values

**Table 4.23** Damage properties for four composite systems

Composite system	CAI (MPa)	CAIT	
		Strength (MPa)	Failure stain
T300/Epoxy A	136	136	2910
T700S/Epoxy B	167	127	2593
CCF300/BMI A	149	142	2730
CCF300/BMI B	194	177	3419

This represents the maximum capacity of a composite system to resist an external impactor.

For quasi-isotropic laminates, the dent depth (or impact energy) versus compression failure strain curve threshold (CAIT), or the compression strength (or failure curve) (CAI) at a dent depth of 1.0 mm (measured immediately after impact) can be used to characterize the damage tolerance of a composite system.

On the basis of these characterizations, composite systems, which are shown to have good damage resistance, will also give aircraft structures with good damage resistance. Similarly, if composite systems have very good damage tolerance behavior, aircraft structures made of these composite systems will also show good damage tolerance.

#### 4.9.5.4 Comparison Between the Recommended Method and the Traditional CAI Evaluation

For a long time, CAI values obtained from NASA RP 1142 or SACMA SRM 2R-94 have been considered to be the main specifications for characterizing damage tolerance. In the NASA standard, an impactor 12.7 mm in diameter with an impact energy of 27 J (about 4.45 J/mm) is used. In the SACMA standard, an impactor 16 mm in diameter with an impact energy of 6.67 J/mm is used.

Here, the obtained damage tolerance values represent the corresponding compression failure strength obtained under testing conditions of 27 J (NASA standard) or 6.67 J/mm (SACMA standard). In fact, the impact energy cannot reflect damage parameters, such that values derived from these methods cannot be used to evaluate the damage tolerance behavior of composite systems perfectly. In Fig. 4.101, the relationship between the damage width versus compression failure strain of two different toughened composite systems is shown. In terms of damage tolerance, the composite systems IM6/3501-6 (brittle epoxy) and IM7/8552-1 (toughened epoxy) have similar damage tolerance behavior, but their CAI values are quite different [15]. According to the above analysis, the composite systems with the higher CAI value at knee point may produce a larger maximum damage area (or diameter) than composite systems with a lower CAI values. Composite systems with higher CAI values may show lower CAIT as given in Fig. 4.102. In Table 4.23, some test results are listed.

## **4.10 Environmental Effects and Protection**

### **4.10.1 Introduction**

Aircraft composite structures in service may be subjected to maneuver and gust loading environments. External environmental conditions, such as temperature, humidity, lightning strikes, sand, hail, rain, snow, ultraviolet light, and atmospheric pollution may influence the structural integrity of composites. The local environment, including fuel, hydraulic fluid, and cleaning solvents can also affect composites. Thus, environmental effects should be considered at the stage of material and configuration selection in the detailed design phase of composite structure design. Environmental design criteria and effective environmental protection methodologies must be established. The influences of hygrothermal and aging environments on airplane composite structures should be considered in structural design and these aspects are discussed in this chapter.

### **4.10.2 Environmental Design Criterion**

Environmental design criteria for aircraft composite structures should be determined based on the service area, flight scope, material systems, mission purpose, and structural status [1, 2, 13].

#### **4.10.2.1 Hygrothermal Environment**

For composite structures, the hygrothermal environment must be considered as part of the overall environment. Two aspects should be carefully considered: first, the degradation of mechanical properties caused by the most extreme potential hygrothermal environments, and second the effects of long-term hygrothermal aging on mechanical behaviors. These aspects should be qualified through analysis and testing of composite structures within the designated service life duration. Structures should maintain sufficient integrity under the individual or combined actions of temperature, humidity, and loading environments. In certain special structural positions, the combined effects of local and overall environments should also be qualified. Detailed requirements are as follows:

- (1) Rigorous structural use environments can be determined based on flight missions, the structural configuration, and the ground rest environment. Thermal spiking effects caused by aerodynamic heating in flight at speeds greater than Mach 2 should also be considered.
- (2) Moisture diffusion behaviors of a chosen material system under a specific hygrothermal environment and the effects of this environment on the physical and mechanical properties of the system should be determined.

- (3) The service moisture absorption content, final moisture content, steady conditions, and hygrothermal allowables of chosen materials and configurations should be determined.

#### 4.10.2.2 Physical Impacts

Aircraft composite structures are susceptible to impact damage from tool dropping, runway detritus, hail stones, and ground service vehicles. Other considerations include lighting strikes, bird-strikes, and bullet damage. In general, lightning strikes will result in visible damage and local ablation of the composite structures,

**Table 4.24** Typical airplane service environmental areas in China

Type	Typical area	Main characteristics	Representative regions
1	Dry-cold	Low air-temperature; annual average air-temperature lower than 10 °C; low rainfall; not more than 500 h of relative humidity more than 80% on average; low levels of industrial pollution and corrosive media in air	Tibet, Qinghai, Ningxia, Jilin and most of the Heilongjiang region
2	Basic warm	Moderate air-temperature; annual average air-temperature lower than 15 °C; moderate rainfall, relatively dry; not more than 3000 h of relative humidity more than 80% on average; moderately serious industrial pollution	Xi'an, Zhengzhou, Beijing, and Shenyang
3	Hot-wet inland	High air-temperature; annual average air-temperature of 15–20 °C; high levels of rainfall, dew, and fog; high air humidity; more than 4000 h hours of relative humidity more than 80% on average; serious industrial pollution and high levels of corrosive media in air; semitropical humid climate	Chongqing, Wuhan, Changsha, Guangzhou, and Nanjing
4	Warm coastal	Moderate air-temperature, annual average air-temperature lower than 15 °C, high levels of rainfall, high air humidity, strong winds, high salt content in air, high salt-fog sedimentation, serious industrial pollution	Qingdao, Xiamen, and coastal regions
5	Hot-wet coastal	High air-temperature, annual average air-temperature more than 20 °C, other characteristics resemble those of the warm coastal region	Hainan coast

introducing through-thickness holes or local delamination. Bird and bullet strikes will produce through-thickness holes.

For composite structures, the requirements of strength and service life after low-energy impacts must still be satisfied, and damage caused by high-energy strikes should not grow further.

### 4.10.2.3 Aging Environment

Here, the aging environments used to study composite structures are discussed, including corrosive liquids (fuel, hydraulic fluid, and antifreeze), ultraviolet radiation, weathering, and sand and rain erosion.

**Table 4.25** Maximum and minimum air-temperature of every month in typical areas °C

Area	1		2		3		4		5	
Month	Dry-cold		Basic warm		Hot-wet inland		Warm coast		Wet-hot coast	
	$T_{max}$	$T_{min}$	$T_{max}$	$T_{min}$	$T_{max}$	$T_{min}$	$T_{max}$	$T_{min}$	$T_{max}$	$T_{min}$
1	-7.4	-21.8	1.4	-9.9	9.6	3.2	3.5	-2.6	20.0	12.0
2	-4.0	-18.4	2.5	-8.5	9.8	3.9	4.4	-0.2	20.0	12.0
3	4.0	-10.4	10.5	-0.5	15.7	6.8	8.1	1.4	24.0	16.0
4	12.6	-0.8	18.6	6.0	20.2	12.8	11.6	5.7	30.0	22.0
5	18.9	5.5	27.0	15.0	26.7	18.8	18.2	11.2	31.0	23.0
6	23.5	10.1	30.0	19.0	28.3	20.5	22.1	16.7	32.0	24.0
7	25.5	12.6	30.8	21.5	31.9	23.5	25.5	21.3	33.0	24.0
8	23.8	11.6	29.5	20.5	31.1	22.5	28.2	23.7	34.0	24.0
9	18.2	5.4	23.5	4.5	29.3	19.5	25.1	19.7	32.0	22.0
10	13.2	-2.4	18.0	6.0	21.4	4.1	20.2	15.4	28.0	22.0
11	1.6	-13.2	9.30	-3.0	16.4	9.3	13.0	6.2	24.0	18.0
12	0.2	-20.2	2.0	-10.0	11.5	3.5	6.9	0.5	21.0	13.0

**Table 4.26** Statistical results of relative humidity in basic warm and dry-cold areas

Area	Relative humidity/%			
	Average monthly maximum	Average monthly minimum	Monthly maximum	Monthly minimum
Basic warm	85	30	100	0
Dry-cold	78	25	100	0

### 4.10.3 *Hygrothermal Environment Effect*

One important key point for composite structure design is to consider the influence of the hygrothermal environment on structural performance. The resin matrix has the ability to absorb moisture, and moisture diffusion can result in a distribution of moisture content in the structure. Thus, both the anti-corrosion resistance of fibers and the glass transition temperature  $T_g$  might decrease. The structural stiffness and strength of the composites might also be reduced through these effects. At all stages of material and configuration selection, detailed design and testing of the composite structure should account for environmental response of the system [1, 2, 13].

#### 4.10.3.1 Aircraft Service Environment in China

The long-term environmental conditions to which an aircraft will be exposed should be determined as the use environment. The most extreme environmental conditions and use environment can be confirmed by a statistical process based on a large volume of measured data. Typical airplane service areas in China are represented in Table 4.24. The average maximum and minimum air-temperature and average relative humidity (RH) each month in typical areas are listed in Tables 4.25 and 4.26.

#### 4.10.3.2 Prediction of Moisture Absorption Diffusion Behaviors

To use composites in structures, first issues related to changes of mechanical performance after moisture absorption by the resin matrix should be addressed. The change of mechanical performance depending on moisture content should be qualified. The composite moisture content in a specific environmental and the time taken for that moisture content to be attained under specified environmental conditions should be determined by theoretical analysis and moisture absorption experiments.

#### Theoretic Predictions

Characteristics of moisture absorption and diffusion can be predicted by the following two models at the initial stages of composite structure design. Moisture diffusion in composites at low relative humidity can be described by the *Fickian* diffusion model, while moisture diffusion processes at high relative humidity are preferably described by the vapor boundary model.

(1) **Fickian model**

Analysis of the moisture diffusion in resin matrix composites can be accomplished with this simple model. The main characteristics of this model are its initial linear moisture absorption curve leading over the long term to a steady moisture level. The model is equivalent to that for moisture absorption of a material immersed in water. The moisture diffusion of bismaleimide (BMI) matrix composites can be described perfectly by this model. In one dimension the model is:

$$\frac{\partial C}{\partial t} = D_z \frac{\partial^2 C}{\partial z^2} \quad t > 0, z \in [-h/2, h/2] \quad (4.102)$$

The boundary conditions are:

$$C(z, 0) = C_0$$

$$C(-h/2, t) = C(h/2, t) = C_\infty \quad t > 0$$

where

- $C$  moisture concentration;
- $C_0, C_\infty$  initial concentration and equilibrium concentration;
- $D_z$  moisture diffusivity through the thickness direction;
- $t$  time;
- $h$  laminate thickness;
- $z$  coordinate in the thickness direction.

The total moisture content is:

$$M(t) = M_\infty - (M_\infty - M_0) \frac{8}{\pi^2} \sum_{n=0}^{\infty} \left\{ \frac{1}{(2n+1)^2} \times \exp(-\lambda_n^2 D t / h^2) \right\} \quad (4.103)$$

where

- $M(t)$  moisture of laminate;
- $M_0, M_\infty$  initial moisture content and equilibrium moisture content

$$\lambda_n = 2\pi + n, \quad n = 0, 1, 2, \dots$$

For long-term moisture absorption, the  $n = 0$  term is unchanging. When diffusivity of the material system and equilibrium moisture content are known the moisture content at any time point can be calculated. Diffusivity can also be calculated from knowledge of the moisture content at two different times.

$$D = \pi \left( \frac{h^2}{4(M_\infty - M_0)} \right)^2 \left( \frac{M(t_1) - M(t_2)}{\sqrt{t_1} - \sqrt{t_2}} \right)^2 \tag{4.104}$$

The disadvantage of this model is the use of fixed boundary conditions, and the shape of the moisture curve at the initial stage are not accurately described. Therefore, the initial moisture absorption is greatly over estimated and the diffusivity is under estimated.

**(2) Vapor boundary model**

When a solid absorbs or desorbs water vapor from the atmospheric environment, the *Fickian* model produces large deviations. A proportionality constant  $F$  may be introduced. Hence,  $F$  is defined as the moisture absorption gradient and is proportion to the difference between the actual surface concentration and equilibrium concentration. The diffusion equation is unchanged from that given in (4.102); however, the boundary conditions are modified as:

$$C(z, 0) = C_0 \tag{4.105}$$

$$C(\pm h/2, t) = C_\infty + \frac{D}{F} \times \frac{\partial C}{\partial z} (\pm h/2, t)$$

Thus, in the limit  $F \rightarrow \infty$ , the vapor boundary model degrades to the *Fickian* model.

The moisture content is:

$$M(t) = M_\infty - (M_\infty - M_0) \sum_{n=0}^{\infty} \left\{ \frac{2 \sin^2 \beta_n}{\beta_n (\sin \beta_n \cos \beta_n + \beta_n)^2} \times \exp(-4\beta_n^2 D t / h^2) \right\} \tag{4.106}$$

$$\beta_n : \beta \tan \beta = hF/2D \quad n = 0, 1, 2, \dots$$

$$\beta_n \in \left\{ n\pi, \frac{\pi}{2} + n\pi \right\}$$

as  $\frac{F}{D} \rightarrow 0, \beta_n \rightarrow n\pi,$

as  $\frac{F}{D} \rightarrow \infty, \beta_n \rightarrow \frac{\pi}{2} + n\pi,$

An iteration of the following form can be adopted.

$$\beta^{i+1} = \beta^i - \frac{(\beta^i \tan \beta^i - hF/2D) \cos^2(\beta^i)}{\sin \beta^i \cos \beta^i + \beta^i} \quad I = 0, 1, 2, \dots$$

The value of  $F$  can be determined from measurements of moisture content at times  $t_1$  and  $t_2$ .



**Table 4.27** Equilibrium moisture content and diffusivity of materials in specified environment

Material	$D$	$D$	$m_e$
	30 °C, 95%RH	50 °C, 95%RH	50 °C, 95%RH
T300/5405	$1.15 \times 10^{-7} \text{ mm}^2/\text{s}$	$3.788 \times 10^{-7} \text{ mm}^2/\text{s}$	0.85%
T300/QY8911	$3.50 \times 10^{-7} \text{ mm}^2/\text{s}$	$7.043 \times 10^{-7} \text{ mm}^2/\text{s}$	1.35%

$$F = \frac{1}{2(C_\infty - C_0)} \left( -\frac{2M_0}{t_2} - \frac{M_0(t_2 - t_1)}{t_1 t_2} + \frac{M(t_1)}{t_1} + \frac{M(t_1)}{t_2 - t_1} - \frac{M(t_2)t_1}{t_2(t_2 - t_1)} \right) \quad (4.107)$$

This model corresponds to a situation in which moisture enters the material from the ambient environment. The initial rate parameters can be obtained easily and have clear physical meanings. Results predicted by this model for high relative humidity are consistent with experimental findings, and at low relative humidity the predictions can satisfy engineering requirements.

In conclusion, for environments with low relative humidity, the moisture absorption diffusion process in composite laminate can be described by the *Fickian* model; however, under environments of high relative humidity, the moisture absorption diffusion process is better described by the vapor boundary model owing to swelling of the composite laminate.

### Moisture Absorption Experiments

Composite material systems require experimental confirmation of moisture absorption and testing should be performed. The purpose of moisture absorption tests is to determine the moisture diffusivity at different temperatures and the equilibrium moisture content at different relative humidity. The test must be performed according to the aviation industry standard *Environmental Moisture Absorption Test Method (HB-7401-96)*. The moisture absorption and desorption behaviors of resin matrix composites are controlled mainly by two parameters; the equilibrium moisture content of the material, which depends on the environmental relative humidity; and the moisture diffusivity, which correlates with the environmental temperature (Table 4.27). The moisture absorption content within a specified time may be determined from these two parameters. Moisture absorption tests should be performed at three different combinations of temperature and humidity for every type material. Two sets of conditions will have the same relative humidity, and two sets of conditions will have the same temperature. Hence, these basic parameters will allow the moisture absorption content to be calculated under a specified environment at different time intervals. Furthermore, the required time to achieve a certain moisture absorption level in a specified environment can be estimated.

### 4.10.3.3 Principle and Methodology of Accelerated Moisture Absorption

The mechanical, thermodynamic, and chemical properties of resin matrix composites will change on exposure to certain hygrothermal environments over a long time. This is a slow accumulative process, and hygrothermal experiments are time consuming and costly. Therefore, accelerated hygrothermal experiments are a necessary part of such studies.

A large volume of experimental results has indicated that there is a direct relationship between the moisture content and the mechanical performances of composite laminates after moisture absorption. Moreover, this relationship is not affected by the hygrothermal history of the composite. This is the basis for accelerated laboratory moisture absorption testing for prediction of mechanical properties after moisture absorption. Additional material degradation should not be induced. The use of high temperatures for accelerated moisture absorption is not generally appropriate.

Two methods for calculating accelerated moisture absorption are given as follows:

- (1) **The accelerated time coefficient  $K$  can be estimated according to following equation:**

$$k = \frac{t_1}{t_2} = \frac{e^{-C/T_2\phi_2}}{e^{-C/T_1\phi_1}} \quad (4.108)$$

where

- $K$  accelerated time coefficient;  
 $t_1$  actual exposed time;  
 $t_2$  time after acceleration;  
 $T_1\phi_1$  temperature ( $^{\circ}\text{C}$ ) and relative humidity of actual exposure environment;  
 $T_2\phi_2$  temperature ( $^{\circ}\text{C}$ ) and relative humidity of accelerated environment.

- (2) **The accelerated time coefficient  $K$  can be estimated from the ratio of diffusivity in the different environments:**

$$K = \frac{t_1}{t_2} = \frac{D_2}{D_1}$$

$$D = D_0 \exp(-C/T) \quad (4.109)$$

where

**Table 4.28** Diffusion constants of different materials under different environments at room temperature

Material Constant	T300/1034		AS/3501-5		T300/5208		934		3501-5		5208	
	$D_0$	$C$	$D_0$	$C$	$D_0$	$C$	$D_0$	$C$	$D_0$	$C$	$D_0$	$C$
Distilled water	16.3	6211	768	7218	132	6750						
Saturated brine	5.85	6020	5.38	6472	6.23	5912						
Moist air	2.28	5554	6.5	5722	0.57	4993	4.85	5113	16.1	5690	4.19	5448

$D_0, C$  —two diffusion constants under different moisture environments at room temperature;

$T$  —absolute temperature.

The diffusion constants of different materials under different moisture environments are shown in Table 4.28.

The results estimated from these two methods are often inconsistent and the more conservative result should be adopted. For example, suppose that T300/5208 laminate is exposed to an environment at 25 °C and 60% relative humidity for 100 days. For accelerated moisture absorption at 60 °C and 95% relative humidity, the accelerated time required is  $t_2 = 10.4$  days according to Eq. (4.108), and  $t_2 = 17.2$  days according to Eq. (4.109). The differences may be caused by the experimental and material constants used. To obtain the most conservative result, both methods should be used and the longer accelerated time selected.

#### 4.10.3.4 Influence of Hygrothermal Environment on Composite Performance

Composites are sensitive to their hygrothermal environment. Moreover, the combination of temperature and humidity has a synergic effect. The influence of hygrothermal environment on the physical and mechanical properties can be predicted based on empirical equations or interpolation of experimental results. Alternatively, the influence could be numerically calculated at a structural level. Namely, the initial strains caused by temperature and humidity could be calculated based on the structural temperature and humidity distribution. The initial strains are transformed to the initial load and the initial load can be superposed with a mechanical load. Finally, the structural stress analysis and strength could be checked by FEMs [46].

## Influence of Hygrothermal Environment on Physical Properties of Composites

### (1) Glass transition temperature

Changes in the physical behavior of composites occur after moisture absorption. The glass transition temperature  $T_g$  will decline with increasing moisture content. The extent of this influence can be predicted by the following equation:

$$T_g = \frac{[\beta_m(1 - v_f)T_{gm} + \beta_f v_f T_{gf}]}{[\beta_m(1 - v_f) + \beta_f v_f]} \quad (4.110)$$

where

- $T_g$  glass transition temperature of matrix under certain moisture content;
- $\beta_m$  wet swelling coefficient of matrix under certain moisture content;
- $\beta_f$  wet swelling coefficient of fiber under certain moisture content, usually equal to zero;
- $V_f$  fiber volume content under certain moisture content;
- $T_{gm}$  glass transition temperature of matrix under certain moisture content;
- $T_{gf}$  glass transition temperature of fiber under certain moisture content.
- $T_{gf}$  —glass transition temperature of fiber under certain moisture content.

The changes of glass transition temperature with moisture content for some composite material systems are given in Table 4.29. The experimentally determined variation of the glass transition temperatures of three material systems is presented in Fig. 4.103. This figure shows that for polymer matrix systems the  $T_g$  declines by approximately 25 °C for at a moisture content of 0.5%. For further increases in the moisture content over 1.2% there is only a slight decrease of  $T_g$ . For cyanate esters matrix composites,  $T_g$  declines by approximately 20 °C when the moisture content is greater than 0.3%. For a BMI matrix composite, moisture content has hardly any effect on  $T_g$ .

### (2) Wet swelling coefficient and thermal expansion coefficient

The wet swelling and thermal expansion coefficients for some materials are shown in Table 4.30. The change of the thermal expansion coefficient with moisture content can be predicted by the following equation:

$$\alpha(T) = \alpha(RT) \left( \frac{T_{gw} - T}{T_{gd} - T_{RT}} \right)^{-\frac{1}{2}} \quad (4.111)$$

where

- $\alpha(T)$  thermal expansion coefficient at temperature  $T$  under a certain moisture content;
- $\alpha(RT)$  thermal expansion coefficient at room temperature;
- $T_{gw}$  glass transition temperature at certain moisture content;



**Fig. 4.103** Change of  $T_g$  with moisture content for three material systems

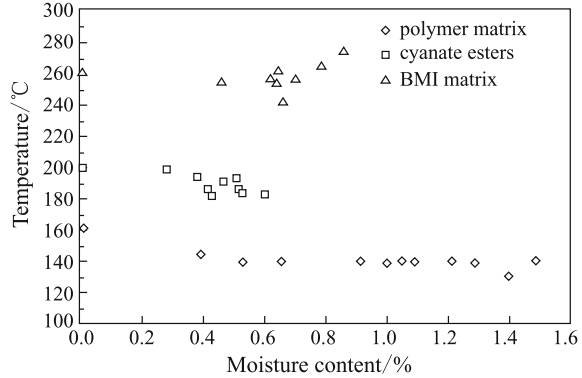


**Table 4.30** Wet swelling and thermal expansion coefficients of some materials

	T300/5208	B/5505	AS/3501	Scotch/1002	Kevlar/epoxy
$\alpha_L/10^{-6}K^{-1}$	0.02	6.1	-0.3	8.6	-0.4
$\alpha_T/10^{-6}K^{-1}$	22.5	30.3	28.1	22.1	79.0
$\beta_L$	0.0	0.0	0.0	0.0	0.0
$\beta_T$	0.6	0.6	0.44	0.6	0.6

$T_{gd}$  the glass transition temperature in dry state;

$T_{RT}$  room temperature.

The changes of the thermal expansion coefficients for 914C pure resin and T300/914C unidirectional laminate with temperature are shown in Table 4.31 and Fig. 4.104. Equation (4.111) is used and has already been validated. The wet swelling coefficient is shown in Fig. 4.105, and the change of wet swelling strain with moisture content is shown in Fig. 4.106. These results indicate that the change of lengthways wet swelling coefficient  $\beta_L$  is small, while the transverse wet swelling coefficient varies linearly with moisture content.

### Influence of Hygrothermal Environment on Mechanical Properties of Composites

Composite mechanical performances, particularly the mechanical performances related to the matrix, are strongly influenced by the hygrothermal environment. Test results have highlighted the importance of considering the influence of hygrothermal environment on the compression, interlaminar shear, compression after impact, and tension and compression strength with an open hole in composite structure design. The non-dimensional parameter  $T^*$  may be introduced.

**Table 4.31** Change of thermal expansion coefficient with temperature

$T/^\circ\text{C}$	$\alpha_T/10^{-6}\text{K}^{-1}$	$\alpha_L/10^{-6}\text{K}^{-1}$
120	38.4	
80	36.0	
40	34.4	-0.8
23	32.8	
0	32.0	
-55	29.6	

**Fig. 4.104** Change of thermal expansion coefficient for 914C pure resin and T300/914C unidirectional laminate with temperature

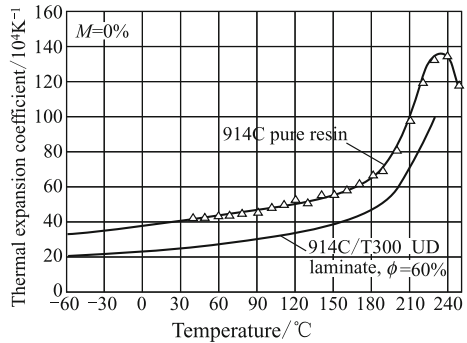


**Fig. 4.105** Change of wet swelling coefficient for 914C pure resin and T300/914C unidirectional laminate with fiber volume content

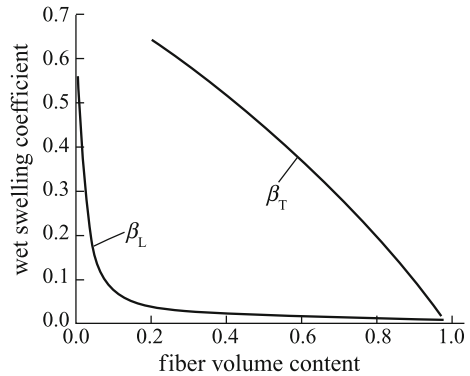
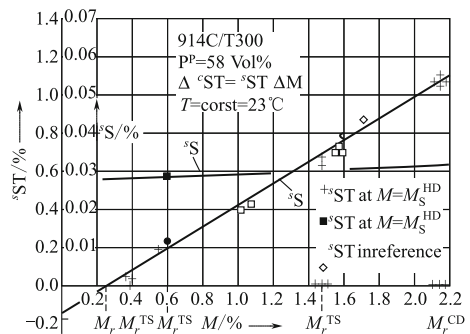


**Fig. 4.106** Change of swelling strain with moisture content for 914C pure resin and T300/914C unidirectional laminate



$$T^* = (T_g - T)/(T_g - T_r) \quad (4.112)$$

where

$T$  operation temperature;

$T_g$  glass transition temperature;

$T_r$  reference temperature or room temperature.

When experimental results on the influence of hygrothermal environment on composite mechanical performance are lacking, the following equations may be used to make predictions:

$$\begin{aligned} X_f/X_f^0 &= (V_f/V_f^0)(T^*)^{0.04} \\ E_1/E_1^0 &= (V_f/V_f^0)(T^*)^{0.04} \\ X_C/X_C^0 &= (V_f/V_f^0)(T^*)^{0.04}(T^*)^{0.05} \\ E_2/E_2^0 &= \left[ (T_g - T)/(T_g^0 - T_r) \right]^{0.5} \\ G_{12}/G_{12}^0 &= \left[ (T_g - T)/(T_g^0 - T_r) \right]^{0.5} \\ S/S_0 &= (T^*)^{0.2} \\ \nu/\nu^0 &= \alpha \left[ (T_g - T)/(T_g^0 - T_r) \right]^{0.5} \end{aligned} \quad (4.113)$$

where

the superscript 0—represents the dry state;

$\alpha$ —parameter related to moisture content, for carbon fiber-reinforced composite (when moisture is not more than 1.0%,  $\alpha \approx 1.0$ );

$V_f$ —fiber volume content.

Tension and compression tests have been performed on different multi-laminate T700S/5405 material systems of different thicknesses immersed in 70 °C distilled water for 3 weeks. The ply ratio of these laminates was 0°-plies 40%, 45°-plies 50%, and 90°-plies 10%. The test results are shown in Table 4.32. The following conclusions could be drawn:

- ① Moisture absorption alone has little influence on the tension strength and modulus.
- ② Moisture absorption alone has little influence on the compression modulus; however, the compression strength of 1.5-, 2.5-, and 3.0-mm-thick laminates dropped 2.2%, 8.6%, and 5.0%, respectively.



**Table 4.32** Tension and compression properties of T700S/5405 system laminate at different thickness

Properties		Nominal thickness of specimen					
		1.5 mm	$C_v / \%$	2.5 mm	$C_v / \%$	3.0 mm	$C_v / \%$
Tension strength/MPa	Dry	1410.0	3.1	1151.8	7.5	1291.1	6.0
	Wet	1326.0	6.6	124.8	3.9	1308.5	6.3
Tension modulus/GPa	Dry	81.77	3.5	64.71	3.3	71.92	3.3
	Wet	81.72	4.6	66.31	1.5	75.56	6.2
Tension Poisson's ratio	Dry	0.34	5.6	0.52	3.5	0.52	5.9
	Wet	0.36	6.7	0.53	2.8	0.53	3.3
Tension extensibility/ %	Dry	2.03	5.0	2.09	6.6	2.11	5.1
	Wet	1.90	8.8	2.17	3.6	2.01	5.9
Compression strength/MPa	Dry	560.28	7.9	716.81	7.1	752.66	6.9
	Wet	548.07	6.8	654.99	4.1	715.10	6.6
Compression modulus/GPa	Dry	79.19	8.7	61.32	2.7	67.71	5.1
	Wet	80.97	10.3	64.00	9.6	73.79	5.2
Compression Poisson's ratio	Dry	0.31	8.5	0.48	8.3	0.49	4.1
	Wet	0.32	9.4	0.48	13.4	0.50	10.6

- ③ The change of the compression strength was more pronounced in thicker laminates.

Mechanical performances tests have been performed on a stitched multi-laminate T300/QY 8911-III material system of different thicknesses immersed in 70 °C distilled water for three weeks. The specimens were divided into types A and B. The ply proportions of the type A laminate were 0°-plies 50%, 45°-plies 40%, and 90°-plies 10%. The ply proportions of the type B laminate were 0° lamina 45%, 45° lamina 40%, and 90° lamina 15%. The test results are shown in Table 4.33, and the following conclusions may be drawn:

- ① The moisture content of stitched T300/QY 8911-III laminate was approximately 1.5 times as large as that of the unstitched laminate.
- ② Moisture absorption only had little influence on the tension strength, modulus, and Poisson ratio of the stitched T300/QY8911-III laminate.
- ③ Moisture absorption alone had little influence on the compression modulus of stitched T300/QY 8911-III laminate. However, the compression strength of the 3.0-, 4.0-, and 4.5-mm-thick laminates dropped 15.3%, 3.3%, and 8.6%, respectively.
- ④ Moisture absorption alone had little influence on the in-plane shear strength of stitched T300/QY  
For 8911-III laminate, however, the in-plane shear strength of 3.0-mm-thick laminates dropped by 11.3%.

**Table 4.33** Mechanical properties of T300/QY8911-III system stitched laminate under different thickness

Properties		Layering and nominal thickness of specimen					
		Type A			Type B		
		3.0 mm	4.0 mm	4.5 mm	3.0 mm	4.0 mm	4.5 mm
Tension strength/MPa	Dry	631.03	565.16	601.80	498.55	671.29	707.15
	Wet	672.38	573.61	609.30	–	–	–
Tension modulus/GPa	Dry	63.21	58.59	56.88	54.97	68.11	69.85
	Wet	64.03	64.92	62.86	–	–	–
Tension Poisson ratio	Dry	0.41	0.49	0.42	0.42	0.54	0.38
	Wet	0.42	0.52	0.45	–	–	–
Tension extensibility/%	Dry	1.22	1.15	1.25	1.08	1.16	1.21
	Wet	1.20	1.05	1.16			
Compression strength/MPa	Dry	613.41	659.89	610.26	435.86	648.97	693.03
	Wet	519.59	637.94	557.81	–	–	–
Compression modulus/GPa	Dry	51.81	52.99	51.42	48.20	65.31	66.57
	Wet	54.38	54.07	52.48	–	–	–
In-plane shear strength/MPa	Dry	247.92	276.32	289.41			
	Wet	219.92	271.09	294.88			
In-plane shear modulus/GPa	Dry	13.13	16.77	17.47			
	Wet	15.37	18.11	18.25			
Flexural strength/MPa	Dry	713.33	699.77	74.61	783.13	801.58	765.60
	Wet	–	700.75	–	793.79	–	771.36
Flexural modulus/GPa	Dry	47.93	40.66	48.30	52.60	44.18	52.03
	Wet	–	40.58	–	53.41	–	51.99
Flexural failure deformation/mm	Dry	10.20	10.70	7.38	10.55	10.58	7.86
	Wet	–	10.73	–	10.45	–	8.00
Interlaminar shear strength/MPa	Dry	53.61	64.28	60.69	57.03	66.23	67.37
	Wet	53.19	62.74	58.48	–	–	–

- ⑤ Moisture absorption had little influence on the flexural performances of stitched T300/QY 8911-III laminate.
- ⑥ The interlaminar shear strength of stitched T300/QY 8911-III laminate decreased appreciably after moisture absorption.

Mechanical performances tests have been performed on nine material systems (T700S/5428, T700S/5429, T700S/5405, T700S/5228, T300/5405, T800/QY9511, T700S/QY 9511, T300/QY8911, and stitched T300/QY9512) immersed in 70 °C distilled water for 3 weeks in six different environments ( $-55 \pm 2$  °C,  $23 \pm 2$  °C and  $(50 \pm 5)\%RH$ ,  $80 \pm 2$  °C and  $(50 \pm 5)\%RH$ ,  $125 \pm 2$  °C,  $150 \pm 2$  °C,  $170 \pm 2$  °C). The ply ratio in the eight unstitched laminates was 0°-plies 33%, 45°-plies 57%, and 90°-plies 10%. The ply ratio in the stitched laminate was 0°-plies 35%, 45°-plies 53%, and 90°-plies 12%.

**Table 4.34** Moisture contents of nine materials systems after immersion in 70 °C distilled water for three weeks

Material	Moisture content/%	Material	Moisture content/%
T700S/5428	0.58	T800/QY9511	0.95
T700S/5429	0.46	T700S/QY9511	0.58
T700S/5405	0.67	T300/QY8911	1.11
T700S/5228	1.00	Stitched T300/QY9512	1.45
T300/5405	0.66		

The moisture contents of the nine materials systems after immersion in 70 °C distilled water for three weeks are shown in Table 4.34. The moisture content of the T700S/5429 system was lowest. The moisture content of the stitched T300/QY9512 system was highest, and approximately 3.2 times as large as that of the T700S/5429 system.

Results of testing tension and compression, and tension and compression with an open hole for nine material systems are shown in Table 4.35 and Figs. 4.107, 4.108, 4.109, 4.110.

- ① The tension strengths of the nine wet open hole specimens were very similar under the six hygrothermal environments. The tension strength of the open-hole specimen of the T700S/5405 system was slightly higher than that of other systems.
- ② The tension strength gradually declined as temperature was elevated. The tension strength of the specimens at −55 °C was basically equivalent to that room temperature. The material most sensitive to elevated temperature was T700S/5405, which at 170 °C featured a tension strength drop of 25.7%. The material most sensitive to cryogenic temperatures was T700S/5429; the tension strength at −55 °C dropped by 8.1% compared with that at room temperature. Among the nine materials, the tension strength of the T700S/5405 system was highest. The tension modulus fluctuated within a range of 20% at the six temperatures.
- ③ The Poisson's ratio at high temperature was elevated increased except for the T700S/5228 system.
- ④ The tension and the tension performance of the open-hole specimen of the stitched laminate gradually declined at elevated temperature. The corresponding strengths decreased by 17.0% and 4.9%, compared with room temperature.
- ⑤ Hygrothermal environment had a strong influence on the compression performance of the open-hole specimens for all the material systems. The residual performances of the various materials are shown in Table 4.36. The compression strength of the open-hole specimens at 170 °C decreased by more than 50%. The residual compression strength of the stitched T300/QY9512 system was only 16.6%.

**Table 4.35** Test results of tension and compression and tension and compression with open hole specimens for nine material systems

Material	Test environment	Test type						
		Tension with an open hole	Tension			Compression with an open hole	Compression	
			$\sigma_{kt}$ /MPa	$\sigma_t$ /MPa	$E_t$ /GPa		$\nu_t$	$\sigma_c$ /MPa
T700S/5428	-55 °C	628.3	991.5	63.36	0.46	347.2	574.5	53.50
	23 °C, 50% RH	675.5	1071.4	59.58	0.51	332.2	549.4	59.39
	80 °C, 50% RH	694.8	1045.6	3.48	0.54	283.8	466.3	54.04
	125 °C	709.4	908.4	72.12	0.55	248.0	419.2	54.54
	150 °C	717.5	934.0	68.29	0.48	204.1	358.4	54.98
	170 °C	728.5	870.1	69.32	0.53	146.0	260.1	55.31
T700S/5429	-55 °C	622.0	1037.2	59.78	0.48	348.4	543.1	50.31
	23 °C, 50% RH	636.9	1129.1	58.51	0.49	304.1	491.3	50.06
	80 °C, 50% RH	626.9	1047.8	57.03	0.53	276.6	495.8	50.73
	125 °C	654.3	990.5	68.54	0.60	263.3	433.4	47.63
	150 °C	637.1	900.0	68.66	0.59	165.3	360.0	53.55
	170 °C	636.4	863.0	68.27	0.53	135.4	234.7	44.57
T700S/5405	-55 °C	706.8	1261.2	65.60	0.50	411.8	525.9	54.84
	23 °C, 50% RH	732.5	1268.7	68.48	0.53	355.4	493.3	51.08
	80 °C, 50% RH	874.0	1151.4	63.46	0.56	306.8	485.9	52.78
T700S/5405	125 °C	722.1	1045.8	69.81	0.60	239.0	411.5	50.69
	150 °C	683.2	1004.3	64.55	0.54	120.8	409.6	52.42
	170 °C	668.9	942.3	50.69	0.45	92.0	250.7	51.04
T700S/5228	-55 °C	522.9	905.7	56.36	0.53	363.0	528.4	45.44
	23 °C, 50% RH	573.5	832.6	49.99	0.51	319.3	497.6	44.15
	80 °C, 50% RH	577.7	899.3	52.65	0.54	258.1	500.5	44.58
	125 °C	532.5	843.6	69.08	0.52	180.2	436.3	44.32
	150 °C	507.7	754.2	59.76	0.50	108.2	315.1	47.22
	170 °C	533.9	685.5	59.70	0.52	81.3	215.4	48.60
T300/5405	-55 °C	355.2	768.2	64.28	0.49	449.9	644.4	61.37
	23 °C, 50% RH	340.3	702.4	69.01	0.50	356.1	570.9	56.12
	80 °C, 50% RH	352.3	688.8	61.60	0.52	299.3	487.7	54.14

(continued)

**Table 4.35** (continued)

Material	Test environment	Test type						
		Tension with an open hole	Tension			Compression with an open hole	Compression	
			$\sigma_{kt}$ /MPa	$\sigma_t$ /MPa	$E_t$ /GPa		$\nu_t$	$\sigma_c$ /MPa
T800/QY9511	125 °C	331.6	650.0			233.5		55.42
	150 °C	339.0	556.6	75.70	0.53	125.1	281.1	55.32
	170 °C	331.2	476.1	70.32	0.46	91.1	210.4	58.46
	-55 °C	470.3	893.7	65.27	0.51	373.33	646.4	70.82
	23 °C, 50% RH	479.9	949.0	61.01	0.52	336.51	628.3	76.89
	80 °C, 50% RH	469.9	901.6	59.36	0.54	311.71	530.7	68.64
	125 °C	505.6	927.9	67.71	0.59	238.05	515.6	70.65
T700S/QY9511	150 °C	518.1	802.0	53.23	0.51	200.77	383.5	74.32
	170 °C	499.1	746.7	60.47	0.53	168.45	321.9	65.77
	-55 °C	591.8	968.9	54.32	0.50	404.7	651.3	62.92
	23 °C, 50% RH	584.2	956.3	55.51	0.51	338.6	636.0	71.16
	80 °C, 50% RH	608.9	956.1	59.58	0.53	317.4	476.8	60.67
	125 °C	586.2	877.4	58.72	0.53	247.8	485.4	56.09
	150 °C	640.1	870.1	51.08	0.53	216.6	413.7	53.25
T300/QY8911	170 °C	613.0	830.9	56.21	0.50	147.3	280.9	58.37
	-55 °C	312.9	743.2	60.33	0.47	378.0	649.1	52.48
	23 °C, 50% RH	329.4	673.8	63.40	0.49	380.2	675.5	59.49
	80 °C, 50% RH	329.7	672.7	58.31	0.53	353.2	605.3	56.76
	125 °C	327.0	591.7	63.93	0.51	249.5	457.7	58.97
	150 °C	317.8	556.3	71.63	0.51	168.4	255.1	60.18
	170 °C	306.9	523.9	64.05	0.52	128.3	200.4	59.29
Stitched T300/QY9512	-55 °C	299.8	577.7	56.30	0.42	376.6	576.5	49.96
	23 °C, 50% RH	323.2	536.1	57.76	0.44	341.3	550.4	46.75
	80 °C, 50% RH	334.2	506.0	61.32	0.54	249.1	432.6	44.46
	125 °C	301.7	498.5	54.72	0.43	127.1	227.8	43.72
	150 °C	291.8	396.9	58.34	0.42	76.5	139.2	47.36
	170 °C	307.4	445.2	53.79	0.46	56.8	80.4	42.13

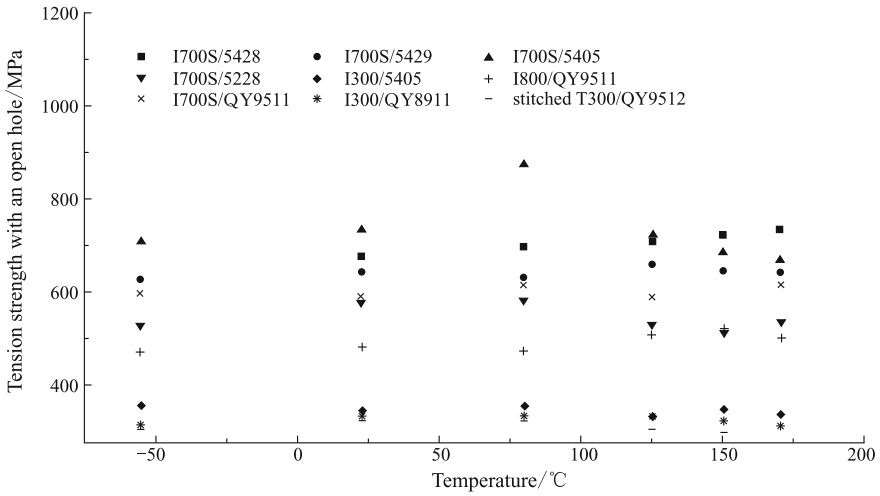


**Fig. 4.107** Influence of temperature on tension strength with an open hole for nine material systems

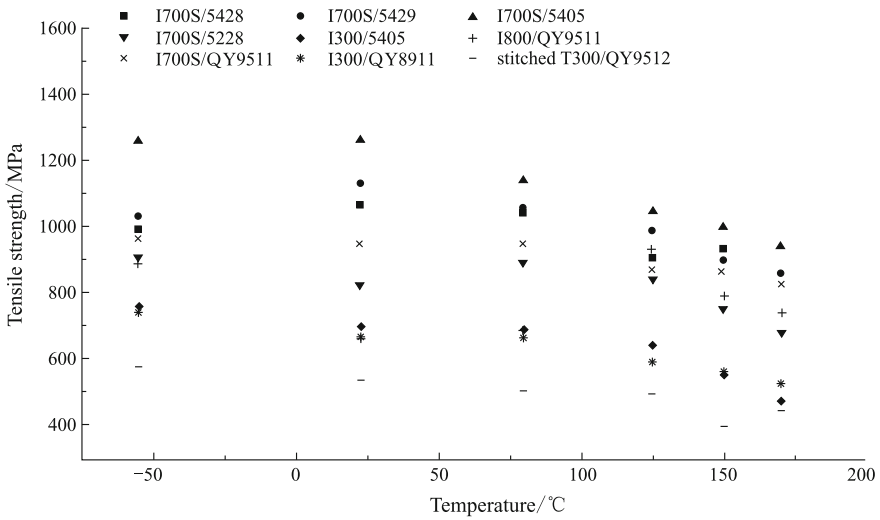


**Fig. 4.108** Influence of temperature on tension strength for nine material systems

- ⑥ The hygrothermal environment also strongly affected the compression strength of the nine material systems. The compression strength at 170 °C dropped to 50% or less, and the residual compression strength of the stitched T300/QY9512 system was only 4.6%. The modulus dropped

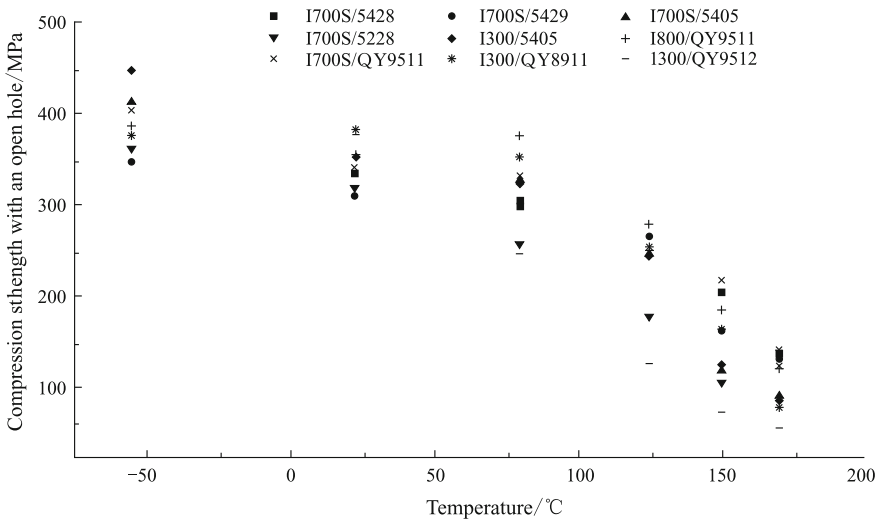


**Fig. 4.109** Influence of temperature on compression strength with an open hole for nine material systems

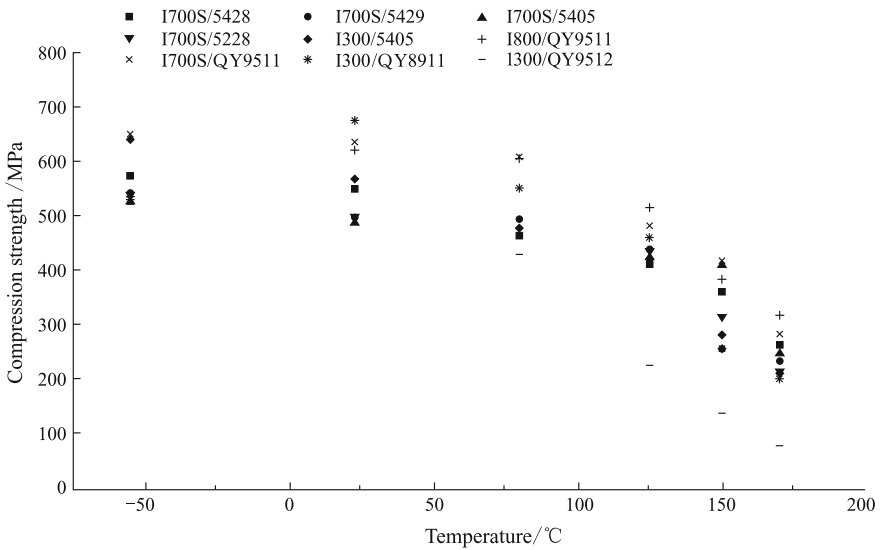


**Fig. 4.110** Influence of temperature on compression strength for nine material systems

approximately 10% on average. The modulus of the T700S/QY9511 system dropped 18%.

- ⑦ The compression strength at  $-55\text{ }^{\circ}\text{C}$  was equivalent to that at room temperature. The most sensitive material to cryogenic temperatures was

**Table 4.36** Strength and modulus survivability of compression and compression with an open hole

Residual performance	T700S/5428					T700S/5429						
	-55 °C	23 °C, C, 50% RH	80 °C, C, 50% RH	125 °C	150 °C	170 °C	-55 °C	23 °C, 50% RH	80 °C, 50% RH	125 °C	150 °C	170 °C
$\sigma_{kc}/\%$	104.5	100	85.4	74.7	61.4	43.9	14.6	100	91.0	86.6	54.4	44.5
$\sigma_c/\%$	104.6	100	84.9	76.3	65.2	47.3	110.5	100	101	88.2	73.2	47.8
$E_c/\%$	90.1	100	91.0	91.8	92.6	93.1	100.5	100	101.3	95.1	107	89.0
Residual performance	T700S/5405					T700S/5228						
	-55 °C	23 °C, C, 50% RH	80 °C, C, 50% RH	125 °C	150 °C	170 °C	-55 °C	23 °C, 50% RH	80 °C, 50% RH	125 °C	150 °C	170 °C
$\sigma_{kc}/\%$	115.9	100	86.3	67.2	34.0	25.9	113.7	100	80.8	56.4	33.9	25.5
$\sigma_c/\%$	106.6	100	98.5	83.4	83.0	50.8	106.2	100	100.6	87.7	63.3	43.3
$E_c/\%$	107.4	100	103.3	99.2	102.6	99.9	102.9	100	101	100.4	107	110.1
Residual performance	T3000/5405					T800/QY9511						
	-55 °C	23 °C, C, 50% RH	80 °C, C, 50% RH	125 °C	150 °C	170 °C	-55 °C	23 °C, 50% RH	80 °C, 50% RH	125 °C	150 °C	170 °C
$\sigma_{kc}/\%$	126.3	100	84.0	65.6	35.1	25.6	110.9	100	92.6	70.7	59.7	50.1
$\sigma_c/\%$	112.9	100	85.4	73.3	49.2	36.9	102.9	100	84.5	82.1	61.0	51.2
$E_c/\%$	109.3	100	96.5	98.8	98.6	104.2	92.1	100	89.3	91.9	96.7	85.5

(continued)



Table 4.36 (continued)

Residual performance	T700S/5428					T700S/5429						
	-55 °C	23 °C, C, 50% RH	80 °C, C, 50% RH	125 °C	150 °C	170 °C	-55 °C	23 °C, 50% RH	80 °C, 50% RH	125 °C	150 °C	170 °C
$\sigma_{kc}/\%$	119.5	100	93.7	73.2	64.0	43.5	99.4	100	92.9	65.6	44.3	33.7
$\sigma_c/\%$	102.4	100	75.0	76.3	65.0	44.1	96.1	100	89.6	67.8	37.8	29.7
$E_c/\%$	88.4	100	85.3	78.8	74.8	82.0	88.2	100	95.4	99.1	101.2	99.7
Residual performance	T300/QY9511											
	T300/QY8911											
Residual performance	Stitched T300/QY9512											
$\sigma_{kc}/\%$	110.3	100	73.0	37.2	22.4	16.6	-55 °C	23 °C, C, 50% RH	80 °C, 50% RH	125 °C	150 °C	170 °C
$\sigma_c/\%$	104.8	100	78.6	41.4	25.3	4.6	-55 °C	23 °C, 50% RH	80 °C, 50% RH	125 °C	150 °C	170 °C
$E_c/\%$	106.9	100	95.1	93.5	101.3	90.1	-55 °C	23 °C, 50% RH	80 °C, 50% RH	125 °C	150 °C	170 °C

T300/QY8911; the compression strength and modulus at  $-55\text{ }^{\circ}\text{C}$  dropped 4.9% and 11.8%, respectively, compared with room-temperature values.

### Influence of Hygrothermal Environment on Composite Failure Mode

The hygrothermal environment not only affects the physical and mechanical properties of composite laminate, but also affects failure modes. The failure modes at low temperatures and in the dry state are related to basic failure of the matrix itself. The failure modes of wet composites at room temperature involve hybrid failure of a matrix/interphase. The failure modes of wet composites at elevated temperature involve failure of the fiber/matrix interface.

### Hygrothermal Stress Analysis

The hygrothermal environment seriously affects the stress distribution of composite structure and composite/metal hybrid structures. The response of the steady or quasi-steady hygrothermal field in structural stress analysis should be dealt with by linear superposition, neglecting coupling. Thermal strain and wet strain can be considered as the initial strain, and the equivalent hygrothermal initial load can be created. The hygrothermal initial load should then be superposed on the mechanical load. The displacement and total strain can be resolved by FEMs and the stress distribution of the structure can be resolved by subtracting the initial strain from the total strain.

The initial strain and the equivalent hygrothermal initial load caused by the hygrothermal environment can be calculated from the following equations.

- ① For an isotropic material:

$$\begin{aligned}\varepsilon_T &= \alpha\Delta T \\ \varepsilon_C &= 0\end{aligned}\tag{4.114}$$

$$\{R_T\}^e = \Delta t \iint [B]^T [D] \{\varepsilon_T\} dx dy$$

- ② For an anisotropic material:

$$\begin{aligned} \begin{pmatrix} \varepsilon_{1T} \\ \varepsilon_{2T} \\ 0 \end{pmatrix} &= \begin{pmatrix} \alpha_1 \Delta T \\ \alpha_2 \Delta T \\ 0 \end{pmatrix} \\ \begin{pmatrix} \varepsilon_{1C} \\ \varepsilon_{2C} \\ 0 \end{pmatrix} &= \begin{pmatrix} \beta_1 \Delta C \\ \beta_2 \Delta C \\ 0 \end{pmatrix} \\ \{R_T\}^e &= \Delta t \iint_e [B]^T [T]^T [Q] \{\varepsilon_T\} dx dy \\ \{R_T\}^e &= \Delta t \iint_e [B]^T [T]^T [Q] \{\varepsilon_T\} dx dy \\ \{R_C\}^e &= \Delta t \iint_e [B]^T [T]^T [Q] \{\varepsilon_C\} dx dy \end{aligned} \quad (4.115)$$

where

- $\alpha$  —thermal expansion coefficient of material,  $1/^\circ\text{C}$ ;
- $\Delta T$  —increment of temperature,  $^\circ\text{C}$ ;
- $\Delta C$  —increment of moisture content;
- $\alpha_1$  —longitudinal thermal expansion coefficient of laminate,  $1/^\circ\text{C}$ ;
- $\alpha_2$  —transverse thermal expansion coefficient of laminate,  $1/^\circ\text{C}$ ;
- $\beta_1$  —longitudinal wet swelling coefficient of laminate;
- $\beta_2$  —transverse wet swelling coefficient of laminate;
- $\varepsilon_T$  —initial strain caused by temperature;
- $\varepsilon_C$  —initial strain caused by moisture absorption;
- $\{R_T\}^e$  —equivalent thermal load at element node;
- $\{R_C\}^e$  —equivalent wet swelling load at element node.

#### 4.10.4 Hygrothermal Aging Response

The strength and stiffness performance of resin matrix composites will vary considerably with extended usage-time, especially in certain hygrothermal environments. Hygrothermal aging of fiber-reinforced composites is a gradual degradation process caused by the combined action of moisture uptake, temperature, and stress. Fibers and the fiber/matrix interface are degraded by physical/chemical reactions. During the moisture absorption process, a swelling stress will be introduced to the interior of composites. A greater swelling stress might be introduced owing to rapid desorption of the surface layer of wet structures under thermal spiking. Under this repeated interior stress, at a certain threshold stress, cracking will occur followed by crazing. The moisture re-absorption and re-desorption rates will be affected by the

crazing, and finally, macroscale cracks will form. Therefore, the hygrothermal aging response of any selected composite material system should be investigated at the design stage. However, this theoretical analysis is difficult owing to uncertainties of the environmental and the coupling effect between hygrothermal stress and exterior loading. In general, experimental methods are used to study these factors based on ground environmental aging, accelerated laboratory aging and aging in actual flights. The experimental data are globally analyzed to obtain design criterion for hygrothermal aging [1, 2, 13].

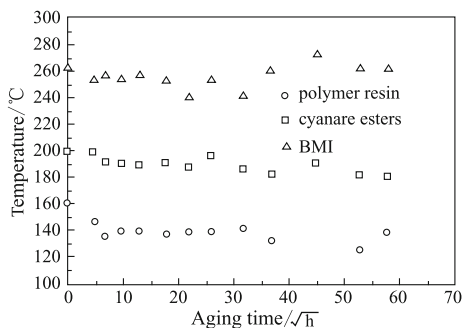
#### 4.10.4.1 Influence of Hygrothermal Aging on Composite Physical Properties

In certain hygrothermal environments over a long period, matrix constituents will undergo chemical reactions, particularly at elevated temperatures. The rate of these reactions will be affected by many factors, including the chemical components of the materials, the aging temperature, fiber volume fraction, and ply stacking sequence of the laminate. For any composite system, the main factors are aging time and temperature.

There have been few investigations on the effect of hygrothermal aging on the physical properties of composites. The changes of  $T_g$  with aging time for three material systems under a 70–85%RH aging environment are shown in Fig. 4.111. The  $T_g$  of the polymer matrix composite was considerably affected by aging. From the start of aging to 50 h,  $T_g$  declined lineally; a maximum decrease of 25 °C was found, after which the  $T_g$  stabilized. Aging up to 900 h, the  $T_g$  underwent a second drop of approximately 10 °C which remained stable with aging for 2700 h. For a cyanate ester matrix composite, the  $T_g$  showed a slow reduction with increasing aging time. After about 1400 h of aging, the  $T_g$  dropped by 20 °C and then stabilized. For BMI composite, aging time had hardly any effect on  $T_g$ .

The influences of hygrothermal aging on the thermal expansion coefficients of a composite matrix can be determined as follows:

**Fig. 4.111** Change of  $T_g$  with aging time under 70 °C/85% RH environment



$$\alpha'_m = \alpha_m [1 + \Delta\alpha_{a1} (a_1)^{n_{za1}}] [1 + \Delta\alpha_{a2} (a_2)^{n_{za2}}] \quad (4.116)$$

$$\alpha_1 = \frac{T_{gd} - T_g^0}{T_{gf} - T_g^0}$$

$$\alpha_2 = \frac{m_0 - m}{m_0 - m_f}$$

where

$\alpha'_m$	matrix thermal expansion coefficient after accounting for aging effects;
$\alpha_m$	matrix thermal expansion coefficient at room temperature in dry state;
$\alpha_1$	degradation parameter of the crosslinking mechanism;
$\alpha_2$	parameter of matrix mass change;
$T_{gd}$	measured glass transition temperature at room temperature in dry state;
$T_g^0$	measured glass transition temperature at initial aged state;
$T_{gf}$	measured glass transition temperature at final aged state;
$m_0$	mass of a small neat matrix specimen at initial aged state;
$m$	mass of a small neat matrix specimen at room temperature and dry state;
$m_f$	mass of a small neat matrix specimen at final aged state.
$\Delta\alpha_{a1}, \Delta\alpha_{a2}, n_{za1}, n_{za2}$	fitting parameters based on the change of $a_1$ and $a_2$ data.

The matrix wet expansion coefficient can also be modified by an analogous methodology.

#### 4.10.4.2 Influence of Hygrothermal Aging on Mechanical Properties of Laminates

The aging of resin matrix composites involves degradation (degeneration) processes. During this process, mechanical properties, in particular matrix controlled properties, such as shear and transverse behavior, are markedly affected.

The thermal aging properties of HT3/QY8911 and HT3/5405 unidirectional laminates are shown in Tables 4.37 and 4.38. Test results of the interlaminar shear strength for a polymer matrix composite at different temperatures after 70–85% RH environmental aging are shown in Figs. 4.112 and 4.113. The influence of aging time and moisture content on interlaminar shear strength at room temperature was slight; however, the interlaminar shear strength at 100 °C decreased linearly with increasing moisture content. For every 1% increase in moisture content, the interlaminar shear strength dropped by approximately 7.9 MPa. The hygrothermal aging

**Table 4.37** Thermal aging properties of T300/QY8911 unidirectional laminate

Aging time	$\tau_b^i$ /MPa		$\sigma_b^f$ /MPa	
	25 °C	150 °C	25 °C	150 °C
0	14.1	77.0	1916	1752
100	118.1	94.4	1925	1748
240	113.2	84.1	1876	1759
400	14.8	92.2	1819	1700
710	117.5	89.1	1914	1684
1000	14.7	88.0	1941	1684

**Table 4.38** Thermal aging properties of T300/5405 unidirectional laminate

		Aging time /h			
		0	310	607	1000
$s_b^i$ (RT)	Average value/MPa	96.8	90.0	88.4	93.1
	Standard deviation/MPa	5.9	3.8	3.6	3.9
	$C_v$ /%	6.1	4.2	4.0	5.2
$t_b^i$ (130 °C)	Average value/MPa	81.2	82.2	81.5	84.9
	Standard deviation/MPa	1.1	1.8	4.9	1.8
	$C_v$ /%	1.4	2.3	6.1	2.1
$s_b^f$ (RT)	Average value/MPa	1770	1764	1876	1865
	Standard deviation/MPa	56.0	29.9	75.4	35.4
	$C_v$ /%	3.2	1.7	4.0	1.9
$s_b^f$ (130 °C)	Average value/MPa	1300	1323	1396	1437
	Standard deviation/MPa	58.7	56.6	86.6	76.2
	$C_v$ /%	2.6	2.4	3.5	3.0
$S$ (RT)	Average value/MPa	113.6	108.2	104.5	97.2
	Standard deviation/MPa	1.3	1.6	6.7	2.3
	$C_v$ /%	1.2	1.5	6.4	2.4
$S$ (130 °C)	Average value/MPa	96.3	102.6	103	99
	Standard deviation/MPa	0.2	1.0	2.6	1.3
	$C_v$ /%	4.3	1.1	1.5	1.4
$G_{12}$ (RT)	Average value/GPa	1.75	4.51	4.60	4.57
	Standard deviation/GPa	0.06	0.08	0.09	0.05
	$C_v$ /%	1.4	1.7	2.0	1.1
$G_{12}$ (130 °C)	Average value/GPa	3.1	3.8	4.0	4.1
	Standard deviation/GPa	0.2	0.6	0.1	0.1
	$C_v$ /%	5.1	1.6	2.7	2.7

responses of BMI matrix composite are shown in Figs. 4.114 and 4.115. When the moisture content was less than 0.6% (corresponding to 70 h of aging), there was little change in the interlaminar shear strength; however, for a moisture content greater than 0.6%, the interlaminar shear strength showed a marked decrease. The interlaminar shear strength of the moisture saturation state dropped by approximately 50% compared with that of the dry state.

**Fig. 4.112** Change of interlaminar shear strength with aging time for polymer matrix composite after 70–85% RH environmental aging at different temperatures

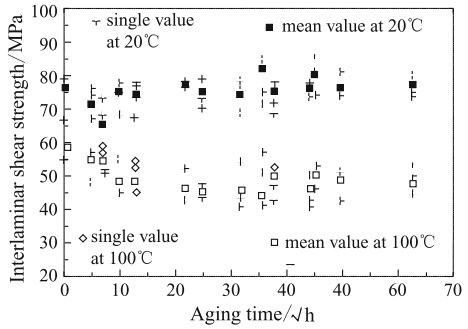


**Fig. 4.113** Change of interlaminar shear strength with moisture content for polymer matrix composite after 70–85% RH environmental aging at different temperatures

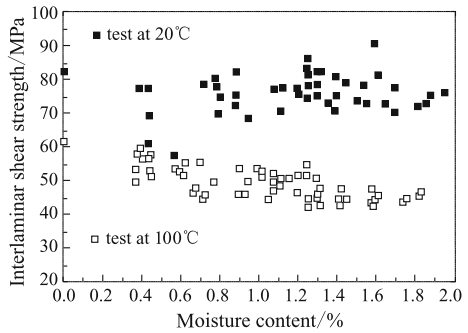


**Fig. 4.114** Change of interlaminar shear strength with aging time for BMI matrix composite after 70–85% RH environmental aging at different temperatures

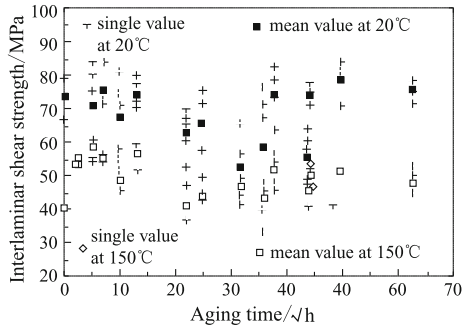
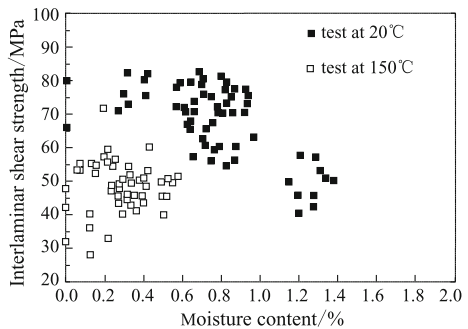


**Fig. 4.115** Change of interlaminar shear strength with moisture content for BMI matrix composite after 70–85% RH environmental aging at different temperatures



This may be explained by the reaction between the water and matrix requiring a certain time. Thus, controlling moisture content is a design criterion for application of MBI matrix composites in structures.

#### 4.10.4.3 Prediction of Composite Aging Effects

##### Physical Aging

When a polymeric matrix material is used below its glass transition temperature for a long time, the mechanical properties will change markedly. This change is termed physical aging. During the physical aging process, the material becomes stiffer, with decreased compliance and an increased modulus. The physical aging responses of resin matrix composites have received considerable research attention. The results of various investigations have shown that the matrix-dominated properties of continuous fiber-reinforced composite (e.g., the shear and transverse responses) are most seriously affected by physical aging in a similar manner to that of a pure polymer.

##### Physical Aging of Polymers

###### (1) Influence of aging time

The polymeric compliance varies with aging time according to:

$$\begin{aligned}
 S(t) &= S_0 e^{(t/t_e)^\beta} \\
 \tau(t_e) &= \tau(t_{\text{ref}})/a_{t_e} \\
 a_{t_e} &= \left(\frac{t_{\text{ref}}}{t_e}\right)^\mu \\
 \mu &= -\frac{d \lg a_{t_e}}{d \lg t_e}
 \end{aligned}
 \tag{4.117}$$

where

- $S(t)$  compliance at time  $t$ ;
- $S_0$  initial compliance;
- $t_e$  aging time;
- $\tau$  relaxation time;
- $T$  time;
- $t_{\text{ref}}$  reference aging time;
- $a_{t_e}$  aging time shift factor at aging time;
- $\beta$  shape parameter;
- $\mu$  shift rate.



Note from Eq. (4.117) that if the initial compliance  $S_0$ , shape parameter  $\beta$ , shift rate  $\mu$  and relaxation time  $\tau$  at reference aging time  $t_{\text{eref}}$  of the polymer are known, then the compliance at any time may be determined. If  $t_e > t_{\text{eref}}$ , then  $a_{t_e} < 1$ ; otherwise,  $a_{t_e} > 1$ . In the case of  $t_e > t_{\text{eref}}$ , the relaxation time at  $t_e$  is also greater than that at the reference aging time [ $\tau(t_e) > \tau(t_{\text{eref}})$ ]. This relation shows that at a given time the modulus of the material is higher and the compliance is lower [ $S(t; t_e) < S(t; t_{\text{eref}})$ ].

For most polymers, if the material is being used at temperatures close to its  $T_g$ , the material changes into an equilibrium state in a relative short time. The time required to achieve the equilibrium state is known as the equilibrium aging time.

The shift factor,  $\mu$  characterizes the influence of aging on material properties. For the same aging time a larger value of  $\mu$  indicates a smaller compliance change. Thus, the shift factor  $\mu$  can be used as a screening parameter for selection of materials. Materials with larger  $\mu$  values should be chosen. In general, experimental results have shown that before the aging equilibrium  $\mu \approx 1$  and after the aging equilibrium  $\mu \approx 0.1$ . These results indicate the dramatic change of materials in the aging equilibrium state. Thus, in the design stage of polymer matrix composite structures, materials with larger  $\mu$  value should be selected, while avoiding aging to an equilibrium state during the full life period, particularly in structures for use in high temperature applications.

## (2) Influence of aging temperature

Although the shift factor  $\mu$  over a large temperature range is constant, in fact, both  $\mu$  and  $a_{t_e}$  are functions of temperature. In general, the relationship of the time temperature-aging time shift factor can be expressed as:

$$\lg a = \lg a_{t_e} + \lg \bar{a}_T \quad (4.118)$$

where  $\bar{a}_T$  is a time temperature shift factor, i.e., a function of temperature and aging time at temperatures below  $T_g$ .

The relationship between  $\bar{a}_T$  and  $\mu(T)$  can be expressed as:

$$\frac{\bar{a}_{T_1/T_2}^{t_{e2}}}{\bar{a}_{T_1/T_2}^{t_{e1}}} = \left( \frac{t_{e2}}{t_{e1}} \right)^{\mu(T_2) - \mu(T_1)} \quad (4.119)$$

where  $\bar{a}_{T_1/T_2}^{t_{e1}}$ —time temperature shift factor between temperature  $T_1$  and  $T_2$  at aging time  $t_{e1}$ .

Thus, if the  $\mu(T)$  value or its expression and the time temperature shift factor at a single aging time are given, then  $\bar{a}_T$  at any aging time can be calculated. Therefore, the shift factor,  $\mu$ , and the time temperature shift factor,  $\bar{a}_T$ , have an effect on aging time.

### Aging Response of Unidirectional Laminate

The effective compliance matrix of a unidirectional laminate under plane stress condition can be described as:

$$[\bar{S}] = [T]^{-1}[S][T] \quad (4.120)$$

where

$[\bar{S}]$ —effective compliance matrix;

$[S]$ —compliance matrix with respect to the fiber coordinate system;

$[T]$ —transformation matrix.

The elastic stress–strain relation under in-plane loading is given by:

$$\begin{bmatrix} \varepsilon_{xx} \\ \varepsilon_{yy} \\ \varepsilon_{xy} \end{bmatrix} = [\bar{S}] \times \begin{bmatrix} \sigma_{xx} \\ \sigma_{yy} \\ \sigma_{xy} \end{bmatrix} \quad (4.121)$$

Experimental studies of polymer matrix composites have shown that the transverse compliance  $S_{22}$  and the shear compliance  $S_{66}$  are related to time temperature and subject to physical aging. Their values can be determined by Eq. (4.122), such that in a functional form:

$$\begin{aligned} S_{22}(t) &= f(S_{22}^0, \beta_{22}, \tau_{22}(t_{\text{ref}}), \mu_{22}, t) \\ S_{66}(t) &= f(S_{66}^0, \beta_{66}, \tau_{66}(t_{\text{ref}}), \mu_{66}, t) \end{aligned} \quad (4.122)$$

Note from Eq. (4.122), the transverse and shear compliance of composite unidirectional laminates are independently described by four viscoelastic parameters, namely the initial compliance, shape parameter, relaxation time at a given reference aging time, and shift factor. For any given material the four independent parameters may be determined by short-term aging tests in the laboratory.

Equation (4.121) is rewritten, accounting for time relativity as:

$$\begin{bmatrix} \varepsilon_{xx}(t) \\ \varepsilon_{yy}(t) \\ \varepsilon_{xy}(t) \end{bmatrix} = [\bar{S}(t)] \begin{bmatrix} \sigma_{xx} \\ \sigma_{yy} \\ \sigma_{xy} \end{bmatrix}, \quad (4.123)$$

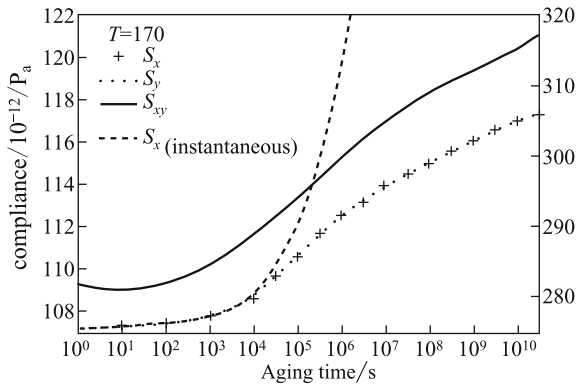
$$\bar{S}_{ij}(t) = f(\theta, S_{ij})$$

Investigations have shown that the compliance of  $0^\circ$ -ply laminates shows essentially no change with aging time, and that the response of other angle plies shows an increasing trend with angle. The compliance change is highest for  $90^\circ$ -ply laminates.

**Table 4.39** Viscoelastic parameters, transverse and shear compliance of IM7/8320 material system

Viscoelastic parameter	$S_{22}$	$S_{66}$
$\mu$	0.77	0.93
$\beta$	0.416	0.456
$\tau$	$1.19 \times 10^6$ s	$4.31 \times 10^5$ s
$S_0$	$750 \times 10^{-9}$ Pa <sup>-1</sup>	$1364 \times 10^9$ Pa <sup>-1</sup>
$t_{\text{eref}}$	$3.24 \times 10^4$ s	$3.24 \times 10^4$ s
Elastic parameters:	$S_{11} = 5.75 \times 10^{-91}$ /psi	$\nu_{12} = 0.348$

**Fig. 4.116** Predicted aging response of IM7/8320 system



Aging Response of Laminate

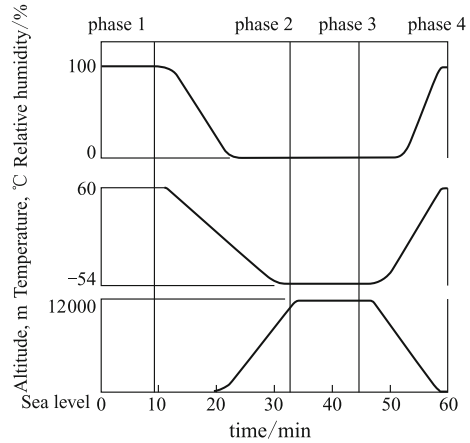
To determine the influence of physical aging on composite properties, first, the transverse and shear compliance in each lamina self-coordinate system under a specific aging environmental condition is determined. These values are transformed in the laminate coordinate system, and finally the laminate response is resolved by laminate theory.

The viscoelastic parameters, transverse and shear compliance of IM7/8320 composite lamina, are listed in Table 4.39. The estimated aging response for a quasi-isotropic laminate  $[0/\pm 45/90]_s$  IM7/8320 is illustrated in Fig. 4.116. The figure shows that although the quasi-isotropic laminate is fiber-dominated, the compliance changes by 8–10% over a 10-year aging period. This type of change must be considered in the composite structure design stage.

**4.10.4.4 Aging Test Results of Boeing Commercial Group**

The influence of environmental exposure on the performance of three composite material systems is experimentally investigated. More than 8000 standard specimens made from T300/5208, T300/5209, T300/934, machined according to the

**Fig. 4.117** Laboratory accelerated aging scheme of Boeing Commercial Group



required test methods, were exposed for approximately 13 years. The exposure tests included ground exposure, flight travel exposure, and accelerated laboratory aging, which simulated the change of temperature, humidity, and pressure during aircraft flight. The ground-based exposure tests were performed at Dallas, NASA Dryden, Honolulu, and Wellington. Aloha Airlines, Air New Zealand Ltd., and Southwest Airlines were selected for flight exposure studies. The laboratory accelerated aging results are shown in Fig. 4.117.

On the basis of global analysis of the test results, the following recommendations for composite structural design were proposed:

- ① The tension and flexure strength at room temperature after aging for the three materials showed a slight overall increase. At elevated temperatures, the results were mixed. For the T300/5209 and T300/934 systems the flexure and tension strength decreased slightly. For the T300/5208 system, both these properties were greater their baseline strength. The T300/934 tension strength also increased. However, in all cases, the differences were relatively small.
- ② Room-temperature compression strength dropped in general. At the end of 10 years' exposure, all three materials showed decreases of approximately 30%. The elevated temperature residual strength was likely seriously decreased; however, the exact test data could not be determined owing to the grab-tab failure.
- ③ The short-beam shear displayed a peculiar pattern for residual strength in both room and elevated temperature tests on all three material systems. The drop of the shear strength was largest after 1, 2, and 3 years of exposure; lesser degradation was found after 5 years exposure; however, the room-temperature residual strength increased slightly, and strength at elevated temperatures remained at or near their baseline levels after 10 years of exposure.

- ④ Accelerated laboratory aging can be useful for predicting the relative durability of composite materials. Accelerated aging over a 6-month aging period was sufficient to predict changes in the properties of all three materials systems.
- ⑤ Strength tests after aging at both room and elevated temperatures should be performed.

#### **4.10.4.5 Accelerated Hygrothermal Aging Scheme for Fighter Aircraft and Test Results**

In general, the designed life of fighter aircraft is 5000 flight hours, or 20–30 years. Complete simulation of both the mechanical and environmental loading history is the most credible evaluation; however, this would be impractical. Acceleration of the actual temperature/humidity time history can be used to obtain the accelerated hygrothermal aging results. Therefore, a large amount of comparable data can be accumulated and the development period for structures can be shortened and the test costs reduced. Furthermore, individual test results can be very easily interpreted and estimated.

In this section, based on the flight environment and service mission of aircraft in China, accelerated hygrothermal aging and test results for composite components of certain fighter aircraft are introduced.

##### **(1). Basis for Establishing Scheme**

On the basis of a typical mission profile, involving 5000 flight hours over 20 years, an accelerated aging program is developed.

##### **(2). Developing Requirements and Basic Rules**

- ① Accelerated tests should yield the same results for composite degradation and residual strength compared with that resulting from the real-time history, or give more conservative results than those from experiments.
- ② The actual aircraft usage environment should be reflected reasonably.
- ③ For accelerated aging, the response of thermal spiking caused by aerodynamic heating should be considered because an elevated temperature environment will have a considerable influence on composite properties over the long term.
- ④ The greatest test acceleration may be achieved by compressing the simulated ground standing time as much as possible. The ambient environmental exposure over 20 years may be simulated by accelerated tests over one year.
- ⑤ The selected accelerated conditions should not have any additional effects on composites. For BMI matrix systems, an accelerated temperature of 70 °C is appropriate.

### (3). Flight Temperature and Humidity Profiles and Their Simulation

In the accelerated spectrum, the temperature profile of composite structures subjected to high loads and sites that experience elevated temperatures should be considered. Elevated temperatures may approach the glass transition temperature of the resin. Elevated temperatures below the glass transition temperature will also diminish the ability of the resin matrix to support fibers against compression buckling and load transfer from fiber to fiber.

Testing should include low-temperature environments; however, these effects are smaller and may be neglected to reduce test time and cost.

The time of flight missions can be described by four stages, namely, ground running, climbing, cruising, gliding and landing. Representative extreme temperature and humidity profiles may be chosen for each of these stages. The detailed conditions are as follows:

- ① Slide running:  $M = 0.6$ ,  $T = 20\text{--}30\text{ }^{\circ}\text{C}$ ;  $M = 0.6\text{--}0.95$ ,  $T = 60\text{ }^{\circ}\text{C}$ ;  $M = 1.8$ ,  $T = 110\text{ }^{\circ}\text{C}$ ;  $M \geq 2.0$ ,  $T = 125\text{ }^{\circ}\text{C}$ ;
- ② On the ground:  $M < 0.6$ , environmental humidity is 95%;  $M = 0.6\text{--}0.8$  (flight altitude  $H = 0\text{--}5\text{ km}$ ), 50% RH;  $M = 0.8\text{--}1.8$  ( $H = 11\text{--}15\text{ km}$ ), 0% RH;
- ③ Change of air pressure can be neglected and pressure was not simulated in the accelerated aging scheme;
- ④ One symmetrical axis may be used to describe sliding/take-off/climbing/cruising/gliding/landing processes, as shown in Fig. 4.118.
- ⑤ The overall flight time should be determined based on Fig. 4.119. According to flight numbers the flight characteristics ( $M$  number, temperature, humidity) may be cycled at the same amplitude. This accelerated model closely replicates the situation of a real flight in terms of the elevated temperatures and the time of the temperature changes.
- ⑥ The test time may be shortened by acceleration for  $M = 0\text{--}0.6$ , as for the case of ground standing.

**Fig. 4.118** Symmetrical assumption

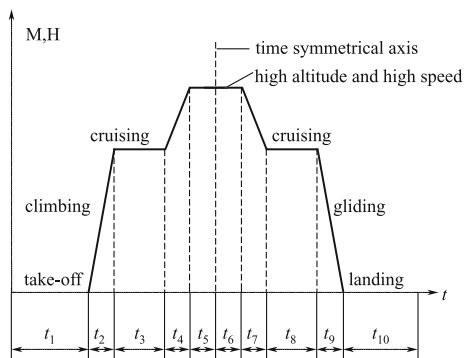
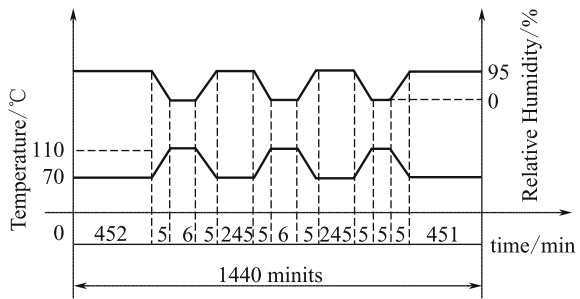


**Fig. 4.119** Accelerated hydrothermal scheme



#### (4). Accelerated Aging Methods for Aircraft at Rest on the Ground

It may be assumed that aircraft are exposed to open air on the ground, which should result in more conservative test results. The effects of ambient temperature, humidity, and solar radiation heating should be considered for outdoor standing conditions.

The airfield temperature and humidity from Guangzhou and Beijing airfield over half a year were adopted, respectively. Thus, conditions of 70 °C/95%RH were chosen for the accelerated testing environment. A ground standing time of one year was simulated by accelerated hydrothermal aging over 14 days.

#### (5). Developed Accelerated Hydrothermal Aging Testing Scheme

The flight life only accounts for about 3% of the total life of a fighter aircraft. In the accelerated testing the moisture recovery between flight intervals and maximum acceleration from rest on the ground are considered adequately. For climbing, high-speed cruising, and gliding, a real simulation may be adopted.

The developed accelerated testing scheme is illustrated in Tables 4.40 and 4.41 and Fig. 4.119. One cycle covers 1 day, and an accelerated laboratory aging of 268 days can be used to simulate the hydrothermal history of a fighter composite structure with a service life of 20 years and 5000 flight hours.

#### (6). Test Results

Tests of the mechanical properties of 312 specimens made from the HT3/QY8911 material system subjected to the hydrothermal aging testing procedures described above were performed. The tests included tension, compression, bend, shear, bond-joint, interlaminar tension–shear, single bolt-joint measurements for multi-laminates and tension, compression, bend, shear measurements for sandwich constructions.

The test results showed:

- (1) Tension strength after hydrothermal aging did not decrease, in fact a slight increase was found.
- (2) Compression strength after aging was markedly decreased.
- (3) Interlaminar shear strength after aging showed the most serious decrease.
- (4) Bearing strength of bolt joints after aging showed a large decrease of approximately 15%.

**Table 4.40** Accelerated hygrothermal aging spectrum

$t_i$	Temperature spectrum		Humidity spectrum		Remarks:
	Durative time/min	Temperature /°C	Durative time/min	Relative humidity /%(RH)	
$t_1$	452	70	450	95	① “2 + 5” represents humidity decrease from 95%RH to 50%RH within 2 min, then from 50%RH to 0% within 5 min. ② Highest temperature: +110 °C. ③ Lowest temperature: +70 °C ④ Maximum humidity: 95% RH ⑤ Minimum humidity: 0% RH ⑥ Rate of temperature increase/decrease: 8.0 °C/min
$T_2$	5	70–110	2 + 5	95–50–0	
$t_3$	6	110	6	0	
$t_4$	5	110–70	5	0–95	
$t_5$	245	70	243	95	
$t_6$	5	70–110	2 + 5	95–50–0	
$t_7$	6	110	6	0	
$t_8$	5	110–70	5	0–95	
$t_9$	245	70	243	95	
$t_{10}$	5	70–110	2 + 5	95–50–0	
$t_{11}$	5	110	5	0	
$t_{12}$	5	110–70	5	0–95	
$t_{13}$	451	70	451	95	

**Table 4.41** Accelerated hot–wet spectrum aging results of laminates and sandwich construction

Strength properties	Baseline value	Accelerated hot–wet spectrum aging
Compression/MPa	525.3	500.4
Tension/MPa	606.7	660.1
SBS/MPa	68.2	46.7
Interlaminar shear/MPa	4.3	13.3
Bearing/MPa	104.1	851.1
Flatwise tension/MPa	2.1	2.1
Core shear/MPa	1.1	1.0
Core shear modulus/MPa	39.6	38.7

- (5) Properties of the sandwich construction after aging were unchanged with the exception of the facing modulus.

#### 4.10.4.6 Accelerated Hygrothermal Aging Spectrum for Transport Airplane and Test Results

Aerodynamic heating effects can be neglected for investigations of hygrothermal aging response of composite structures used in transport airplanes. The accelerated aging spectrum may be developed based on the ground standing environment. A coastal tropical environment was simulated, and 80%RH adopted as the average humidity. The accelerated environment was 70 °C/100%RH (distilled water



immersion). On the basis of the acceleration principle, 1 year of the natural environment could be simulated by 28 days of in the accelerated environment. The effects of midday solar radiation in June, July, August, and September were considered. If the irradiation time each day is 2 h, and the irradiation temperature is 50 °C, and then the total irradiation time of each month is 60 h, or 240 h in 4 months. Therefore, 1 year of ambient environmental aging could be simulated using our accelerated testing method for 38 days. This scheme involved the following steps:

$$4 + \textcircled{1} + 4 + \textcircled{1} + 4 + \textcircled{2} + 4 + \textcircled{2} + 4 + \textcircled{2} + 4 + \textcircled{1} + 4 + \textcircled{1} \quad (4.124)$$

where

4—Immersion in 70 °C/100% RH (70 °C distilled water immersion) for 4 days;

• —50 °C heating for 1 day;

②—50 °C heating for 2 days.

For an aging duration of 3 years, the above spectrum may be repeated three times.

Ambient environmental aging for 1 and 3 years was performed at an environmental experiment field in Hainan Province in China. The corresponding accelerated aging was performed in a laboratory of the Aircraft Strength Research Institute. The test results are shown in Tables 4.42 and 4.43. The test results indicated:

- ① Ambient aging has no measurable influence on tensile and compressive strength.
- ② Ambient aging has a large influence on short-beam shear (SBS) strength. The SBS strength after 1 and 3 years of ambient aging decreased by 26.5% and 37.0%, respectively. The shear strength of single- and double-lag bonds after 1 and 3 years of ambient aging decreased by 45.1% and 12.7%, and 51% and 30.2%, respectively. The tension–shear strength after 1 and 3 years of ambient aging decreased by 9.8% and 30.2%, respectively.

**Table 4.42** Ambient aging and accelerated laboratory aging results of laminates

Strength properties	Baseline value	1 year ambient aging	3 years ambient aging (unpainted)	3 years ambient aging (painted)	1 year accelerated aging	3 years accelerated aging
Compression/MPa	525.3	533.3	659.7	695.6		482.8
Tension/MPa	606.7		662.4	682.6		
SBS/MPa	68.2	50.1	43.0		65.9	55.1
Bonded I/MPa	37.7	20.7	18.5			
Bonded II/MPa		32.9	26.3			
Tension–shear/MPa	4.3	12.9	11.8			

**Table 4.43** Ambient aging and accelerated laboratory aging results of sandwich construction

Strength properties	Baseline value	1 year ambient aging	3 years ambient aging (unpainted)	3 years ambient aging (painted)	1 year accelerated aging	3 years accelerated aging
Flatwise compression ( $H = 19$ )/MPa	3.62	3.49	2.96			
Flatwise compression ( $H = 44$ )/MPa	2.88	3.03	2.97			
Core shear ( $H = 19$ )/MPa	1.21	1.23	0.77	0.76		
Core shear ( $H = 44$ )/MPa	1.11	1.04	1.03	1.06		
Core shear modulus ( $H = 19$ )/MPa	39.2	33.7	45.0	44.4		

- ③ Ambient aging had little influence on the properties of the sandwich construction. The residual strength after accelerated ambient aging was higher than that of ambient aging. This indicates that the above-mentioned accelerated ambient aging scheme is less conservative than ambient conditions. It is recommended that to simulate the aging effects of 1 year, the testing method described in this section may be repeated 2 or 3 times.

#### 4.10.5 *Protection of Composite Structures in Corrosive Environments*

Aircraft composite structures in service may encounter a range of environmental conditions, including temperature, humidity, rain and snow, sun light, lightning strikes, wind borne sand, dust, salt-fog, noise, and industrial pollution. These conditions may degrade composite structures [1, 2, 13].

This process may be considered to be a corrosive process. However, there are no satisfactory explanations of the corrosive mechanisms of composites because of their complexity. The relationship between corrosion–strength–time is difficult to predict. In service, aircraft structures may be affected by the exterior environments, and interior fuel, hydraulic fluid, refrigerants, and sealants. Acidic and alkali substances may be introduced in fabrication and service processes. Furthermore, composites are considered to be high electrode potential materials; thus, in connection with a low electrode potential materials galvanic erosion may occur. Corresponding protection methodologies should be considered during the

composite structure design. These protective measured should also be tested to ensure the integrity of the composite structure.

**4.10.5.1 Control of Corrosion in Composites**

**(1) Corrosive Effects of Environment on the Constituents of Composites**

The following effects may occur to constituents of composites exposed to corrosive environments: corrosion of the resin matrix, reinforced fiber, interface, and corrosive fatigue. The chemical erosion behaviors of general thermoset resins are given in Table 4.44. Epoxy resin matrices used for aircraft structures appear to have good corrosion resistance against acid and alkali.

**(2) Influence of Environmental Media on Mechanical Performance of Composites**

The influence of hygrothermal aging on composite performance have been discussed in detail in 4.10.4. On the basis of experiments and usage experiences, the influences of other corrosive agents in the aging environment can be summarized as follows:

- ① Composites are not susceptible to corrosive liquids, such as interior fuel, hydraulic fluid, and antifreeze. Hence, the influence of these liquids can be neglected.
- ② Damage caused by ultraviolet radiation is a slow cumulate process. This type damage can be neglected if the protective coating of the structural surface is in good condition. If the surface coating brushes off, a new layer of coating should be applied to the surface. The most feasible method is to spray paint an acrylate paint. If a varnish is adopted an appropriate ultraviolet absorber should be applied. Light colored paints are more effective. If no protecting coat is applied, ultraviolet radiation

**Table 4.44** Anti-chemical erosion behaviors of typical thermoset resins

Medium	Phenol ether	Polyester	Epoxy (amine cure)	Epoxy (acid anhydride cure)
Thin acid	Slight corroded	Slight corroded	Uncorroded	Uncorroded
Strong acid	Eroded	Eroded	Eroded	Slight corroded
Thin alkali	Slight corroded	Slight corroded	Uncorroded	Slight corroded
Strong alkali	Decomposed	Decomposed	Slight corroded	Eroded
Solvent	Decomposed by some solvent	Eroded	Anti-erosion	Anti-erosion

might have an effect on laminate performance. The effects of ultraviolet radiation on the modulus of unidirectional laminate have been investigated by MBB Company.

The results showed that under 12260–40866 equivalent hours of solar irradiation the specimen tensile stiffness dropped approximately 6–10% (see Fig. 4.120), under 17,800 and 22,800 equivalent hours' sun irradiation the bending modulus dropped 12.5% and 28.0%, respectively (see Fig. 4.121).

- ③ Damage caused by wind, sand, and rain erosion is a slow cumulative process. This type of damage can be prevented provided that an anti-rain erosion protective paint is sprayed on structural surfaces. If the surface coat brushes off, applying a new layer of the coat to surface will give sufficient protection. The mechanism of rain erosion and respective anti-rain erosion measures has been widely investigated. It has been shown that the pressure impulse and fluid of rainwater impacts are physical factors of rain erosion. The main factors influencing rain erosion are the angle of incidence of the raindrop and raindrop parameters,

**Fig. 4.120** Effects of ultraviolet radiation on tensile stiffness of unidirectional laminate

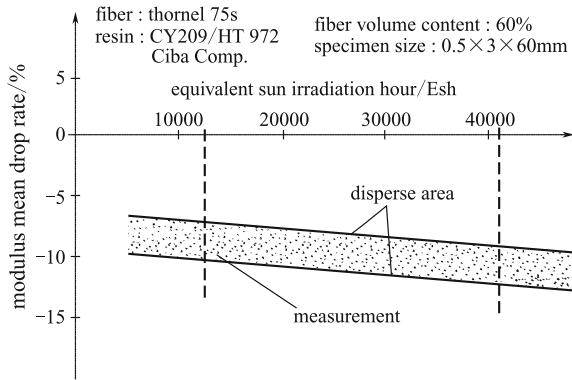
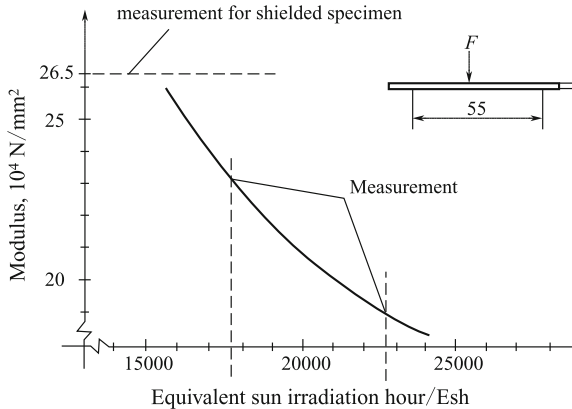


**Fig. 4.121** Effects of ultraviolet radiation on flexural modulus of unidirectional laminate



such as its size and velocity. When the angle of incidence of a raindrop is  $90^\circ$  and the raindrop velocity is more than 200 m/s an anti-rain erosion protective coat should be applied to the surface of the composite structure. At the design stage, the layout of components should attempt to minimize the area of impacted surfaces and lower the angle of rain drop incidence in addition to protective coatings. Anti-erosion paint and metal or ceramic protective coatings may be adopted as anti-rain water erosion measures.

### (3) Corrosive Control

There are two main principles for controlling composite corrosion caused by environmental media.

- (1) Enhance innate material corrosion resistance: In some cases it is possible to improve the crystallinity, tropism grade, or crosslinking density of composites. The matrix compactness can also be enhanced to reduce the diffusion coefficient and penetrative coefficient of the medium. A surface cleanup solvent may be used to enforce the adherence strength between the reinforced fiber and matrix, reduce the interface clearance, and enhance impermeability.
- 2) Use of protective coatings: A protecting coat is sprayed on the composite surface to avoid direct corrosion of the composite by environmental media.

### (4) Biological Corrosion and its Control

Biological corrosion occurs mainly at the fuel box position of aircraft structures. The combination of moisture and other impurities in fuel can provide appropriate conditions for biological organisms to grow. The main microorganisms that might affect composites are germs, epiphyte, and mildew. Such microorganisms may reproduce and excrete acidic substances, such as lactic acid and grass fungus. These acidic substances might react with composites. Biological corrosion of composite structures used in a sea environment can pose a threat. Composite destruction caused by oceanic organisms can occur. The composite might be bitten away by hexapods and chisel-ship worms, and the above-mentioned microbe encroachment can become more serious. The following steps should be taken to control biological corrosion:

- ① Fuel quality should be controlled. The content of moisture and impurities in fuel and possible pollution during the fuel transport process should be minimized to remove the conditions necessary for microbial growth.
- ② An effective drainage system should be designed in the fuel tank. A fluent-fuel mouth should be installed at the lowermost position and water should be drained at intervals.
- ③ Anti-bioerosion protective coatings may be applied. A coating in common use is SF-9 epoxy, which can effectively prevent biological growth.

- ④ Additives made be added to fuel. Typical additives include: chromic acid, strontium glycol ether and organic borides. These additives can kill microorganisms and effectively limit bioerosion.

#### 4.10.5.2 Galvanic Erosion Between Composites and Metals

When two types of materials with different electrode potentials are directly connected or in contacted through an electrolyte, accelerated corrosion might be caused in the lower potential material. This is known as galvanic or electrical dipolar erosion. Carbon has good electrical conductivity and a relatively high electrode potential. Carbon fiber-reinforced composites under general environmental conditions show inert behavior similar to that of noble metals with high electrode potentials. Thus, when carbon fiber-reinforced composites are joined with metal the cathode-like behavior could accelerate corrosion of the metal. The electrode potential difference between carbon fiber-reinforced composite and most metals is 0.5–1.0 V, and in some cases, may reach as high as 1–2 V. Therefore, anti-electrical dipolar erosion steps must be adopted in areas of connected metals and composites. The generation of electrical dipolar erosion requires three conditions: an electrode potential difference, electrolyte, and an electrical conductive connection. Protective measures against galvanic erosion should consider these three aspects.

##### (1) Structural Design

The accumulation of electrolyte can be prevented to a large extent by careful structural design to avoid formation of corrosion batteries.

- ① Attention should be paid to structural seals, to avoid infiltration of rainwater, fog, and seawater. Holes and places where contamination may accumulate should be reduced. Countermeasures should be mounted at positions subject to seepage.
- ② Small metallic elements surrounded by a large area of composite should be avoided. Strict protecting steps should be adopted for mechanical fastener joints.
- ③ The lumen and blind holes should be designed with perforation to prevent condensation water cohesion.

##### (2) Selection of Materials

Consistent materials should be selected to prevent galvanic erosion.

- ① Anticorrosive materials and materials with a low potential difference compared with that of the composite should be chosen. Pay special attention to small parts such as fasteners.
- ② Insulated and closed down materials should be non-hygroscopic and should not contain any corrosive components. When a single layer of

co-cured glass-cloth on a surface is used as an insulating coat, the edge must be sealed. Otherwise, counterproductive effects may be caused.

### (3) Protective Methodologies

Effective protective measures must be adopted for metals, which show corrosion in direct contact with composites and the contact is otherwise unavoidable.

- ① An appropriate overlay coating for the metal or a non-metal may be used as a transition layer or adjustment. For example, anodization, chemical oxygenation, passivation, and phosphorization are commonly used treatments. The contact resistance is increased and the electrical dipolar erosion can be reduced providing that the covering coat is perfect. Selection principles for the thickness of an over coat and its applicable range can be found in the standard HB5033.
- ② Efforts to insulate the component should be made; however, steps to reduce the electrode area should also be taken through the use of appropriate coatings on the surfaces. Protective coats should be applied to both the metal and composite to avoid forming large cathode and small anode areas in case electrolyte in-leakage occurs via microholes or local damage of the protecting coats. Furthermore, the protective coats should be resistant to alkali because alkaline substances are generated at the cathode by electrical dipolar erosion.
- ③ Gaskets, cannula, and adhesive tapes made from inert materials should be used between metals and composites to form an insulated coating.
- ④ Appropriate hermetic sealing materials should be used to form gapless seals that insulate against electrolyte formation. Such sealants are effective at slowing corrosion.

### (4). Protection of Metals Against Galvanic Erosion of Carbon Fiber-Reinforced Composite

- ① The composite should not be connected with magnesium or magnesium alloy.
- ② Aluminum and its alloys should be treated as follows: The metal may be placed in a recycling hot water or chromate solution after an anodization process. Typical coatings include chromate +H06-2 zinc yellow epoxy resin priming and chromate +SF-9 for fuel tank dope (used interior of fuel tank).
- ③ Steel and low-carbon steel should be treated by any of the following: coating by galvanization and H06-2 zinc yellow epoxy resin priming; phosphorized and coated with X04-1 acetal phosphoric paint and X04-1 varnish (oil proof); phosphorized and coated with H06-2 iron red epoxy resin priming and X04-2 epoxy nitril magnetism paint (available in various colors); phosphorized and two-layer zinc yellow epoxy resin priming (add  $FLU_{1-4}$  aluminum powder) and H61-2 steel gray organic silicon epoxy polyamide magnetism paint applied.

- ④ Stainless steel should be treated as follows: The unmodified surface may be used or one of the passivation process described above.
- ⑤ Titanium alloy should be treated as follows: The unmodified surface may be used; an anodized process; souring or sand blasting and H06-2 zinc yellow epoxy resin priming and 13-2 propenoic acid polyurethane magnetism paint; souring or sand blasting and F06-9 zinc yellow phenolic priming and 13-2 propenoic acid polyurethane magnetism paint.

The above-mentioned methodologies may be selected based on the service environment and structural conditions. Under poor environmental condition metals should also be sealed, with sealants such as XM 22, XM 23, XM30, and XM 34.

#### **4.10.5.3 Protective Coatings for Composites**

Protective coatings for composite components can not only improve the appearance of faces but are also important for slowing moisture absorption and aging processes of the material. The application of an anti-friction dope on the front structural features can improve resistance to sand and rain erosion. Application of anti-friction dope on interior surfaces can prevent direct contact of composites with metal and avoid electrical dipolar erosion.

##### **(1) Cover Coatings and their Effects**

Different cover coat materials are used at different positions and fall mainly into the following types:

- ① For interior surfaces and end faces a protective coat formed by priming should be applied.
- ② For general exterior surfaces with ornamental protective coatings, priming, sealants, transition priming, and surface paint may be applied.
- ③ For front structural features, an anti-friction and antiscouring protective coating system formed by priming, an elastic anti-friction dope, and surface paint should be applied.
- ④ For upright surfaces or other surfaces requiring anti-static protection, anti-static protective coatings system formed by priming, and anti-static or elastic anti-static dopes should be applied.
- ⑤ For the interior surfaces of the fuel tank an anti-static protective coat system formed by priming, and anti-static and oil proof dopes should be applied.
- ⑥ For exterior surfaces of the fuel tank, an electrical protective coating system formed by priming, an electrical layer, and painting of the surfaces should be applied.

##### **(2) Surface Dopes and Coating Systems**

Currently, the most widely used dopes are epoxy- and polyurethane-based. Epoxy dopes are strongly adherent, show low contraction, and good toughness.



Epoxy dopes are versatile and can be applied with many types of surface paint. However, because this dope has poor gloss retention after film formation and it is prone to pulverization, it is mainly applied in priming coats.

A large variety of polyurethane dopes are available, which shows excellent performance, strong adherence, and high rigidity. Polyurethane dopes form bright films with excellent oil and moisture proofing, heat endurance, and wear and chemical resistance. Therefore, these dopes are widely applied in the aviation industry.

Dopes and coating systems in common use for aircraft composite structures are shown in Tables 4.45 and 4.46.

#### ***4.10.6 Relationships Between Atmospheric Aging, Accelerated Atmosphere Aging, and Hygrothermal Aging and Recommendations***

The relationships between three different types of aging methods are investigated to determine an optimal method for studying aging response. It is important for the method to not only reflect the real history of an aircraft but also to be convenient and simple. On the basis of real investigations, the following recommendations are given.

- ① For the composite structures of military aircraft, the accelerated testing scheme shown in Fig. 4.119 may be considered to be a standard accelerated hygrothermal scheme. An actual history of 5000 flight hours and 20-year service life can be simulated in approximately 1 year. The highest temperature of thermal spiking can be determined based on the type of fighter plane ( $M = 2.0$ ,  $T = 110$  °C;  $M = 2.2$ ,  $T = 125$  °C).
- ② In general, the compression, interlaminar shear and compression after impact strength are sensitive to hygrothermal aging. Thus, the aforementioned properties must be tested for all material selected during the structural design phase.  
In particular, the residual strength should be tested at the operating temperatures.
- ③ Hygrothermal aging has an influence on the facing properties of sandwich constructions, but it has no obvious influence on other properties providing that the facing is undamaged and sealed.
- ④ Ultraviolet radiation and rain erosion have no obvious effects on composite properties providing that a protective coating is maintained.
- ⑤ Cryogenic temperatures and changes of air pressure have little effect on the properties of composites and may be neglected to reduce the test costs.

Table 4.45 Paint and coatings commonly used for composites

Number	Title	Sign Standard	Main constituent	Elasticity /mm	Impact /N·cm	Grade of adherent force	Properties	Dry criterion	
								77°C	t/h
1	Epoxy polyamide varnish	H01-101H Q/6s72-80	E-20 epoxy and polyamide resin	1	490	1	Paint film tenacity, good adhesiveness with composites, liquid proof, waterproof, low air permeability	18-25 50-60 110-120	24-26 6-8 1-2
2	Epoxy polyamide priming	H01-102H Q/6s455-85	E-20 epoxy and polyamide resin, strontium yellow	1	490	1	Liquid proof, matches with many other surface paints, high interlaminar adhesion force, good adaptability	18-25 50-60 110-120	24-26 6-8 1-2
3	Polyurethane surface paint	13-2	Acrylic resin, HOI, paint, padding	1	490	1	Good adhesiveness, waterproof, hygrothermal resistance, excellent resistance to radiation and weatherability	18-25 50-60 110-120	24-26 6-8 1-2
4	Elastic polyurethane magnetism paint	HTY/B-80-15(1)	TDI mixed polyamine prepolymer, MOCA curing agent, paint padding	1	490	180° peel off ≥ 39.2 N/cm	Paint film tenacity and good elastic behavior, good wear, rain, and scouring resistance, good adhesiveness to priming	18-25 50-60	24-26 8-12

(continued)

Table 4.45 (continued)

Number	Title	Sign Standard	Main constituent	Elasticity /mm	Impact /N-cm	Grade of adherent force	Properties	Dry criterion	
								77°C	t/h
5	Epoxy polyamide sealant	Q/6sz358-83	Epoxy polyamide varnish, talcum powder				Good adhesiveness to fundus varnish and transition priming, easily scraped, easily polished, low contraction	18-25 50-60	36-48 6-8
6	Thinner	X-7 X-10	Xylene, positive butyl alcohol, butyl-resin, cyclohexanone				Use to dilute epoxy type paints Use to dilute polyurethane type paints		
7	Epoxy black polysulfide electric dope	HL04-1019 H.D Q/6s530-90	Epoxy resin, Thiokol, electriccarbon black	1	490	1	Good electrical properties (0.5-15 MΩ/m), oil proof, good adhesiveness to sealant, apply as a thin glue in the interior surface of the fuel tank	70	24
8	Epoxy polyamide electric dope	H06-1020 H.D Q/6s530-90	Epoxy and polyamideresin, ST-3 electric powder	1	490	1	Good electric properties (0.5-15 MΩ/m), oil proof, apply to the bottom priming in the interior surface of the fuel tank	90 - 100 100- 120	4 2

**Table 4.46** Dopes in common use for composites

Number	Coating system	Dry criterion		Coat thickness		Coating property	Location of use
		T/°C	t/h	Monolayer /μm	Total/μm		
1	First or second epoxy polyamide varnish (lower varnish)	18–50–110–120	24–36–6–8–1–2	First 15–20 Second 25–35	15–20 25–35	Low air permeability, good adhesiveness, and waterproof as a sealant	Interior and exterior surfaces, end faces and walls of holes
2	First epoxy polyamide varnish	18–25	24–36	First 15–20	80–100 100–120	Good interlaminar adhesion force, waterproof, hydrothermal proof	Exterior surfaces of components
	Smearred locally polyamide sealant	18–25 50–60	24–36 6–8				
	First polyamide priming (filtration priming)	18–25 50–60	24–36 6–8	15–20			
	Second polyurethane surface paint	18–25 50–60	36–48 6–8	50–60			
3	First epoxy polyamide varnish	18–25	24–36	15–20	240–260	Good interlaminar adhesiveness, excellent wearability, anti-scourability; Facing- paint is hydrothermal proof and has good weatherability	Front facing surfaces and those requiring anti-friction coatings
	Eight elastic polyurethane magnetism paint	18–25 50–60	24–36 8–12	180–200			
	Second polyurethane surface paint	18–25 50–60	36–48 6–8	40–50			
4	Epoxy polyamide varnish, epoxy polysulfide electric dope	18–25 50–60 70	18–25 6–8 24	15–20 50–60	80–100	Good electrical properties, oil proof, and good interlaminar adhesion force	Fuel tank, up panels and other position requiring oil proofing
5	Epoxy polyamide varnish, epoxy polyamide electric dope, XM-electric thin glue, epoxy black polysulfide electric dope	18–25 50–60 70 70 70	24–36 6–8 24 24 24	25–30 40–50 50–60	200–400	Good electrical properties, oil proof, and good interlaminar adhesion force	Fuel tank, erect gaps, horizontal gaps, down panels and edges

## 4.11 Impact Damage Tolerance Reliability of Composite Structures

### 4.11.1 Introduction of Structural Reliability Design and Analysis

#### 4.11.1.1 General

Composite materials are widely used in modern structures for their high performance and reliability. However, because these structures usually operate in hostile and variable service environments, it is difficult to predict their structural performance. In addition, experiments show that composite structural behavior exhibits a wide scatter as a result of the inherent uncertainties in design variables.

Design variables, known as primitive variables, include: the fiber and matrix material properties at the constituent level; fiber and void volume ratios; ply misalignment and ply thickness; the fabrication process; size of random structures; boundary conditions; loadings; and the operating environment.

The full range of structural behavior cannot be computationally simulated by traditional deterministic methods, which use a safety factor to account for uncertain structural behavior. Thus, the true structural reliability cannot be discerned. A probabilistic design methodology is needed to accurately determine the structural reliability of composite structures.

For the purposes of structural reliability analysis, it is necessary to distinguish between at least three types of uncertainty: physical uncertainty, statistical uncertainty, and model uncertainty.

#### 4.11.1.2 Reliability Function

The probability of failure  $F(t)$

$$F(t) = P\{T \leq t\} \quad (4.125)$$

The probability density function  $f(t)$

$$f(t) = \frac{dF(t)}{dt} \quad (4.126)$$

The reliability function  $R(t)$ , which is the probability that the system will still be operational at time  $t$  is given by

$$R(t) = P\{T > t\} = 1 - F(t) \quad (4.127)$$

### 4.11.1.3 Structural Reliability

According to Chinese standard GB/T 3187 (Reliability and maintainability terms), the reliability of a structure is its ability to fulfill its design purpose for some specified time.

## 4.11.2 Types of In-Service Damage

To analyze the rate of occurrence of in-service damage to composite structures, potential mechanical impact and types of in-service damage should be categorized. Depending on the projectile speed ( $V$ ), mechanical impacts causing damage in composites may be subdivided into low-speed ( $V < 6\text{--}8$  m/s) and mid-speed ( $V < 30\text{--}200$  m/s) phenomena.

Unlike metals, where impacts may be absorbed by plastic deformation, polymer composites fail as brittle materials. Therefore, low- and mid-speed impacts cause damage to a composite skin which may be categorized as follows:

- ① Surface damage, scratches, and fracture notches. Such damage has a negligible effect on the load-bearing capabilities of a structure and may be neglected in analyses.
- ② Delamination followed by matrix cracking and fiber failure. This damage occurs inside the composite layer. The external skin surface may feature indentation. Delamination may be categorized as: internal delamination, visually undetectable at both skin surfaces, which may be followed by matrix cracking at the face opposite to the impacted surface; delamination visually detectable at the external skin surface, with respect to the impact surface.
- ③ Through damage cracks and punctures. In this case, the damaged area will feature failure of layers through the thickness of the composite. Through damage may be characterized as either clean holes or other damaged material. Puncture edges usually show delamination and cracking.

Damage types 2 and 3 may considerably reduce the load-bearing capability of a structure and must be accounted for in analyses.

### 4.11.3 Random Variables

Variables that need to be considered in the stiffness reduction model can be classified into three categories:

- ① Material parameters, which include strength of the undamaged laminate, fracture toughness of the material system, laminate thickness, and laminate layer pattern.
- ② Structural parameters, which include boundary conditions and sub-structural configurations.
- ③ Impact threat parameters, which include impact energy and impactor size. The model assumes that the severity of stiffness reduction, for a given material system and impact condition, depend on the impact energy.

In considering the structural integrity of a structural component containing damage, potential random variables should be accounted for including the number of damage sites, damage size, time to detection/repair of damage, load, and strength properties. The effectiveness of inspections is another potential random variable. The effectiveness of an inspection can be characterized by the probability of damage detection distribution. In total, nine random variables are considered:

- ① Number of damages sites per life, for each type of damage;
- ② Time of damage initiation;
- ③ Damage size, for each type of damage;
- ④ Time from damage initiation to repair, i.e., a random function of damage size and damage initiation;
- ⑤ Initial failure load, for each load case;
- ⑥ Residual strength of damaged structure for each type of damage and each load case;
- ⑦ Failure load of repaired structure, for each type of damage;
- ⑧ Structural load for each load case;
- ⑨ Structural temperatures at the sites when maximum external loads occur.

#### ***4.11.4 Impact Threat Distribution***

At the beginning of advanced certification methodology for composite structures, no detailed data existed on the actual impact threat encountered by in-service composite structures. Consequently, some scenarios for impact threat distributions were developed. The impact threat scenarios clearly depend on the location of the structure and its structural configuration. To establish realistic impact damage requirements, a structural zoning procedure is used to categorize the structure. On the basis of available data, the impact threat can be tentatively divided into three levels — high, medium, and low. The probabilistic distributions of these impact threats are discussed below [3, 47–52].

To quantify the different levels of impact threat, it is assumed that the probability of a structure being exposed to a given impact can be described by a two-parameter Weibull distribution in terms of the impact energy. Instead of expressing the

distribution by the usual scale ( $\beta$ ) and shape ( $\alpha$ ) parameters, the threat is characterized by two impact energy levels. These are the model energy level associated with a high possibility of occurrence ( $X_m$ ), and the high energy level associated with a low probability of occurrence ( $X_p$ ). The relationships between the energy parameters and the Weibull scale and shape parameters can be expressed by the following two equations.

$$X_m = \left(\frac{\alpha - 1}{\alpha}\right)^{1/\alpha} \beta \tag{4.128}$$

and

$$X_p = \beta[-\ln(P)]^{1/\alpha} \tag{4.129}$$

where  $P$  is the probability of occurrence of the impact energy  $P(X > X_p)$ .

Combining Eqs. (4.128) and (4.129) gives:

$$\frac{X_m}{X_p} = \left[\frac{\alpha - 1}{-\alpha \ln(P)}\right]^{1/\alpha} \tag{4.130}$$

Equation (4.130) is solved for  $\alpha$  by iteration and  $\beta$  is then obtained from Eq. (4.128). The Weibull distribution for the impact threat to a structure is then defined from the obtained values of  $\alpha$  and  $\beta$ .

The three scenarios of impact threats, denoted as high, medium and low, are defined as shown in Table 4.47. The high threat distribution is considered to be a conservative estimate of the impact threat to a structure. The medium threat is a more realistic estimate of the impact damage threat for composite structures. The table shows the computed Weibull parameters corresponding to these threats. Figure 4.122 shows that all three assumed threat scenarios are conservative compared with the MCAIR in-service survey results.

**Table 4.47** Impact threat scenarios

	High threat	Medium threat	Low threat	MCAIR Data fitting
Modal energy $X_m(\times 1.36 \text{ J})$	15	6	4	1
$X_p(\times 1.36 \text{ J})$	100	100	100	35
$P(X > X_p)$	0.1	0.01	0.0001	0.00005
$\alpha$	1.264	1.192	1.221	1.177
$\beta$	57.7	27.8	16.2	4.992



### 4.11.5 Cases and Solution Steps

In this section, four cases will be introduced as follows:

(1) **Case one**

Calculate the structure reliability  $R$  at a given applied stress and impact energy as shown in Fig. 4.123.

(2) **Case two**

Establish the relation between the reliability  $R$  and impact energy  $E$  as shown in Fig. 4.124.

(3) **Case three**

Calculate the cumulative damage tolerance strength reliability  $\bar{R}$  at a given stress and impact threat as shown in Fig. 4.125.

(4) **Case Four**

Establish the relationship between stress and cumulative damage tolerance strength reliability as shown in Fig. 4.126.

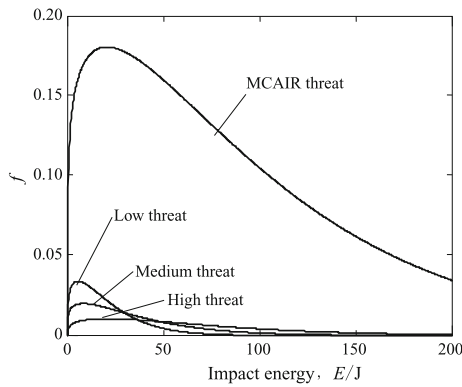


**Fig. 4.122** Impact threat distributions

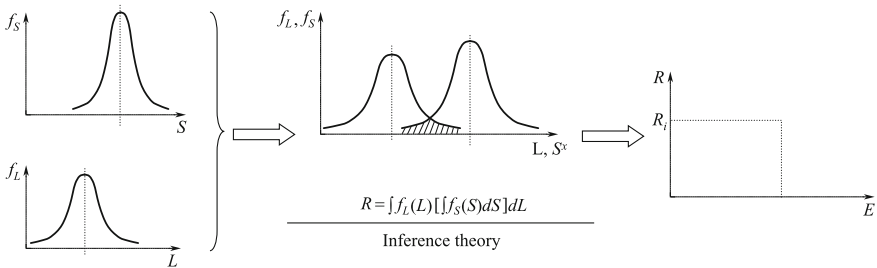


**Fig. 4.123** Inference theory

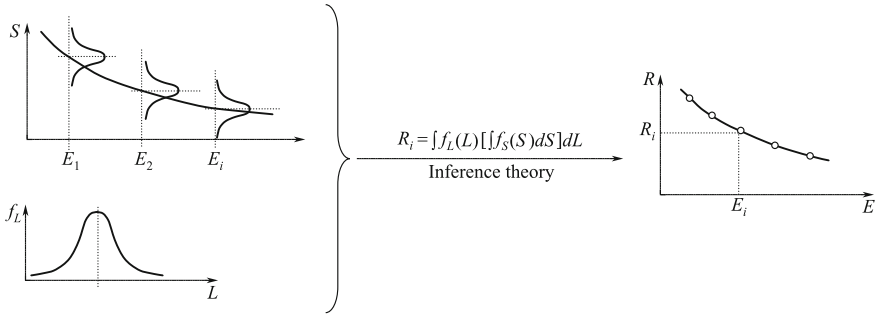


**Fig. 4.124** Relation between the reliability  $R$  and impact energy  $E$

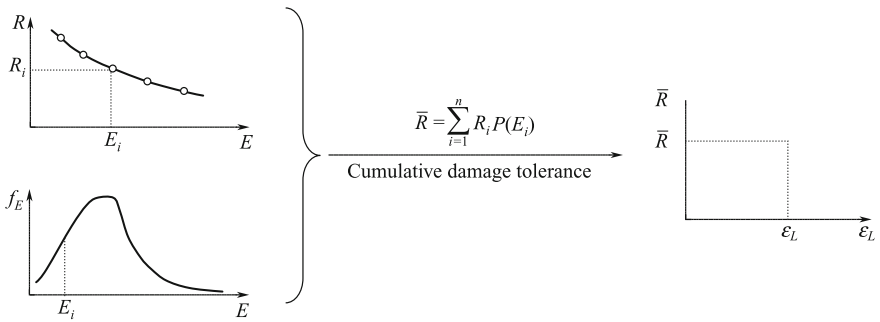


**Fig. 4.125** Cumulative damage tolerance strength reliability  $\bar{R}$

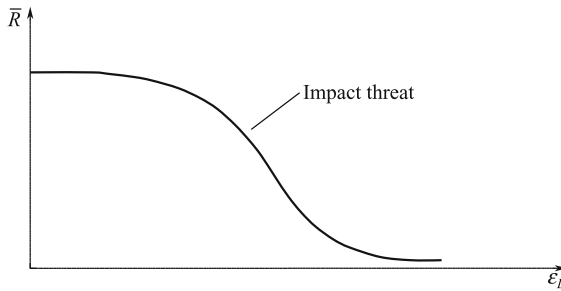


**Fig. 4.126** Relation between Stress and Cumulative Damage Tolerance Strength Reliability

(In the Chapter, 4.1–4.6 and 4.9 were translated by Jianmao Tang; 4.7 was translated by Jiahui Xie.)

(4.1–4.6 and 4.9 were translated by Jianmao Tang, 4.7 was translated by Jiahui Xie.)

## References

1. Shen Z (1995) design guideline of durability/damage tolerance for composite aircraft structures. Aviation Industry Publisher, Beijing
2. Shen Z (2001) Design Handbook for Composite Structures. Aviation Industry Publisher, Beijing
3. U.S. Department of Defense (2002) MIL-HDBK-17F. Composite material handbook, vol 3. Polymer matrix composites materials usage, design, and analysis
4. Briston JW (1986) Airworthiness of composite structures—some experiences from civil certification. In: Proceedings of the 2nd international conference on fiber reinforced composites
5. Soderquist JR (1987) Design/certification considerations in civil composite aircraft structure. SAE 871846
6. Brandecker B, Hilgert RS (1988) A320 full scale structural testing for fatigue and damage tolerance certification of metallic and composite structure. In: Proceedings of the 16th ICAS
7. Shen Z (1988) The design allowables of composite aircraft structures and their determination principle. *Acta Aeronautica Et Astronautica Sinica* 19(4):385–392
8. Jones RM (1981) (trans: Zhu YL) Mechanics of composite materials. Science and Technology of Shanghai Publisher, Shanghai
9. Zhou L, Fan FQ (1991) Mechanics of composite materials. Higher Education Press, Beijing
10. Zhu YL (1979) Review on mechanical properties of advanced composites. glass-fiber reinforced plastics. GFRP Structures Research Institute of Shanghai
11. Yang NB, Zhang YN (2002) Composite aircraft structure design. Aviation Industry Publisher, Beijing
12. Jiang YQ, Lu FS, Gu ZS (1990) Mechanics of composite materials. Xi'an Jiaotong University Press, Xi'an
13. Chen SJ (1990) Design handbook of composite materials. Aviation Industry Publisher, Beijing
14. Tong XX (2002) Guideline of stability analysis for composite structures. Aviation Industry Press, Beijing
15. Niu MC (1992) Composite aircraft structures. Cinmilit Press Ltd, Hong Kong
16. Zhu JF, Wang H (1996). Analysis code of post-buckling strength and failure for composite stiffened panel and shell structures (COMPOSS). *Comput Struct Mech Its Appl* 13(4)
17. Xie MJ (1995) Handbook for composite joints. Aviation Industry Press, Beijing
18. ASM International Handbook Committee (1987) Engineered materials handbook, vol 1. Composites
19. Hart-Smith LJ (1973) Adhesive bonded single lap joints. NASA CR-112236
20. Hart-Smith LJ (1973) Adhesive bonded double lap joints. NASA-CR-112235
21. Hart-Smith LJ (1973) Adhesive bonded scarf and stepped lap joints. NASA CR-112237
22. Hart-Smith LJ (1982) Design methodology for bonded-bolted composite joints. AD-A117342 (AFWAL TR 81-3154)
23. Collings TA (1977) The strength of bolted joints in multidirectional CFRP laminates. ARC CP 1380
24. Garbo SP, Ogonowski JM (1981) Effect of variance and manufacturing tolerances on the design strength and life of mechanically fastened composite joints. AD- A101657
25. Chi J, Xie MJ (1988) FE analysis investigation on bolt-load distribution in composite laminate joints. *Acta Aeronautica Et Astro- Nautica Sinica* 19(7) (in Chinese)
26. Hart-Smith LJ (1976) Bolted joints in graphite composites. NASA-TR-144899
27. Hart-Smith LJ (1978) Mechanically fastened joints for advanced composite-phenomenological consideration and simple analysis. In: Presented to the conference on fibrous composites in structure design
28. Bunin BL (1985) Critical joints in large composite primary aircraft structures. NASA-CR-3914 Vol. I — Technical summary

29. Bunin BL (1985) Critical joints in large composite primary aircraft structures vol II — Technology demonstration test report. NASA-CR-172587
30. Bunin BL, Sagui RL (1985) Critical joints in large composite primary aircraft structures vol III—Ancillary data test results. NASA-CR-172588
31. Nelson WD, Bunin BL, Hart-Smith LJ (1983) Critical joints in large composite primary aircraft structures. NASA-CR-3710
32. Hortin RE, McCarty JE (1987) Damage tolerance of composites. In: Engineered materials handbook Vol.1 Composites. ASM International, Ohio, USA, pp 259–267
33. Tang XD, Shen Z, Chen PH, Gaedke M (1997). A methodology for residual strength of damaged laminated composites. AIAA Paper 97–1220
34. Chen PH (1999). Damage tolerance analysis for composite laminates and stiffened panel. PhD thesis of Nanjing Aeronautical and Astronautical University
35. Chen PH, Shen Z, Wang JY (2001) Damage tolerance analysis of cracked stiffened composite panels. *J Compos Mater* 35(20)
36. Chen PH, Shen Z, Wang JY (2001). Impact damage tolerance analysis of stiffened composite panels. *J Compos Mater* 35(20)
37. Chen PH, Shen Z, Wang JY (2001) Prediction of the strength of notched composite laminates. *Compos Sci Technol* 61(10)
38. Chen PH, Shen Z, Wang JY (2002) A new method for compression after impact strength prediction of composite laminates. *J Compos Mater* 36(5)
39. ASTM D 3878-07 (2004) Standard terminology for composite materials
40. ACEE Composites Project Office (1985) NASA/Aircraft industry standard specification for graphite fiber/toughened thermoset resin composite material. NASA RP 1142
41. SACMA 2R-94 (1994) SACMA recommended test method for compression after impact of oriented fiber-resin composites
42. Dost EF, Avery WB, Finn LB, Ilciewicz LB, Scholz DB, Wishart RE (1993) Impact damage resistance of composite fuselage structure, Part 3. In: Paper presented at fourth ACT conference
43. Shen Z, Zhang ZL, Wang J, Yang SC, Ye L (2004) Characterization on damage resistance and damage tolerance behavior of composite laminates. *Acta Materiae Composite Sinica* 21 (5):140–145 (in Chinese)
44. Chen PH, Shen Z et al (2006) Failure mechanisms of laminated composites subjected to static indentation. *J Compos Struct* 75(1–4):486–495
45. Shen Z, Yang SC, Chen PH (2008) Experimental study on the behavior and characterization methods of composite laminates to withstand impact. *Acta Materiae Composite Sinica* 25 (5):125–133 (in Chinese)
46. Li Y (1998). Effect of hygrothermal spectrum aging on composite laminates. NCCM-10. Hunan Science and Technology Press, Changsha, pp 143–146
47. Kan HP, Whitehead RS, Kauts E (1992). Damage tolerance certification methodology for composite structures, N92-32579
48. Bai G (1997). Reliability evaluation of composite laminates under impact threat. MSC thesis of Northwestern Polytechnical University
49. Ma ZK, Yang L (1998) Analysis method of cumulative damage tolerance reliability for composite laminated structures. Design and Research of Commercial Aircraft
50. Chen PH, Shen Z (2004). Statistical analysis and reliability evaluation of post- impact compressive residual strength. *Acta Aeronautica Et Astronautica Sinica* 25(6)
51. Tong MB, Chen P H, Shen Z (2004). Reliability analysis of impact damage tolerance for composite materials. *Acta Materiae Composite Sinica*, 21(6)
52. JSSG-2006 (1998) Joint service specification guide—Aircraft structures